Density Functional Theory Studies on CC Bond Metathesis by Grubbs and Schrock Catalysts: Metal-Carbon Bonding, Mechanisms, and Metallacycles

Thesis Submitted to AcSIR for the Award of the Degree of
DOCTOR OF PHILOSOPHY
in Chemical Sciences

By
Remya P. R.
Registration No: 10CC12A39011

Under the Guidance of
Dr. C. H. Suresh

Chemical Sciences and Technology Division
CSIR-National Institute for Interdisciplinary Science and Technology
Thiruvananthapuram-695019, Kerala, India

January, 2018

DECLARATION

I hereby declare that the Ph.D. thesis entitled "**Density Functional Theory Studies on CC Bond Metathesis by Grubbs and Schrock Catalysts: Metal-Carbon Bonding, Mechanisms, and Metallacycles**" is an original work carried out by me at Chemical Science and Technology Division(CSTD), CSIR-National Institute for Interdisciplinary Science and Technology (CSIR-NIIST), Thiruvananthapuram, under the supervision of Dr. C. H. Suresh, Principal Scientist, CSTD, CSIR-NIIST, and it has not been submitted elsewhere for any other degree, diploma or title.

CSIR-NIIST

24/01/18 **Remya P. R.**

Council of Scientific & Industrial Research
National Institute for Interdisciplinary Science and Technology
Thiruvananthapuram-695019, Kerala, India

Dr. C. H. Suresh
Principal Scientist
Chemical Sciences & Technology Division
Tel: +91- 4712515472
E-mail: sureshch@gmail.com
sureshch@niist.res.in

24th January 2018

CERTIFICATE

This is to certify that the work incorporated in this Ph.D. thesis entitled "**Density Functional Theory Studies on CC Bond Metathesis by Grubbs and Schrock Catalysts: Metal-Carbon Bonding, Mechanisms, and Metallacycles**" submitted by Ms. Remya P.R to Academy of Scientific and Innovative Research (AcSIR) in fulfillment of the requirements for the award of the Degree of Doctor of Philosophy, embodies original research work done under my supervision. I further certify that this work has not been submitted to any other University or Institution in part or full for the award of any degree or diploma. Research material obtained from other sources has been duly acknowledged in the thesis. Any text, illustration, table etc., used in the thesis from other sources, have been duly cited and acknowledged.

Dr. C. H. Suresh
(Thesis Supervisor)

ACKNOWLEDGEMENT

At this moment of accomplishment, I wish to express my sincere appreciation to those who have contributed to this thesis and supported me in one way or the other during this amazing journey.

It is difficult to overstate my gratitude to my Ph.D. supervisor, Dr. C. H. Suresh for his enthusiasm, inspiration, timely advice, continued encouragement, thoughtful guidance and strong motivation throughout my research period.

I am deeply indebted to Dr. A. Ajayaghosh-Director, CSIR-NIIST, and former directors, Dr. Suresh Das and Dr. Gangan Pratap for providing the academic support and excellent infrastructure facilities which made my Ph.D. experience productive and stimulating.

I am greatly influenced by AcSIR coordinators Dr. Mangalam S. Nair and Dr. Luxmi Varma- HOD, Chemical Sciences and Technology Division with their valuable advice and constructive criticisms throughout my coursework.

I also extend my sincere thanks to former HODs Dr. D. Ramaiah and Dr. K.R. Gopidas for all the support and guidelines.

I wish to thank my Doctoral Committee members Dr. M.L.P. Reddy, Dr. K.V. Radhakrishnan, and Dr. Vasundhara Mutta for their valuable suggestions, timely help, and support.

I wish to thank the current and former members of CHS Group for their support and friendship. Dr. Sajith, Dr. Basha, Dr. Sandhya, Dr. Neetha, Dr. Prabha, and Dr. Remya are acknowledged for their help and guidelines in understanding the computational tools and research methods. Current members of the lab; Rakhi, Della, Anjali, Remya, Bijina, Divya, Anila, and Dr. Renjith are acknowledged for their warm friendship which created a pleasant working atmosphere in the lab.

Many thanks to, Anjali, Afeefah, Maya, Sayana, Shimi, and Swetha for their invaluable friendship, support, and encouragement. I greatly appreciate the friendship and support of Ivy, Honey, Sreejith Kumar, and Rajesh.

I wholeheartedly extend my thanks to all my friends at CSIR-NIIST for making my days in NIIST memorable. I would also like to thank the administrative and technical staff members of the Institute for the cooperation and help in their respective roles.

I gratefully acknowledge UGC for providing me financial support.

High-performance computational facilities at CSIR-NCL, Pune, and CSIR-CMMACS, Bangalore is greatly acknowledged.

The mere expression of thanks does not suffice for the unconditional love and care of my family. Above all, I owe it all to the Almighty for granting me the wisdom, health, and strength to undertake this research task and enabling me to its completion.

Remya P. R.

CONTENTS

Chapter 2

Unusual Bonding Features of Metallacycles of Alkene and Alkyne Metathesis

Part A: Hypercoordinate β-Carbon in Grubbs and Schrock Olefin Metathesis

List of Figures

List of Schemes

List of Tables

List of Abbreviation

ACID : Anisotropy of Current Induced Density
ACM : Alkyne Cross Metathesis
ADIMET : Acyclic Diyne Metathesis Polymerization
ADMET : Acyclic Diene Metathesis
AIMD : *Ab Initio* Molecular Dynamics
AMBER : Assisted Model Building with Energy Refinement
AO : Atomic Orbitals
BCP : Bond Critical Point
BO : Born Oppenheimer
BP : Bond Path
BSI : Bond Stretch Isomerism
CASSCF : Complete Active Space Self-Consistent Field
CC : Coupled Cluster Theory
CCD : Cambridge Crystal Database

CCP : Cage Critical Point

CGTO : Contracted Gaussian Type Orbitals

CHARMM : Chemistry At Harvard Macromolecular Mechanics

CHEAT : Carbohydrate Hydroxyls Represented By External Atoms

CI : Configuration Interaction

CM : Cross Metathesis

CP : Critical Point

CSGT : Continuous Set of Gauge Transformation

DFT : Density Functional Theory

DI : Distortional Isomerism

ECPs : Effective Core Potentials

EFF : Empirical Force Field

G09 : Gaussian 09

GGA : Generalized Gradient Approximation

GIAO : Guage Invariant Atomic Orbitals

GROMOS : Gronien Molecular Simulation

GTO : Gaussian Type Orbitals

HF : Hartree-Fock

IEF-PCM : Integral Equation-Formalism Polarizable Continuum Model

IGAIM : individual gauge for atoms in molecules

IGLO : individual gauge for localized orbitals

IRC : Intrinsic Reaction Coordinate

LDA : Local Density Approximation

LSDA : Local Spin Density Approximation

MC : Monte Carlo

MCB : Metallacyclobutane

MCBD : Metallacyclobutadiene

MCSCF : Multi-Configurational Self-Consistent Field

MD : Molecular Dynamics

MM : Molecular Mechanics

MRCI : Multi-Reference-Configuration Interaction

NBO : Natural Bond Orbital

NHC : N-Heterocyclic Carbene

NICS : Nucleus Independent Chemical Shift

NMR : Nuclear Magnetic Resonance

ONIOM : our Own N-Layered Integrated Molecular Orbital and Molecular Mechanics

PCM : Polarizable Continuum Model

PES : Potential Energy Surface

QM : Quantum Mechanics

QTAIM : Quantum Theory of Atoms in Molecules

RCAM : Ring-Closing Alkyne Metathesis

RCEYM : Ring Closing Enyne Metathesis

RCM : Ring Closing Metathesis

RCP : Ring Critical Point

ROAMP : Ring-Opening Alkyne Metathesis Polymerization

ROMP : Ring Opening Metathesis Polymerization

RuCB : Ruthenacyclobutane

SCF : Self-Consistent Field

SCRF : Self-Consistent Reaction Field

SMD : Solvation Model Based on Density

STQN : Synchronous Transit-Guided Quasi-Newton

SP : Square Pyramidal

STOs : Slater-Type Orbitals

TBP : Trigonal-Bipyramidal

TS : Transition State

W_{bo} : Wiberg Bond Order

WCB : Tungstenacyclobutane

UFF : Universal Force Field

PREFACE

Metathesis reaction is a well established synthetic strategy for the clean production of numerous classes of chemical structures. Grubbs ruthenium-based catalysts and Schrock's tungsten-based catalysts are the widely used in metathesis. Mechanistic studies reveal the presence of a metallacycle intermediate in the pathway which plays an important role in the reaction. The metallacyclobutane (MCB) of alkene metathesis and metallacyclobutadiene (MCBD) of alkyne metathesis shows unusual bonding features such as short metal C_β bond distance and longer $C_\alpha C_\beta$ bonds and wider CCC bond angle. The thesis entitled "**Density Functional Theory Studies on CC Bond Metathesis by Grubbs and Schrock Catalysts: Metal-Carbon Bonding, Mechanisms, and Metallacycles**" is our attempt to quantify the metal-C_β interaction in the metallacycle and thus confirm the 1,3-metal carbon interaction in metathesis using density functional theory (DFT) methods. Further, these insights are utilized in providing a theoretical explanation for reactions of experimental importance.

The thesis is divided in to four chapters. Chapter 1 gives an overview of metathesis reactions and the metallacycle intermediates (Part A) and computational methodologies and the techniques employed in the thesis (Part B).

Chapter 2 is divided into two parts. Part A of Chapter 2 discusses the unusual bonding features of the metallacyclobutane intermediate of Grubbs and Schrock catalysts. The unique bonding feature of MCB is attributed to the interaction of electron deficient metal center with both the CC-σ bonds. This kind of interaction termed as α,β-agostic interaction brought C_β closer to the metal center (~2.20 Å) and activate the CC bonds (~1.60 Å). The M-C_β interaction can be considered as a fifth bond for the C_β, thus making it hypercoordinate ($_{hyper}C$). The metallacycles with agostic type interaction are called agostic complexes. The MCB can exist in another isomeric form with no such interaction and that isomer termed as non-agostic complex exhibit longer M-C_β interaction and shorter CC bonds. The hypercoordinate character of C_β in both MCB of Grubbs and Schrock system are quantified using structural, bonding, electronic, and NMR analysis. These analyses reveal that there exists a direct correlation between the

metal-C_β interaction and CC bond activation and explains the low activation barrier required for the CC multiple bond breaking in metathesis reaction. Part B of Chapter 2 quantifies the metal-C_β interaction (1,3-MC bonding) in the tungstenacyclobutadienes (WCBD) of alkyne metathesis. The strong 1,3-MC bonding in these metallacycles is the result of d_π-p_π interaction and can be treated as a direct bond. The 1,3-MC bond becomes the fourth bond of C_β in the same plane that makes the C_β a planar tetracoordinate center ($_{pt}C$). This section also contains discussion on metallorganic frameworkes containing more than one $_{pt}C$ center with WCBD as the basic unit.

Chapter 3 of the thesis invokes the concept of Bond stretch isomerism (BSI) in explaining the mechanism and catalyst design of olefin metathesis catalyzed by Grubbs system. BSI is a rare phenomenon in chemistry where the isomers differ only in one more bond lengths. The agostic (RuCB) and non-agostic (RuCB′) metallacycle of ruthenium catalyzed alkene metathesis are found to be connected by a transition state of significant barrier and satisfy the conditions of BSI. All possible pathways *viz.* the dissociative, associative and associative-dissociative mechanism of alkene metathesis leading to MCB formation are analyzed to answer many fundamentals of olefin metathesis such as the non-preference of associative mechanism and preference for bulky ligands in the catalyst design.

Chapter 4 is focused on the mechanistic aspect of cyclotrimerization reaction involving CC and CN triple bonds catalyzed by Grubbs type catalysts. First part of this chapter discusses the cyclotrimerization reaction of acetylene to benzene catalyzed by Grubbs first and second generation catalysts. Two possible pathways *viz.* metathesis and non-metathesis for the reaction are discussed in detail using four catalyst models. A new decomposition pathway for the Grubbs catalyst involving the chloro ligand migration is brought in to explain the non-metathesis pathway. In the second part, findings from the acetylene cyclotrimerization reaction are applied in explaining an experimentally known cyclotrimerization reaction of a diyne and nitrile leading to pyridine derivative.

It may be mentioned that each chapter of the thesis is presented as an independent unit and therefore the structural formulae, schemes and figures are numbered chapter wise.

Chapter 1

Introduction

Part A- Metathesis Reactions

&

Part B - Theoretical Concepts and Computational Methodology

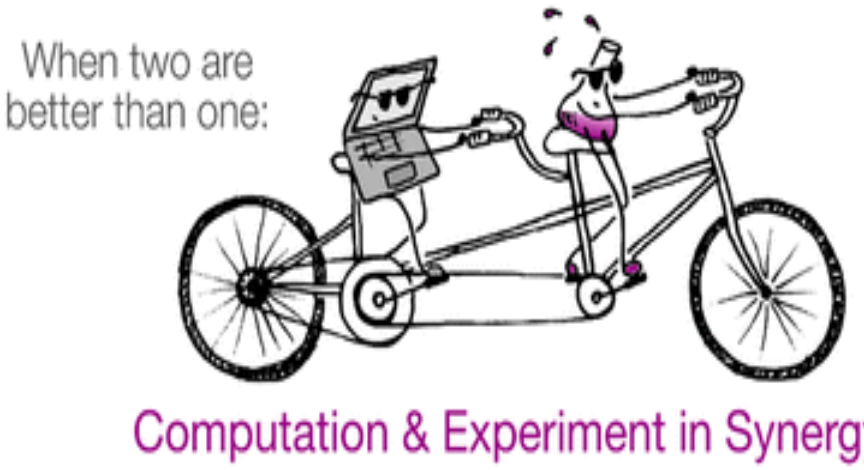

Theresa Sperger *et al. Acc. Chem. Res.*, **2016**, 49,1311

Part A: Metathesis Reactions

1.1 An Overview of Metathesis Reactions

Metathesis reaction is a well-established synthetic strategy for the clean production of numerous classes of chemical structures. The Greek word 'metathesis' means transposition,[1] and in the context of chemistry, it is described as a double displacement reaction involving the exchange of bonds between the reactants. A general representation of such a reaction, also known as 'salt metathesis' is represented in (Eq. 1.1) where the compounds A-B and C-D transform to products A-C and B-D.

$$A\text{-}B + C\text{-}D \rightarrow A\text{-}C + B\text{-}D \qquad \text{(Eq.1.1)}$$

Though the 'salt metathesis' reaction where the counter ion exchange occurs is known in chemistry for a while reactions involving the exchange of organic fragments by cleaving and rearranging CC bonds were unknown till 1950s.[2-5] Breaking and making of CC bond is not an easy process and it often requires a catalyst.[5-6] The idea of 'metathesis' in organic chemistry provides one of the simple and elegant mechanistic pathways for the synthesis of molecules which are otherwise difficult to synthesize. The 2005 Nobel Prize in chemistry was awarded to Yves Chauvin, Robert H. Grubbs, and Richard R. Schrock for the development of metathesis reaction in chemistry. The advances in metathesis reaction in the last four decades have enhanced the scope of organic chemistry to the easy synthesis of a large variety of complex organic molecules leading to profound and growing influence in related areas such as medicine, biochemistry, and material science.[7-11] Also, metathesis provides a greener way for the synthesis of complex molecules as the byproducts and wastes are less compared to similar reactions.[12]

Though different types of metathesis reactions such as alkene metathesis,[13] alkyne metathesis,[14] alkane metathesis,[15] enyne metathesis,[16] are known; the most important and well-developed class is the alkene metathesis.

1.1.1 Alkene Metathesis

Alkene/olefin metathesis reaction involves the redistribution of double bonds in the presence of a transition metal catalyst (Scheme 1.1).[2-3, 13, 17-21] First observation of olefin transformation was made in the 1950s by the chemists at a petroleum industry when they detected ethylene and 1-butene during the copolymerization of propylene in the presence of metal salts.[22] It was later found that the unexpected products are formed as a result of the breaking and making of the olefinic bonds, and the reaction was named as alkene/olefin metathesis.[2] Recognizing the potential of metathesis reaction, many groups put themselves out to understand this reaction and designed new catalyst systems to enable the practical application of this reaction. Among the many, Grubbs and Schrock are well-known for their contribution towards the catalyst design.[12, 23]

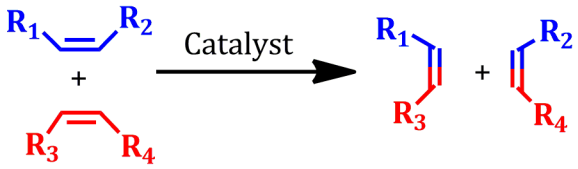

Scheme1.1 A schematic representation of alkene metathesis reaction.

1.1.1.1 Mechanism of Alkene Metathesis

Calderon and group after a series of experimental analysis found that alkene transformation occurs *via* CC double bond cleavage rather than a transfer of alkyl groups between olefins *via* single-bond cleavage.[24] This critical observation paved the foundation for further mechanistic studies of metathesis reaction. Banks and Bailey proposed a "quasicyclobutane" mechanism to account for their alkene interchange reaction. All these studies suggested a mechanism in which both the alkenes interact with the metal center simultaneously and exchange the carbon fragments. This type of mechanism is known as pair-wise mechanism and is depicted in Scheme 1.2. However, the pair-wise mechanism failed to explain the product formation in the polymerization or cross metathesis between cyclic olefin and an acyclic olefin.

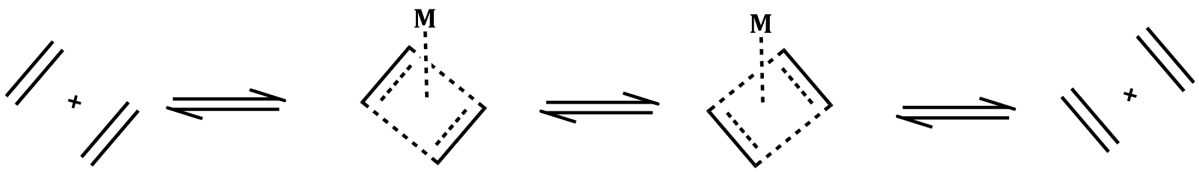

Scheme 1.2 The pair-wise mechanism of olefin metathesis.

Later, Chauvin and Hérisson suggested the possibility of a metal-carbon double bond formation to explain the formation of products in the metathesis reaction.[25] They proposed the possible interconversion of an alkene bond with the metal-carbene bond. Conducting a large number of experiments, Grubbs, Katz and MacGinis and co-workers verified the metal-carbene mechanism proposed by Chauvin.[26-27] This observation led to the development of metal-carbene catalysts for metathesis reaction. According to the metal-carbene mechanism or now known as Chauvin mechanism, the metal-carbene complex couples with the CC double bond to form a metallacyclobutane (MCB) intermediate (Scheme 1.3). It suggests a series of cycloaddition and cycloreversion for the scrambling of alkenes. The Chauvin mechanism and MCB intermediate were further confirmed by many experimental and theoretical studies.[28-33]

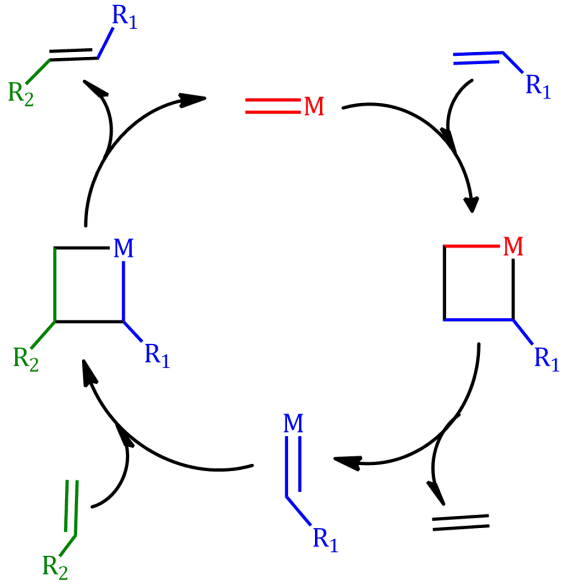

Scheme 1.3 Chauvin mechanism showing a series of cycloaddition and cycloreversion in the olefin metathesis process catalyzed by a metal alkylidene complex.

1.1.1.2 Catalysts for Alkene Metathesis

The large area of application found for the metathesis reaction is because of the development of catalysts with high selectivity and efficiency. In the earlier days of metathesis, a combination of transition metal salts and main group alkylating agents (such as WCl_6/Bu_4Sn, $WOCl_4/EtAlCl_2$, $MoO_3/SiO2$) were used as catalysts under very harsh conditions.[23] Further attempts for the catalyst development focused on the metal alkylidene complexes as suggested by Chauvin mechanism.[25] Schrock group reported metal-carbene complexes (**a, b**) of molybdenum and tungsten of formula $M(NAr)(CHR)(R')_2$ for alkene metathesis that show high activity under mild conditions (Figure 1.1).[18, 34-36] The ancillary ligands especially the alkoxo group plays an important role in the catalytic activity and tuning the ligand environment around the metal center using electron withdrawing ligands increases the metathesis activity.[37] Though these catalysts are found to be highly reactive to catalyze the metathesis of both internal and terminal alkynes, oxophilicity of the metal center made them vulnerable to air and moisture. Also, these early transition metal complexes are found to be intolerant to many functional groups such as aldehydes and alcohols leading to many unwanted byproducts in the course of the reaction.

Following the results from Schrock group, Grubbs and coworkers started the quest for robust catalysts for olefin metathesis which selectively reacts with olefins. Since early transition metals show poor functional group tolerance, Grubbs group focused on late or middle transition metal with high oxidation state. They tested the tolerance of different metal centers with functional groups and found that ruthenium(II) is highly selective for CC double bonds than any other functional group.[13] The Ru(II) based catalysts which are less active compared to Schrock alkylidene systems become widely accepted because of their stability and functional group tolerance. It is optimized that ruthenium(II) metal center with five ligand coordination (two neutral electron donating species, two monoanionic groups, and one alkylidene ligand) is a good candidate for the metathesis reaction. It is found that large and more electron donating phosphine ligands increase the catalytic activity and PCy_3 becomes the best choice for catalyst design. The PCy_3 derivative (first generation catalyst **c**) is

found to activate the low strain rings and even acyclic olefins for metathesis reaction.[31, 38-39] The first generation Grubbs catalyst was further modified to improve the catalytic activity by replacing the phosphine ligands with more electron donating groups.[40]

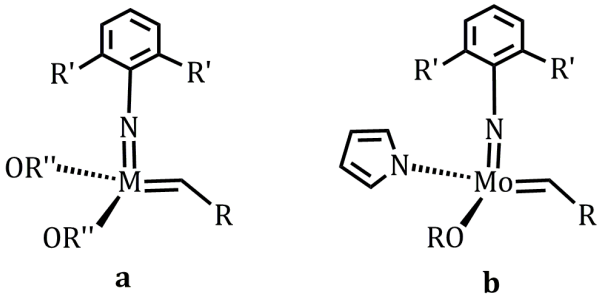

Schrock type catalysts

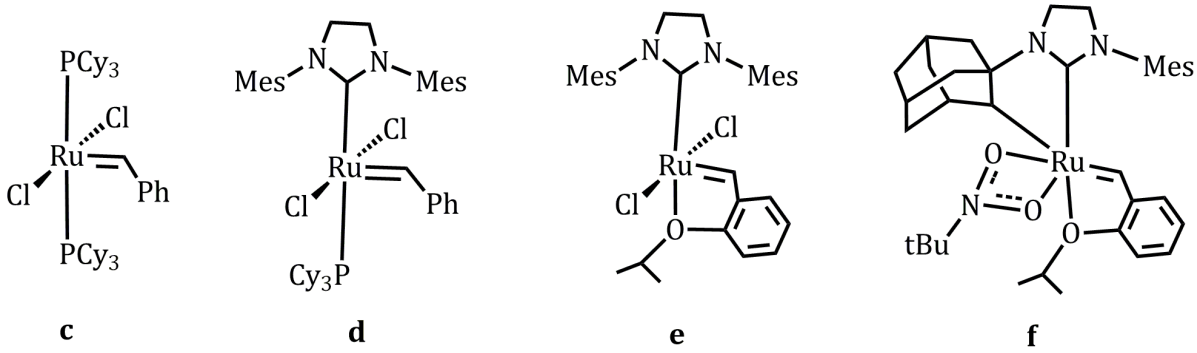

Grubbs type catalysts

Figure 1.1 Schrock and Grubbs catalysts used in the olefin metathesis reaction.

Further modification was attempted by replacing one of the phosphine ligands with an N-heterocyclic carbene (NHC) as its electron rich character, and the ligand bulk improve the catalytic activity (**d**).[41] With saturated NHC ring the catalyst becomes more efficient as the lack of π interaction increases the basic nature of NHC ligand.[42-43] Another significant contribution to the Grubbs catalysts development was made by replacing the labile phosphine ligand with a chelating ligand (**e**).[6, 44-45] This new catalyst system often referred to as Hoveyda–Grubbs catalyst has a chelating ortho-isopropoxy group attached to the benzene rings and gives a completely phosphine-free structure. Although these catalysts are slower to initiate and expensive compared to the Grubbs

catalysts, Hoveyda–Grubbs type system gained the popularity in chemistry because of their improved stability.

The single component catalytic systems developed by Grubbs and Schrock works well under mild reaction conditions and popularize alkene metathesis by providing an atom economic path for the synthesis of complex molecules.[46-47] Though the above-mentioned catalyst systems significantly reduce the intricacy of the organic synthesis, most of these catalysts are non-selective and give thermodynamically favored *E*-olefins as the major product. However, the quest for *Z*-selective catalyst was indeed high, as it will enable the efficient total synthesis of natural products. Schrock and Hoveyda reported tungsten and molybdenum complexes of formula M(NR)(CHR')(X)(Y), [where X is an oxygen based ligand (such as alkoxide, aryloxide, binaphtholates) and Y is a pyrollide such as mono aryl oxypyrolidene] for selective synthesis of *Z*-olefins (**b**).[48-50] Modifications are done on Grubbs ruthenium catalysts to increase its enantioselectivity which is mainly achieved by developing cyclometallated ruthenium complexes (**f**).[51-54] Olefin metatheses are now widely applied in the area of polymer synthesis, total synthesis of natural products, and organic materials.

Initiation *via* the dissociation of a labile ligand L (for first and second generation catalysts) or by the cleavage of Ru-O bonds (for Hoveyda type systems) is the most accepted mechanism for Grubbs ruthenium catalysts (Scheme 1.4).[29-31, 55-56] In the next step of dissociative pathway, an olefin coordinate with the metal center to form a 16-electron complex. Theoretical studies found that the bottom bound coordination of alkene is preferred to the side bound attack.[32-33, 57-58] The coordinated alkene undergoes a [2+2] cycloaddition with the metal-carbene bond to form a 14-electron metallacyclobutane (MCB) intermediate. The formation of metallacycle changes the oxidation of the metal center from +2 to +4. Although the relative stability of the carbenes and MCBs can vary with reaction conditions, catalyst composition, and alkene substitutions, the mechanism of alkene metathesis appears to be the same for all types of catalysts. Though the dissociative mechanism given in Scheme 1.4 is mostly accepted,[56] there is a chance for alkene coordination without the labile ligand dissociation and is termed as the associative mechanism.[29] In such cases, an 18-electron

olefin adduct complex will be formed as an intermediate. Detailed information on the possible mechanism of alkene metathesis using Grubbs type catalysts are added in Chapters 2 and 3.

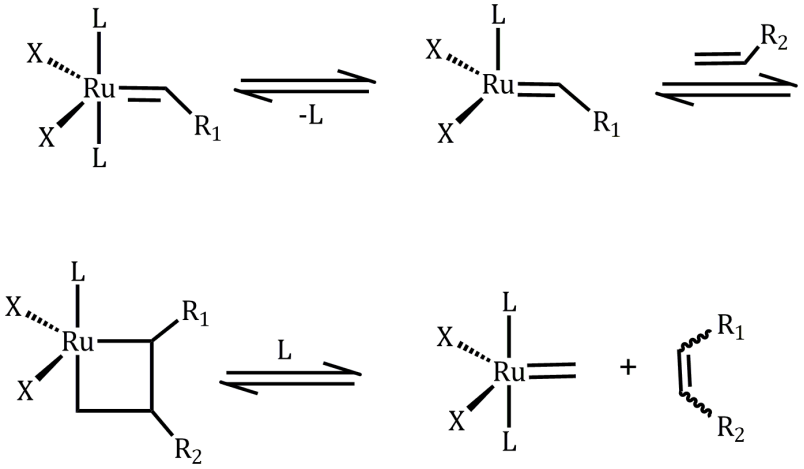

Scheme 1.4 A general scheme for alkene metathesis using Grubbs type catalyst showing the involvement of a metallacyclobutane intermediate.

1.1.1.3 Decomposition of Grubbs Ruthenium Catalysts

Grubbs ruthenium based catalysts found extensive application in the field of organic and polymer chemistry. Though these catalysts provide best functional group tolerance and stability, it is observed that at special reaction condition the catalysts may undergo decomposition or degradation. As the industrial application of metathesis reaction is increasing, it is important to understand the decomposition pathways of the catalysts to use them efficiently. Mol and coworkers attempted to decompose ruthenium carbene based complexes using primary alcohols to get a highly active ruthenium hydride system.[59-60] Van Rensburg and coworkers using density functional techniques suggested a substrate induced decomposition mechanism for Grubbs ruthenium carbene catalysts.[61] They proposed a β-hydride transfer from the ruthenacyclobutane intermediate. Grubbs group reported the thermal decomposition of phosphonium based Grubbs catalyst to a dinuclear ruthenium hydride complex.[62] They proposed that the dissociated phosphine ligand can attack the nucleophilic methylidene center of the catalyst to form a ruthenium hydride complex.[62] Grubbs group proposed yet another decomposition path

involving a double C-H bond activation for second generation catalyst with benzylidene ligand[63] which was later theoretically supported by Jomon and Suresh, using DFT techniques.[64] Blechert *et al.* reported deactivation pathway for Hoveyda-Grubbs type complexes with alkoxy benzylidene ligands. Their report suggested that Hoveyda-Grubbs type complexes with N-aryl substituted NHC ligands, lacking steric hindrance at the ortho position of the arene ligand, can give rise to intramolecular C-H insertion. This insertion leads to metathesis inactive ruthenium complexes.[65] Decomposition of a Z-selective ruthenium metathesis catalysts have been attempted by Grubbs, Houk and coworkers using X-ray crystallography and density functional theory.[66] Fogg *et al.* reported a donor induced decomposition of Grubbs first generation catalysts.[67] Recently the same group reported that Brønsted bases can decompose the metathesis-active Ru intermediates of Hoveyda and Grubbs second-generation catalysts. The resulting decomposed system is found to catalyze some reactions such as olefin isomerization, cycloaddition which are often observed as side reactions in a metathesis reaction.[68-71]

1.1.1.4 Types of Alkene Metathesis Reactions

Olefin metathesis reactions have enabled the synthesis of a wide range of unsaturated molecules, which were challenging or even impossible to prepare otherwise. Alkene metathesis can be classified in to different classes based on the reactants and products formed in the reaction. Cross metathesis (CM) is a common type of metathesis reaction where transalkylidation occurs in the presence of metal alkylidene catalysts with the release of ethylene gas (Scheme 1.5). It is a convenient route for the synthesis of higher alkenes from smaller alkenes.[72-73] Though the development of active catalysts increased the application of CM reaction, lack of predictability in the product selectivity and stereoselectivity was an issue hindering the wider use of CM in organic synthesis. Selectivity issues are solved by using modified catalysts and/or using specifically substituted olefins.[74-76] Ring closing metathesis (RCM) is a powerful and widely used method for the synthesis of cyclic structures of ring size 5 to 7 atoms (Scheme 1.5).[35, 77-79] The release of ethene during the reaction is the driving force for the reaction. RCM proceeds *via* a sequence of [2+2] cycloaddition and cycloreversion and found use in the synthesis of natural products,[80] drug molecules,[81] and polymers.[82] Like CM, the RCM

reaction also fails to predict the control of stereochemistry about the CC bond formed and the yield of the reaction highly depends on the reaction conditions.

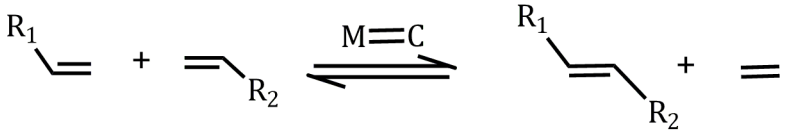

Cross metathesis

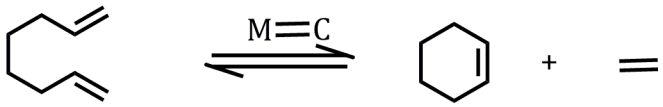

Ring closing metathesis

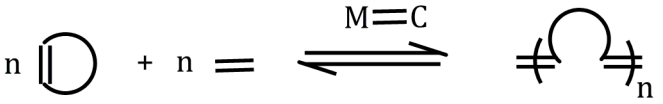

Ring openng metathesis polymerization

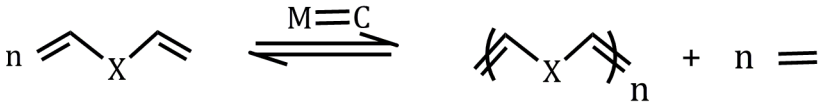

Acyclic diene metathesis polymerization

Scheme 1.5 Representation of various olefin metathesis reactions.

Ring opening metathesis polymerization (ROMP) is a chain growth, addition polymerization technique, widely used for the synthesis of macromolecular materials (Scheme 1.5).[34, 52, 83-85] In ROMP, a mixture of strained cyclic structures are converted to the polymeric material of high molecular weights, and low dispersity and release of the ring strain during the reaction acts as the driving force for the reaction to occur.[86-87] Substituted cyclobutenes and cyclooctenes are the commonly used substrates for the

synthesis of linear polymers with a wide range of functionality.[88-89] During the reaction, metal carbene bond couples with the double bond of the ring to form a metallacyclobutane structure which opens up to give a linear chain with a terminal metal-carbene bond. This new carbene center attacks the double bond of the next monomer and thus propagates the reaction until all monomers are consumed. In the case of living ROMP, the reaction is quenched by adding a quencher, which removes or deactivates the active metal-carbene from the growing polymer chain and install a functional group to terminate the reaction. ROMP reaction is unique as the double bond of the monomer is conserved in the polymer.

Acyclic diene metathesis (ADMET) polymerization is a step-growth condensation of terminal diene monomers to produce well-defined and strictly linear polymers with unsaturated polyethylene backbones (Scheme 1.5).[75, 90-94] Constant removal of the condensate (ethylene) drives the ADMET reaction. It is demonstrated that nearly any unsaturated polymer can be synthesized *via* ADMET reaction and is used in the production of polymers with a specific structure which are difficult to synthesize using other techniques.[95-98]

1.1.2 Alkyne Metathesis

The redistribution of alkyne bonds was first described by Bailey *et al.* using heterogeneous catalysts system of a mixture of tungsten and silicon oxides.[99] Later Mortreux *et al.* used a homogeneous mixture of $Mo(CO)_6$ (a molybdenum source) and simple phenol additives to catalyze the scrambling of alkynes.[100] Katz *et al.* proposed a mechanism similar to the Chauvin mechanism of alkene metathesis, which suggested a metallacyclobutadiene (MCBD) intermediate formation after a [2+2] cycloaddition between the metal-carbon triple bond and the alkyne.[26] The MCBD intermediate in the presence of excess reactant opens up to release the product and regenerate the catalysts system (Figure 1.2). This proposal paved the base for the metal alkylidyne complexes as alkyne metathesis catalysts.[5, 101-102] Compared to alkene metathesis, alkyne metathesis is still in the growing stage and development of active and efficient

catalysts improved the status of alkyne metathesis as an important tool in the organic synthesis.[14, 103]

The best catalyst known for alkyne metathesis is a high-valent Schrock type catalyst of formula X_3WCR where the ancillary ligand X plays a crucial role in the catalytic reaction (**g**). The alkyl group on the carbyne carbon plays an important role in the synthesis and stability of the catalysts but does not play a crucial role in the catalyst activity as they are replaced in each metathesis step. Apart from tungsten alkylidynes, rhenium and molybdenum alkylidynes are also tested for their catalytic activity in alkyne metathesis. Though molybdenum complexes of type X_3MoCR are found to give significant results, the synthesis of these catalysts is found to be a problem.[37, 104] Recently Tamm and coworkers developed metal-carbyne complexes of tungsten with Imidazolin-2-iminato ligand (**h**) which shows high activity at room temperature.[105-108]

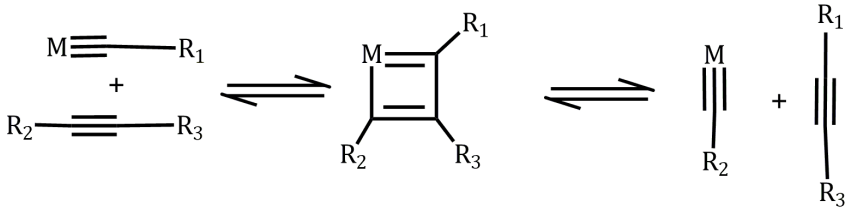

(i)

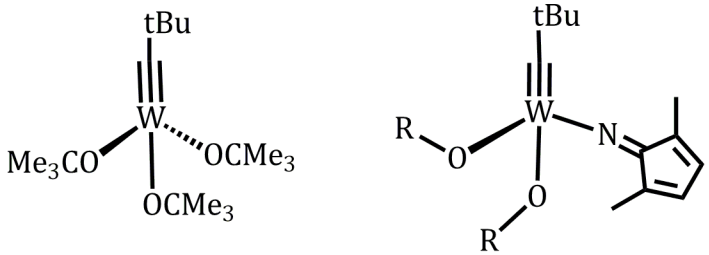

g **h**

(ii)

Figure 1.2 (i) Representation of Katz mechanism for alkyne metathesis and (ii) common catalysts used in the alkyne metathesis.

Similar to alkene metathesis, there are many types of alkyne metathesis such as alkyne cross metathesis (ACM),[109-110] ring-closing alkyne metathesis (RCAM),[111-112]

ring-opening alkyne metathesis polymerization (ROAMP) and acyclic diyne metathesis polymerization (ADIMET) (Scheme 1.6). RCAM reaction is found to be useful in the synthesis of macrocyclic structures, and these cyclic structures can be stereoselectively hydrogenated to obtain *Z*- or *E* alkenes. ROAMP and ADIMET techniques have been widely used in the synthesis of various polymers like nonconjugated polyalkynylenes as well as conjugated poly-(arylene ethynylene)s.[113] These alkyne metathesis techniques often found application in the total synthesis of natural products and material science.

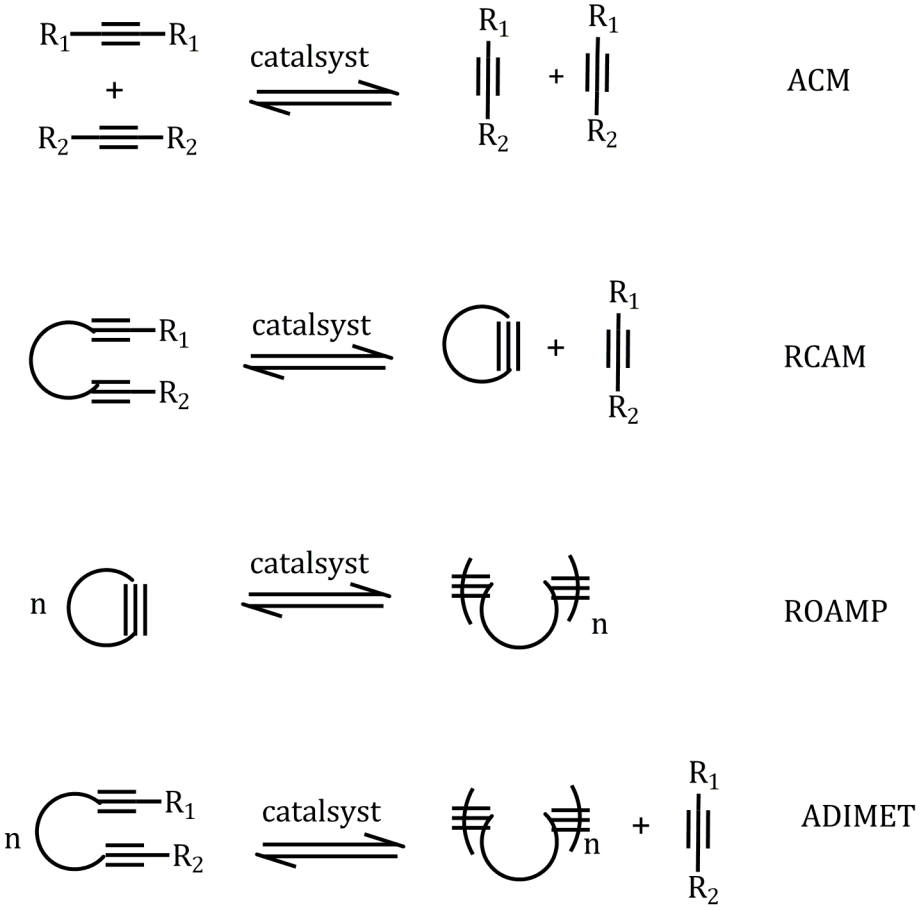

Scheme 1.6 Representation of various alkyne metathesis reactions.

1.1.3 Enyne Metathesis

Enyne metathesis is a bond reorganization reaction between an alkene and an alkyne to form a 1,3-diene and can be used both in intra- and intermolecular applications

(Scheme 1.7).[16] History of enyne metathesis began when alkene polymerization by metal-carbenes was tested in the presence of alkynes, and the reaction was first reported in the presence of Pd(II) and Pt(II) complexes.[114-115] Metal-Fischer carbene catalysts found to be useful in the enyne bond reorganization and were used stoichiometrically to produce a variety of products. Grubbs ruthenium carbene complexes replaced the metal Fischer carbene catalysts as the former dominates with the catalytic efficiency and functional group tolerance. Choice of using metal-carbene complexes in the enyne bond reorganization transformed the fate of enyne metathesis reaction.[115-116] Today many ring closing, ring opening and cross metathesis involving alkene and alkynes are conducted using ruthenium carbene complexes and becomes a good synthetic tool in organic chemistry. The intermolecular enyne metathesis also known as ring closing enyne metathesis (RCEYM) is an important technique for the synthesis of heterocycles.[117] The enyne metathesis reaction is driven by the formation of a stable conjugated 1,3-diene molecule.[117-122]

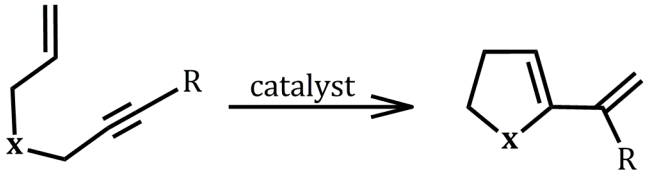

Intramolecular enyne metathesis

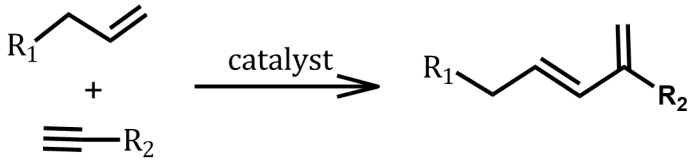

Inter molecular enyne metathesis

Scheme 1.7 Representation of intra- and intermolecular enyne metathesis.

The mechanism of enyne metathesis catalyzed by metal-carbene is parallel to that of alkene metathesis, and a metallacyclobutene is formed as an intermediate in the course of the reaction. The reaction can be initiated either by the coordination of a

triple bond (alkyne first mechanism or yne-then-ene mechanism) or by the coordination of alkene (alkene first or ene-then-yne mechanism) (Scheme 1.8). The mechanism highly depends on the type of reaction *viz.* inter- or intramolecular, reaction condition, and substrates. Experimental and theoretical studies on the reaction mechanism suggest the formation of an η^3 vinyl carbene complex instead of a metallacyclobutene intermediate.[123-125]

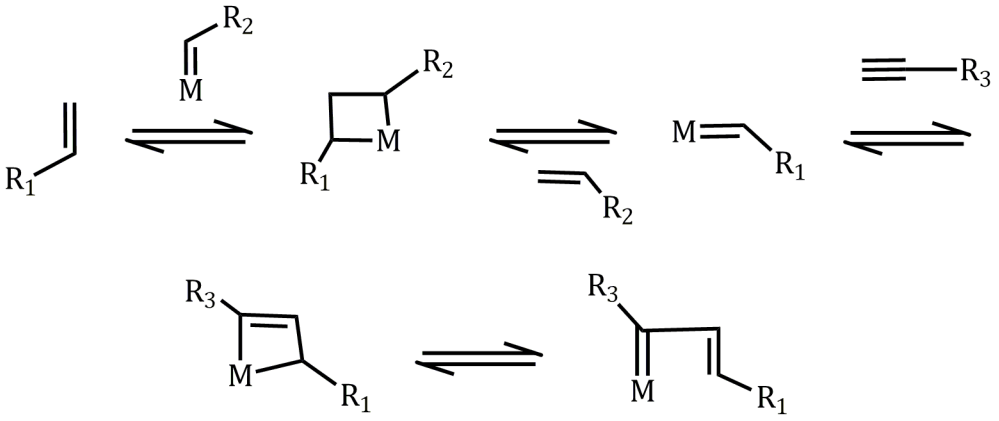

Alkene first mechanism

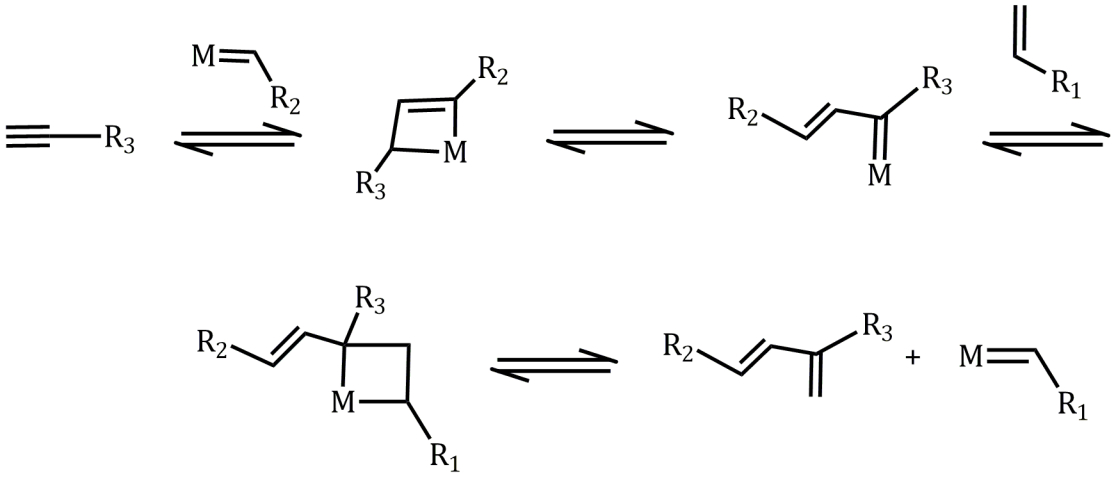

Alkyne first mechanism

Scheme 1.8 Probable mechanisms of enyne metathesis.

1.1.4 Applications of Metathesis Reactions

Development of stable active catalysts (Grubbs type and Schrock type) enabled the profound application of metathesis in a wide range of fields, including petrochemicals, pharmaceuticals, and materials. The metathesis catalysts are readily available in the market. Main advantages of metathesis method over other synthetic techniques are (i) the reaction occurs at or near room temperature (ii) less amount of waste or byproducts, often the byproducts are volatile substances such as ethylene or acetylene, and (iii) can be used for the conversion of highly functionalized or strained alkenes as the catalysts are highly selective for double bonds.

Various types of metathesis reactions such as CM, RCM, RCAM, CAM, enyne metathesis, can be applied for the construction of novel molecular architectures which are otherwise difficult to synthesize. RCM is found to be an important method for the production of macrocycles and is widely applied in the total synthesis.[126] The metathesis polymerization techniques such as ADMET and ROMP are used for the synthesis of polymer structures which are else difficult to synthesize. Alkyne metathesis is used as a general solution to nonselectivity of alkene metathesis, as the hydrogenation of the alkyne products to *Z*-alkene is a straightforward reaction. Also, reduction of the isolated alkyne to the *E*-alkene is achieved by ruthenium mediated hydrosilylation followed by protodesilylation.[127]

Metathesis reaction often found application in the industry for development of various polymers and materials. Materia, the company which holds the right for Grubbs catalysis is applying various metathesis techniques for the large-scale production of a variety of products such as resins. Recently this company traded pheromones synthesized based on olefin metathesis based techniques which in fact offered the cheaper root of synthesis. The CM reaction is applied in the industrial production of various alkenes especially in the petrochemical industries where a large amount of alkenes are produced. For example, propylene, an excellent raw material for a wide variety of products is manufactured by the CM of butene and ethane. Metathesis techniques are applied in the oleochemical industries for the production of various molecules such as civetone.

1.1.5 Metallacycle Intermediates

Chauvin mechanism of alkene metathesis and Katz mechanism of alkyne metathesis propose a metallacycle intermediate in the reaction pathway. A metallacyclobutane (MCB) is formed in the course of alkene metathesis, while a metallacyclobutadiene (MCBD) is formed in alkyne metathesis (Scheme 1.9). The metallacycles of Grubbs complexes are never isolated while those of Schrock systems are isolated and characterized using crystallographic techniques.

i ii

Scheme 1.9 Representation of metallacycles of (i) alkene and (ii) alkyne metathesis (Substituents on carbon are omitted for clarity).

In the early development of metathesis mechanism, the metallacycle was speculated as a transition state, whereas later theoretical studies[33] and some experimental studies have confirmed it as an intermediate. In 2004, Romero and Piers[128] based on ^{1}H and ^{13}C NMR analysis gave convincing evidence for the existence of 14-electron ruthenacyclobutane as an observable intermediate in Grubbs second generation (N-heterocyclic carbene (NHC)-stabilized) catalysts. Adlhart *et al.*[30] and Cavallo[32] provided theoretical explanation for the formation of ruthenacyclobutane in Grubbs olefin metathesis. Formation of MCB suggests the conversion of MC and CC double bonds to the corresponding single bonds along with the formation of a new CC bond. To be precise, a CC double bond is activated to a single bond during the metallacycle formation. In the subsequent step of cycloreversion, one MC and one CC single bonds of the metallacycle are cleaved. Literature shows that the activation barrier for cycloreversion is 5-10 kcal/mol for Grubbs and Schrock olefin metathesis which is the most noteworthy feature of the mechanism as this value is astonishingly

low for the cleavage of a CC single bond.[32, 129-135] Such a low barrier for CC bond cleavage can be justified only if the strength of the CC bonds in MCB is largely deteriorated from a typical CC single bond. On examination of the reported MCB structures of olefin metathesis in the literature for Ru, Ti, Nb, W, Mo and Ta, one could easily identify that the CC bonds of the metallacycles are weak as they show significant elongation (~1.60 Å) compared to a normal CC single bond, (~1.52 Å).[130, 136] The substantial activation of CC bonds in the metallacycles explains the low activation barrier for the metathesis reaction. The X-ray structure determination of Grubbs metallacycle intermediate is never reported in the literature whereas, in the case of Schrock catalyst, several stable tungstenacyclobutanes have been reported. It is also known that depending on the ligand environment and metal centers, the metallacycle can form either trigonal-bipyramidal (TBP) geometry or a square pyramidal (SP) geometry.[137-142] Experimental and theoretical studies on these tungstenacyclobutane isomers[50, 132-133, 138, 141-147] revealed that C_β of the TBP isomer is different from a typical sp^3 carbon center as it shows single bond-like metal-C_β distance.

Suresh and Koga interpreted the C-C bond weakening in MCB in terms of unusual orbital interactions in the metallacycle intermediates of Grubbs first and second generation catalysts.[148] Suresh and Baik using detailed molecular orbital interaction diagrams confirmed that both CC-σ bonds of the metallacycle simultaneously interact with the highly electron deficient metal center.[130] Such an interaction was named as α,β-CCC agostic interaction. The α,β-CCC agostic interaction is found to be a common feature in many metallacycle intermediates of metathesis reaction with metal centers Ru, Ti, Nb, W, Ta, Zr, Hf, V, Cr, Mo[136] and it provided substantial values for the bond order between metal and the β-carbon which explained the significantly short metal-C_β distance. Suresh proposed that the α,β -CCC agostic interaction can be considered as a π orbital formed between the electron deficient metal and the carbon which has no σ bond connectivity with the metal.[136] Suresh and Baik used an arrow to represent the agostic bonding in the metallacycle structure (Figure 1.3).[130]

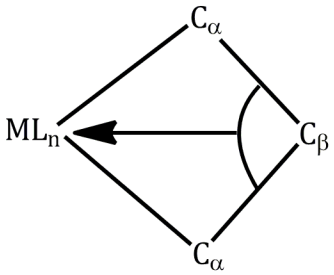

(i)

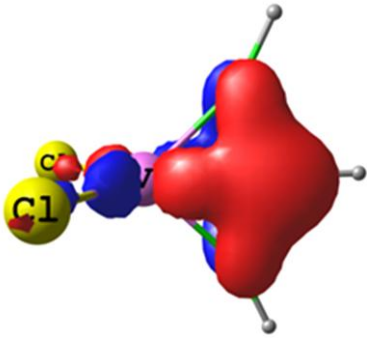

(ii)

Figure 1.3 (i) Representation of the α,β,-CCC agostic interaction in the metallacyclobutane. The agostic bond is indicated in the structure with an arrow.[130] (ii) d_π–p_π orbital interaction between the metal center and C_β in the metallacyclobutadiene.[149]

Brookhart and Green introduced the concept of agostic bonding in organometallic chemistry by describing the bonding interactions between C-H σ-bonds and d orbital on transition metals.[150] Agostic interactions refer to the covalent intra-molecular interactions of an electron deficient metal with a σ-bond which is in close geometrical proximity to the metal atom.[151-152] The strength of such interactions depends on the metal (its position in the periodic table, electron deficiency, and oxidation state), type of bonds, the distance between the σ-bond and the metal center, etc. The classic case of C–H agostic bonding is now considered as a general phenomenon in organometallic chemistry. Further, many more agostic systems have been proposed which contain Si-H, B-H, C-C and Si-C σ-bonds coordinated to a range of metal atoms.[153-154] Agostic bonding interaction results in partial removal of electron density from the concerned bond, leading to the weakening of that bond and thus acts as an important component in many catalytic bond breaking processes. Donation of σ-electron density from an otherwise inert C–H bond to an electron-deficient metal center is found to be the key to CH bond activation in many reactions.[150, 155] Similar to C-H bonds, C–C bonds also show metal induced polarization as their bond energies are ~10 kcal/mol lower than those of typical C–H bonds and thus qualify as good candidates for agostic type bonding with the metals (Scheme 1.10). C–C--M interactions have been proposed as

intermediates or transition states in C–C cleavage reactions mediated by transition metals. C–C bond activation by transition metal complexes generally involves CC bonds, which are intrinsically strained, or they are held in close proximity to the metal centre.[148, 156-160]

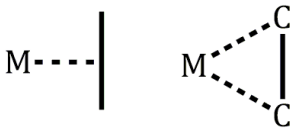

Scheme 1.10 Representations of C-C---M agostic interaction.

The metallacyclobutadiene (MCBD) of alkyne metathesis are quite stable intermediates and are characterized both experimentally and theoretically. A characteristic feature of these MCBD is the short across the ring metal C bond length, which is ~2.20 Å for tungsten complexes. This is quite unusual as this WC_β distance is comparable with the WC_α bond length, which is found to be ~2.00 Å in the tungstenacyclobutadienes. The unusual bonding in MCBD has extensively studied by Suresh and Frenking in a series of scientific papers.[149, 161-162] They suggest a direct 1,3 metal β-carbon bonding interaction is present in these metallacycles with the help of computational techniques. They explained the direct 1,3-MC bond by defining d_π–p_π orbital interaction between the metal center and C_β (Figure 1.3).

It is now an undisputed fact that metallacycle is the key intermediate in metathesis reaction and play a major role in deciding the regio- and stereochemical outcome of the reaction. Hence a complete understanding of the structural and electronic properties of metallacycle is important to fully unravel the beauty of metathesis, and computational chemistry tools can play an important role in this.

Part B: Theoretical Concepts and Computational Methodology

1.2 An Overview of Computational Chemistry

The studies presented in this thesis come under the domain of computational chemistry. Two important theories which form the foundation for computational chemistry are classical mechanics (based Newton's equation of motion) and quantum mechanics (based on Schrödinger equation). The important computational methods are molecular mechanics (MM), semiempirical quantum chemical methods, density functional theory (DFT) methods, *ab initio* quantum chemical methods, molecular dynamics (MD), Monte-Carlo (MC) simulations and hybrid quantum mechanics/molecular mechanics (QM/MM) methods which are developed based on different theories and approximations in the classical and quantum mechanical domains. Depending on the sophistication of the theoretical approach, computational chemistry methods range from highly accurate to very approximate which can be applied to systems with hundreds of atoms to thousands of atoms. Such methods implemented on powerful computer systems enable the modeling and simulation of complex chemical systems and provide an in-depth understanding of the electronic and structural properties of molecular systems.[163] Taking advantage of the incredible progress in the speed and capacities of computers; computational chemistry has grown as an essential tool in chemistry like any other experimental technique. It has become an indispensable tool in many aspects of chemistry such as structure prediction and elucidation, predicting reactions and mechanisms, drug designing, protein folding, designing of functional material. The interplay of computation and experiment is important as it will be helpful in doing chemistry as both complements each other.[164]

1.2.1 *Ab initio* Quantum Chemical Methods

All quantum chemical methods describe the electronic structure of matter in terms of time-independent Schrödinger equation which can be written in its simple form as

$$H\Psi = E\Psi \qquad \text{(Eq. 1.2)}$$

where H is the Hamiltonian operator, Ψ is the N-body wave function and E is the energy eigenvalue of the system. The Hamiltonian for a system containing N electrons and M nuclei can be written as,

$$H = -\sum_{i=1}^{N}\frac{1}{2}\nabla_{i}^{2} - \sum_{A=1}^{M}\frac{1}{2M_A}\nabla_{A}^{2} - \sum_{i=1}^{N}\sum_{A=1}^{M}\frac{Z_A}{r_{iA}} + \sum_{i=1}^{N}\sum_{j>i}^{N}\frac{1}{r_{ij}} + \sum_{A=1}^{N}\sum_{B>1}^{M}\frac{Z_A Z_B}{R_{AB}} \qquad \text{(Eq. 1.3)}$$

In (Eq. 1.3), first two terms represent the kinetic energy (KE) operator of electrons and nuclei respectively. The third term represents coulombic attraction between the electrons and nuclei. The fourth and fifth term represents the repulsion between electrons and between nuclei respectively. M_A is the ratio of the mass of the nucleus A to the mass of an electron, r_{ij} is the distance between the ith and jth electrons and R_{AB} is the distance between Ath and Bth nuclei.

An approximation has been proposed by Born and Oppenheimer to solve the complex Schrödinger equation given in (Eq. 1.3).[165] According to Born Oppenheimer (BO) approximation, the nuclear and electronic motions take place at different time scales, such that the electrons in a molecule are moving in the field of static nuclei. With this approximation, the second term (KE of nuclei) in (Eq. 1.3) becomes zero, and the last term (repulsion between the nuclei) becomes a constant. The remaining part of the electronic Hamiltonian can be written as,

$$H_{elec} = -\sum_{i=1}^{N}\frac{1}{2}\nabla_{i}^{2} - \sum_{i=1}^{N}\sum_{A=1}^{M}\frac{Z_A}{r_{iA}} + \sum_{i=1}^{N}\sum_{j>i}^{N}\frac{1}{r_{ij}} \qquad \text{(Eq. 1.4)}$$

The Schrödinger equation corresponding to the electronic Hamiltonian is

$$H_{elec}\Phi_{elec}\left(\{\mathbf{r}_i\};\{\mathbf{R}_A\}\right) = E_{elec}\Phi_{elec}\left(\{\mathbf{r}_i\};\{\mathbf{R}_A\}\right) \qquad \text{(Eq. 1.5)}$$

where, $\{\mathbf{r_i}\}$ and $\{\mathbf{R_A}\}$ are the positions of electrons and nuclei, respectively. The electronic wave function describes the motion of electrons and depends explicitly on the electronic coordinates and parametrically on nuclear coordinates. BO approximation made possible the separation of electronic and nuclear Hamiltonians

and their corresponding wave functions as well. Thus the molecular wave function can then be represented as a product of electronic and nuclear counterparts,

$$\Psi\left(\{\mathbf{r}_i\};\{\mathbf{R}_A\}\right)=\Phi_{\text{elec}}\left(\{\mathbf{r}_i\};\{\mathbf{R}_A\}\right)\Phi_{\text{nuc}}\left(\{\mathbf{R}_A\}\right) \qquad \text{(Eq. 1.6)}$$

Once the wave function Ψ is known from the Schrödinger equation, any experimental observable can be computed as the expectation value of appropriate operator. An exact solution to the Schrödinger equation is not easy and hence approximations are needed to get qualitatively correct solutions to the many-body Schrödinger equation.

1.2.1.1 Hartree-Fock Theory

Since it is difficult to solve Schrödinger equation for multi-electron systems, approximations are needed to obtain solutions for Schrödinger equation. The Hartree-Fock method is an important approach towards solving the Schrödinger equation and is the foundation for most of the approximation methods in *ab initio* calculation. This method assumes that each electron's motion can be described by a single-particle function (orbital) which does not depend explicitly on the instantaneous motions of other electrons. That is the total Hamiltonian (*H*) of a many-electron system can be represented as the sum of single electron Hamiltonian (*h*),

$$H=\sum_{i=1}^{N}h(i) \qquad \text{(Eq. 1.7)}$$

Also, the corresponding wave function can be written as the product of individual one electron function called Hartree product (HP),

$$\Psi^{\text{HP}}(\mathbf{x}_1,\mathbf{x}_2,.....,\mathbf{x}_N)=\chi_i(\mathbf{x}_1)\chi_j(\mathbf{x}_2).....\chi_k(\mathbf{x}_N) \qquad \text{(Eq. 1.8)}$$

where χ*'s* are the spin orbitals, and $\mathbf{x_1}$, $\mathbf{x_2}$, etc. represents the combined spatial and spin coordinates of each electron. The problem with the Hartree product function is that the electrons are indistinguishable; that is it does not satisfy the anti-symmetry principle. According to Pauli's exclusion principle, no two electrons of an atom shall have identical value of all the four quantum numbers *viz.* n, l, m, and s.[166] Anti-symmetrization is achieved by arranging the one electron spin-orbital in a determinant form called Slater

determinant.[167-168] Slater determinant for an N-electron wave function can be written as,

$$\Psi(\mathbf{x_1},\mathbf{x_2},....,\mathbf{x_N}) = \frac{1}{\sqrt{N!}}\begin{vmatrix} \chi_i(\mathbf{x_1}) & \chi_j(\mathbf{x_1}) & ..... & \chi_N(\mathbf{x_1}) \\ \chi_i(\mathbf{x_2}) & \chi_j(\mathbf{x_2}) & ..... & \chi_N(\mathbf{x_2}) \\ ... & ... & ..... & ... \\ \chi_i(\mathbf{x_N}) & \chi_j(\mathbf{x_N}) & ..... & \chi_N(\mathbf{x_N}) \end{vmatrix} \quad \text{(Eq. 1.9)}$$

where $\frac{1}{\sqrt{N!}}$ is a normalization factor.

In (Eq. 1.9), interchange of two electrons will result in the interchange of two rows of the determinant which will alter the sign of the determinant thus satisfying the condition of anti-symmetry. Also, all the electrons are indistinguishable as two electrons occupying the same spin-orbital will result in two columns being equal, which will make the determinant equal to zero. Slater determinant in shorter notation can be represented as

$$\Psi\left(\mathbf{x_1},\mathbf{x_2}.....\mathbf{x_N}\right) = \left| \chi_i\chi_j.....\chi_N \right\rangle \quad \text{(Eq. 1.10)}$$

According to the variational principle, the best wave function is the one giving lowest energy and can be calculated as an expectation value of the Hamiltonian over this approximate wave function. With the increase in the basis set size, the energy goes on decreasing, until a limit, called the Hartree-Fock limit is attained. The best approximate wave function Ψ_0, is obtained by varying all the wave function parameters so that the energy expectation value is a minimum (E_o), as shown in (Eq. 1.11).

$$E_0 = \left\langle \Psi_0 \middle| H \middle| \Psi_0 \right\rangle \quad \text{(Eq. 1.11)}$$

This minimization procedure leads to an eigenvalue equation called Hartree-Fock equations for individual spin-orbital $\mathbf{x_i}$.

$$f(i)\chi(\mathbf{x}i) = \varepsilon\chi(\mathbf{x}i) \quad \text{(Eq. 1.12)}$$

where *f(i)* is a one-electron operator called the Fock operator, which has the form,

$$f(i) = -\frac{1}{2}\nabla_i^2 - \sum_{A=1}^{M}\frac{Z_A}{r_{iA}} + V^{HF}(i) \quad \text{(Eq. 1.13)}$$

where $V^{HF}(i)$ is the Hartree-Fock potential and is defined as the average potential seen by the i^{th} electron due to the remaining electrons. That is, the complicated many-

electron problem is replaced by a one-electron problem where the electronic interaction is treated in an average way. The HF potential of a particular electron $V^{HF}(i)$ depends on the spin orbitals of the remaining electrons. The HF potential for the electron (1) can be defined as,

$$V^{HF}(1) = \sum_{j}^{N} \left(J_j(1) - K_j(1) \right) \qquad \text{(Eq. 1.14)}$$

where J_j is the Coulomb operator which accounts for the Coulombic repulsion between the electrons and K_j is the exchange operator which represents the quantum correlation due to the Pauli exclusion principle.

$$J_j(1) = \int d\mathbf{x_2} \left| \chi_j(2) \right|^2 \frac{1}{r_{12}} \qquad \text{(Eq. 1.15)}$$

$$K_j(1)\chi_i(1) = \left[\int d\mathbf{x_2} \chi_j(2) \frac{1}{r_{12}} \chi_i(2) \right] \chi_j(1) \qquad \text{(Eq. 1.16)}$$

For closed shell systems, HF equations were proposed by Roothaan and Hall.[169-170] The HF equation in (Eq. 1.12) may be rewritten by substituting (Eq. 1.17), where the spin-orbital is expressed as the linear combination of basis functions (Φ_μ) and leads to (Eq. 1.18).

$$\Psi_i = \sum_{\mu=1}^{K} C_{\mu i} \varphi_\mu \qquad \text{i = 1, 2,....., K} \qquad \text{(Eq. 1.17)}$$

where $C_{\mu i}$ are the coefficients of Φ_μ, and K is the total number of basis functions.

The Roothan-Hall equation developed for closed shell systems are also called restricted Hartree-Fock theory (RHF) and can be written in a single matrix form as

$$\mathbf{FC=SC}\varepsilon \qquad \text{(Eq. 1.18)}$$

where ε are orbital energies, **S** is the overlap matrix, and **F** is the Fock matrix which is the matrix representation of the Fock operator in (Eq. 1.13) in the basis function Φ_μ. Diagonalization of Fock matrix yields the unknown molecular orbital coefficients in order to determine the eigenvalues from Roothaan Hall equation.

The HF equation is a non-linear equation and can be solved iteratively using a method called self-consistent field (SCF) method in which a trial set of spin orbitals are guessed and used to construct the Fock operator. First, the average potential $V^{HF}(i)$

calculated from the initial guess spin-orbital is used to solve eigenvalue equation given in (Eq. 1.13) for a new set of orbitals. These new sets of spin orbitals are used to generate a new field, and the procedure of calculation and reformulation are continued until the self-consistency is reached, which means the fields do not change and the spin orbitals used to build the Fock operator remains same as its eigenfunctions. HF equation (Eq. 1.12) gives a set of orthonormal spin orbitals $\{\chi_K\}$ along with their orbital energies $\{\varepsilon_K\}$). Among these N lowest energy orbitals will be occupied and the rest will be unoccupied or virtual orbitals.

1.2.1.2 Post-Hartree-Fock Methods

The main problem with the HF approximation is that it ignores all electron correlation except exchange interaction. The approaches which try to include the electron correlation to HF theory are known as post-HF methods. Configuration interaction (CI),[171] multi-configurational self-consistent field (MCSCF), Møller-Plesset perturbation theory (MPn, where n is the order of correlation), coupled cluster theory[172] etc., are examples of post HF methods. The post HF methods try to calculate the correlation energy as the difference between the exact *ab initio* energy and exact (complete basis) HF energy.

1.2.1.2.1 Configuration Interaction Method

Configuration interaction methods are one of the popular methods to solve many electron problems and include excited states to describe the electronic state. In CI, the HF wave function is used as the reference determinant and the energy is minimized variationally with respect to the determinant expansion coefficients and the wave function is written as a linear combination of Slater determinants with all the permutations of electron occupancies. In general, CI wave function can be written as,

$$\left|\Phi_0\right\rangle = c_0\left|\Psi_0\right\rangle + \sum_{ar} c_a^r\left|\Psi_a^r\right\rangle + \sum_{\substack{a<b\\r<s}} c_{ab}^{rs}\left|\Psi_{ab}^{rs}\right\rangle + \sum_{\substack{a<b<c\\r<s<t}} c_{abc}^{rst}\left|\Psi_{abc}^{rst}\right\rangle + ... \qquad \text{(Eq. 1.19)}$$

The first term in Eq. (1.19) represents the Slater determinant corresponding to the HF wave function and rest of the terms constitute singly, doubly, triply, etc. excited determinants with appropriate expansion coefficients. The indices *a, b*, etc. signify the occupied orbitals and *r, s*, etc. signify the virtual orbitals involved in the electron

excitations. The CI methods are classified according to the number of excitations made to construct each new determinant.[173-174] If only one electron has been moved from each determinant, it is called a configuration interaction single-excitation (CIS) calculation. CIS calculations give an approximation to the excited states of the molecule, but do not change the ground-state energy. Single and double excitation (CISD) calculations yield ground-state energy that has been corrected for correlation. Triple-excitation (CISDT) and quadruple-excitation (CISDTQ) calculations are done only when very-high-accuracy results are desired. Full CI calculation describes all possible excitation and yield a very accurate quantum mechanical result but requires an immense amount of computational resources.[175-176]

1.2.1.2.2 Multi-Configurational Self-Consistent Field (MCSCF)

MCSCF uses multiple determinants and gives a most accurate result for a given CPU time. The user should determine the molecular orbital to be used in the calculation, and there should be a correlation between the bonding and anti-bonding orbitals.[177] A complete active space self-consistent field (CASSCF) calculation is an MCSCF calculation in which all combinations of the active space orbitals are included. This calculation gives the maximum correlation in the valence region. A multi-reference-configuration interaction (MRCI) method uses an MCSCF wave function instead of an HF wave function as a starting point of CI calculation. Though this methodology provides accurate results, it is costly in terms of computational power utilized.[175, 178]

1.2.1.2.3 Coupled Cluster Theory

Coupled cluster (CC) is a more advanced method than CI in treating multi-electron system.[179-181] CC is a more mathematically refined method for calculating the electron correlation, and the total wave function is a linear combination of several determinants similar to CI. But the method for choosing the wave function is different and more complex than that of CI. The various orders of CC expansion are CCSD, CCSDT, etc. Coupled cluster calculations are size extensive but not variational. By including many excitation terms in the expansion, CC methods are computationally very expensive relative to HF calculations.[175-176]

1.2.1.2.4 Møller-Plesset Perturbation Theory

Møller and Plesset proposed a method based on Perturbation theory to tackle the electron correlation problem in HF method and the difference between the exact Hamiltonian, and the Fock operator is considered as a perturbation.[182-183] First order perturbation is HF itself and second-order perturbation method (MP2), adds a minimal amount of correlation. The fourth order perturbation method (MP4) is roughly similar to that of a CISD calculation. MPn methods, especially at the MP2, are the most popular way to incorporate electron correlation in molecular quantum mechanical calculations, level. At the same time, Möller-Plesset calculations are restricted to single point calculations at geometry obtained using a lower level of theory as the calculations are computationally intensive.[184-185]

1.2.1.3 Basis Set

A basis set is a set of non-orthogonal one-particle wave functions used for creating molecular orbitals which are expanded as a linear combination with coefficients to be determined. The basis functions are usually centred on the atoms and are sometimes referred as atomic orbitals (AO). In the early days of computational chemistry, Slater-type orbitals (STOs) were used to mimic AOs as it is not possible to locate the AOs for many-electron systems.[186] STO refers to a set of function which has an exponential relation with the radius.[187] The mathematical form of STO is

$$\Phi_{abc}^{STO}(x,y,z) = Nx^a y^b z^c e^{-\zeta r} \qquad \text{(Eq. 1.20)}$$

where N is the normalization constant, *a*, *b*, *c* are the components of angular momentum (L = *a* +*b* + *c*), ζ is the orbital exponent which determines the width or spread of the orbital and x, y, z represent the cartesian coordinates, r is the radius in angstrom. STO type treatment involves tedious calculations and longer time to calculate the integrals. Also, STOs are difficult to analyze especially when the orbitals are centered on different nuclei. Use of standard Gaussian functions centered on atoms (Gaussian type orbitals, GTO) helped in overcoming this difficulty associated with STO.[188-190] A Gaussian function can be written as

$$\Phi_{abc}^{GTO}(x,y,z) = Nx^a y^b z^c e^{-\zeta r^2} \qquad \text{(Eq. 1.21)}$$

The advantage of the GTO over STO is because of Gaussian product theorem which says the product of two GTOs is also a Gaussian function centered at the weighted midpoint of the two functions.[191-192] It is a common practice to bunch together a set of primitive GTO described in (Eq. 1.21) to form a Gaussian function also called contracted GTO (CGTO) to represent the AO as

$$\Phi_{abc}^{CGTO}(x,y,z) = N\sum_{i}^{n} c_i \, x^a y^b z^c e^{-\zeta_i r^2} \qquad \text{(Eq. 1.22)}$$

where n is number of Gaussians needed to mimic an STO and c_i represents coefficients. Number of CGTOs used to describe an atomic orbital decides the complexity and accuracy of a basis set.[193-195]

There are many variations of Gaussian basis sets and a single zeta basis set is the simplest among all. In a single zeta basis set also known as minimal basis set, each AO is represented using one basis function. STO-3G is the most popular single zeta basis set which is formed by a linear combination of three contracted functions for each basis function.[196-197] Furthermore accurate basis sets are formed by describing the AOs with two (double zeta) three (triple zeta) or more basis functions.[198] Pople and co-workers designed the split-valence basis sets of type 'k-nlmG' where 'k' indicates how many primitive Gaussians are used for representing the core orbitals and 'nlm' indicates both how many functions the valence orbitals are split into and how many primitive Gaussians are used for their representation.[199] The basis set can be further improved by adding additional functions to describe the atomic orbital more accurately. Polarization function can be added to the existing basis sets to define the polarization of electron density of the atom in a molecule and is denoted by adding * or (d) or ** or (d, p) after G in the notation of basis set. These * represent the use of an extra set of d-orbitals on heavy atoms and p-orbitals on hydrogens. Another important addition is the diffuse functions which spread the electron density over the molecule. Diffuse functions are added by + or ++ signs. Diffuse functions are a must for treating anions and electronegative atoms.[200] A three dimensional periodic system can be better described by a plane wave basis set than with a localized basis functions.[201]

For heavier atoms such as transition metals with large inner core, number of basis functions needed to describe the system is high. Since only the valence electrons

are involved in the bonding, the core electrons can be replaced by a potential which fit to all-electron calculations called Effective core potentials (ECPs).[202-204] ECP treatment on the core electrons gives good results at a fraction of the cost needed for a calculation involving all electrons. For a large core ECP, all orbitals except (n+1)s, (n+1)p and nd orbitals are treated as core electrons. Such a treatment usually gives a good geometry for the molecule but the energetics are often found to be approximate. This can be rectified by using a small core ECP where the ns, np, nd and (n+1)s forms the valence orbitals. Such a treatment often increases the computational cost.

Today most widely used basis sets are those developed by the groups of Pople,[205] Dunning,[206-207] and Ahlrichs.[208-209] Computational work discussed in this thesis are carried out using a variety of basis sets. Pople basis sets 6-31G* and 6-31+G** are used to define smaller atoms such as H, C, N, O, P, and Cl, while the metal centers are defined using basis sets along with the corresponding ECP on core electrons. def2-Def2-TZVPP[210] is a much advanced level of basis set developed by Ahlrichs and group and contains a triple zeta basis set with two sets of polarization and is used in this thesis to define Ru and W atoms. We also used Stuttgart-Dresden (SDD) effective core potential for the 28 core electrons and the associated double-zeta basis set for the 16 valence electrons to describe Ru center.[211] LANL2DZ developed by Los Alamos National Laboratory (LANL) is a commonly used basis set for defining transition metals which is also used in this thesis to define the metal center.[212]

1.2.2 Molecular Mechanics

Molecular mechanics (MM) also known as force field methods use the classical laws of physics to predict the structure and energy of a molecule ignoring the electronic motion. In MM methodology the molecule is considered as a bunch of balls (atoms) connected through springs (chemical bonds). MM methods can handle macromolecular systems containing thousands of atoms such as DNA, proteins, enzymes and the calculations are quite inexpensive. Molecular mechanics calculate energy (E) based on the geometry or conformation of a molecule and it can be written as an algebraic sum of stretching energy (E_{str}), bending energy (E_{bend}), torsion energy (E_{tor}), non-bonded

interaction energies such as van der Waals energy (E_{vdw}), and electrostatic energy (E_{elec}),

$$E = E_{str} + E_{bend} + E_{tor} + E_{vdw} + E_{elec} \quad \text{(Eq. 1.23)}$$

In molecular mechanics, potential energy is calculated using force field instead of the wave function. A set of equations with their associated constants is called a force field. The constants are obtained either from *ab initio* calculations or experimental data. Transferability of a parameter is the foundation of the force field methods; which means the features (energy, bond length, molecular motion, etc.) associated with a group or atom types such as C-H bond or sp^3 carbon is same in all molecules. This assumption, in fact, simplifies the molecular mechanics and success of a force field depends on the energy expression, data used for parameterization, and the experience and ability of the user with the strengths and weaknesses of each method. Force fields differ in the number of terms in the energy expression, the complexity of the terms used, and the way in which the constants were obtained. Most of the software packages for MM methods are built in with specific force fields. MM2, MM3, and Merck (MMFF) force fields are found to perform well for a wide range of organic molecules.[213-214] For protein and nucleic acid studies, force fields such as AMBER (Assisted model building with energy refinement) and CHARMM (Chemistry at Harvard macromolecular mechanics) are used.[215-216] Customization is required for the molecular mechanics studies of inorganic molecules. MOMEC is a widely used force field for the transition metal coordination complex.[217] UFF (Universal force field) is a full periodic table force field method and is used for studying systems containing inorganic elements.[218] CHEAT (carbohydrate hydroxyls represented by external atoms) and EFF (Empirical force field) are force fields developed for modeling carbohydrates.[219] GROMOS (Groningen molecular simulation) are used to predict the dynamical motion of molecules and bulk liquids, and modeling of biomolecules.[175]

1.2.3 Semiempirical Methods

Semiempirical methods are based on quantum mechanics but use many approximations based on empirical data. In these methods, the core electrons are treated with the nucleus and some expensive two-electron integral calculations are omitted. In order to

correct this omissions, the method is parameterized by adding data from empirical or *ab initio* calculations.[220] These are much faster than *ab initio* methods but the results are less accurate. In general, such methods provide more accurate results than MM methods at a higher computational cost.

Depending on the type of approximations and empirical data used, a variety of semiempirical methods are available for different types of molecules in software packages. The π electron method of Hückel and extended Hückel theory of Hoffmann are the early approximation in semiempirical quantum chemistry. [221] The PPP (Pariser-Parr-Pople) method is another variation of the Hückel method.[222] All these early approximations are restricted on the π electrons. Pople proposed all valance electron MO methods (CNDO, complete neglect of differential overlap; INDO, intermediate neglect of differential overlap; NDDO, neglect of diatomic differential overlap) which are parameterized to produce *ab initio* Hartree-Fock results with a minimal basis set. A different parameterization technique using experimental values is used for analyzing the ground state potential energy surface of organic molecules. MINDO, AM1, PMx are the prominent examples of this class developed after extensive parameterization.[224] PM6 and PM7 methods essentially cover the whole periodic table and are used for the calculation of molecular solid state properties.[225-226]

1.2.4 Density Functional Theory

The main drawback of a wave function method is the 3N level dependence of wave function with the number of electron (N). As the number of electron increases, the wave function becomes too complicated to work with. In DFT, the system is defined *via* its density $\rho(\mathbf{r})$ which is a function of its many body wave function and the dependence is reduced to 3 spatial coordinates (or four, if the spin is included) regardless the value of N. This enables the application of DFT on systems with hundreds or even thousands of atoms. Also, electron density, when integrated over all space, gives the total number of electrons, N. ie.,

$$N = \int \rho(\mathbf{r}) d\mathbf{r} \qquad \text{(Eq. 1.24)}$$

According to the DFT formalism, the electronic energy is a functional of electron density, or in other words, there exists a one-to-one correspondence between the electron density and its energy.

1.2.4.1 Thomas-Fermi Model

The idea of expressing the energy of a system as a function of the total electron density introduced by Thomas and Fermi is often viewed as a precursor of DFT formalism.[227-228] Thomas and Fermi derived a kinetic energy expression based on uniform electron gas where electron-nucleus and electron-electron interactions are treated classically. That is, kinetic energy of the electron gas, T_{TF} which exclusively depends on the electron density $\rho(r)$ can be written as

$$T_{TF}[\rho(\mathbf{r})] = \frac{3}{10}(3\pi^2)^{2/3}\int \rho(\mathbf{r})^{5/3} d\mathbf{r} \qquad \text{(Eq. 1.25)}$$

Although the Thomas-Fermi model was the first step in the development of DFT, it is not accurate enough to be chemically useful.

1.2.4.2 Hohenberg-Kohn Theorems

Hohenberg and Kohn proposed and formulated two theorems which established DFT as a rigorous quantum chemical methodology.[223] In their landmark paper Hohenberg and Kohn stated that (i) external potential (V_{ext}) and the total energy (E) is a functional of electron density $\rho(r)$ and (ii) the ground state energy can be obtained variationally: the density that minimizes the total energy is the exact ground state density. A straightforward consequence of the Hohenberg-Kohn theorem is that the ground state energy E is uniquely determined by the ground-state charge density. The energy functional can be written as a sum of two terms,

$$E[\rho(\mathbf{r})] = \int V_{ext}(\mathbf{r})\rho(\mathbf{r})d\mathbf{r} + F[\rho(\mathbf{r})] \qquad \text{(Eq. 1.26)}$$

where the first term arises from the interaction of the electrons with an external potential $V_{ext}(\mathbf{r})$. $F[\rho(\mathbf{r})]$ is the sum of the kinetic energy of the electrons and the contribution from the inter-electronic interactions. The minimum value in the energy corresponds to the exact ground-state electron density, enabling a variational approach to be used. The DFT equivalent of the Schrödinger equation may be written as,

$$\left(\frac{\delta E[\rho(\mathbf{r})]}{\delta\rho(\mathbf{r})}\right)_{V_{\text{ext}}} = \mu \qquad \text{(Eq. 1.27)}$$

where μ is a Lagrangian multiplier which can be identified with the chemical potential for the electron for its nuclei.

Although the Hohenberg-Kohn theorems are extremely powerful, they do not offer a way of computing the ground-state density of a system in practice. Later Kohn and Sham devised a simple method for carrying out DFT calculations, that retains the exact nature of DFT.[229]

1.2.4.3 Kohn-Sham Equations

Kohn and Sham proposed a practical way to solve the Hohenberg-Kohn theorem for a set of interacting electrons and showed that $E[\rho(\mathbf{r})]$ should be approximated as the sum of three terms,

$$E[\rho(\mathbf{r})] = E_{\text{KE}}[\rho(\mathbf{r})] + E_{\text{H}}[\rho(\mathbf{r})] + E_{\text{XC}}[\rho(\mathbf{r})] \qquad \text{(Eq. 1.28)}$$

where $E_{\text{KE}}[\rho(\mathbf{r})]$ is the kinetic energy of non-interacting electrons, $E_{\text{H}}[\rho(\mathbf{r})]$ is the Hartree electrostatic energy of the electrons, and $E_{\text{XC}}[\rho(\mathbf{r})]$ is contributions of exchange and correlation to energy. The first term, $E_{\text{KE}}[\rho(\mathbf{r})]$, is defined as the kinetic energy of a system of non-interacting electrons with the same density $\rho(\mathbf{r})$ as the real system,

$$E_{\text{KE}}[\rho(\mathbf{r})] = \sum_{i=1}^{N}\int \Psi_{\text{i}}(\mathbf{r})\left(-\frac{\nabla^2}{2}\right)\Psi_{\text{i}}(\mathbf{r})\mathrm{d}\mathbf{r} \qquad \text{(Eq. 1.29)}$$

$$\text{Hartree electrostatic energy, } E_{\text{H}}[\rho(\mathbf{r})] = \frac{1}{2}\iint \frac{\rho(\mathbf{r}_1)\rho(\mathbf{r}_2)}{|\mathbf{r}_1 - \mathbf{r}_2|}\mathrm{d}\mathbf{r}_1\mathrm{d}\mathbf{r}_2 \qquad \text{(Eq. 1.30)}$$

The total energy of an N-electron system within the Kohn-Sham scheme can be written as

$$E[\rho(\mathbf{r})] = \sum_{i=1}^{N}\int \Psi_{\text{i}}(\mathbf{r})\left(-\frac{\nabla^2}{2}\right)\Psi_{\text{i}}(\mathbf{r})\mathrm{d}\mathbf{r} + \frac{1}{2}\iint \frac{\rho(\mathbf{r}_1)\rho(\mathbf{r}_2)}{|\mathbf{r}_1 - \mathbf{r}_2|}\mathrm{d}\mathbf{r}_1\mathrm{d}\mathbf{r}_2 + E_{\text{XC}}[\rho(\mathbf{r})] - \sum_{A=1}^{M}\int \frac{Z_A}{r - R_A}\rho(\mathbf{r})\mathrm{d}\mathbf{r}$$

(Eq. 1.31)

The exchange-correlation energy term contains the difference between the exact and non-interacting kinetic energies along with the contribution due to exchange and correlation.

Kohn and Sham proposed that electron density of an N electron system can be written as the sum of the square moduli of N one-electron orbitals,

$$\rho(\mathbf{r}) = \sum_{i=1}^{N} \left|\Psi_i(\mathbf{r})\right|^2 \qquad \text{(Eq. 1.32)}$$

Using this expression for electron density and applying the appropriate variational condition the functional in terms of, the one-electron Kohn-Sham equation takes the form,

$$\left\{ -\frac{\nabla_1^2}{2} - \left(\sum_{A=1}^{M} \frac{Z_A}{r_{1A}} \right) + \frac{\rho(\mathbf{r_2})}{r_{12}} \mathrm{d}\mathbf{r}_2 + V_{\mathrm{XC}}\left[\mathbf{r_1}\right] \right\} \Psi_i(\mathbf{r}_1) = \varepsilon_i \Psi_i(\mathbf{r}_1) \qquad \text{(Eq. 1.33)}$$

where ε_i are the orbital energies, and V_{XC} is the exchange-correlation functional which is related to the exchange-correlation energy by,

$$V_{\mathrm{XC}}[\mathbf{r}] = \frac{\delta E_{\mathrm{XC}}[\rho(\mathbf{r})]}{\delta \rho(\mathbf{r})} \qquad \text{(Eq. 1.34)}$$

The exchange-correlation potential describes the effects of the Pauli principle and the Coulomb potential beyond a pure electrostatic interaction of the electrons. The exchange-correlation energy, E_{XC} is generally divided into two terms, an exchange term E_X (associated with the interaction of electrons of the same spin) and a correlation term E_C (associated with the interaction of electrons of opposite spin). The corresponding functionals are exchange functional and correlation functional, respectively,

$$E_{\mathrm{XC}}[\rho(\mathbf{r})] = E_{\mathrm{X}}[\rho(\mathbf{r})] + E_{\mathrm{C}}[\rho(\mathbf{r})] \qquad \text{(Eq. 1.35)}$$

Though the KS method gives a good description of the ground state properties, practical applications of DFT are often based on approximations for the exchange-correlation potential such as (i) Local density approximation (LDA) (ii) Generalized gradient approximation (GGA) (iii) meta-GGA and, (iv) Hybrid functionals.

LDA is the simplest approximation for the exchange-correlation functional and is the basis for all approximate exchange-correlation functionals.[230-231] In LDA, the exchange-correlation energy at any point in space is a function of the electron density at that point and can be given by the electron density of a homogeneous electron gas of the same density. Within the LDA approach, the exchange function is given by,

$$E_X^{LDA}[\rho(\mathbf{r})] = -\frac{3}{4}\left(\frac{3}{\pi}\right)^{1/3}\int \rho^{4/3}(\mathbf{r})d\mathbf{r} \qquad \text{(Eq. 1.36)}$$

A further modification to the LDA is made by introducing the spin densities to the functional and is called local spin density approximation (LSDA). LSDA approximation proposed by Slater solve many conceptual problems associated with the LDA.[232] The exchange functional in LSDA approach is given by,

$$E_X^{LSDA}[\rho(\mathbf{r})] = -2^{1/3}\left(-\frac{3}{4}\left(\frac{3}{\pi}\right)^{1/3}\right)\int\left(\rho_\alpha^{4/3}(\mathbf{r}) + \rho_\beta^{4/3}(\mathbf{r})\right)d\mathbf{r} \qquad \text{(Eq. 1.37)}$$

where α and β represent spin up and down, respectively.

In generalized gradient approximation methods (GGAs) the exchange-correlation energies depend not only on the density but also on the gradient of the density, $\nabla(\rho)$.[233-234]

$$E_{XC}\left[\rho_\alpha(\mathbf{r}), \rho_\beta(\mathbf{r})\right] \equiv \int \varepsilon_{XC}(\rho_\alpha(\mathbf{r}), \rho_\beta(\mathbf{r}), \vec{\nabla}\rho_\alpha(\mathbf{r}), \vec{\nabla}\rho_\beta(\mathbf{r}))d^3\mathbf{r} \qquad \text{(Eq. 1.38)}$$

Most of the GGA functionals are constructed by adding a correction term to the LDA functionals. The development of GGA methods is based on two main lines; one based on numerical fitting procedures proposed by Becke and a more rational-based one advocated by Perdew. Among the exchange functionals based on this principle are Becke88 (B), Perdew-Wang (PW), modified Perdew-Wang (mPW), Becke86 (B86), Perdew86 (P), Perdew-Burke-Ernzerhof (PBE) and modified Perdew-Burke-Ernzerhof (mPBE). For the correlation functional, several formulations have been developed including Becke88 (B88),[234] Perdew 86,[235] Perdew-Wang 91 (PW91)[236] and Lee-Yang-Par (LYP). Meta-GGA functionals represent further improvement over GGA functionals by adding the Laplacian of the density $\nabla^2(\rho)$.

Hybrid density functionals are an approximation to the exchange-correlation part by combining the exchange-correlation of a conventional GGA method with a percentage of HF exchange. The exact amount of HF exchange is fitted semiempirically from experimental atomization energies, ionization potentials, proton affinities, total atomic energies, and other data, for a representative set of small molecules.[237-238] Examples of hybrid density functionals include B3LYP, B3P86, B3PW91, B97-1, MPWB1K and X3LYP. Hybrid-meta GGA methods represent a new class of density

functionals, based on a similar concept of hybrid functionals, but start from meta-GGAs instead of standard GGAs. These methods depend on Hartree-Fock exchange, the electron density and its gradient and the kinetic energy density. Examples include B1B95, BB1K, MPW1B95 and TPSS1KCIS.

Minnesota functionals are a group of exchange-correlation functional developed by Truhlar and co-workers.[239-243] Most commonly used Minnesota functionals are M06-L, a local functional (no HF exchange);[240] M06, a global-hybrid meta-GGA with 27% of HF exchange, leading to a well-balanced functional for overall good performance for chemistry;[244] M06-2X, a global hybrid meta-GGA with 54% HF exchange, for top-level across-the-board performances in all areas of chemistry including thermochemistry and reaction kinetics, but excluding multi-reference system such as many systems containing transition metals; and M06-HF, a global-hybrid meta-GGA with 100% HF exchange, suitable for calculation of spectroscopic properties of charge-transfer transitions, where elimination of self-interaction error is of paramount importance.[245]

Dispersion corrections can be added to the KS-DFT functionals to define the long-range Van der Waals type interaction in molecules.[246-248] The total energy of the system using dispersion correction is,

$$E_{DFT-D} = E_{KS-DFT} + E_{disp} \qquad \text{(Eq. 1.39)}$$

where $E_{KS\text{-}DFT}$ is the self-consistent Kohn-Sham energy obtained from the chosen density functional, and the dispersion energy is,

$$E_{disp} = -S_6 \sum_{i=1}^{N_{at}-1} \sum_{j=i+1}^{N_{at}} \frac{C_6^{ij}}{R_{ij}^6} f_{dmp}(R_{ij}) \qquad \text{(Eq. 1.40)}$$

where N_{at} is the number of atoms in the system, C_6^{ij} is the dispersion coefficient for atom pair ij. S_6 is a global scaling factor that depends only on the dispersion function used and R_{ij} is the interatomic distance. f_{dmp} is the damping function which must be used to avoid near-singularities for small interatomic distance.

In this thesis, we have used BP86 functional for the structural and spectroscopic analysis of metathesis reaction catalyzed by Grubbs and Schrock type catalysts. BP86 functional is a GGA composed of the Becke 1988 exchange functional and the Perdew 86 correlation functional.[234-235] We also used dispersion corrected BP86 functional for

studying the reaction mechanism catalyzed by Grubbs type catalysts. Suresh and Frenking found that BP86 functional is able to reproduce the experimental structural data in the case of alkene and alkyne metathesis reaction. We also benchmarked our findings using a series of hybrid and Minnesota functionals. All calculations discussed in this thesis (minimizations, single points, vibrational analysis) are carried out using Gaussian 09 (G09) program suite.[249]

1.2.5 Molecular Dynamics and Monte-Carlo Simulations

Simulation techniques use the classical equations of motion to understand the dynamical behavior of gases, liquids, solids, surfaces, and clusters. There are two main kinds of simulations named molecular dynamics (MD), and Monte-Carlo simulation (MC) and the hybrid of these two are used in a wide range. Molecular simulations act as a bridge between theory and experiment. Simulation techniques are useful to understand the reaction which is impossible to conduct such as high temperature and pressure reactions. In molecular dynamics, the forces acting on each molecule are calculated from the molecular positions; which are used to advance the positions and velocities through a small time step, and then the procedure is repeated. That is MD uses a step by step algorithm to solve Newton's equation of motion using a time scale ranging from picoseconds to nanoseconds. MD techniques can be used to get thermodynamic, structural and dynamic features of the molecule. Monte-Carlo simulations, on the other hand, moves molecule randomly in each stage and random numbers are used to decide whether or not to accept the move. The decision depends on how favorable the energy change would be and the procedure is repeated. Both methods employ system sizes from a few hundred to a few million molecules.

Ab initio Molecular Dynamics (AIMD) unifies the Newton's and Schrödinger's equations, to allow complex simulations without relying on any adjustable parameter. In AIMD, the motions of the atoms are computed classically and the difference with standard MD lies in the way the interatomic forces are calculated.[250-253]

1.2.6 Hybrid QM/MM Method

The hybrid QM/MM (quantum mechanics/molecular mechanics) approach is a molecular simulation method which combines the strengths of the QM (accuracy) and MM (speed) approaches. The QM/MM approach was introduced by Warshel and Levitt in 1976.[254] They won the 2013 Chemistry Nobel Prize along with Martin Karplus, for "the development of multi-scale models for complex chemical systems".[255-256] In QM/MM method, the region of the system in which the chemical process takes place is described with a suitable quantum chemical theory, while the remaining part is treated by a molecular mechanics force field. With this approach, chemical reactivity of large systems, such as enzymes can be studied.[257-258]

Among the various hybrid methods, ONIOM (our Own N-layered Integrated molecular Orbital and molecular Mechanics) method developed by Morokuma and co-workers is a general one. In this method, the molecular system is divided into layers and is treated with different model chemistries. The layers are known as low, medium and high layers, and the layer assignment depends on the molecule specification.[96, 259] This method offers a wide application in thermochemistry analysis, enzymatic reactions, and molecular dynamics.

1.2.7 Computational Methods for Studying Organometallic Systems

Computational chemistry is an important tool in the chemical analysis and describes the use of computer modeling and simulations for studying the structure and properties of molecules. Computational and theoretical studies of transition metal complexes especially organometallic systems and associated reactions are of great importance as their application in the chemistry and industry are wide. Transition metals are difficult to model as they exhibit varieties of geometry, bonding nature and often require a non-classical understanding. The valence electrons of transition and inner transition metals are placed in the d and f orbitals respectively. Compared to s and p orbitals, d and f orbitals can occupy more electrons and have more complex shapes and higher angular momentum, and causes complexity in the chemical bonding features of complexes of d and f metals complexes. Also, transition metals can exhibit multiple oxidation states, and the higher oxidation states result in a highly charged system which can cause long-

range effects. Further, transition metals show multiple coordination numbers. As a result of these, the bonding in a transition metal compound become complex compared to the ionic and covalent bonding pattern of main group elements making it difficult to model a general force field to define the metal.

The molecular mechanics force fields such as AMBER and CHARMM are found to be useful in studying systems with millions of atoms, but only a few are applicable to transition metal complexes as the metal centers show different coordination numbers and the ligand coordination. MOMEC,[260-263] VALBOND (based on valence bond theory), LFMM (based on ligand field theory),[264-265] SIBFA (sum of interactions between fragments *ab Initio)*[266] are some of the successful force fields applied for describing transition metal complexes.[267] The Hartree-Fock method is not suitable for transition metal complexes as the HF theory uses a single-determinant and omits correlation effects in the calculation. The post HF method includes correlation function and is found to be useful in the calculation involving transition metal complexes. It is found that multi-reference wave function based methods provide a better description of transition metal complexes than the single reference methods. But the computational cost of the multi-reference method is very high.[268-269] Density functional theory is the most popular quantum chemical tool in the study of transition metal system. Development of improved functionals widens the application of DFT in the area of transition metal chemistry, and today DFT techniques are used in the prediction and elucidation of molecular structures, various spectroscopic analysis, and reactivity studies involving transition metal coordination or organometallic complexes. Functionals such as B3LYP, BP86 and Truhlar's Minnesota functionals are found to be very good in reproducing the experimental values and are the widely used in the study of transition metal complexes. Often the electronic structure approach can be combined with classical or *ab initio* molecular dynamics to understand the time-related properties of transition metal complexes.[270] *Ab initio* molecular dynamics (AIMD) techniques along with DFT calculation can be used to exploit the inaccessible dynamical features of transition metal catalyzed reactions.[271-272] AIMD method is widely used to sample the potential

energy surface of a system at a finite temperature which in turn provides insights on the reaction mechanism.[273-274]

Among the quantum chemical methods, DFT methodology has an upper hand in the study of reaction mechanism studies.[275] The development of DFT along with the growth of computer power enabled the quantum chemical treatment of wide variety of catalytic system involving large systems with reasonable accuracy. Also, these methods are used in the designing of new catalyst systems.[276] Mechanistic studies require the calculation of detailed free energy profile of the reaction involving all the possible intermediates and transition state. The hybrid functional B3LYP is the most commonly employed method in the mechanistic studies. The main drawback of the B3LYP and most of the other methods for the mechanistic study is their inability to describe the attractive dispersion interaction properly. Inclusion of Grimme dispersion functionals, in fact, helped in overcoming this problem.[248]

Metathesis is a remarkable reaction in chemistry and is applied widely in small-scale laboratory research and also in large-scale industrial production. Computational studies on this topic helped the tremendous growth it achieved today as the important synthetic tool for CC forming reaction. Different aspects of metathesis chemistry such as reactivity, selectivity, reaction mechanism, the effect of ligands and substituent's and decomposition of catalysts are well studied using computational methods.[277] Detailed analysis of the mechanistic aspect of metathesis reaction by Thiel, Cavallo, Adhlart, Chen and their coworkers using DFT techniques has in fact helped in understanding how the shed light into the possible mechanism of metathesis reaction.[33] [278]B3LYP, BP86, M06 are the most common methods used in the analysis of metathesis reaction.

This thesis describes the computational analysis of metathesis reactions which shed light on the complex bonding nature of the reaction intermediates. Along with DFT methodology, other quantum chemical tools for electronic and bonding analysis are utilized and are described below.

1.2.8 Solvation Models

Molecular properties obtained from a gas phase calculation are sometimes inadequate to explain a system completely as the surrounding environment such as solvent can considerably influence it. Solvent effect can be incorporated in to a system either by using continuum solvation model which treat the solvent as a continuous medium or explicit solvation model which describes individual solvent molecules(Figure 1.4).[279-280] Though the explicit solvation model provides an accurate way of modeling chemistry in solvent; their application is restricted as they are computationally expensive. Treating the solvent as a polarizable continuum as a substitute for modeling individual molecules reduces the computational expenses makes computation feasible. In continuum solvent model the solute M is placed in a suitably shaped cavity in the polarizable medium with dielectric constant ε.[281]

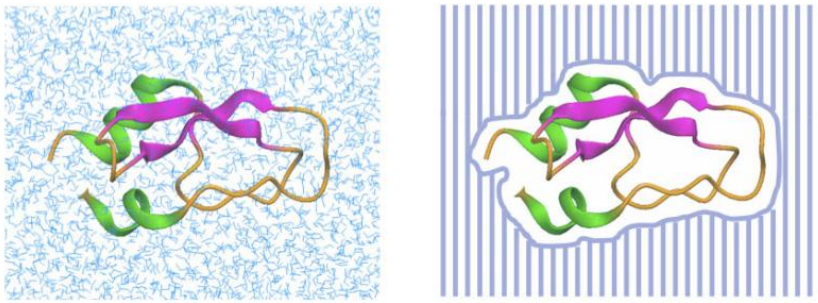

(i) (ii)

Figure 1.4 A representation of (i) explicit and (ii) implicit solvation models.

Self-Consistent Reaction Field (SCRF) is a method used for accounting the effect of polarizable medium on a quantum system and varies with the way they define the cavity and reaction field.[282-283] Polarizable continuum model (PCM) is one of the most frequently used SCRF methods. In PCM the cavity is defined as the union of a series of interlocking atomic spheres.[284] In PCM, the free energy of solvation, ΔG_{sol} is expressed as the sum of three terms *viz*. the electrostatic (ΔG_{elec}), dispersion-repulsion (ΔG_{disp}) contributions to free energy, and the cavitation energy (ΔG_{cav}).

$$\Delta G_{sol} = \Delta G_{elec} + \Delta G_{disp} + \Delta G_{cav} \qquad \text{(Eq. 1.41)}$$

ΔG_{elec} accounts for the electrostatic solute-solvent interaction while ΔG_{disp} arises due to the solute and solvent dispersion interaction and the resulting repulsion. ΔG_{cav} is

the cavitation energy needed to form the molecular cavity inside the continuum. There are many variants of PCM available which perform well in analyzing the solvent effect on chemical systems. [285]

Solvation model based on density (SMD) works similar to PCM but uses specifically parametrized radii to construct the cavity.[286] SMD is a universal solvation model, since it can be applied to any charged or uncharged solute in any solvent. According to this model, the electron density of the solute as a whole is interacting with the solvent rather than its partial atomic charge. In SMD the solvation free energy can be written as the sum of two terms *viz.* electrostatic term and cavity-dispersion solvent-structure term. The first component is due to a self-consistent reaction field treatment that involves the solution of the nonhomogeneous Poisson equation for electrostatics in terms of the integral equation-formalism polarizable continuum model (IEF-PCM). The second component is the contribution arising from short-range interactions between the solute and solvent molecules in the first solvation shell. This contribution is a sum of terms that are proportional (with geometry-dependent proportionality constants called atomic surface tensions) to the solvent-accessible surface areas of the individual atoms of the solute.

1.2.9 Potential Energy Surface (PES)

A potential energy surface is a mathematical function that gives the energy of a molecule as a function of its geometry. The Born-Oppenheimer approximation is one of the foundations for computational chemistry as it defines the concept of molecular geometry and thus enables the concept of potential energy surface. PES of a system gives a complete description of all conformers and isomers and energetically possible motions of a system. Minima on the PES correspond to a minimum energy structure or optimized geometry. A PES can have a global minimum and several local minima on it. The global minimum represents the lowest-energy minimum structure, and the local minima represent higher energy conformers or isomers. A simple PES can be compared to mountainous landscapes and can be represented as a topological surface with valleys and hill where the minima are represented as valleys (Figure 1.5).[287-289] Analyses of PES can provide information regarding the molecular system. Reaction rates can be

determined from the height and profile of the pathway connecting reactant and product valleys. Analysis of the shape of a valley gives information on the vibrational spectrum of the molecule. Also, the response of the energy to electric and magnetic fields determines molecular properties such as dipole moment, polarizability, NMR shielding.[290-291]

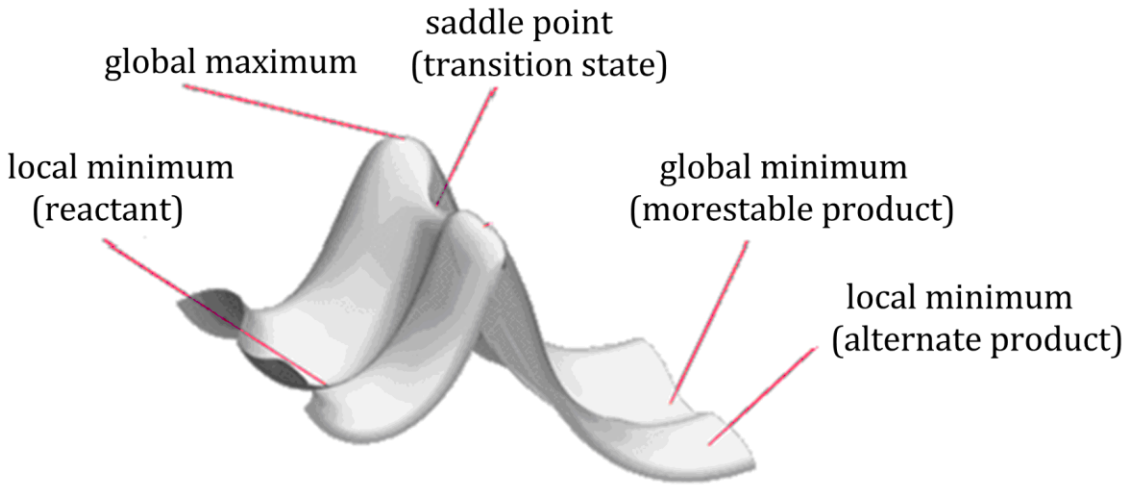

Figure 1.5 A model representation of potential energy surface.

Considering a PES of a chemical reaction, the reactant and products are located as minima, and the transition state (TS) of the reaction is represented as first-order saddle point. Thus finding the TS is vital to calculate the reaction barriers and reaction rates. For a first-order saddle point, it should be a maximum in one direction and minimum in all other direction. Compared to minimization, transition state location is a tricky job in computational chemistry.[292-294] A common method used for locating transition state is an eigenvalue following algorithm in which the optimization looks for a negative eigenvalue and follow the most negative eigenvalue.[295-296] Synchronous transit-guided quasi-Newton (STQN) method is another widely used technique for locating transition state.[297] This method by Schlegel and co-workers uses two basic approaches called linear synchronous transit for getting closer to the transition state guess and an eigenvalues following method quasi-Newton algorithm to complete the optimization.[298-299] Two variables of this method *viz.* QST2 and QST3 are available in the Gaussian program suite. The QST2 method requires the geometry of reactant and

product only while in QST3 a guess structure of the transition state is also needed. For both methods, the reactant and product geometry must be described with all atoms in the same order. A large part of the thesis deals with PES analysis of various metathesis reactions.

1.2.10 Bond Order Calculations

According to the qualitative molecular orbital theory, the formal bond order (BO) of a diatomic molecule is defined as the equation

$$BO = \frac{N_{bondng} - N_{antibonding}}{2} \qquad \text{(Eq. 1.42)}$$

where $N_{bonding}$ is the number of electrons in the bonding orbital and $N_{antibonding}$ is the number of electrons in the anti bonding orbital. Quantum chemical methods for calculating BO are later developed and these bond index values played a conceptual role in describing the molecules as atoms held together by bonds. Today most widely used methods of bond order calculation are Wiberg and Mayer bond orders. The Wiberg bond order index defined by K. B. Wiberg in 1968, is originally introduced for close-shell semi-empirical wave functions and are found to give values very close to formal bond order.[300] The main limitation of Wiberg bond order is that it is not directly applicable to *ab initio* wave functions as the former assumes the orthonormal condition of basis functions while later used non-orthonormal basis functions. Mayer bond order can be viewed as a generalization of Wiberg bond order for *ab initio* cases, as the overlap matrix is considered for the calculation[301] and the property of Mayer bond order is found to be very similar to the Wiberg bond order. Recently Manz introduced new, efficient computational method for the bond order calculation of diverse materials including elements from each chemical group and period.[302]

Wiberg bond order (W_{bo}) values reported in the thesis are calculated using Natural Bond Orbital (NBO) analysis implemented in Gaussian 09.[303] NBO analysis is an effective tool for calculating and understanding the intuitive picture of both electron orbitals and population analysis. NBO attempts to connect the numerical content of wave function with concepts of bonding theory. In natural bond analysis, it classifies and localizes orbitals into three distinct groups: non-bonding natural atomic orbitals

(NAOs), orbitals involved in bonding and anti-bonding (NBOs), and Rydberg type orbital. The NAOs and Rydberg type orbitals are made up of basis sets of single atoms and the NBOs are a combination of basis set atomic orbitals of two atoms.

1.2.11 Quantum Theory of Atoms in Molecule

Bader *et al.* developed the quantum theory of atoms in molecules (QTAIM) based on the electron density, as it is a fundamental function to describe the electron distribution in a molecule.[304-306] He proposed that the topology of electron density $\rho(\mathbf{r})$ yields an accurate mapping of the molecular structure, and each topological feature can be described by a set of critical points (CPs). A critical point (CP) is a point in the electron density surface where the gradient of electron density vanishes (Eq. 1.43).

$$\nabla\rho(\mathbf{r}) = i\frac{d\rho(\mathbf{r})}{dx} + j\frac{d\rho(\mathbf{r})}{dy} + k\frac{d\rho(\mathbf{r})}{dz} \longrightarrow \begin{cases} = \vec{0} \text{ (at critical points } (r_c) \text{ and at } \infty) \\ \# \vec{0} \text{ (at all other points)} \end{cases} \quad \text{(Eq. 1.43)}$$

There are critical points corresponding to the maxima, minima and saddle points of $\rho(r)$. Collection of nine possible second derivative electron density at r_c can be written in a matrix form called Hessian matrix ($A(r_c)$),

$$A(r_c) = \begin{pmatrix} \frac{\partial^2\rho}{\partial x^2} & \frac{\partial^2\rho}{\partial x\partial y} & \frac{\partial^2\rho}{\partial x\partial z} \\ \frac{\partial^2\rho}{\partial y\partial x} & \frac{\partial^2\rho}{\partial y^2} & \frac{\partial^2\rho}{\partial y\partial z} \\ \frac{\partial^2\rho}{\partial z\partial x} & \frac{\partial^2\rho}{\partial z\partial y} & \frac{\partial^2\rho}{\partial z^2} \end{pmatrix} \quad \text{(Eq. 1.44)}$$

Diagonalization of Hessian matrix gives a set of eigenvalues and associated eigenvectors. All type of CPs can be distinguished based on the eigenvalues associated with it. Each critical point can be labeled by an ordered pair (r,ω), where r is the rank of the CP and ω the signature. The rank is the number of non-zero eigenvalues of the electron density at the CP and signature is the algebraic sum of the signs of eigenvalues. CPs associated with the energetically stable configuration of nuclei show three non-zero eigenvalues (ω= 3). CPs with ω < 3 are called degenerate and are unstable. A CP with

rank three can exist in four types. (3, -3) CP corresponds to the local maximum, the nuclear attractor; (3, -1) is the bond critical point (BCP); (3, +1) is the ring critical point (RCP); and (3, -3) is the local minimum, called the cage critical point (CCP). A BCP between two nuclei indicate the bonding interaction between them, and a line called bond path (BP) can be drawn connecting the two nuclei through the BCP. BP is the line of maximum electron density connecting and bond critical point is the minimum of electron density on the bond path. A collection of bond paths linking the nuclei of bonded atoms in equilibrium geometry with the associated critical points is known as the molecular graph. The Laplacian of electron density ($\nabla^2(\rho)$) offers an understanding of the local charge concentration or depletion in the molecule. Positive $\nabla^2(\rho)$ values indicate local charge depletion and negative values represent local charge concentration. The local charge concentration does not represent a maximum.

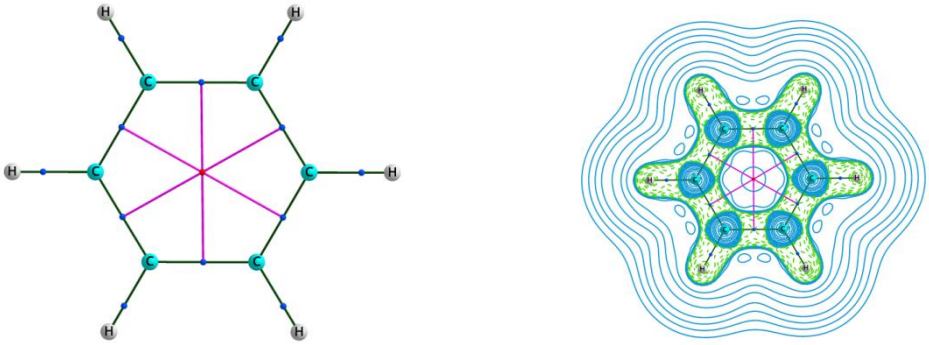

(i) (ii)

Figure 1.6 (i) Molecular graph of benzene (BP86/6-31+g(d,p)) showing bond paths (solid green line) and ring paths (solid pink line) along with the critical points. Different critical points are represented as small colored spheres (blue for (3, -1) or bond CP, red for (3, +1) or ring CP, and green for (3, +3) or cage CP). (ii) The contour of Laplacian of electron density in the plane of the ring along with the molecular graph.

Figure 1.6 represents the molecular graph of benzene along with the contour of Laplacian of electron density. The dark green lines correspond to bond paths between interacting nuclei while the pink lines indicate ring paths connecting BCP and RCP. Dashed green curves show the area of relative electron concentration (positive $\nabla^2(\rho)$) and solid blue curves are areas of relative charge depletion (negative $\nabla^2(\rho)$). The thesis

extensively uses the QTAIM analysis to understand the metal-carbon bonding in various metallacycles of metathesis reactions.

In this thesis, the topological analysis of electron density is done using the AIMAll program developed by Keith *et al.*[307]

1.2.12 NMR Chemical Shift Calculations

Nuclear Magnetic resonance (NMR) spectroscopy is one of the basic and fundamental tools in chemistry for the structural interpretation of molecules. The NMR chemical shift of a nucleus is defined as the resonant frequency of the nucleus relative to a standard in a magnetic field. NMR shielding tensors and magnetic susceptibility can be calculated using computational tools at different levels of theory using different modeling program suits such as Gaussian, Gamess, NWChem, etc. In computational program suits the chemical shifts are calculated by subtracting the nuclear shielding tensors of reference compound such as TMS (trimethylsilane) from the isotropic nuclear magnetic shielding tensors calculated for each atom.[308] Several methods such as, (i) Gauge invariant atomic orbitals (GIAO),[309] (ii) individual gauge for localized orbitals (IGLO),[310-311] (iii) localized orbital/local origin (LORG),[312] (iv) individual gauges for atoms in molecules (IGAIM),[313] and (v) continuous set of gauge transformation (CSGT)[314] for computing the NMR properties.[315-316] Structures used for NMR calculations should have been optimized at a good level of theory. Spin-spin coupling constants can also be computed using these methods.[317-319] Among these methods, the most widely used method is the GIAO method developed based on the perturbation theory.[316] In this case, the MOs are calculated as a linear combination of GIAO instead of the LCAO formin presence of a magnetic field. The NMR chemical shift values reported in this thesis are calculated based on GIAO-DFT formalism implemented in Gaussian 09 program.

1.2.13 Nucleus Independent Chemical Shift (NICS)

Nucleus independent chemical shift is the most widely used aromaticity probe in quantum chemistry due to its simplicity and efficiency. Schleyer *et al.* used NICS index for the first time for the estimation of aromaticity of hydrocarbons.[320-322] The NICS

index can be used in the evaluation of aromaticity, antiaromaticity, and nonaromaticity of single ring systems and individual rings in polycyclic systems and is widely used to evaluate the aromaticity and antiaromaticity of many organic and inorganic compounds, intermediates, and transition states.[323-324] NICS is defined as the negative value of the absolute shielding computed at the ring center of a molecule (NICS(0)) or at some other point, usually at 1 Å perpendicularly above the ring center (NICS(1)) (Figure 1.7).[324] Negative NICS values at each point of the ring exhibit the presence of induced diatropic ring currents (aromaticity), whereas positive NICS values at the same point show paratropic ring currents (antiaromaticity) and NICS values close to zero belong to nonaromatic species. In this thesis we have used GIAO-DFT formalism implemented in Gaussian 09 program for calculating various NICS parameters.

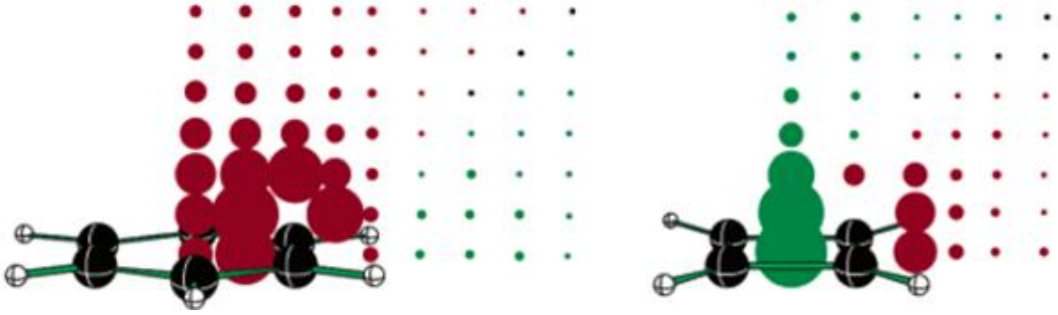

(i) (ii)

Figure 1.7 NICS grid plot of (i) benzene and (ii) cyclobutadiene. Red and green dots denote the diatropic (aromatic) and paratropic (antiaromatic) ring currents respectively.[322]

1.2.14 Anisotropy of Current Induced Density (ACID)

Anisotropy of current induced density is a quantum chemical method for the analysis and visualization of delocalization and conjugation (σ, π, through the bond, and through-space conjugation) in molecules. ACID can be used in investigating ground, excited, and transition states and also in organometallic compounds.[325-326] This method can be used to study conjugative effects such as stereoelectronic effects in reactions, anomeric effect, aromaticity, homoaromaticity of molecules. As a quantum theoretical tool for the investigation of molecular properties, it provides information about charge

and steric interactions. ACID isosurfaces are complementary to the electrostatic surface and electron density. Current density vectors can be plotted on to the ACID isosurface which could provide information on the magnitude and direction of currents (e.g., diatropic or paratropic). Diatropic arrangement of the vectors on the ACID isosurface represents aromatic nature of the molecule while the paratropic arrangement of the vectors on the surface indicates the antiaromatic character.[327] Figure 1.8 shows the ACID isosurface (at an isosurface value of 0.5 au) of benzene and cyclobutadiene. Benzene shows clockwise arrangements of the current vectors (green arrows) on the isosurface indicating its aromatic character, while anti-aromatic molecule cyclobutadiene shows an anti-clockwise arrangement of vectors on the isosurface. This tool is used for the characterization of certain metallacycles discussed in the thesis.

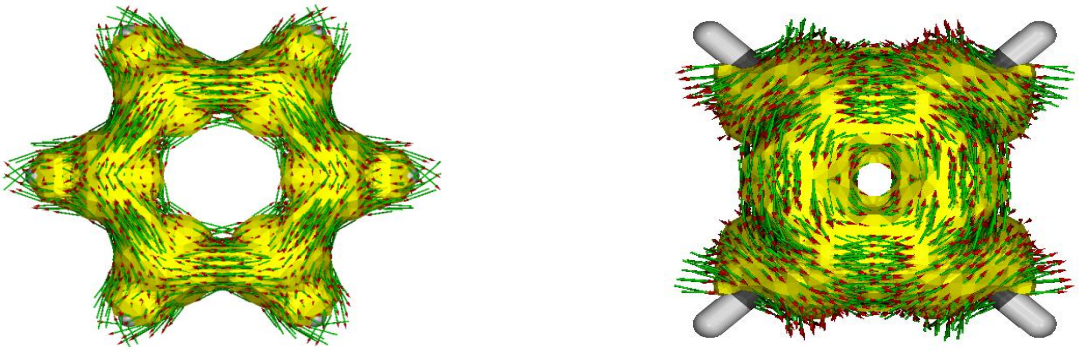

(i) (ii)

Figure 1.8 ACID isosurface (0.05 au) plot of (i) benzene and (ii) cyclobutadiene calculated at BP86/6-31g* level of DFT. Aromatic molecule benzene shows a clock-wise arrangement of the current vectors (green arrows) while anti-aromatic molecule cyclobutadiene shows an anti-clockwise arrangement of vectors on the isosurface.

1.3 Conclusions

Metathesis is an important synthetic technique in organic chemistry for the CC bond forming reactions. The first part of the Chapter 1 gives a brief discussion on the various types of metathesis reactions such as alkene metathesis, alkyne metathesis and enyne metathesis. A detailed discussion on the alkene metathesis mechanism, catalysts and decomposition of Grubbs type catalysts are included in the chapter. A discussion on the

application of metathesis reaction clearly marks the growth of metathesis reaction from a synthetic technique to an industrially important reaction. The metallacycle intermediates of metathesis reaction are found to play a crucial role in deciding the outcome of the reaction. A detailed discussion on the experimental and theoretical studies of metallacycle and its unusual bonding characters are also included in the chapter.

Computational chemistry methods become an integral part in solving and understanding chemical problems. These techniques play a crucial role in predicting reactions and mechanisms which are otherwise difficult to explain. Second part of the chapter discusses the common computational methods such as molecular mechanics, *ab initio* methods, semiempirical methods, DFT, molecular dynamics. Part B of Chapter 1 also includes discussion on the computational techniques used for calculating and quantifying electronic properties and energetics of organometallic systems.

1.4 References

1. A. D. M. a. A. Wilkinson., *IUPAC. Compendium of Chemical Terminology, 2nd ed. (the "Gold Book")*, Blackwell Scientific Publications, Oxford, **1997**.
2. N. Calderon, H. Y. Chen and K. W. Scott, *Tetrahedron Lett.*, **1967**, *8*, 3327-3329.
3. T. M. Trnka and R. H. Grubbs, *Acc. Chem. Res*, **2001**, *34*, 18-29.
4. D. Astruc, *New J. Chem.*, **2005**, *29*, 42-56.
5. R. R. Schrock, *Acc. Chem. Res.*, **1986**, *19*, 342-348.
6. J. S. Kingsbury, J. P. A. Harrity, P. J. Bonitatebus and A. H. Hoveyda, *J. Am. Chem. Soc.*, **1999**, *121*, 791-799.
7. S. A. Janine Cossy , Christophe Meyer , Robert H. Grubbs, *Metathesis in Natural Product Synthesis: Strategies, Substrates and Catalysts*, **2010**.
8. J. C. Mol, *J. Mol. Catal. A-Chem.*, **2004**, *213*, 39-45.
9. A. D. Piscopio and J. E. Robinson, *Curr. Opin. Chem. Biol.*, **2004**, *8*, 245-254.
10. A. Wojtkielewicz, *Current Organic Synthesis*, **2013**, *10*, 43-66.
11. S. Leimgruber and G. Trimmel, *Monatshefte Fur Chemie*, **2015**, *146*, 1081-1097.

12. A. D. Valerian Dragutan, Ileana Dragutan, Eugene Sh. Finkelshtein, *Green Metathesis Chemistry - Great Challenges in Synthesis, Catalysis and Nanotechnology*, Springer, **2010**.
13. T. M. Trnka and R. H. Grubbs, *Acc. Chem. Res.*, **2001**, *34*, 18-29.
14. A. Fürstner, *Angew. Chem. Int. Ed.*, **2013**, *52*, 2794-2819.
15. A. S. Goldman, A. H. Roy, Z. Huang, R. Ahuja, W. Schinski and M. Brookhart, *Science*, **2006**, *312*, 257-261.
16. S. T. Diver and A. J. Giessert, *Chem. Rev.*, **2004**, *104*, 1317-1382.
17. J. Huang, E. D. Stevens, S. P. Nolan and J. L. Petersen, *J. Am. Chem. Soc.*, **1999**, *121*, 2674-2678.
18. R. R. Schrock, *Tetrahedron*, **1999**, *55*, 8141-8153.
19. A. Furstner, *Angew. Chem. Int. Ed.*, **2000**, *39*, 3012-3043.
20. S. J. Connon and S. Blechert, *Angew. Chem. Int. Ed.*, **2003**, *42*, 1900-1923.
21. R. H. Grubbs, *Tetrahedron*, **2004**, *60*, 7117-7140.
22. R. L. Banks and G. C. Bailey, *I&EC Product Research and Development*, **1964**, *3*, 170-173.
23. J. C. M. K.J. Ivin, *Olefin Metathesis and Metathesis Polymerization*, Elsevier **1997**.
24. N. Calderon, E. A. Ofstead and W. A. Judy, *Angew. Chem. Int. Ed.*, **1976**, *15*, 401-409.
25. P. Jean-Louis Hérisson and Y. Chauvin, *Die Makromolekulare Chemie*, **1971**, *141*, 161-176.
26. T. J. Katz and J. McGinnis, *J. Am. Chem. Soc.*, **1975**, *97*, 1592-1594.
27. R. H. Grubbs, P. L. Burk and D. D. Carr, *J. Am. Chem. Soc.*, **1975**, *97*, 3265-3267.
28. M. Ulman and R. H. Grubbs, *Organometallics*, **1998**, *17*, 2484-2489.
29. E. L. Dias, S. T. Nguyen and R. H. Grubbs, *J. Am. Chem. Soc.*, **1997**, *119*, 3887-3897.
30. C. Adlhart, C. Hinderling, H. Baumann and P. Chen, *J. Am. Chem. Soc.*, **2000**, *122*, 8204-8214.
31. M. S. Sanford, J. A. Love and R. H. Grubbs, *J. Am. Chem. Soc.*, **2001**, *123*, 6543-6554.
32. L. Cavallo, *J. Am. Chem. Soc.*, **2002**, *124*, 8965-8973.
33. S. F. Vyboishchikov, M. Bühl and W. Thiel, *Chem. Eur. J.*, **2002**, *8*, 3962-3975.

34. R. R. Schrock, *Acc. Chem. Res.*, **1990**, *23*, 158-165.
35. R. H. Grubbs, S. J. Miller and G. C. Fu, *Acc. Chem. Res.*, **1995**, *28*, 446-452.
36. R. R. Schrock, *Chem. Rev.*, **2009**, *109*, 3211-3226.
37. L. G. McCullough, R. R. Schrock, J. C. Dewan and J. C. Murdzek, *J. Am. Chem. Soc.*, **1985**, *107*, 5987-5998.
38. S. T. Nguyen, R. H. Grubbs and J. W. Ziller, *J. Am. Chem. Soc.*, **1993**, *115*, 9858-9859.
39. T. E. Wilhelm, T. R. Belderrain, S. N. Brown and R. H. Grubbs, *Organometallics*, **1997**, *16*, 3867-3869.
40. S. T. Nguyen, L. K. Johnson, R. H. Grubbs and J. W. Ziller, *J. Am. Chem. Soc.*, **1992**, *114*, 3974-3975.
41. M. Scholl, T. M. Trnka, J. P. Morgan and R. H. Grubbs, *Tetrahedron Lett.*, **1999**, *40*, 2247-2250.
42. M. Scholl, S. Ding, C. W. Lee and R. H. Grubbs, *Org. Lett.*, **1999**, *1*, 953-956.
43. G. C. Vougioukalakis and R. H. Grubbs, *Chem. Rev.*, **2010**, *110*, 1746-1787.
44. S. B. Garber, J. S. Kingsbury, B. L. Gray and A. H. Hoveyda, *J. Am. Chem. Soc.*, **2000**, *122*, 8168-8179.
45. S. Gessler, S. Randl and S. Blechert, *Tetrahedron Lett.*, **2000**, *41*, 9973-9976.
46. R. H. Grubbs and S. Chang, *Tetrahedron*, **1998**, *54*, 4413-4450.
47. M. Schuster and S. Blechert, *Angew. Chem. Int. Ed.*, **1997**, *36*, 2036-2056.
48. S. C. Marinescu, R. R. Schrock, P. Müller, M. K. Takase and A. H. Hoveyda, *Organometallics*, **2011**, *30*, 1780-1782.
49. S. J. Meek, R. V. O'Brien, J. Llaveria, R. R. Schrock and A. H. Hoveyda, *Nature*, **2011**, *471*, 461-466.
50. A. J. Jiang, J. H. Simpson, P. Müller and R. R. Schrock, *J. Am. Chem. Soc.*, **2009**, *131*, 7770-7780.
51. K. Endo and R. H. Grubbs, *J. Am. Chem. Soc.*, **2011**, *133*, 8525-8527.
52. H. Martinez, P. Miró, P. Charbonneau, M. A. Hillmyer and C. J. Cramer, *ACS Catal.*, **2012**, *2*, 2547-2556.
53. J. Hartung, P. K. Dornan and R. H. Grubbs, *J. Am. Chem. Soc.*, **2014**, *136*, 13029-13037.

54. T. P. Montgomery, T. S. Ahmed and R. H. Grubbs, *Angew. Chem. Int. Ed.*, **2017**, *56*, 11024-11036.
55. I. W. Ashworth, I. H. Hillier, D. J. Nelson, J. M. Percy and M. A. Vincent, *ACS Catal.*, **2013**, *3*, 1929-1939.
56. M. S. Sanford, M. Ulman and R. H. Grubbs, *J. Am. Chem. Soc.*, **2001**, *123*, 749-750.
57. J. Mathew and C. H. Suresh, *Organometallics*, **2011**, *30*, 3106-3112.
58. C. A. Urbina-Blanco, A. Poater, T. Lebl, S. Manzini, A. M. Z. Slawin, L. Cavallo and S. P. Nolan, *J. Am. Chem. Soc.*, **2013**, *135*, 7073-7079.
59. M. B. Dinger and J. C. Mol, *Organometallics*, **2003**, *22*, 1089-1095.
60. D. Banti and J. C. Mol, *J. Organomet. Chem.*, **2004**, *689*, 3113-3116.
61. W. Janse van Rensburg, P. J. Steynberg, W. H. Meyer, M. M. Kirk and G. S. Forman, *J. Am. Chem. Soc.*, **2004**, *126*, 14332-14333.
62. S. H. Hong, A. G. Wenzel, T. T. Salguero, M. W. Day and R. H. Grubbs, *J. Am. Chem. Soc.*, **2007**, *129*, 7961-7968.
63. S. H. Hong, A. Chlenov, M. W. Day and R. H. Grubbs, *Angew. Chem. Int. Ed.*, **2007**, *46*, 5148-5151.
64. J. Mathew, N. Koga and C. H. Suresh, *Organometallics*, **2008**, *27*, 4666-4670.
65. K. Vehlow, S. Gessler and S. Blechert, *Angew. Chem. Int. Ed.*, **2007**, *46*, 8082-8085.
66. M. B. Herbert, Y. Lan, B. K. Keitz, P. Liu, K. Endo, M. W. Day, K. N. Houk and R. H. Grubbs, *J. Am. Chem. Soc.*, **2012**, *134*, 7861-7866.
67. J. A. Lummiss, W. L. McClennan, R. McDonald and D. E. Fogg, *Organometallics*, **2014**, *33*, 6738-6741.
68. A. Mukherjee, *Synlett*, **2006**, 1128-1129.
69. D. D. Young, R. S. Senaiar and A. Deiters, *Chem. Eur. J.*, **2006**, *12*, 5563-5568.
70. B. Alcaide, P. Almendros and A. Luna, *Chem. Rev.*, **2009**, *109*, 3817-3858.
71. S. Y. Yun, K.-P. Wang, M. Kim and D. Lee, *J. Am. Chem. Soc.*, **2012**, *134*, 10783-10786.
72. A. K. Chatterjee, in *Handbook of Metathesis*, Wiley-VCH Verlag GmbH, **2008**,246-295.
73. A. K. Chatterjee, T.-L. Choi, D. P. Sanders and R. H. Grubbs, *J. Am. Chem. Soc.*, **2003**, *125*, 11360-11370.

74. Y. Dong, J. B. Matson and K. J. Edgar, *Biomacromolecules*, **2017**, *18*, 1661-1676.
75. J. E. Schwendeman, A. C. Church and K. B. Wagener, *Adv. Synth. Catal.*, **2002**, *344*, 597-613.
76. H. E. Blackwell, D. J. O'Leary, A. K. Chatterjee, R. A. Washenfelder, D. A. Bussmann and R. H. Grubbs, *J. Am. Chem. Soc.*, **2000**, *122*, 58-71.
77. H.-G. Schmalz, *Angew. Chem. Int. Ed.*, **1995**, *34*, 1833-1836.
78. S. Monfette and D. E. Fogg, *Chem. Rev.*, **2009**, *109*, 3783-3816.
79. B. J. van Lierop, J. A. M. Lummiss and D. E. Fogg, in *Olefin Metathesis*, John Wiley & Sons, Inc., **2014**,85-152.
80. A. Gradillas and J. Pérez-Castells, *Angew. Chem. Int. Ed.*, **2006**, *45*, 6086-6101.
81. N. K. Yee, V. Farina, I. N. Houpis, N. Haddad, R. P. Frutos, F. Gallou, X.-j. Wang, X. Wei, R. D. Simpson, X. Feng, V. Fuchs, Y. Xu, J. Tan, L. Zhang, J. Xu, L. L. Smith-Keenan, J. Vitous, M. D. Ridges, E. M. Spinelli, M. Johnson, K. Donsbach, T. Nicola, M. Brenner, E. Winter, P. Kreye and W. Samstag, *J. Org. Chem.*, **2006**, *71*, 7133-7145.
82. F. Sinclair, M. Alkattan, J. Prunet and M. P. Shaver, *Polym. Chem.*, **2017**, *8*, 3385-3398.
83. A. Hejl, O. A. Scherman and R. H. Grubbs, *Macromolecules*, **2005**, *38*, 7214-7218.
84. D. M. Lynn, S. Kanaoka and R. H. Grubbs, *J. Am. Chem. Soc.*, **1996**, *118*, 784-790.
85. C. W. Bielawski and R. H. Grubbs, *Prog. Polym. Sci.*, **2007**, *32*, 1-29.
86. T.-L. Choi and R. H. Grubbs, *Angew. Chem. Int. Ed.*, **2003**, *42*, 1743-1746.
87. S. Penczek, M. Cypryk, A. Duda, P. Kubisa and S. Słomkowski, *Prog. Polym. Sci.*, **2007**, *32*, 247-282.
88. M. A. Hillmyer, W. R. Laredo and R. H. Grubbs, *Macromolecules*, **1995**, *28*, 6311-6316.
89. B. R. Maughon and R. H. Grubbs, *Macromolecules*, **1997**, *30*, 3459-3469.
90. K. B. Wagener, J. M. Boncella and J. G. Nel, *Macromolecules*, **1991**, *24*, 2649-2657.
91. T. W. Baughman and K. B. Wagener, in *Metathesis Polymerization: Advances in Polymer Science*, ed. M. R. Buchmeiser, Springer Berlin Heidelberg, **2005**, *vol. 176*,1-42.
92. P. Atallah, K. B. Wagener and M. D. Schulz, *Macromolecules*, **2013**, *46*, 4735-4741.

93. M. D. Schulz and K. B. Wagener, in *Handbook of Metathesis*, Wiley-VCH Verlag GmbH & Co. KGaA, **2015**,313-355.
94. H. Mutlu, L. M. de Espinosa and M. A. R. Meier, *Chem. Soc. Rev.*, **2011**, *40*, 1404-1445.
95. M. D. Schulz and K. B. Wagener, *Macromol. Chem. Phys.*, **2014**, *215*, 1936-1945.
96. L. W. Chung, W. M. C. Sameera, R. Ramozzi, A. J. Page, M. Hatanaka, G. P. Petrova, T. V. Harris, X. Li, Z. Ke, F. Liu, H.-B. Li, L. Ding and K. Morokuma, *Chem. Rev.*, **2015**, *115*, 5678-5796.
97. Z. Zhang and Y. Qin, *ACS Macro Lett.*, **2015**, *4*, 679-683.
98. H. Li, L. Caire da Silva, M. D. Schulz, G. Rojas and K. B. Wagener, *Polymer International*, **2017**, *66*, 7-12.
99. F. Pennella, R. L. Banks and G. C. Bailey, *Chem. Commun.*, **1968**, *0*, 1548-1549.
100. A. Mortreux and M. Blanchard, *J. Chem. Soc., Chem. Commun.*, **1974**, 786-787.
101. J. H. Wengrovius, J. Sancho and R. R. Schrock, *J. Am. Chem. Soc.*, **1981**, *103*, 3932-3934.
102. S. F. Pedersen, R. R. Schrock, M. R. Churchill and H. J. Wasserman, *J. Am. Chem. Soc.*, **1982**, *104*, 6808-6809.
103. A. Furstner and P. W. Davies, *Chem. Commun.*, **2005**, *0*, 2307-2320.
104. L. G. McCullough and R. R. Schrock, *J. Am. Chem. Soc.*, **1984**, *106*, 4067-4068.
105. B. Haberlag, M. Freytag, C. G. Daniliuc, P. G. Jones and M. Tamm, *Angew. Chem. Int. Ed.*, **2012**, *51*, 13019-13022.
106. X. Wu and M. Tamm, *Beilstein J. Org. Chem.*, **2011**, *7*, 82-93.
107. S. Beer, C. G. Hrib, P. G. Jones, K. Brandhorst, J. Grunenberg and M. Tamm, *Angew. Chem. Int. Ed.*, **2007**, *46*, 8890-8894.
108. B. Haberlag, X. Wu, K. Brandhorst, J. Grunenberg, C. G. Daniliuc, P. G. Jones and M. Tamm, *Chem. Eur. J.*, **2010**, *16*, 8868-8877.
109. A. Fürstner and C. Mathes, *Org. Lett.*, **2001**, *3*, 221-223.
110. R. Lhermet and A. Fürstner, *Chem. Eur. J*, **2014**, *20*, 13188-13193.
111. A. Fürstner and G. Seidel, *J. Organomet. Chem.*, **2000**, *606*, 75-78.
112. K. Grela and J. Ignatowska, *Org. Lett.*, **2002**, *4*, 3747-3749.

113. K. Weiss, A. Michel, E.-M. Auth, U. H. F. Bunz, T. Mangel and K. Müllen, *Angew. Chem. Int. Ed.*, **1997**, *36*, 506-509.
114. T. J. Katz and S. J. Lee, *J. Am. Chem. Soc.*, **1980**, *102*, 422-424.
115. T. J. Katz, E. B. Savage, S. J. Lee and M. Nair, *J. Am. Chem. Soc.*, **1980**, *102*, 7942-7944.
116. T. J. Katz and T. M. Sivavec, *J. Am. Chem. Soc.*, **1985**, *107*, 737-738.
117. H. Villar, M. Frings and C. Bolm, *Chem.Soc. Rev.*, **2007**, *36*, 55-66.
118. A. Kinoshita and M. Mori, *Synlett*, **1994**, *1994*, 1020-1022.
119. A. Kinoshita, N. Sakakibara and M. Mori, *J. Am. Chem. Soc.*, **1997**, *119*, 12388-12389.
120. M. Mori, *J. Mol. Catal. A-Chem.*, **2004**, *213*, 73-79.
121. M. Mori, *Materials*, **2010**, *3*, 2087-2140.
122. C. Fischmeister and C. Bruneau, *Beilstein J. Org. Chem.*, **2011**, *7*, 156-166.
123. J. J. Lippstreu and B. F. Straub, *J. Am. Chem. Soc.*, **2005**, *127*, 7444-7457.
124. S. T. Diver, *Coord. Chem. Rev.*, **2007**, *251*, 671-701.
125. T. M. Trnka, M. W. Day and R. H. Grubbs, *Organometallics*, **2001**, *20*, 3845-3847.
126. K. Nicolaou, P. G. Bulger and D. Sarlah, *Angew. Chem. Int. Ed.*, **2005**, *44*, 4490-4527.
127. F. Lacombe, K. Radkowski, G. Seidel and A. Fürstner, *Tetrahedron*, **2004**, *60*, 7315-7324.
128. P. E. Romero and W. E. Piers, *J. Am. Chem. Soc.*, **2005**, *127*, 5032-5033.
129. C. Adlhart and P. Chen, *J. Am. Chem. Soc.*, **2004**, *126*, 3496-3510.
130. C. H. Suresh and M.-H. Baik, *Dalton Trans.*, **2005**, *0*, 2982-2984.
131. S. E. Vyboishchikov and W. Thiel, *Chem. Eur. J.*, **2005**, *11*, 3921-3935.
132. X. Solans-Monfort, C. Copéret and O. Eisenstein, *Organometallics*, **2012**, *31*, 6812-6822.
133. X. Solans-Monfort, C. Copéret and O. Eisenstein, *Organometallics*, **2015**, *34*, 1668-1680.
134. A. Poater, X. Solans-Monfort, E. Clot, C. Coperet and O. Eisenstein, *J. Am. Chem. Soc.*, **2007**, *129*, 8207-8216.

135. A. Poater, X. Solans-Monfort, E. Clot, C. Coperet and O. Eisenstein, *Dalton Trans.*, **2006**, *0*, 3077-3087.
136. C. H. Suresh, *J. Organomet. Chem*, **2006**, *691*, 5366-5374.
137. R. R. Schrock, R. T. DePue, J. Feldman, C. J. Schaverien, J. C. Dewan and A. H. Liu, *J. Am. Chem. Soc.*, **1988**, *110*, 1423-1435.
138. J. Feldman, W. M. Davis and R. R. Schrock, *Organometallics*, **1989**, *8*, 2266-2268.
139. J. Feldman, W. M. Davis, J. K. Thomas and R. R. Schrock, *Organometallics*, **1990**, *9*, 2535-2548.
140. R. R. Schrock, A. J. Jiang, S. C. Marinescu, J. H. Simpson and P. Müller, *Organometallics*, **2010**, *29*, 5241-5251.
141. D. V. Peryshkov and R. R. Schrock, *Organometallics*, **2012**, *31*, 7278-7286.
142. E. Folga and T. Ziegler, *Organometallics*, **1993**, *12*, 325-337.
143. R. R. Schrock and A. H. Hoveyda, *Angew. Chem. Int. Ed.*, **2003**, *42*, 4592-4633.
144. M. M. Flook, A. J. Jiang, R. R. Schrock, P. Müller and A. H. Hoveyda, *J. Am. Chem. Soc.*, **2009**, *131*, 7962-7963.
145. M. R. Reithofer, G. E. Dobereiner, R. R. Schrock and P. Müller, *Organometallics*, **2013**, *32*, 2489-2492.
146. X. Solans-Monfort, J.-S. Filhol, C. Coperet and O. Eisenstein, *New J. Chem.*, **2006**, *30*, 842-850.
147. A. Poater, X. Solans-Monfort, E. Clot, C. Copéret and O. Eisenstein, *J. Am. Chem. Soc.*, **2007**, *129*, 8207-8216.
148. C. H. Suresh and N. Koga, *Organometallics*, **2003**, *23*, 76-80.
149. C. H. Suresh and G. Frenking, *Organometallics*, **2012**, *31*, 7171-7180.
150. M. Brookhart, M. L. H. Green and G. Parkin, *Proc. Natl. Acad. Sci.*, **2007**, *104*, 6908-6914.
151. W. Scherer and G. S. McGrady, *Angew. Chem. Int. Ed.*, **2004**, *43*, 1782-1806.
152. M. Lein, *Coord. Chem. Rev.*, **2009**, *253*, 625-634.
153. H. Weiss, F. Haase and R. Ahlrichs, *Chem. Phys. Lett.*, **1992**, *194*, 492-496.
154. M. Etienne, J. E. McGrady and F. Maseras, *Coord. Chem. Rev.*, **2009**, *253*, 635-646.
155. M. Brookhart and M. L. H. Green, *J. Organomet. Chem.*, **1983**, *250*, 395-408.

156. R. Tomaszewski, I. Hyla-Kryspin, C. L. Mayne, A. M. Arif, R. Gleiter and R. D. Ernst, *J. Am. Chem. Soc.*, **1998**, *120*, 2959-2960.
157. A. Vigalok and D. Milstein, *Acc. Chem. Res.*, **2001**, *34*, 798-807.
158. B. G. Harvey, C. L. Mayne, A. M. Arif and R. D. Ernst, *J. Am. Chem. Soc.*, **2005**, *127*, 16426-16435.
159. M. Etienne and A. S. Weller, *Chem. Soc. Rev.*, **2014**, *43*, 242-259.
160. B. G. Harvey and R. D. Ernst, *Eur. J. Inorg. Chem.*, **2017**, *2017*, 1205-1226.
161. C. H. Suresh and G. Frenking, *Organometallics*, **2010**, *29*, 4766-4769.
162. C. H. Suresh and G. Frenking, *Organometallics*, **2013**, *32*, 1531-1536.
163. S. Grimme and P. R. Schreiner, *Angew. Chem. Int. Ed.*, **2017**.
164. T. Sperger, I. A. Sanhueza and F. Schoenebeck, *Acc. Chem. Res.*, **2016**, *49*, 1311-1319.
165. M. Born and R. Oppenheimer, *Annalen der Physik*, **1927**, *389*, 457-484.
166. W. Pauli, *Zeitschrift für Physik A Hadrons and Nuclei*, **1925**, *31*, 765-783.
167. V. Fock, *Zeitschrift für Physik A Hadrons and Nuclei*, **1930**, *61*, 126-148.
168. J. C. Slater, *Phys. Rev.*, **1930**, *35*, 210-211.
169. G. G. Hall, *Proc. Royal Soc. A*, **1951**, *205*, 541-552.
170. C. C. J. Roothaan, *Rev. Mod. Phys.*, **1951**, *23*, 69-89.
171. I. Shavitt, *Mol. Phys.*, **1998**, *94*, 3-17.
172. R. J. Bartlett and M. Musiał, *Rev. Mod. Phys.*, **2007**, *79*, 291.
173. H. J. Werner and P. J. Knowles, *J. Chem. Phys.*, **1988**, *89*, 5803-5814.
174. P. J. Knowles and H.-J. Werner, *Chem. Phys. Lett.*, **1988**, *145*, 514-522.
175. D. C. Young, *Computational Chemistry: A Practical Guide for Applying Techniques to Real World Problems*, **2001**, 19-31.
176. A. Szabo and N. S. Ostlund, *Modern Quantum Chemistry: Introduction to Advanced Electronic Structure Theory*, Courier Corporation, **2012**.
177. H. Nakano, *J. Chem. Phys.*, **1993**, *99*, 7983-7992.
178. J. Olsen, D. L. Yeager and P. Jørgensen, *Advances in Chemical Physics, Volume 54*, **1983**, 1-176.
179. J. Čížek, *Theor. Chim. Acta*, **1991**, *80*, 91-94.
180. J. Čížek and J. Paldus, *Phys. Scr.*, **1980**, *21*, 251.

181. J. Čížek, *J. Chem. Phys.*, **1966**, *45*, 4256-4266.
182. D. Cremer, *Wiley Interdiscip. Rev. Comput. Mol. Sci.*, **2011**, *1*, 509-530.
183. C. Møller and M. S. Plesset, *Phys. Rev.*, **1934**, *46*, 618-622.
184. D. Cremer, *Encyclopedia of computational chemistry*, **1998**.
185. D. G. Fedorov and K. Kitaura, *J. Chem. Phys.*, **2004**, *121*, 2483-2490.
186. L. C. Allen and A. M. Karo, *Rev. Mod. Phys.*, **1960**, *32*, 275-285.
187. J. C. Slater, *Phys. Rev.*, **1930**, *36*, 57-64.
188. P. M. W. Gill, in *Advances in Quantum Chemistry*, eds. J. R. Sabin and M. C. Zerner, Academic Press, **1994**, *vol. 25*,141-205.
189. D. Feller and E. R. Davidson, in *Rev. Computat. Chem.*, John Wiley & Sons, Inc., **2007**,1-43.
190. S. F. Boys, *Proc. Royal Soc. A*, **1950**, *200*, 542-554.
191. E. Besalú and R. Carbó-Dorca, *J. Math. Chem.*, **2011**, *49*, 1769-1784.
192. I. Shavitt and M. Karplus, *J. Chem. Phys.*, **1965**, *43*, 398-414.
193. Y. Sakai, H. Tatewaki and S. Huzinaga, *J. Comput. Chem.*, **1981**, *2*, 100-107.
194. R. F. Stewart and W. J. Hehre, *J. Chem. Phys.*, **1970**, *52*, 5243-5247.
195. H. Tatewaki and S. Huzinaga, *J. Chem. Phys.*, **1979**, *71*, 4339-4348.
196. J. B. Collins, P. v. R. Schleyer, J. S. Binkley and J. A. Pople, *J. Chem. Phys.*, **1976**, *64*, 5142-5151.
197. W. J. Hehre, R. F. Stewart and J. A. Pople, *J. Chem. Phys.*, **1969**, *51*, 2657-2664.
198. E. R. Davidson and D. Feller, *Chem. Rev.*, **1986**, *86*, 681-696.
199. R. Ditchfield, W. J. Hehre and J. A. Pople, *J. Chem. Phys.*, **1971**, *54*, 724-728.
200. M. J. Frisch, J. A. Pople and J. S. Binkley, *J. Chem. Phys.*, **1984**, *80*, 3265-3269.
201. G. Kresse and J. Furthmüller, *Comput. Mater. Sci.*, **1996**, *6*, 15-50.
202. J. G. Hill, *Int. J. Quantum Chem.*, **2013**, *113*, 21-34.
203. P. J. Hay and W. R. Wadt, *J. Chem. Phys.*, **1985**, *82*, 270-283.
204. F. Jensen, *Introduction to Computational Chemistry*, John wiley & sons, **2017**.
205. W. J. Hehre, *Acc. Chem. Res.*, **1976**, *9*, 399-406.
206. A. K. Wilson, D. E. Woon, K. A. Peterson and T. H. Dunning Jr, *J. Chem. Phys.*, **1999**, *110*, 7667-7676.
207. T. H. Dunning Jr, *J. Chem. Phys.*, **1989**, *90*, 1007-1023.

208. F. Weigend and R. Ahlrichs, *Phys. Chem. Chem. Phys.*, **2005**, *7*, 3297-3305.
209. F. Weigend, F. Furche and R. Ahlrichs, *J. Chem. Phys.*, **2003**, *119*, 12753-12762.
210. A. Schäfer, C. Huber and R. Ahlrichs, *J. Chem. Phys.*, **1994**, *100*, 5829-5835.
211. K. A. Peterson, D. Figgen, M. Dolg and H. Stoll, *J. Chem. Phys.*, **2007**, *126*, 124101.
212. A. W. Ehlers, M. Böhme, S. Dapprich, A. Gobbi, A. Höllwarth, V. Jonas, K. F. Köhler, R. Stegmann, A. Veldkamp and G. Frenking, *Chem. Phys. Lett.*, **1993**, *208*, 111-114.
213. N. L. Allinger, Y. H. Yuh and J. H. Lii, *J. Am. Chem. Soc.*, **1989**, *111*, 8551-8566.
214. T. A. Halgren, *J. Comput. Chem.*, **1999**, *20*, 730-748.
215. J. Wang, R. M. Wolf, J. W. Caldwell, P. A. Kollman and D. A. Case, *J. Comput. Chem.*, **2004**, *25*, 1157-1174.
216. K. Vanommeslaeghe, E. Hatcher, C. Acharya, S. Kundu, S. Zhong, J. Shim, E. Darian, O. Guvench, P. Lopes and I. Vorobyov, *J. Comput. Chem.*, **2010**, *31*, 671-690.
217. P. Comba and M. Zimmer, *J. Chem. Educ.*, **1996**, *73*, 108.
218. A. K. Rappé, C. J. Casewit, K. Colwell, W. Goddard Iii and W. Skiff, *J. Am. Chem. Soc.*, **1992**, *114*, 10024-10035.
219. M. L. Kouwizjer and P. D. Grootenhuis, *J. Phys. Chem.*, **1995**, *99*, 13426-13436.
220. W. Thiel, *Wiley Interdiscip. Rev. Comput. Mol. Sci.*, **2014**, *4*, 145-157.
221. R. Hoffmann, *J. Chem. Phys.*, **1963**, *39*, 1397-1412.
222. R. Pariser and R. G. Parr, *J. Chem. Phys.*, **1953**, *21*, 767-776.
223. A. D. Becke, *J. Chem. Phys.*, **2014**, *140*, 18A301.
224. M. J. S. Dewar and W. Thiel, *J. Am. Chem. Soc.*, **1977**, *99*, 4899-4907.
225. J. J. P. Stewart, *J. Mol. Model.*, **2013**, *19*, 1-32.
226. J. J. P. Stewart, *J. Mol. Model.*, **2007**, *13*, 1173-1213.
227. E. Fermi, *Rend. Accad. Naz. Lincei*, **1927**, *6*, 32.
228. L. H. Thomas, presented in part at the Math. Proc. Camb. Philos.Soc., **1927**.
229. W. Kohn and L. J. Sham, *Phys. Rev.*, **1965**, *140*, A1133-A1138.
230. P. A. Dirac, presented in part at the Math. Proc. Camb. Philos.Soc., **1930**.
231. M. Gell-Mann and K. A. Brueckner, *Phys. Rev.*, **1957**, *106*, 364-368.
232. J. C. Slater, *Phys. Rev.*, **1951**, *81*, 385-390.
233. J. P. Perdew, K. Burke and M. Ernzerhof, *Phys. Rev. Lett.*, **1996**, *77*, 3865-3868.
234. A. D. Becke, *Phys. Rev. A*, **1988**, *38*, 3098-3100.

235. J. P. Perdew, *Phys. Rev. B*, **1986**, *33*, 8822-8824.
236. K. Burke, J. P. Perdew and Y. Wang, in *Electronic Density Functional Theory*, Springer, **1998**,81-111.
237. J. P. Perdew, M. Ernzerhof and K. Burke, *J. Chem. Phys.*, **1996**, *105*, 9982-9985.
238. A. D. Becke, *J. Chem. Phys.*, **1993**, *98*, 1372-1377.
239. R. Peverati and D. G. Truhlar, *Phil. Trans. R. Soc. A*, **2014**, *372*, 20120476.
240. Y. Zhao and D. G. Truhlar, *J. Chem. Phys.*, **2006**, *125*, 194101.
241. Y.-S. Lin, C.-W. Tsai, G.-D. Li and J.-D. Chai, *J. Chem. Phys.*, **2012**, *136*, 154109.
242. Y. Zhao, N. E. Schultz and D. G. Truhlar, *J. Chem. Phys.*, **2005**, *123*, 161103.
243. R. Peverati and D. G. Truhlar, *J. Chem. Theory Comput.*, **2012**, *8*, 2310-2319.
244. Y. Zhao and D. G. Truhlar, *Theor. Chem. Acc.*, **2008**, *120*, 215-241.
245. Y. Zhao and D. G. Truhlar, *Acc.Chem. Res.*, **2008**, *41*, 157-167.
246. E. R. Johnson, I. D. Mackie and G. A. DiLabio, *J. Phys. Org. Chem.*, **2009**, *22*, 1127-1135.
247. S. Grimme, J. Antony, T. Schwabe and C. Muck-Lichtenfeld, *Org. Biomol. Chem.*, **2007**, *5*, 741-758.
248. S. Grimme, *Wiley Interdiscip. Rev. Comput. Mol. Sci.*, **2011**, *1*, 211-228.
249. M. J. Frisch, G. W. Trucks, H. B. Schlegel, G. E. Scuseria, M. A. Robb, J. R. Cheeseman, G. Scalmani, V. Barone, B. Mennucci, G. A. Petersson, H. Nakatsuji, M. Caricato, X. Li, H. P. Hratchian, A. F. Izmaylov, J. Bloino, G. Zheng, J. L. Sonnenberg, M. Hada, M. Ehara, K. Toyota, R. Fukuda, J. Hasegawa, M. Ishida, T. Nakajima, Y. Honda, O. Kitao, H. Nakai, T. Vreven, J. J. A. Montgomery, J. E. Peralta, F. Ogliaro, M. Bearpark, J. J. Heyd, E. Brothers, K. N. Kudin, V. N. Staroverov, T. Keith, R. Kobayashi, J. Normand, K. Raghavachari, A. Rendell, J. C. Burant, S. S. Iyengar, J. Tomasi, M. Cossi, N. Rega, J. M. Millam, M. Klene, J. E. Knox, J. B. Cross, V. Bakken, C. Adamo, J. Jaramillo, R. Gomperts, R. E. Stratmann, O. Yazyev, A. J. Austin, R. Cammi, C. Pomelli, J. W. Ochterski, R. L. Martin, K. Morokuma, V. G. Zakrzewski, G. A. Voth, P. Salvador, J. J. Dannenberg, S. Dapprich, A. D. Daniels, O. Farkas, J. B. Foresman, J. V. Ortiz, J. Cioslowski and and D. J. Fox *Gaussian 09, Revision D.01*, Gaussian, Inc. Wallingford CT: **2013**.

250. T. D. Kühne, *Wiley Interdisciplinary Reviews: Computational Molecular Science*, **2014**, *4*, 391-406.
251. H. B. Schlegel, J. M. Millam, S. S. Iyengar, G. A. Voth, A. D. Daniels, G. E. Scuseria and M. J. Frisch, *J. Chem. Phys.*, **2001**, *114*, 9758-9763.
252. R. Car and M. Parrinello, *Phys. Rev. Lett.*, **1985**, *55*, 2471-2474.
253. E. T. Mark, *J. Phys.: Condens. Matter.*, **2002**, *14*, R1297.
254. A. Warshel and M. Levitt, *J. Mol. Biol.*, **1976**, *103*, 227-249.
255. M. Karplus, *Annu. Rev. Biophys. Biomol. Struct.*, **2006**, *35*, 1-47.
256. M. Levitt, *Nat. Struct. Mol. Biol.*, **2001**, *8*, 392-393.
257. U. C. Singh and P. A. Kollman, *J. Comput. Chem.*, **1986**, *7*, 718-730.
258. J. Gao and M. A. Thompson, *Combined Quantum Mechanical and Molecular Mechanical Methods*, ACS Publications, **1998**.
259. L. W. Chung, H. Hirao, X. Li and K. Morokuma, *Wiley Interdiscip. Rev. Comput. Mol. Sci.*, **2012**, *2*, 327-350.
260. P. Comba and R. Remenyi, *Coord. Chem. Rev.*, **2003**, *238*, 9-20.
261. P. Comba, *Coord. Chem. Rev.*, **1999**, *182*, 343-371.
262. A. Bentz, P. Comba, R. J. Deeth, M. Kerscher, B. Seibold and H. Wadepohl, *Inorg. Chem.*, **2008**, *47*, 9518-9527.
263. P. Comba, B. Martin, A. Sanyal and H. Stephan, *Dalton Trans.*, **2013**, *42*, 11066-11073.
264. R. J. Deeth, *Coord. Chem. Rev.*, **2001**, *212*, 11-34.
265. R. Brodbeck and R. J. Deeth, *Dalton Trans.*, **2011**, *40*, 11147-11155.
266. N. Gresh, C. Policar and C. Giessner-Prettre, *J. Phys.Chem. A*, **2002**, *106*, 5660-5670.
267. P. Li and K. M. Merz, *Chem. Rev.*, **2017**, *117*, 1564-1686.
268. J. Wang, S. Manivasagam and A. K. Wilson, *J. Chem. Theory Comput.*, **2015**, *11*, 5865-5872.
269. W. Jiang, N. J. DeYonker and A. K. Wilson, *J. Chem. Theory Comput.*, **2012**, *8*, 460-468.
270. F. De Angelis, S. Fantacci and A. Sgamellotti, *Coord. Chem. Rev.*, **2006**, *250*, 1497-1513.

271. G. Kresse and J. Hafner, *Phys.Rev. B*, **1993**, *48*, 13115-13118.
272. M. A. Caro, O. Lopez-Acevedo and T. Laurila, *J. Chem. Theory Comput.*, **2017**, *13*, 3432-3441.
273. A. Stirling, N. N. Nair, A. Lledós and G. Ujaque, *Chem. Soc. Rev.*, **2014**, *43*, 4940-4952.
274. J. M. Skelton, T. H. Lee and S. R. Elliott, *Appl. Phys. Lett.*, **2012**, *101*, 024106.
275. M. J. S. Dewar, *Int. J. Quantum Chem.*, **1988**, *34*, 557-566.
276. J. Jover and N. Fey, *Chem. Asian J.*, **2014**, *9*, 1714-1723.
277. P. Liu, B. L. H. Taylor, J. Garcia-Lopez and K. N. Houk, in *Handbook of Metathesis*, Wiley-VCH Verlag GmbH & Co. KGaA, **2015**,199-252.
278. C. Adlhart and P. Chen, *J. Am. Chem. Soc.*, **2004**, *126*, 3496-3510.
279. C. J. Cramer and D. G. Truhlar, *Chem. Rev.*, **1999**, *99*, 2161-2200.
280. J. Tomasi, B. Mennucci and R. Cammi, *Chem. Rev.*, **2005**, *105*, 2999-3094.
281. J. B. Foresman, T. A. Keith, K. B. Wiberg, J. Snoonian and M. J. Frisch, *J. Phys. Chem.*, **1996**, *100*, 16098-16104.
282. J. Tomasi and M. Persico, *Chem. Rev.*, **1994**, *94*, 2027-2094.
283. J. Thyssen, T. Fleig and H. J. A. Jensen, *J. Chem. Phys.*, **2008**, *129*, 034109.
284. B. Mennucci, *Wiley Interdiscip. Rev. Comput. Mol. Sci.*, **2012**, *2*, 386-404.
285. J. Tomasi, E. Cancès, C. S. Pomelli, M. Caricato, G. Scalmani, M. J. Frisch, R. Cammi, M. V. Basilevsky, G. N. Chuev and B. Mennucci, in *Continuum Solvation Models in Chemical Physics*, John Wiley & Sons, Ltd, **2007**,1-123.
286. A. V. Marenich, C. J. Cramer and D. G. Truhlar, *J. Phys. Chem. B*, **2009**, *113*, 6378-6396.
287. C. E. Dykstra, *J. Comput. Chem.*, **1988**, *9*, 476-487.
288. J. Simons, P. Joergensen, H. Taylor and J. Ozment, *J. Phys. Chem.*, **1983**, *87*, 2745-2753.
289. T. Helgaker, E. Uggerud and H. J. A. Jensen, *Chem. Phys. Lett.*, **1990**, *173*, 145-150.
290. F. Bernardi, M. Olivucci and M. A. Robb, *Chem. Soc. Rev.*, **1996**, *25*, 321-328.
291. V. Barone, *J. Chem. Phys.*, **1994**, *101*, 10666-10676.
292. J. Baker and F. Chan, *J. Comput. Chem.*, **1996**, *17*, 888-904.
293. J. Baker, *J. Comput. Chem.*, **1986**, *7*, 385-395.

294. H. B. Schlegel, *J. Comput. Chem.*, **1982**, *3*, 214-218.
295. J. C. Mauro, R. J. Loucks and J. Balakrishnan, *J. Phys. Chem. A*, **2005**, *109*, 9578-9583.
296. C. Peng, P. Y. Ayala, H. B. Schlegel and M. J. Frisch, *J. Comput. Chem.*, **1996**, *17*, 49-56.
297. C. Peng and H. Bernhard Schlegel, *Isr. J. Chem.*, **1993**, *33*, 449-454.
298. T. A. Halgren and W. N. Lipscomb, *Chem. Phys. Lett.*, **1977**, *49*, 225-232.
299. P. Y. Ayala and H. B. Schlegel, *J. Chem. Phys.*, **1997**, *107*, 375-384.
300. K. B. Wiberg, *Tetrahedron*, **1968**, *24*, 1083-1096.
301. I. Mayer, *J. Comput. Chem.*, **2007**, *28*, 204-221.
302. T. A. Manz, *RSC Adv.*, **2017**, *7*, 45552-45581.
303. T. K. Brunck and F. Weinhold, *J. Am. Chem. Soc*, **1979**, *101*, 1700-1709.
304. R. F. W. Bader, *Acc. Chem. Res*, **1985**, *18*, 9-15.
305. R. F. W. Bader, in *Encyclopedia of Computational Chemistry*, John Wiley & Sons, Ltd, **2002**.
306. R. F. W. Bader, *Atoms in Molecules: A Quantum Theory*, Clarendon Press,Oxford, UK, , **1990.**
307. T. A. Keith *AIMAll*, *14.04.17*; TK Gristmill Software, Overland Park KS, USA, 2014 **2014**.
308. J. Vaara, *Phys. Chem. Chem. Phys.*, **2007**, *9*, 5399-5418.
309. R. Ditchfield, *Mol. Phys.*, **1974**, *27*, 789-807.
310. M. Schindler and W. Kutzelnigg, *J. Chem. Phys.*, **1982**, *76*, 1919-1933.
311. M. Schindler and W. Kutzelnigg, *J. Am. Chem. Soc.*, **1983**, *105*, 1360-1370.
312. A. E. Hansen and T. D. Bouman, *J. Chem. Phys.*, **1985**, *82*, 5035-5047.
313. T. A. Keith and R. F. W. Bader, *Chem. Phys. Lett.*, **1992**, *194*, 1-8.
314. T. A. Keith and R. F. W. Bader, *Chem. Phys. Lett.*, **1993**, *210*, 223-231.
315. J. R. Cheeseman, G. W. Trucks, T. A. Keith and M. J. Frisch, *J. Chem. Phys.*, **1996**, *104*, 5497-5509.
316. T. Gregor, F. Mauri and R. Car, *J. Chem. Phys.*, **1999**, *111*, 1815-1822.
317. V. r. Sychrovský, J. Gräfenstein and D. Cremer, *J. Chem. Phys.*, **2000**, *113*, 3530-3547.

318. T. Helgaker, M. Watson and N. C. Handy, *J. Chem. Phys.*, **2000**, *113*, 9402-9409.
319. L. B. Casabianca and A. C. d. Dios, *J. Chem. Phys.*, **2008**, *128*, 052201.
320. P. v. R. Schleyer, C. Maerker, A. Dransfeld, H. Jiao and N. J. R. v. E. Hommes, *J. Am. Chem. Soc.*, **1996**, *118*, 6317-6318.
321. P. v. R. Schleyer, M. Manoharan, Z.-X. Wang, B. Kiran, H. Jiao, R. Puchta and N. J. van Eikema Hommes, *Org. Lett.*, **2001**, *3*, 2465-2468.
322. Z. Chen, C. S. Wannere, C. Corminboeuf, R. Puchta and P. v. R. Schleyer, *Chem. Rev.*, **2005**, *105*, 3842-3888.
323. M. K. Cyrañski, T. M. Krygowski, M. Wisiorowski, N. J. van Eikema Hommes and P. v. R. Schleyer, *Angew. Chem. Int. Ed.*, **1998**, *37*, 177-180.
324. J. O. C. Jiménez-Halla, E. Matito, J. Robles and M. Solà, *J. Organomet. Chem.*, **2006**, *691*, 4359-4366.
325. R. Herges and D. Geuenich, *J. Phys. Chem. A*, **2001**, *105*, 3214-3220.
326. D. Geuenich, K. Hess, F. Köhler and R. Herges, *Chem. Rev.*, **2005**, *105*, 3758-3772.
327. K. An, T. Shen and J. Zhu, *Organometallics*, **2017**, *36*, 3199-3204.

Chapter 2

Unusual Bonding Features of Metallacycles of Alkene and Alkyne Metathesis

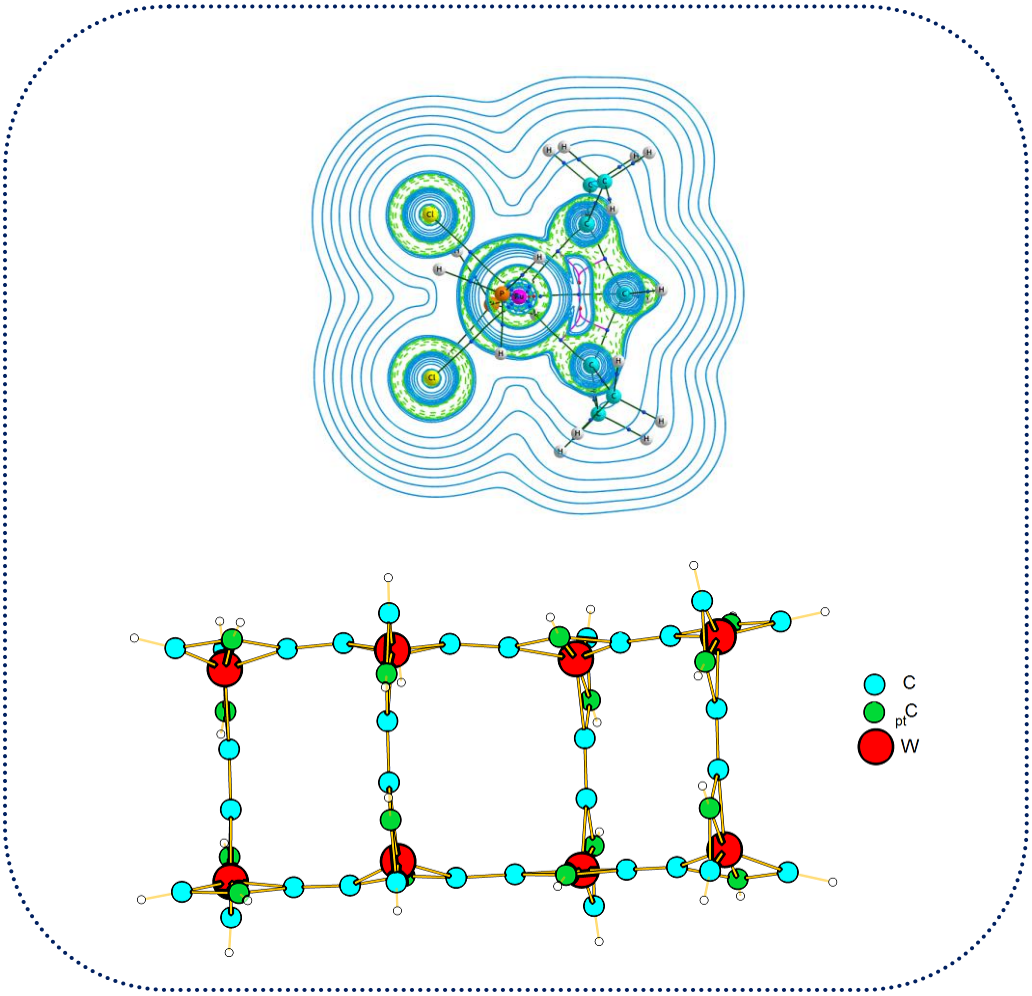

Part A: Hypercoordinate β-Carbon in Grubbs and Schrock Olefin Metathesis Metallacycles

2.1 Abstract

Metallacyclobutane (MCB) intermediates of Grubbs and Schrock olefin metathesis catalysts are well-known for their unusually short single bond-like metal to C_β distance and unusually long $C_\alpha C_\beta$ distances. From the analysis of structural, bond order, electron density and ^{13}C NMR data of a large variety of MCB systems, we show that the C_β of the metallacycle possesses pentacoordinate geometry due to agostic type interaction of the metal with the $C_\alpha C_\beta$ bonds. The pentacoordination of C_β to the metal center is characterized by a catastrophe ring critical point (RCP) in the quantum theory of atoms-in-molecule (QTAIM) analysis. Fine tuning of the ligand environment changes the catastrophe point to a fifth bond critical point (BCP) which is clearly brought out in the case of two ruthenium olefin metathesis systems. Several Ru and W agostic MCB complexes exhibiting pentacoordinate C_β as well as their non-agostic isomers have been reported at the BP86/def2-TZVPP level of DFT. The agostic systems showed significant bond order between metal and C_β (0.17 – 0.36), single bond-like electron density values at the catastrophe RCP/BCP and the significantly large difference in ^{13}C NMR chemical shift values between C_α and C_β atoms.

2.2 Introduction

The Chauvin mechanism[1] of olefin metathesis, applicable to Grubbs-, Schrock- and other related complexes is one of the most elegant mechanistic pathways known in synthetic organic chemistry for the last five decades.[2-3] This general mechanism suggests the formation of a metallacyclobutane (MCB) as a key intermediate in the reaction. Though the catalyst and the olefin-coordinated metal complex possess 16-electron configuration, the MCB, due to its +4 oxidation state is formally a 14-electron system. Therefore, in the early development of metathesis mechanism, MCB has been

speculated as a transition state whereas later experimental and theoretical studies have confirmed it as an intermediate.[4-33] The most striking feature of MCB structure is the unusually short MC_β distance and long CC bond lengths than usual. Such unusual structural features of ruthenacyclobutane (RuCB) have been supported by ^{13}C and proton NMR techniques[14] while direct evidence from crystal structures exist for tungstenacyclobutane (WCB).[4, 34-35]

Though the single bond-like RuC_β and WC_β distances in trigonal bipyramidal (TBP) configuration of a metallacycle is described to be well within the range of a typical bonding distance, a clear identification of this type of metal-C_β interaction as a regular bond is yet to be made. Proposing a regular bond between metal and C_β in MCB will lead to the immediate identification of a large number of pentacoordinate carbons in organometallic chemistry. The hypercoordination of carbon is a well-established phenomenon both experimentally and theoretically.[36-41] Most of the hypercoordinate carbon centers known are either part of an organic system (**a**[42]) or are coordinated to non-metals (**b**[39]).[36 42-47] Some rare examples of hypercoordination of carbon to metal centers are CLi_5 (**c**[48]), CLi_6, $HC[Au(PPh_3)]_4^{2+}$ and the iron-molybdenum nitrogenase cofactor.[38, 48-50]

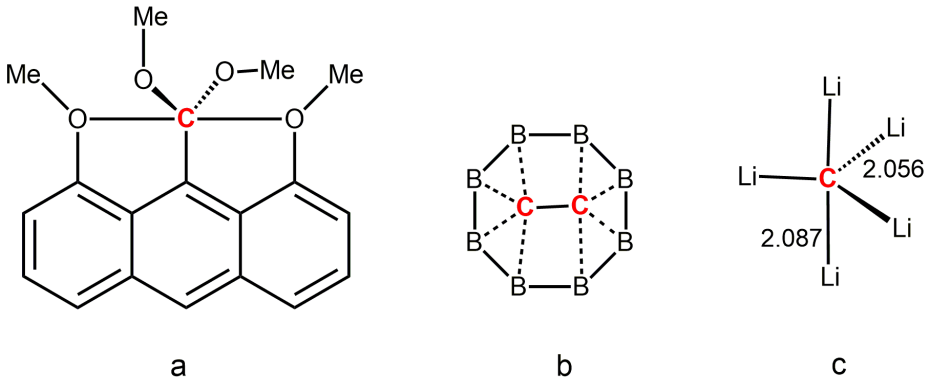

Figure 2.1 Examples of molecules containing hypercoordinate carbon (red coloured).

The main aim of this study is to show that C_β possesses an undeniable amount of pentacoordination in the metallacycle intermediate of Grubbs and Schrock olefin metathesis catalysts. We also attempt to tune the strength of the metal-C_β interaction in

the Grubbs systems by varying the ligand environment of the metal center. In certain cases, the RuC_β interaction attains extreme prominence and leads to the formation of a fifth bond path in the quantum theory of atoms-in-molecule (QTAIM) electron density analysis. Further, geometrical, bond order and ^{13}C NMR data will be used to support our arguments to ascertain the fifth coordination of C_β in MCBs. We start with a systematic study on ruthenacyclobutanes in the TBP and square pyramidal (SP) configurations. This is followed by a study on the X-ray structures reported for tungstenacyclobutanes in the TBP configuration along with a comparison on the SP isomer.

2.3 Computational Details

All the calculations have been done at the BP86/def2-TZVPP level.[51-53] This level of theory is previously used in the study of metallacyclobutadienes and found to yield structural data in good agreement with experimental results.[54-57] For Ru and W, the def2-TZVPP basis set augmented with effective core potential is used. Vibrational frequency calculation is performed on all optimized structures to verify their minimum energy configuration (zero imaginary frequency). The topological analysis of electron density (QTAIM analysis) is done using the AIMAll program.[58] Wiberg bond order (W_{bo})[59] for all the complexes is calculated using Natural Bond Orbital (NBO) analysis[60] implemented in G09. For NMR calculation, the Gauge-Independent Atomic Orbital (GIAO) method is used.[61-62] Since this chapter deals with the bonding analysis in MCB systems, gas phase calculations are adequate for such analyses. A full optimization in solvent phase is not considered as they are computationally more demanding and they do not alter the bonding scenario in MCB systems.

2.4 Results and Discussions

2.4.1 Structural Analysis of Ruthenacyclobutanes

The 14-electron ruthenacyclobutane, the key intermediate of the widely accepted dissociative olefin metathesis mechanism possesses trigonal bipyramidal (TBP) geometry. The halo ligands occupy apical positions of the TBP while the equatorial positions are fulfilled by one N-heterocyclic carbene/phosphine ligand and two RuC_α

bonds of the metallacycle (Scheme 2.1). The ligands considered in the present study include fluoro, chloro, bromo and iodo ligands at the apical positions and N-heterocyclic carbene (1,3-bis(methyl)-4,5-dihydroimidazole and 1,3-bis(2,4,6-trimethylphenyl)-4,5-dihydroimidazole), phosphines (PH_3, PH_2Me, $PHMe_2$, PMe_3, and PCy_3) and pyridine ligands at the equatorial positions. The PCy_3 ligand is used in Grubbs first generation catalyst while N-heterocyclic carbenes (NHC) are well known in Grubbs second generation catalyst. Sometimes pyridine is used as a leaving group instead of PCy_3 in metathesis catalysts.[63] Further, the effect of methyl substitution on α-carbon atoms of the metallacycle as well as the effect of o-isopropoxyphenyl on one of the α-carbons has been studied. Recently Jaque *et al.*[26] reported that alkyl substituents at the α-carbons improve the stability of the ruthenacyclobutanes.

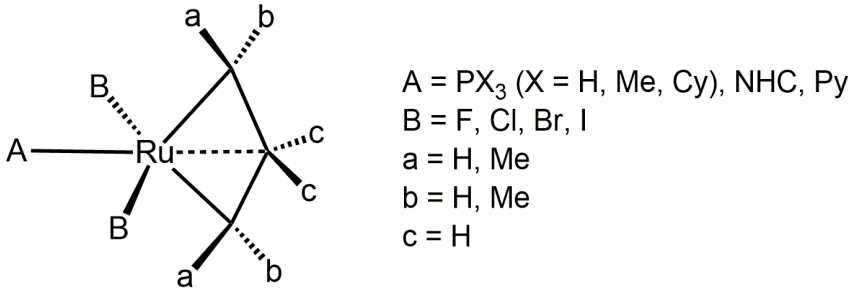

Scheme 2.1 Representation of a 14-electron MCB of TBP geometry.

The optimized structure of all the 14-electron ruthenacyclobutane complexes **1** – **16** with the general formula $Ru(CR_2CH_2CR_2)X_2L$ where R = H/CH_3/o-isopropoxyphenyl; X = F, Cl, Br, I; L = NHC, PCy_3, Py, NC_5F_5 are shown in Figure 2.2 along with the important structural parameters such as $C_\alpha C_\beta$, RuC_α, RuC_β bond distances and $C_\alpha C_\beta C_\alpha$ bond angle. Among these structures **9**, **11**, and **12** are the ruthenacyclobutane intermediates of, Grubbs second, Hoveyda-Grubbs[64] and Grubbs first generation catalysts. The **1** - **16** complexes are characterized by significantly elongated $C_\alpha C_\beta$ bonds (1.581 - 1.612 Å) and RuC_α bonds (1.936 - 2.021 Å) shorter than a typical single bond distance ~2.10 Å. The single bond-like RuC_β distance (2.169 - 2.265 Å) is yet another striking structural feature of all these complexes. Further, the $C_\alpha C_\beta C_\alpha$ bond angle (114.7 - 121.7°) is significantly deviated from the typical C_{sp3} angle 109.5°. All these structural

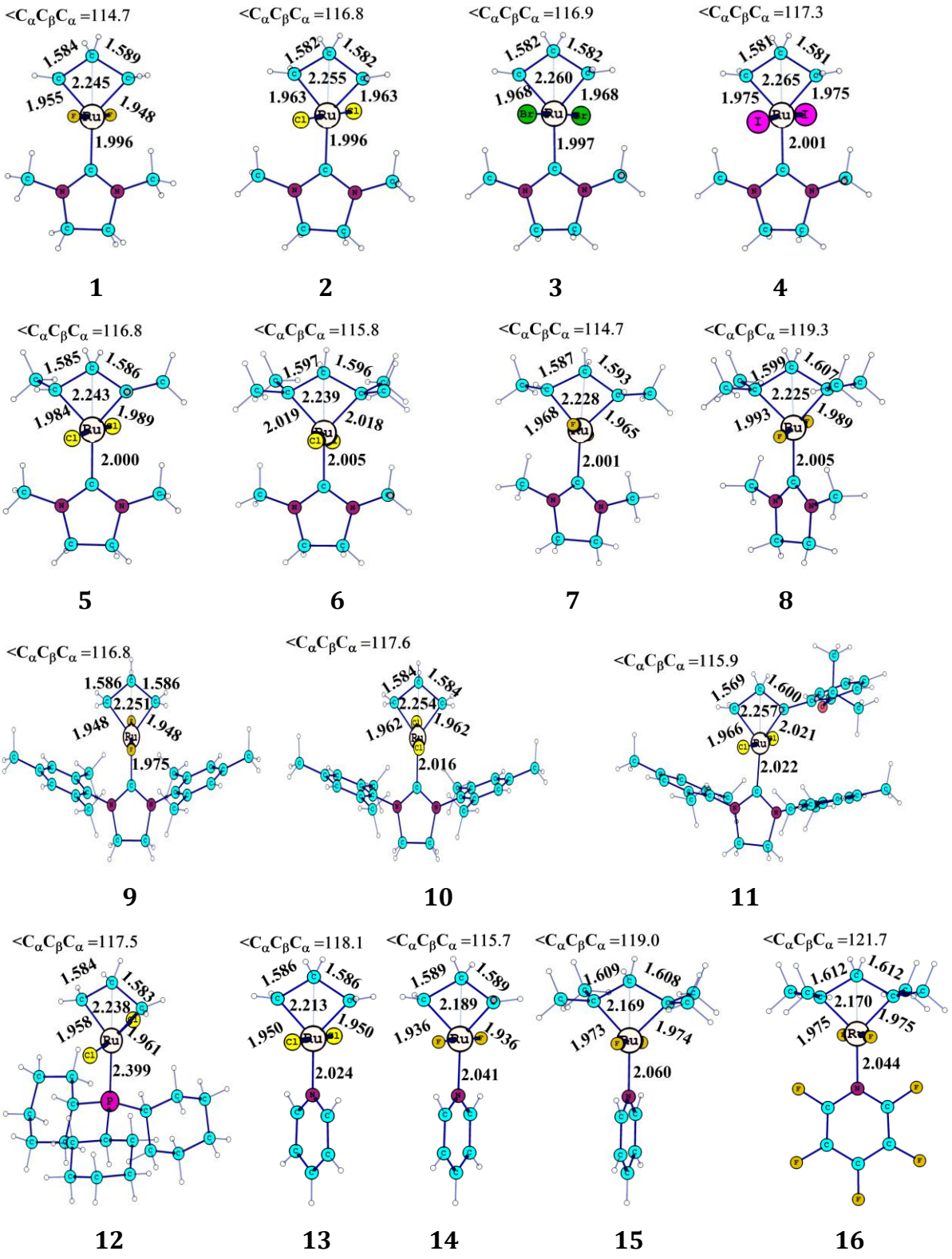

Figure 2.2 Optimized geometries of the 14-electron agostic complexes **1 – 16**.

features clearly suggest the existence of unusual metal-carbon bonding interactions in the metallacycle.

Among the fluoro (**1**), chloro (**2**), bromo (**3**) and iodo (**4**) ligated Grubbs second generation metathesis intermediates, the $C_\alpha C_\beta$ distance decreases from **1** to **4** in the range 1.589 – 1.581 Å whereas the RuC_β and RuC_α distances increase from **1** to **4**; 2.245 – 2.265 Å for the former and 1.948 - 1.975 Å for the latter. These results suggest that with an increase in electron rich character of Ru from **1** - **4**, the RuC_β interaction decreases. Complex **1** shows a slight amount of puckering at the C_β center with $RuC_\alpha C_\beta C_\alpha$ dihedral angle 14.0°, and in all other cases, the metallacycle is planar. Apart from these geometrical parameters, fluoro ligated system **1** shows a twist angle (θ) 25.8° between the plane of NHC ring and the plane of the metallacycle defined by Ru and two C_α atoms. The θ, for the chloro, bromo, and iodo ligated systems **2**, **3** and **4** are 18.0, 10.7 and 2.9°, respectively suggesting that the halo ligands also provide some amount of steric hindrance to the orientation of the NHC ring. In the case of **1**, a CH bond in the methyl substituent shows CH---F interaction with a distance 2.076 Å.

Compared to the unsubstituted **2**, the corresponding methyl substituted **5** at C_α position shows slight elongation of $C_\alpha C_\beta$ and RuC_α bonds and slight compression of RuC_β bond. With dimethyl substitution on each C_α position (**6**), these distance features are further enhanced suggesting that methyl substitution on the C_α-position improves RuC_β interaction by lowering the RuC_α and $C_\alpha C_\beta$ interactions. The steric effect of the methyl group is obvious in **6** as the unhindered C_β comes closer to the metal center. This aspect is clearly seen in $C_\alpha C_\beta C_\alpha$ angle as a value of 116.8° in **2** increases to 117.6° in **5** and 119.0° in **6**. Very similar structural features can be obtained by comparing the unsubstituted **1** with the corresponding dimethyl substituted **7** or tetramethyl substituted **8**.

In **9**, **10** and **11**, the NHC ring plane is coplanar to the metallacycle which can be mainly attributed to the steric hindrance offered by the mesityl substituent to the halo ligands as another orientation of the NHC will give rise to electrostatically unfavourable approach of the π-region of mesityl substituent and the lone pair region of the halo

ligands. RuC_α bond of **9** is 0.014 Å shorter than **10** whereas RuC_β bond of **9** is only 0.003 Å shorter than **10**. In both cases, $C_\alpha C_\beta$ distances (1.584 and 1.586 Å) are significantly longer than a typical CC single bond. The geometrical features of the Grubbs-Hoveyda intermediate **11** agree close to those of **10** except for the $C_\alpha C_\beta$ bond defined by the o-isopropoxyphenyl bearing α-carbon shows more elongation and the other shows more contraction than the typical values. In the case of Grubbs first generation RuCB **12**, the RuC bond distances and the CCC bond angle parameters show a close resemblance to the values observed for the second generation RuCB **10**. The shorter RuC_β (2.238 Å) bond distance of the Grubbs first generation metallacycle **12** compared to the second generation metallacycle **10** (2.254 Å) is noteworthy.

The pyridine ligated MCBs (**13 – 16)** show shorter RuC_α, and RuC_β bond distances compared to their corresponding phosphine or NHC ligated systems. For instance, in the case of **13**, the RuC_α bond distance 1.950 Å and RuC_β bond distance 2.213 Å are significantly shorter than those of the analogs phosphine complex **12** as well as the NHC complex **2** and **10**. Further, **13** – 1**6** show more elongated CC bonds than their corresponding phosphine or NHC ligated systems.

Though the dissociative 14-electron pathway is the most widely accepted olefin metathesis mechanism, the associative 16-electron pathway can also lead to CC bond metathesis activity.[13] The ruthenacyclobutane formed in this pathway for four Grubbs first generation systems (**17, 18, 19** and **20**) and one Grubbs second generation system (**21**) are also considered in this study (Figure 2.3). The **17**, **18**, **19** and **20** systems differ only in the type of phosphine ligand used, *viz*. PH_3, PH_2Me, $PHMe_2$, and PMe_3, respectively. This ligand variation is useful to assess the stereoelectronic effect of alkyl substitution on phosphorus. In **21**, the unsubstituted NHC and one PMe_3 phosphine ligand are coordinated to the metal. The **17** - **21** complexes possess octahedral geometry as they show a nearly orthogonal orientation of the chloro ligands (ClRuCl angle 79.0 – 95.0°). The structural features of the metallacycle region of **17** - **21** are similar to the structural features of the 14-electron metallacycles obtained in the dissociative pathway. They show single bond-like distance parameters for RuC_β

(~2.200 Å), unusually long $C_\alpha C_\beta$ single bond distances (1.580 - 1.680 Å) and unusually large $C_\alpha C_\beta C_\alpha$ bond angle (122.0 – 126.0°). It is noteworthy that all these features are more dominant in the 16-electron metallacycles than the 14-electron metallacycles.

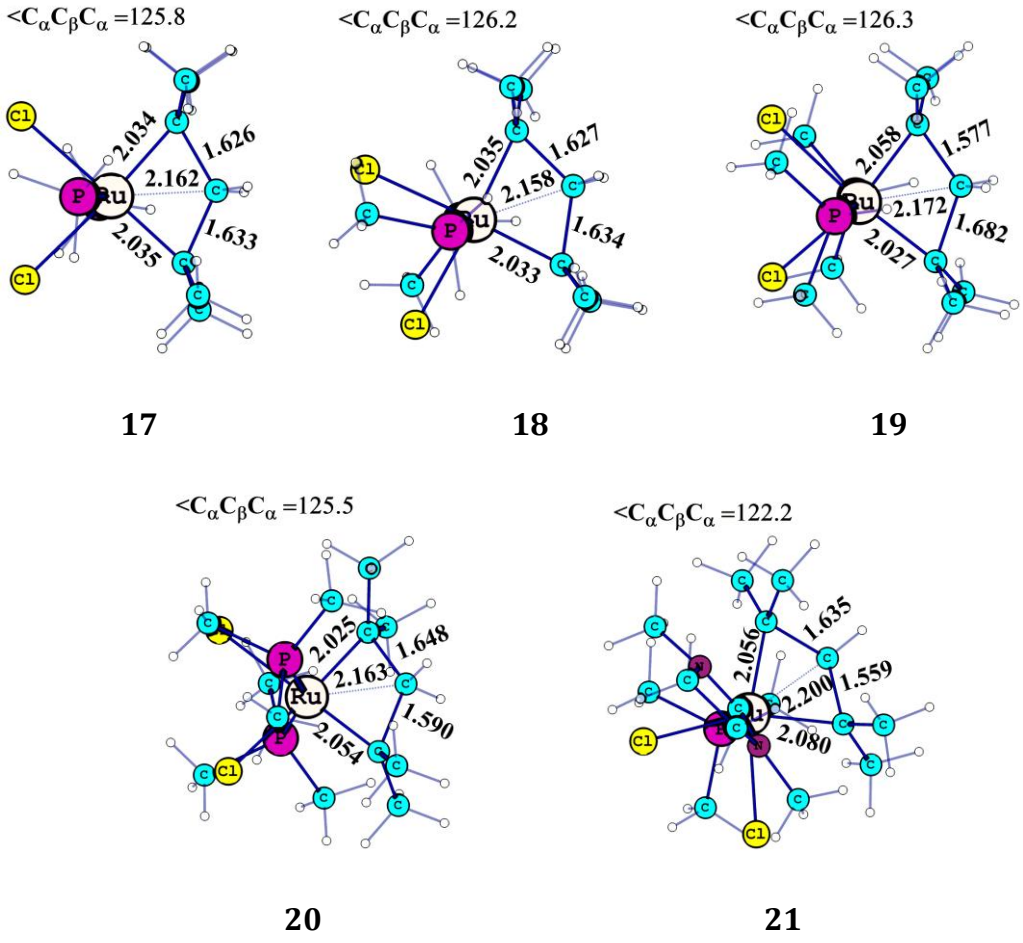

Figure 2.3 Optimized geometries of 16-electron agostic complexes.

The unusually long $C_\alpha C_\beta$ bonds in the ruthenacyclobutanes of 14-electron complexes (**1** - **16**) as well as 16-electron complexes (**17** - **21**) can be interpreted on the basis of α,β-CCC agostic interaction.[15] The molecular orbital responsible for the agostic interaction is shown for the 14-electron complex **2** and 16-electron complex **17** (Figure 2.4). It appears that the highly electron deficient Ru(IV) in a desperate search for electrons finds a way by directly interacting with both the CC σ-bonds.[15] The agostic sharing of the electron density of the CC σ-bonds to the metal leads to significant activation of those bonds in all the complexes (**1** - **21**). At this point, it is imperative to

think about the existence of non-agostic isomers of **1** - **21** as they will provide a clear demarcation between the agostic versus non-agostic consequences of structural changes in the metallacycle.

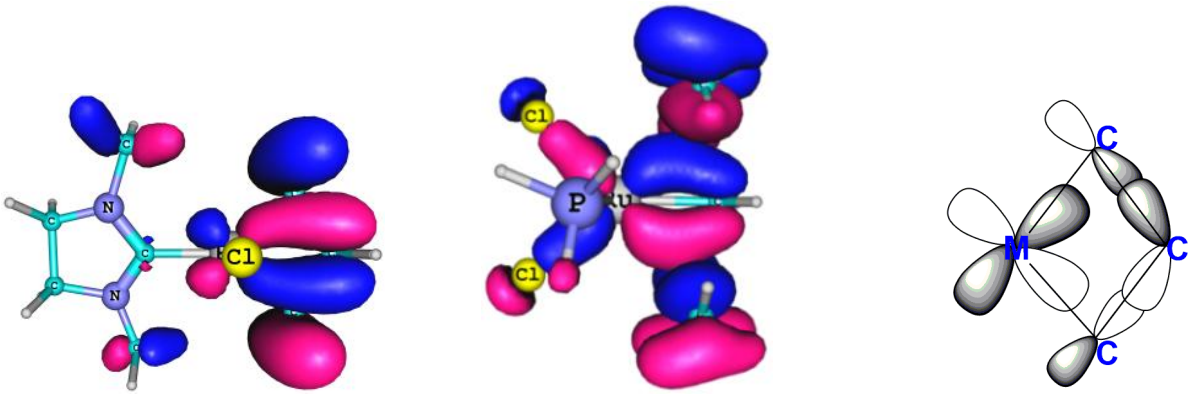

(a) (b) (c)

Figure 2.4 Molecular orbitals showing α,β-CCC agostic interaction in (a) **2** and in (b) **17**. (c) A schematic diagram showing the orbital overlap between the metal and the CCC region.

The SP configuration of all the 14-electron metallacycles exists as energy minimum (**1'** - **16'**). These systems show typical CC single bond distance 1.52 - 1.54 Å and typical RuC_{α} single bond distance 2.100 - 2.200 Å. Moreover, the RuC_{β} bond distance of all these structures are significantly longer (2.690 - 2.790 Å) than any of the agostic complexes while their $C_{\alpha}C_{\beta}C_{\alpha}$ bond angle (96.0 – 102.0°) is substantially smaller than a C_{sp3} angle. Some representative examples (**2'** and **6'**) showing these structural features are given in Figure 2.5. These structural data clearly suggest that RuC_{β} distances are well outside the bonding distances of these atoms, confirming the absence of agostic type interaction in **1'** - **16'**. Hence these systems are described as 'non-agostic complexes' to distinguish them from the agostic isomers **1** - **16**. Among the 14-electron agostic TBP structures and their non-agostic SP isomers, the agostic one is more stable except for the case of **1**. The **1** is 3.21 kcal/mol less stable than the non-agostic isomer **1'** while all other agostic complexes show 1.19 - 15.90 kcal/mol more stabilization than their non-agostic isomers.

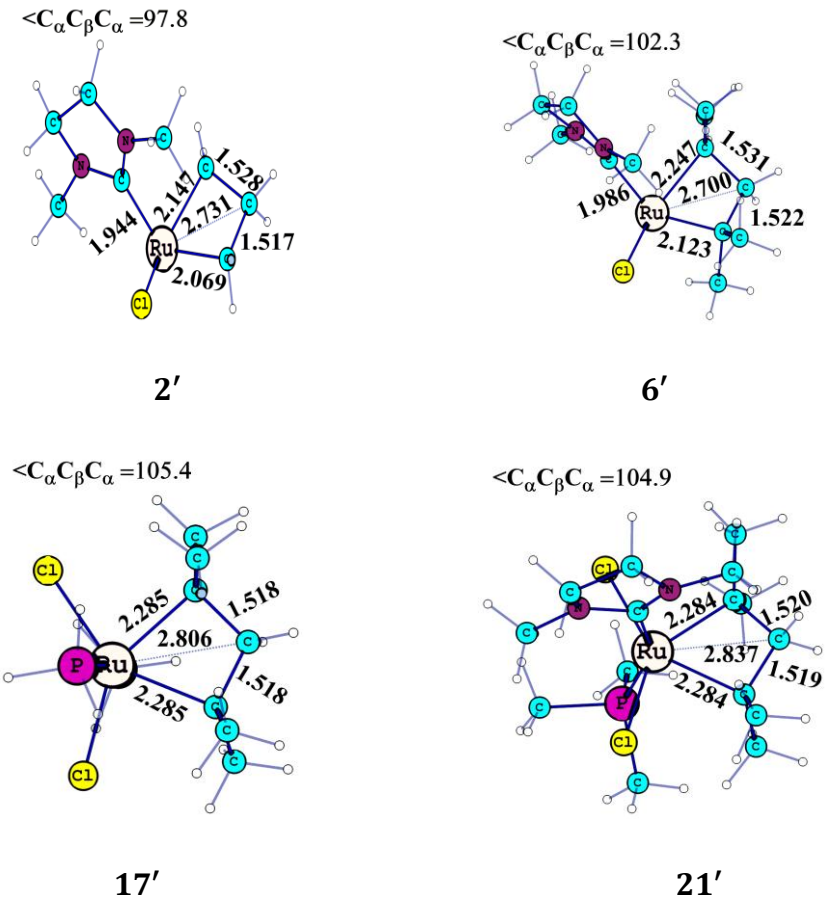

Figure 2.5 Optimized geometries of 14- and 16-electron non-agostic complexes.

It is noteworthy that non-agostic isomers **17'** - **21'** exist for all the 16-electron agostic metallacycles **17** - **21**. These systems show values of CC, RuC_α and RuC_β bond lengths and CCC bond angle very similar to that of 14-electron non-agostic complexes. Two representative examples **17'** and **21'** are depicted in Figure 2.5 to illustrate these structural features. One intriguing fact is that the structures of both agostic (**17** - **21**) and non-agostic (**17'** - **21'**) complexes can be described in a distorted octahedral configuration. If we choose the N-heterocyclic carbene/phosphine ligands to define the axial positions of these complexes, the halo ligands and the RuC_α bonds can be used to define the equatorial positions. The distortion from the octahedral geometry is higher in non-agostic complexes than agostic complexes as the former systems show wider ClRuCl bond angle (132.0 – 165.0°) than the latter. Mainly these two types of complexes differ in the metal-to-ligand and CC bond distance parameters which suggest the

possibility of a rare condition of bond stretch isomerism in organometallics.[65-67] Since the bond stretch isomerism is a highly debated subject, and the focus of the paper is on the hypercoordination of carbon, further study on this phenomenon in CC bond metathesis is discussed in Chapter 3. In the case of 16- electron MCB, all non-agostic models are more stable than the agostic models except **18** by 1.70 - 10.30 kcal/mol. The **18** is 2.57 kcal/mol more stable than the non-agostic **18'**.

2.4.2 Bond Order Analysis of Ruthenacyclobutanes

Table 2.1 compares the Wiberg bond order (W_{bo}) for the agostic complexes with that of non-agostic complexes of ruthenium. All the 14-electron agostic complexes show a bond order ~0.20 for Ru and C_β interaction suggesting significant bonding effect. Hence, the single bond-like RuC_β distance observed in these complexes cannot be attributed to the structural restriction imposed by the four-membered ring. The RuC_α bond order above 0.95 is observed for those systems without any substitution in the ring. Once the ring has a substitution on the C_α, the RuC_α bond order drops down to 0.931 - 0.869. This indicates steric influence of the substituents on the strength of the bonds. In all the 14-electron agostic cases, the CC bond order (0.932 – 0.858) is less than 1.00, whereas that of non-agostic complexes (0.990 – 1.030) indicate stronger bonds. The bond order ~0.03 observed for the RuC_β interaction in non-agostic complexes suggests no bonding effect between Ru and C_β.

The RuC_β bond order (0.301 – 0.362) observed for the 16-electron agostic complexes **17** - **21** suggests that the bonding interaction between Ru and C_β is stronger in these systems than the corresponding 14-electron agostic complexes. The increase in the RuC_β interaction leads to weakening of the CC bonds as they show bond order 0.793 – 0.858. The non-agostic 16-electron complexes **17'** - **21'** show RuC_β bond order ~0.03 suggesting practically no bonding interaction between the two atoms. The correlation plot in Figure 2.6 shows that the increased bonding effect between Ru and C_β proportionally decreases the bonding effect between C_α and C_β atoms. This also means that increasing the α,β-CCC agostic interaction increases the bonding effect between Ru and C_β.

Table 2.1 Wiberg bond order (W_{bo}) values for the agostic **1** - **21** and non-agostic **1'** - **21'** complexes

	Agostic complex			Non-agostic complex		
MCB	RuC_α	$C_\alpha C_\beta$	RuC_β	RuC_α	$C_\alpha C_\beta$	RuC_β
1	1.008	0.908	0.190	0.858	1.029	0.025
2	0.995	0.925	0.198	0.852	1.024	0.031
3	0.989	0.928	0.195	0.845	1.025	0.032
4	0.978	0.932	0.191	0.834	1.026	0.032
5	0.931	0.912	0.207	0.787	1.011	0.034
6	0.869	0.895	0.214	0.722	0.994	0.038
7	0.951	0.918	0.201	0.800	1.011	0.024
8	0.893	0.896	0.211	0.760	0.991	0.035
9	1.009	0.932	0.178	0.845	1.026	0.025
10	0.994	0.925	0.197	0.821	1.028	0.029
11	0.919	0.897	0.195	0.761	1.019	0.032
12	0.994	0.924	0.204	0.787	1.030	0.024
13	1.070	0.905	0.251	0.913	1.026	0.036
14	1.085	0.911	0.253	0.886	1.029	0.028
15	0.875	0.866	0.278	0.757	0.999	0.030
16	0.844	0.858	0.294	0.736	1.002	0.029
17	0.783	0.829	0.358	0.674	1.001	0.030
18	0.785	0.823	0.362	0.681	1.001	0.030
19	0.780	0.829	0.347	0.677	1.003	0.031
20	0.777	0.793	0.346	0.674	1.004	0.033
21	0.770	0.800	0.301	0.683	0.996	0.031

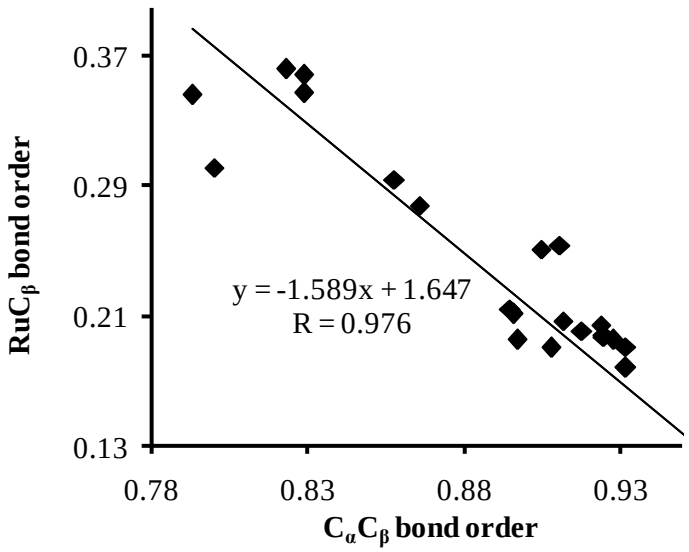

Figure 2.6 Correlation between $C_\alpha C_\beta$ and RuC_β bond orders.

2.4.3 QTAIM Analysis

The QTAIM parameters such as electron density (ρ) at the bond critical point (BCP) and ρ at the ring critical point (RCP) for the metallacycle region are given in Table 2.2. The ρ values in the range 0.135 - 0.158 au and 0.197 – 0.209 au are respectively observed for the BCP's of RuC_α and $C_\alpha C_\beta$ bonds of **1 – 16** whereas the corresponding values for the non-agostic complex **1' – 16'** are in the range 0.102 – 0.131 and 0.243 - 0.255 au. The ρ values of RCPs clearly indicate that agostic complexes show significant electron concentration (0.070 – 0.083 au) towards the center of the metallacycle than the non-agostic systems (0.052 - 0.061 au).

The QTAIM molecular graph along with the Laplacian ($\nabla^2\rho$) contour plots for the metallacycle region in the plane of metallacycle for a representative Grubbs system **2** and its non-agostic isomer **2'** are given in Figure 2.7. In the molecular graph, dark green lines correspond to bond paths while pink lines indicate ring paths connecting BCP and RCP. Dashed green curves show area of relative electron concentration and solid blue curves are areas of relative charge depletion. The Laplacian contours of the agostic complexes are markedly different from the non-agostic complexes. It is clear from Figure 2.7a that charge concentration from C_β towards the metal center is significant in the agostic complex **2** whereas Figure 2.7b shows significant charge depletion from the

Table 2.2 QTAIM parameters for agostic **1** - **21** and non-agostic **1'** - **21'** complexes (all values in au)

	Agostic complex			Non-agostic complex		
MCB	RuC_α BCP	$C_\alpha C_\beta$ BCP	RCP	RuC_α BCP	$C_\alpha C_\beta$ BCP	RCP
1	0.153	0.208	0.073	0.122	0.248	0.059
2	0.149	0.209	0.071	0.119	0.246	0.058
3	0.148	0.209	0.071	0.118	0.246	0.058
4	0.146	0.209	0.070	0.116	0.246	0.057
5	0.143	0.209	0.072	0.113	0.249	0.057
6	0.135	0.206	0.071	0.102	0.246	0.052
7	0.150	0.208	0.074	0.116	0.247	0.055
8	0.142	0.203	0.073	0.111	0.245	0.054
9	0.154	0.207	0.072	0.120	0.246	0.060
10	0.150	0.208	0.072	0.115	0.248	0.058
11	0.140	0.209	0.070	0.109	0.248	0.056
12	0.150	0.207	0.074	0.107	0.252	0.056
13	0.154	0.205	0.077	0.131	0.241	0.061
14	0.158	0.205	0.079	0.127	0.246	0.061
15	0.148	0.199	0.081	0.110	0.243	0.053
16	0.148	0.197	0.083	0.106	0.255	0.052
17	0.129	0.187	0.086	0.086	0.252	0.045
18	0.129	0.187	0.087	0.087	0.252	0.045
19	0.127	0.189	0.083	0.085	0.253	0.045
20	0.127	0.192	0.084	0.084	0.254	0.045
21	0.120	0.202	0.077	0.086	0.250	0.045

central region of the metallacycle in **2'**. This argument is supported by the higher ρ value at RCP of **2** (0.071 au) than that of **2'** (0.058 au).

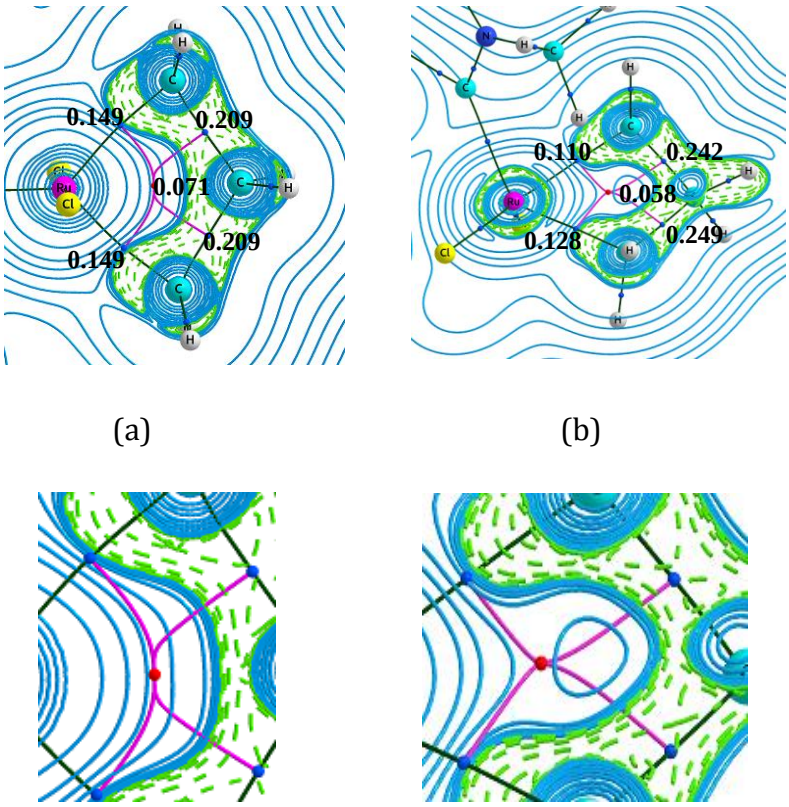

(a) (b)

(c)

Figure 2.7 Contour map of the Laplacian of electron density in the plane of metallacycle for (a) **2** and (b) **2'**. Only metallacyclobutane region is shown for clarity. The ρ values are depicted in au. (c) Magnified image of the RCP region showing the flat (left) and sharp (right) meeting point of the ring paths of **2** and **2'**, respectively.

In a typical ring system, the ring paths has a sharp meeting point as observed in the case of the non-agostic system **2'** (Figure 2.7b) whereas the agostic complex **2** shows a characteristic flat curvature for the ring paths meeting at the RCP (Figure 2.7a) and this aspect is clearer in the magnified image of the RCP region of **2** and **2'** given in Figure 2.7c. Although the existence of a bond path is not a necessary condition to describe a bonding interaction between two atoms, a strong follower of Bader's theory would have liked the existence of a bond path between Ru and C_β to unequivocally

assign the fifth bond to C_β. But none of the 14-electron agostic complexes showed the fifth bond path for C_β whereas all of them showed the characteristic flat curvature of ring paths meeting at the RCP. The $\nabla^2\rho$ plots of **1** - **16** complexes were very similar and markedly different from that of their non-agostic isomers.

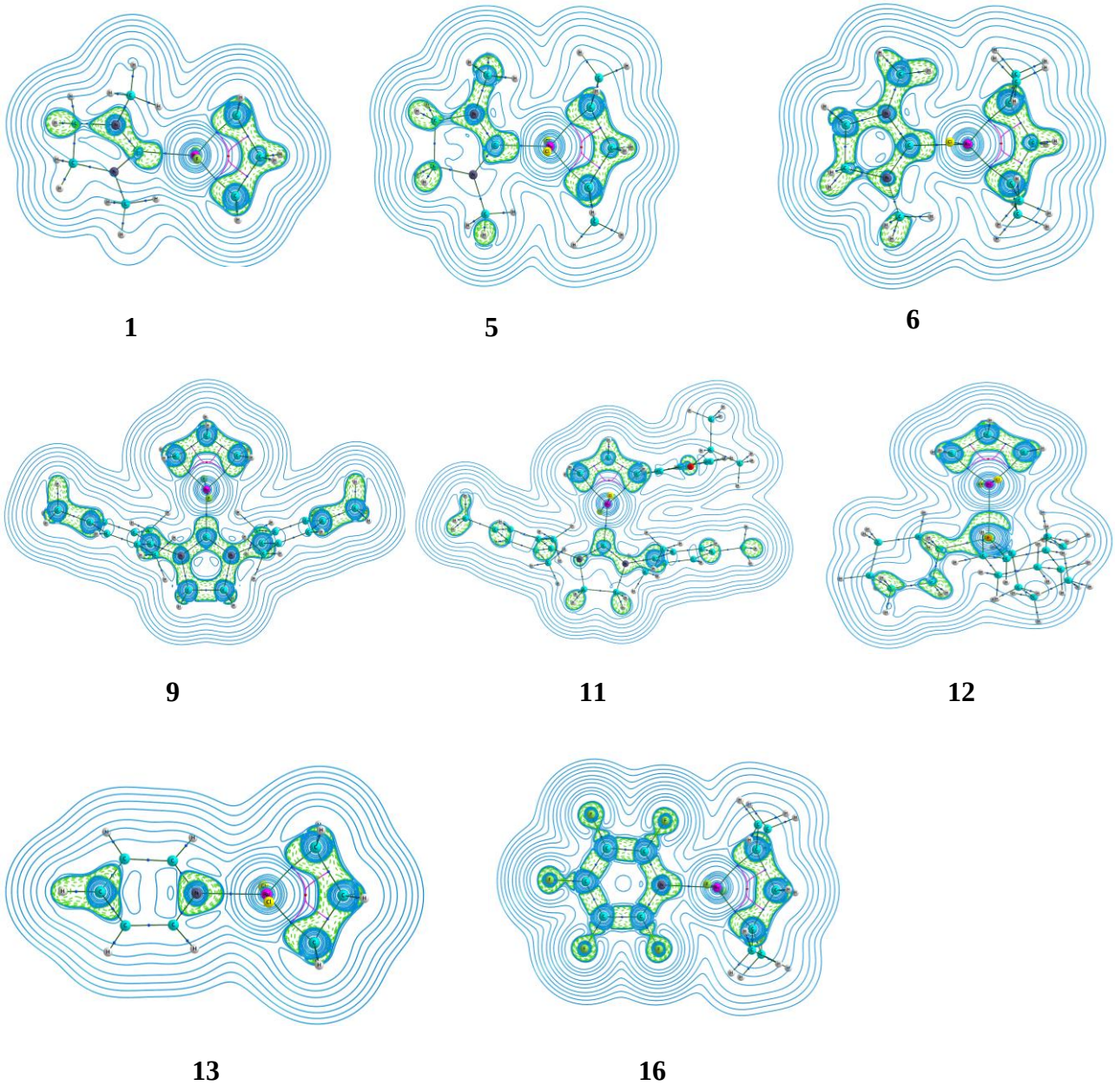

Figure 2.8 Contour map of the Laplacian of electron density in the plane of metallacycle for selected RuCBs.

Recently Suresh and Frenking reported similar flat curvature for ring paths in the case of metallacyclobutadienes (MCBD) of alkyne metathesis intermediates.[68] They suggested that such a feature is due to the existence of a catastrophe point - a point where both RCP and BCP could merge. They also showed that by restricting the metal-C_β distance to a slightly shorter distance than the optimized one, QTAIM topography of MCBD can exhibit a fourth bond path for C_β along with two RCPs. The fourth bond path named as 1,3-MC bond occupied the same plane of the other three regular bonds (two CC and one CH) and suggested a planar tetracoordinate character to C_β in MCBD. We did a similar study in the case of **2** by restricting the RuC_β distance to a value shorter than the optimized value 2.255 Å and found that at RuC_β distance 2.010 Å a BCP emerges for RuC_β bonding interaction along with two RCPs (Figure 2.9a). The constrained geometry at RuC_β distance 2.010 Å is 11.4 kcal/mol less stable than the equilibrium geometry. The two RCPs and BCP lie very close to each other in the constrained geometry indicating the mergence of these CPs as the RuC_β distance increases to the equilibrium value. This leads to a catastrophe situation which can be seen from the values of the three eigenvalues (curvatures) of RCP/BCP as one goes from the equilibrium geometry to the constrained geometry (Figure 2.9b). At the equilibrium geometry, the three eigenvalues of the (3, +1) RCP are -0.0526, +0.0693 and +0.3000 au. As the RuC_β distance decreases, the positive eigenvalue close to zero becomes smaller and smaller and changes its sign at RuC_β distance 2.010 Å whereas the magnitude of the other two eigenvalues increases. This means that the (3, +1) RCP which represents a minimum ρ point in the plane of metallacycle and maximum ρ point with respect to the path perpendicular to that plane, changes its character drastically to (3, -1) due to a small structural perturbation. At the (3, -1) BCP, the ρ value is minimum with respect to the maximum density path connecting Ru and C_β, but maximum to the rest of the directions. Thus catastrophe nature can be assigned to RCP as this point is at the verge of a critical change in character from (3, +1) to (3, -1). It is also noteworthy that the ρ value 0.113 au for the RuC_β interaction in the constrained geometry is slightly higher than the ρ value 0.110 au observed for one of the RuC_α bonds of the non-agostic complex **2'**

meaning that by slightly adjusting the RuC_β interaction, one could achieve bonding effect as strong as RuC_α for the RuC_β interaction.

The QTAIM data of the 14-electron agostic complexes in Table 2.2 and the QTAIM features of the constrained geometry in Figure 2.9 clearly suggest that development of significant bonding interaction between Ru and C_β is responsible for the catastrophe character of the RCP. Therefore, it is imperative to assume that the C_β in the agostic complexes possesses a fifth bonding interaction with the metal in addition to the existing two CC and two CH bonds.[69]

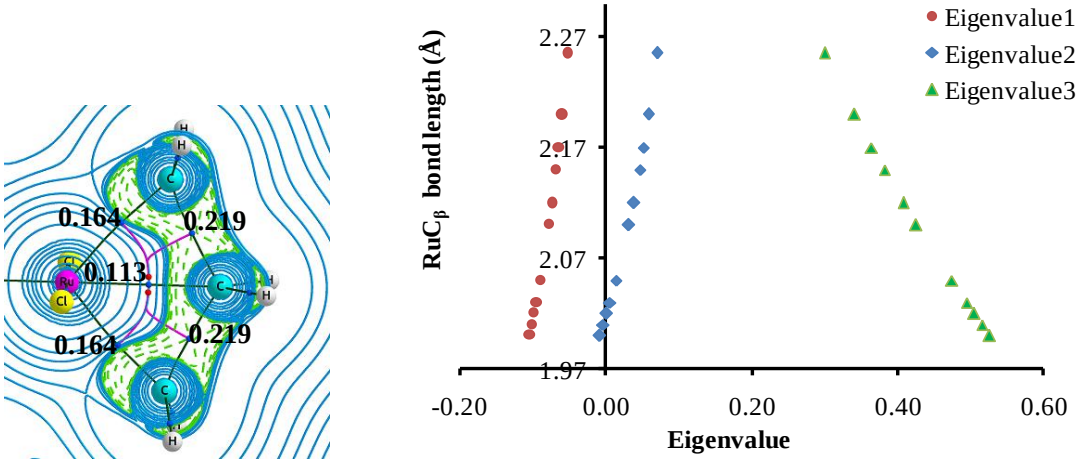

(a) (b)

Figure 2.9 (a) Contour map of the Laplacian of electron density in the plane of metallacycle for the constrained geometry of **2** showing fifth bond for C_β to Ru. Some portions of the complex are omitted for clarity. The ρ values are depicted in au. (b) Plot showing correlation between eigenvalues and RuC_β bond length.

Among the five 16-electron agostic systems studied, the equilibrium geometries of **17** and **18** showed the presence of the fifth bond path between Ru and C_β in QTAIM. The fifth bond path leads to two triangular ring structures defined by Ru, C_α and C_β (Figure 2.10). As in the case of the constrained 14-electron agostic complex **2** given in Figure 2.9, the two RCPs and the BCP lie very close to each other in **17** and **18**. Further, all these CPs possess nearly same ρ value (0.086 au). The QTAIM data of **17** and **18** clearly

suggest that with sufficiently strong interaction between metal and C_β, the catastrophe RCP in the MCB can be resolved into a BCP and two RCPs. The $\nabla^2\rho$ plots of **17** and **18** are very similar to the 14-electron agostic complexes as well as the 16-electron agostic complexes **19**, **20** and **21** except for the fifth bond path. This suggests that the bonding interaction between Ru and C_β is present in every agostic complex which cannot be ignored due to the absence of a well defined fifth bond path. Instead, the fifth bond of C_β could be judged from the significant build up of electron density at the RCP and its catastrophe character. A well-defined fifth bond path will arise only by very fine tuning of the electron deficiency at the metal center by adjusting the stereoelectronic properties of the ligands.

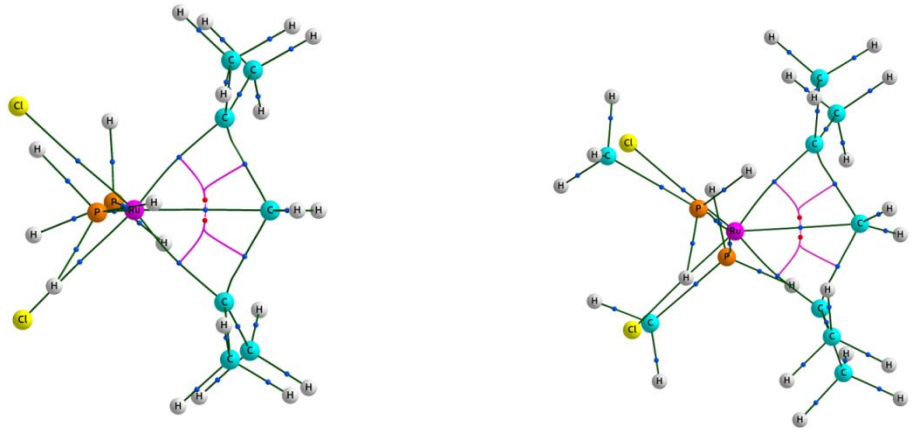

(a) (b)

Figure 2.10 QTAIM molecular graph of (a) **17** and (b) **18** showing the fifth bond path for the C_β.

In general, QTAIM ρ value of **17** - **21** as well as **17'** - **21'** for RuC_α, RuC_β (either RCP or BCP) and $C_\alpha C_\beta$ bonds (Table 2.2) agree closely with the corresponding bond order trends (Figure 2.11a). Among all the systems discussed so far, **18** has the highest RuC_β bond order (0.362) as well as the highest ρ value at the RuC_β BCP (0.087 au). A decreasing linear trend in W_{bo} with an increase in the RuC distance (both α and β carbon atoms) is observed (Figure 2.11b). These correlations suggest that QTAIM ρ data is complementary to W_{bo} data. The highest values of the ordered pair of (ρ in au, W_{bo}) data for the RuC_α bond, *viz*. (0.158, 1.085), (0.154, 1.009), (0.153, 1.008) are seen

in complexes **14**, **9** and **1**, respectively. For the RuC_β bond, the highest values of (ρ in au, W_{bo}), *viz*. (0.087, 0.362), (0.086, 0.358), (0.084, 0.346) are obtained for complexes **18**, **17**, and **20**, respectively. Thus from the W_{bo} assessment, we may conclude that the strength of the fifth RuC_β bond in **18**, **17** and **20** is around 35% of the strength of the strongest RuC_α bonds in **14**, **10** and **1** whereas the ρ data suggests that RuC_β bond strength is more than half the RuC_α bond strength. The comparison of (ρ in au, W_{bo}) data of RuC_β with that of the weakest RuC_α bonds, *viz*. (0.086, 0.674), (0.084, 0.674), (0.086, 0.683) for **17'**, **20'** and **21'**, respectively suggests that the fifth bond is as strong as RuC_α (from ρ data) or at least half as strong as RuC_α (from W_{bo} data). From all these analyses, it is clear that RuC_β interaction could be called as a fifth bond in all the agostic MCBs. This bonding leads to small RuC_β distance, longer $C_\alpha C_\beta$ bonds and wider $C_\alpha C_\beta C_\alpha$ angles than typical sp^3 hybridized carbon centers. The W_{bo} values and ρ values of the fifth RuC_β bond are in the range 0.18 – 0.36 au and 0.07 - 0.09 au respectively.

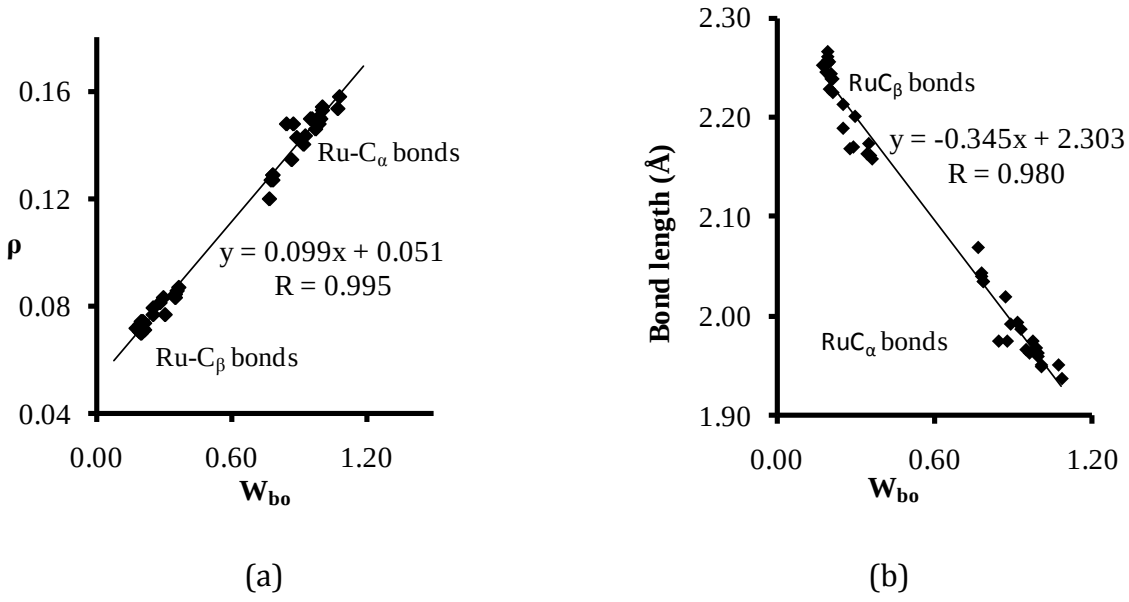

Figure 2.11 Plots showing correlation of (a) ρ against Wiberg bond order (b) bond length against Wiberg bond order.

2.4.4 Tungstenacyclobutanes

In the case of Grubbs MCB systems, the structural data are available only from computations while metathesis intermediates of Schrock's alkylidene catalysts are well

characterized using X-ray crystallography. Hence it would be a nice test to show that the computationally predicted features of the Grubbs systems can be ascertained with the help of metallacycles of similar origin in the Schrock olefin catalysis. We do this comparative study by examining the hypercoordinate state of C_β in known structures of tungstenacyclobutane, available in the Cambridge Crystal Database (CCD).[18, 70-74] The collected structures depicted in Figure 2.12 show TBP geometry. The TBP geometries are compared with the X-ray structure of the SP isomer WUWNOR (CCD ID is used to name the crystal structures).[75]

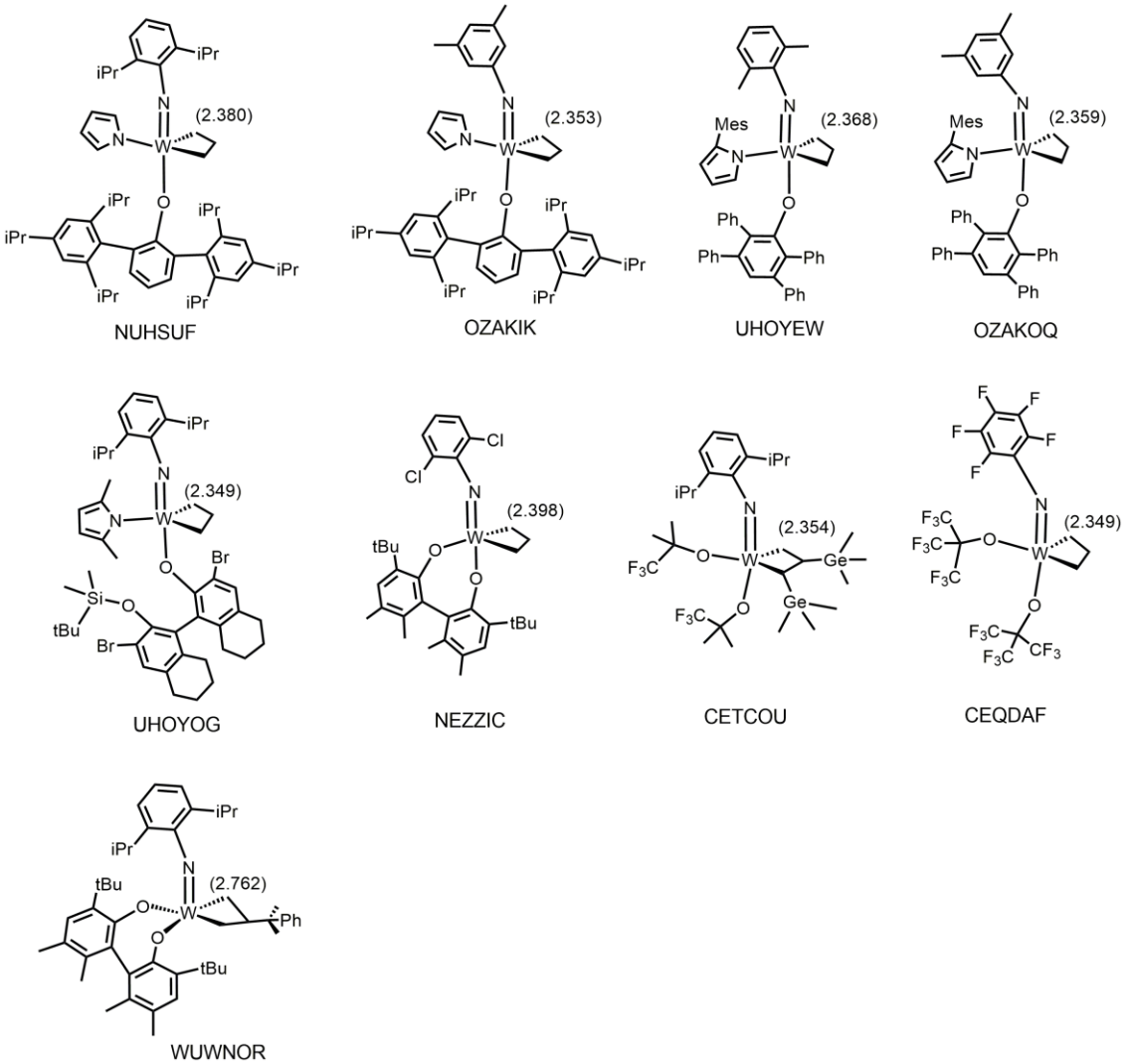

Figure 2.12 Schematic structures of tungstenacyclobutane obtained from CCD database. CCD ID is used to name them. The WCβ bond length is given in the parenthesis.

Table 2.3, discuss the structural parameters of tungstenacyclobutane region of all these systems given in Figure 2.12. All the TBP geometries show single bond-like WC_β distance in the range 2.349 - 2.398 Å, long $C_\alpha C_\beta$ bonds (1.584 - 1.634 Å) and wide $C_\alpha C_\beta C_\alpha$ angle (115 - 118°). These structural features are very similar to the agostic metallacycles of the Grubbs ruthenium systems and strongly point to the presence of pentacoordinate carbon in the tungstenacycle. Compared to the TBP complexes, the SP complex WUWNOR shows longer WC_β (2.76 Å), longer WC_α (2.17 Å) and shorter CC (1.52 Å) bonds as well as smaller CCC angle (97.3). It is clear that tungstenacycle in the SP configuration is very much like any of the non-agostic ruthenacycles.

Table 2.3 Structural parameters of the selected crystal structures and models **22** and **23**. Distances are in Å and angles in degrees

MCB	WC_α	WC_α	WC_β	$C_\alpha C_\beta$	$C_\alpha C_\beta$	$<C_\alpha C_\beta C_\alpha$
NUHSUF[18]	2.039	2.037	2.380	1.590	1.634	115.2
OZAKIK[73]	2.070	2.043	2.353	1.600	1.605	118.2
UHOYEW[72]	2.059	2.057	2.368	1.597	1.603	117.4
OZAKOQ[73]	2.076	2.048	2.359	1.590	1.602	118.3
UHOYOG[72]	2.040	2.056	2.349	1.592	1.585	118.0
NEZZIC[70]	2.078	2.016	2.398	1.586	1.584	115.0
CETCOU[71]	2.057	2.079	2.354	1.589	1.592	117.3
CEQDAF[74]	2.042	2.065	2.349	1.604	1.603	118.1
22	2.093	2.082	2.401	1.599	1.604	117.8
23	2.071	2.073	2.379	1.604	1.602	117.8
WUWNOR[75]	2.165	2.169	2.762	1.521	1.528	97.3

We also analyzed the W_{bo} values and QTAIM features of the X-ray structures using the wavefunction obtained from single point energy calculation (Table 2.4). The W_{bo} values are in the range 0.187 – 0.237 for WC_β, strongly indicating pentacoordination for

C_β. Similar to the agostic ruthenacycles, all the TBP systems showed a catastrophe RCP for the WC_β interaction, but with higher ρ values (~0.10 au) at the RCP than the ruthenium systems. We also optimized two structures (Figure 2.13), one analogous to UHOYEW (**22**) without the isopropyl and methyl substituents on the aromatic rings and the second analogous to CEQDAF (**23**) wherein $-OCF_3$ ligand is used instead of $-OC(CF_3)_3$). The ligand environment of **22** mimics the basic features of NUHSUF, OZAKIK, UHOYOG, UHOYEW and OZAKOQ while **23** mimics the ligand environment of CETCOU, NEZZIC and CEQDAF.

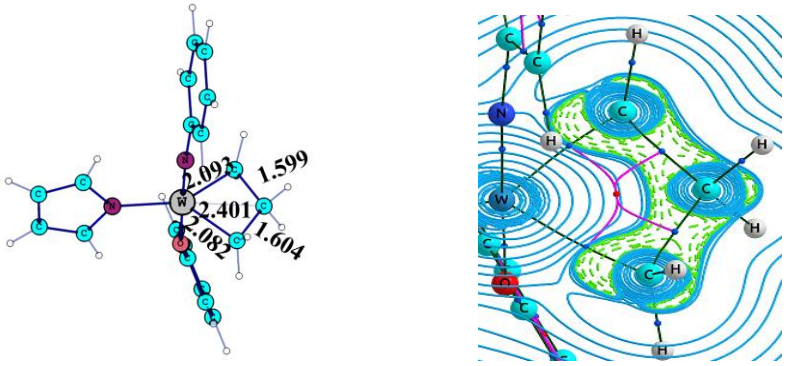

22

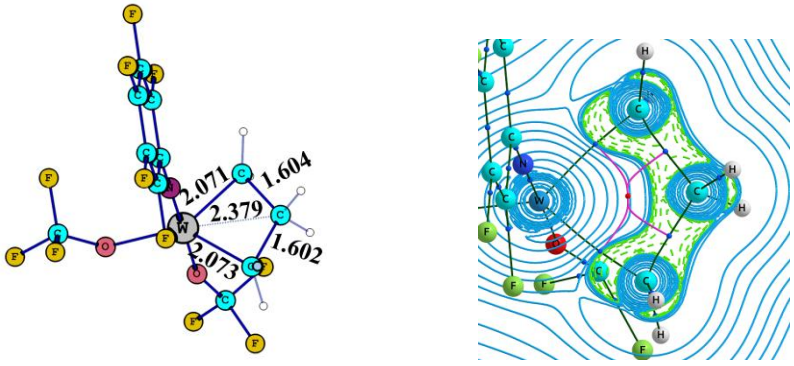

23

Figure 2.13 Optimized geometries and contour of Laplacian of electron density in the plane metallacycle (only metallacycle part is shown for clarity) of WCB.

The optimized structural parameters given in Table 2.3 for the metallacycle region of **22** and **23** are very similar to that of UHOYEW and CEQDAF, respectively.

These data suggest that the single bond-like WC_β distance observed in the X-ray structures cannot be accounted by the crystal packing forces or by invoking the geometrical restrictions (strain) imposed by the four-membered ring. The QTAIM data and W_{bo} values of **22** and **23** are similar to those reported for the X-ray structures (Table 2.4). The Laplacian contour plots of **22** and **23** depicted in Figure 2.13 illustrate the catastrophe nature of the fifth bonding interaction between W and C_β (the ring paths meet at RCP with a flat curvature).

Table 2.4 Wiberg bond order and QTAIM ρ parameters calculated for tungstenacyclobutanes. The average value is shown for the two WC_α and two $C_\alpha C_\beta$ bonds

MCB	Wiberg bond order			AIM ρ parameters (in au)		
	WC_α	$C_\alpha C_\beta$	WC_β	WC_α BCP	$C_\alpha C_\beta$ CP	RCP
NUHSUF	1.001	0.905	0.202	0.195	0.199	0.097
OZAKIK	0.995	0.912	0.200	0.190	0.203	0.099
UHOYEW	0.990	0.905	0.207	0.187	0.205	0.099
OZAKOQ	0.990	0.905	0.207	0.187	0.207	0.099
UHOYOG	1.016	0.912	0.198	0.192	0.209	0.101
NEZZIC	0.985	0.912	0.187	0.195	0.210	0.096
CETCOU	0.958	0.927	0.237	0.185	0.206	0.100
CEQDAF	1.008	0.899	0.227	0.191	0.202	0.102
22	0.985	0.931	0.191	0.180	0.206	0.092
23	1.013	0.923	0.218	0.186	0.205	0.097
WUWNOR	0.841	0.863	0.039	0.165	0.244	0.075

2.4.5 NMR Analysis

Schrock *et al*. have proposed that significant WC_β interaction in a tungstenacyclobutane can be ascertained from the large difference it shows for ^{13}C NMR signals (δC) of C_α and C_β.[35] Similarly, the strongest evidence to the formation ruthenacyclobutane in Grubbs

Table 2.5 ^{13}C NMR data for agostic and non-agostic complexes

MCB	Agostic complex			Non-agostic complex		
	δC_α	δC_β	δC_α-δC_β	δC_α	δC_β	δC_α-δC_β
1	99	5	94	44	36	8
2	104	8	96	41	38	3
3	103	8	95	40	40	0
4	104	8	96	38	41	-3
5	129	23	106	58	57	1
6	154	36	118	81	72	9
7	125	22	103	57	51	6
8	149	36	113	77	67	10
9	101	7	94	39	31	8
10	104	8	96	40	37	3
11	116	17	99	44	44	0
12	106	7	99	33	36	-3
13	114	2	112	78	43	35
14	111	-3	114	57	38	19
15	158	27	131	76	67	9
16	171	30	141	78	63	15
17	172	27	146	88	74	14
18	172	26	146	85	75	10
19	170	26	143	85	76	9
20	171	26	145	83	77	6
21	161	23	138	75	73	2

olefin metathesis is derived from ^{13}C NMR measurements by Romero and Piers[14] who showed that the difference in chemical shift values of C_α and C_β (δC_α-δC_β) value is 92 ppm for **10**, which is due to significant degree of metal to C_β interaction. Later Rowley *et al*.[76] theoretically supported this observation and suggested that the large difference in the chemical shift (δC_α -δC_β) value also indicates $C_\alpha C_\beta$ activation. In Table 2.5, ^{13}C NMR values of the agostic and non-agostic ruthenacyclobutanes are depicted while Table 2.6 depicts those of the Schrock complexes. Computed (δC_α-δC_β) value 96 ppm for **10** is only 4 units deviated from the experimental value reported by Romero and Piers.[14] Similarly a large difference in the chemical shift value (δC_α-δC_β) is observed for all the agostic MCBs whereas the (δC_α-δC_β) values are negligible for the non-agostic MCBs.

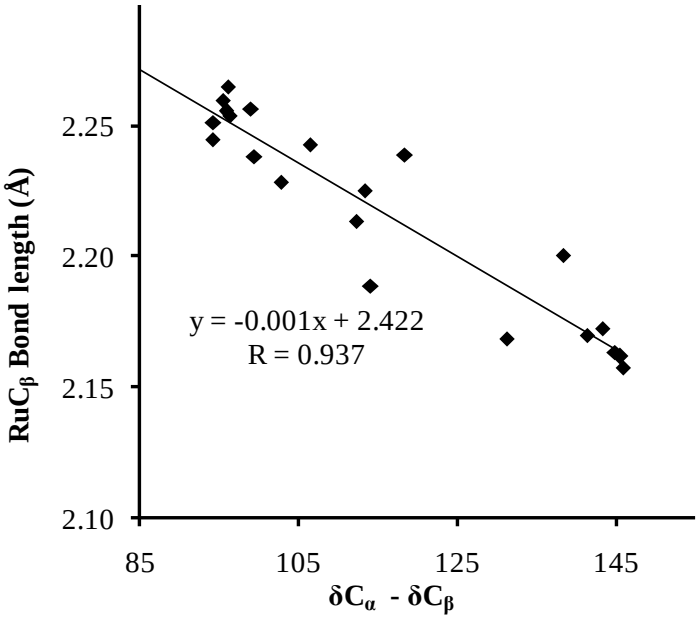

Figure 2.14 Plot showing correlation between the δC_α – δC_β and RuC_β bond length for ruthenacyclobutanes.

The 16-electron MCB systems show high (δC_α-δC_β) values ~ 140ppm. It is noteworthy that **17** and **18** which show the highest (δC_α-δC_β) value (146 ppm) possesses the fifth bond path in the QTAIM analysis. Also the computed ^{13}C NMR values of Schrock complexes agreed well with the experimental values (Table 2.6).[35] These NMR data clearly suggest that δC_α and δC_β of agostic complexes are markedly different

from that for the non-agostic complexes. In the agostic complexes of ruthenium, the the (δC_α-δC_β) values are always very large (94 - 146 ppm) compared to the non-agostic complexes (-3 to 35 ppm). Similarly, all the agostic complexes of tungsten show (δC_α-δC_β) in the range 81 - 93 ppm while that of the non-agostic WUWNOR is -14 ppm. In general, (δC_α-δC_β) values show a linear trend with respect to the MC_β distance (Figure 2.14). These findings that a large value of (δC_α-δC_β) is a characteristic feature of metal-C_β interaction in the metallacycles are in complete agreement with the earlier conclusions drawn by Schrock *et al*.[35].

Table 2.6 ^{13}C NMR data for tungstenacyclobutane complexes

MCB	δC_α	δC_β	δC_α-δC_β
NUHSUF	68	-13	81
OZAKIK	72	-17	89
UHOYEW	73	-16	89
OZAKOQ	68	-22	90
UHOYOG	75	-16	91
NEZZIC	63	-13	76
CETCOU	85	3	82
CEQDAF	77	-16	93
22	83	-3	86
23	90	-3	93
WUWNOR	20	34	-14

2.5 Conclusions

Analysis of the structural, bonding, electron density and ^{13}C NMR features of metallacyclobutane (MCB) intermediates of Grubbs and Schrock olefin metathesis catalysts has revealed a unique pentacoordinate state of the C_β in the system. The high oxidation state of metal center in MCB propels the metal center to accept electron density from the CC σ bonds leading to agostic bonding interaction between metal and

CC bonds.[77] As a result, single bond-like metal-C_β distance is observed in MCB systems. The fifth bond of C_β to the metal is clearly brought out in terms of significant Wiberg bond order values and appearance of a catastrophe QTAIM RCP in the metallacycle. The ρ at the RCP of Grubbs systems is found to be comparable to the ρ value of a normal RuC bond and for some cases, Wiberg bond order values indicated half the strength of a normal RuC bond for the RuC_β bond. In two Grubbs systems, the fifth BCP is clearly observed. The appearance of the catastrophe RCP is proposed as a strong indicator of the fifth bonding interaction between C_β in MCB. To resolve this RCP to a BCP, fine tuning of the stereoelectronic properties of the ligand environment is needed. Further, an MCB system showing a catastrophic RCP or fifth BCP is characterized by significantly large (δC_α-δC_β) value than a normal MCB structure. Thus pentacoordination of C_β is strongly supported by ^{13}C NMR data, and it also provides an experimental way to monitor the formation of such metallacycles. The pentacoordination of C_β to the metal inherently weakens the CC bonds and facilitates the metathesis reaction.

Part B: Planar Tetracoordinate Carbon in Tungstenacyclobutadiene of Alkyne Metathesis and Expanded Structures

2.6 Abstract

Planar tetracoordinate ($_{pt}C$) character of C_β in the tungstenacyclobutadiene (WCBD) of alkyne metathesis is analyzed with the support of structural, electronic, molecular orbital, and electron density data obtained from density functional theory calculations. The $_{pt}C$ character of C_β is due to 1,3-WC bonding which is established by single bond-like WC_β distance in X-ray structures and calculated structures, catastrophe ring critical point for the WCBD ring in the quantum theory of atoms in molecule analysis (QTAIM) and the large difference in ^{13}C NMR data of C_α and C_β atoms. The metalloaromatic character of WCBD is revealed from nuclear independent chemical shift (NICS) values, and diatropic ring current observed in the anisotropy of the current induced density (ACID) plot. These WCBD structural motifs provide a new strategy to build 1-, 2- and 3-dimensional organometallic polymeric structures containing multiple $_{pt}C$ centers. Several such structures are reported, and the 3-dimensional extensions of them provide access to novel $_{pt}C$-incorporated metal-organic framework.

2.7 Introduction

Ever since Hoffmann *et al.*[78] brought the concept of planar tetracoordinate carbon ($_{pt}C$) to world's attention; stabilization of a $_{pt}C$ has been viewed as a fascinating challenge given to chemist. Hoffmann and co-workers proposed that stabilization of $_{pt}C$ can be achieved either through a mechanical approach by constraining the geometry in such a way that the central carbon and its neighbors are in one plane or through an electronic approach by incorporating suitable substituents (ions, metal centers) where at least one of the coordinations should be an atom other than carbon (Figure 2.15).[78-80] Schleyer and co-workers proposed that stabilization of $_{pt}C$ is also possible by incorporating the carbon to small ring systems.[81-83] Another widely used approach for

the stabilization of $_{pt}C$ centers is through the introduction of transition metals. A divanadium complex of formula $V_2[(OMe)_2C_6H_3]_2$ was the first crystallographically characterized molecule to show a $_{pt}C$ center.[84] Later many bimetallic complexes containing $_{pt}C$ centers have been reported with different metal centers like Ti, Pd, W, Re, and Ce.[85-90] Along with bimetallic systems, some monometallic complexes are known to possess $_{pt}C$ centers where the planar tetracoordination results from the additional interaction of the carbon with the metal center.[91] It was observed that in some zirconocene complexes the fourth bond of the carbon is the result of the CH agostic interaction with the metal center.[92-93] Similar unusual bonding interactions were reported in the case of metallacyclobutadienes, metallacyclopentadienes, and other small metallacycles.[34, 94-96] Many reviews dealing with the progress in the field of planar tetra- and hypercoordinate carbon systems are available in the literature.[89, 97-101]

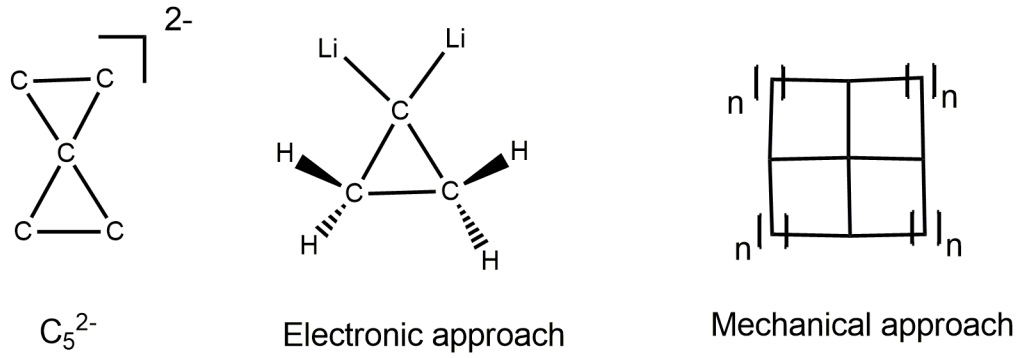

Figure 2.15 Examples of molecules containing $_{pt}C$ centers

Recently, the metallacyclobutadiene (MCBD) intermediate of alkyne metathesis has been proposed as a $_{pt}C$ complex wherein the $_{pt}C$ center is the β-carbon of the MCBD.[54-55] MCBD intermediates of alkyne metathesis especially with tungsten catalysts are stable, and many crystal structures[102-104] are available in Cambridge structural database (CSD). Also, theoretical studies established them as minimum energy structures.[105-106] Structurally, the $_{pt}C$ nature of the MCBD is assigned on the basis of short single-bond like MC_β distance (2.20 – 2.40 Å). Based on energy decomposition, bond order and electron density analyses, the significant bonding interaction between metal and the β-carbon has been unambiguously proven in the case of a Schrock

tungsten complex Cl_3W(C-MeC-MeC-tBu) (CSD ID BONXOR) (Figure 2.16a). This bond named as 1,3-MC bond provided the fourth coordination for the carbon along with three other bonds (two CC and one CH bonds) in the plane of the metallacycle (Figure 2.16).[54]

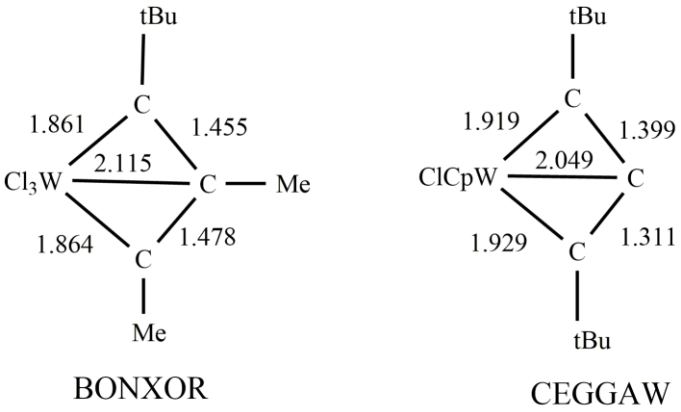

(a)

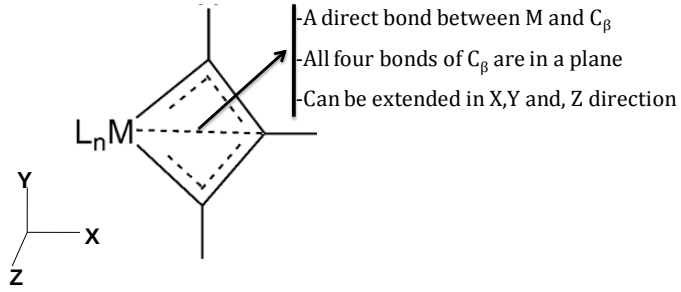

(b)

Figure 2.16 (a) Molecular drawings of the crystal structures of tungstenacyclobutadiene, BONXOR and 'deprotio' tungstenacyclobutadiene, CEGGAW (b) Schematic representation of a bond between metal and C_β in an MCBD complex.

Three decades ago, Schrock *et al.* reported the unexpected formation of 'deprotio' metallacycles during the course of metathesis reaction of terminal alkynes with molybdenum and tungsten catalysts.[107-108] For instance, the reaction of WCp(C-tBu)CI_2 with C-tBuCH in triethyl amine yielded the metallacycle WCpCI[C-tBuCC-tBu] (CSD ID CEGGAW, Figure 2.16a) instead of the expected MCBD $WCpCl_2$[C-tBuC-HC-tBu) due to

dehydrohalogenation. Short WC_β distance (2.049 Å) in WCpCI[C-tBuCC-tBu], indicated bond formation. Recently Jemmis *et al.* have studied structurally similar group 4 'deprotio' metallacycles known as metallacycloallenes using molecular orbital and natural bond orbital analyses and confirmed that four-membered metallacycloallenes are stabilized through metal-C_β bonding interaction.[109] Although the C_β of metallcycloallene or a 'deprotio' metallacycle is not a $_{pt}C$ center (only 3 atoms, *viz*. two C_α and the metal center are bonded to C_β), WCpCl[C-tBuCC-tBu] has been considered in this study to assess the strength of the 1,3-MC type interaction in the MCBD.

Recently, Suresh and Frenking showed the existence of 1,3-MC bond in the MCBD systems of group 4, 5 and 6 transition metals.[54-55] This bonding is due to considerable d_π-p_π interaction[110-111] between the metal and C_β and this finding pave the way for a new type of $_{pt}C$ chemistry in organometallics. Compared to the previous theoretical and experimental discoveries on $_{pt}C$ centers, the finding that a $_{pt}C$ center is available in MCBD is fascinating because of the role it plays in alkyne metathesis reaction as well as the status of the complex as a well-defined, stable, structurally characterized organometallic complex. MCBD system can also be viewed as a system wherein the metal center is incorporated into a small carbon framework. Such metallic incorporation in carbon frameworks can drastically change the properties of the resulting molecules, and based this, new materials exhibiting interesting optical, electronic, and magnetic properties can be designed and developed. Thus, the stable form of $_{pt}C$ in MCBD offers new design strategies for the development of $_{pt}C$ based materials. Using the extension of the building block in Figure 2.16b, Suresh and Frenking have computationally designed "edge complexes" of group 4 transition metals by utilizing the 1,3-MC bonding at the edges of aromatic hydrocarbons.[56] Herein, we propose that the structural motif given in Figure 2.16b for a $_{pt}C$ center can be extended to design more complex architectures in 1-, 2- and 3-dimensions. The larger structures can be envisaged by extending the structure in the X-, Y- and Z-direction *via* the β-carbon, α-carbon, and the metal center, respectively (Figure 2.16b). Many computational attempts have been made in the past to design the possible extension of molecules possessing multiple $_{pt}C$ centers in complex networks.[100, 112-115] Prediction of

edge decorated graphene systems possessing $_{pt}$C centers is also proposed by many groups by incorporating metal centers and some non-metals.[116-117]

In this study, we emphasize that the $_{pt}$C center, as well as the 1,3-MC bond observed in a MCBD system of alkyne metathesis is fundamental to organometallic chemistry and these findings immediately open up new room for expanding the chemistry of $_{pt}$C through 1,3-MC bond in CC frameworks. We perform this study as a computational endeavour to the design of $_{pt}$C incorporated metal-organic frameworks.

2.8 Computational Details

For the optimization of crystal structures, and 1- and 2- dimensional structures, the BP86/BS1[53] level of density functional theory is used wherein BS1 stands for triple-zeta quality basis set def2-tzvpp for all the atoms and the use of effective core potential for W to treat the core electrons. For the optimization of large 3-dimensional cage structures, BP86/BS2[118] level is used wherein BS2 stands for the all electron basis set SDD with effective core potential for W and 6-31g* basis set for other elements. All the structures discussed in this work have been confirmed as energy minima by locating only positive frequency for all the normal modes of vibration unless otherwise specified. Wiberg bond order analysis[59] is done to quantify bond strength using Natural Bond Orbital analysis (NBO) as implemented in G09. Electron density topology analysis is done with AIMALL program.[58] For ^{13}C NMR analysis, GIAO method[61, 119] in G09 is used. The same method is used to calculate Nucleus Independent Chemical Shift values at the center of the ring, NICS(0), at 1 Å above the ring center, NICS(1) and also the zz-tensor component of NICS(1), NICS(1)$_{zz}$.[120] Aromaticity of MCBD ring is visualized in terms of Anisotropy of Current Induced Density (ACID) developed by Herges group.[121-122]

2.9 Results and Discussion

At first we consider X-ray crystal structures of seven tungstenacyclobutadiene (WCBD) systems (Figure 2.17) for the structural and bonding analysis to confirm the existence

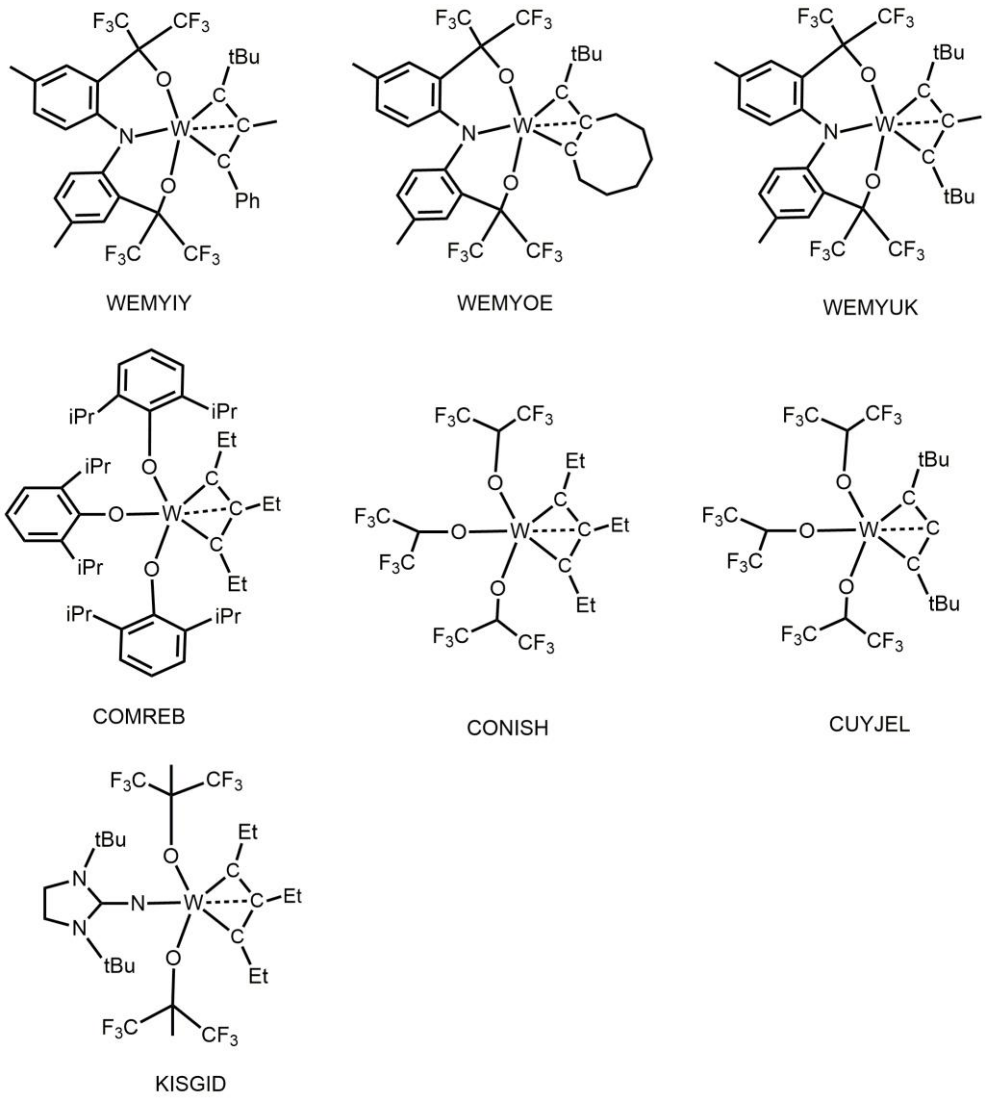

Figure 2.17 Molecular drawing of the crystal structures of tungstenacyclobutadienes. CSD ID is used to name the molecules.

of 1,3-MC bond. Among them the first three systems, identified in the CSD as WEMYIY, WEMYOE, and WEMYUK, are reported in a very recent work by Veige *et al.*[123] They have synthesized the first neutral trianionic ONO pincer-type tungsten alkylidyne complexes and showed that these complexes can react rapidly with alkynes to yield WCBDs. Though the possibility of 1,3-MC bond in these structures are obvious from the single bond-like WC_{β} distance (~2.150 Å), this kind of a bonding was not discussed by Veige *et al.* In Figure 2.17, we also depict the schematics of the molecular geometries of WCBD systems reported by Schrock and co-workers and identified in CSD as COMREB,[34]

CONISH,[94] and CUYJEL.[95] Yet another WCBD system is KISGID reported by Tamm *et al.*[104] In Table 2.7, the bond lengths (WC_α, WC_β, and $C_\alpha C_\beta$) and bond angle ($C_\alpha C_\beta C_\alpha$) parameters of the metallacycle region are depicted for the X-ray structures and the corresponding theoretically derived structures.

Table 2.7 Structural parameters of WCBD in the crystal and in the optimized geometries given in parenthesis (bond distances are given in Å and angles in degree)

MCBD	WC_α	WC_α	$C_\alpha C_\beta$	$C_\alpha C_\beta$	WC_β	$<C_\alpha C_\beta C_\alpha$
WEMYIY	1.905	1.911	1.450	1.473	2.159	119.9
	(1.935)	(1.943)	(1.452)	(1.468)	(2.192)	(120.5)
WEMYOE	1.897	1.911	1.443	1.473	2.156	119.9
	(1.930)	(1. 938)	(1.450)	(1.467)	(2.185)	(120.5)
WEMYUK	1.882	1.908	1.453	1.456	2.143	120.0
	(1.927)	(1.936)	(1.459)	(1. 464)	(2.185)	(120.3)
COMREB	1.883	1.949	1.433	1.466	2.159	120.8
	(1.903)	(1.986)	(1.417)	(1. 490)	(2.193)	(121.0)
CONISH	1.864	1.903	1.428	1.437	2.093	122.5
	(1.926)	(1. 930)	(1.436)	(1.481)	(2.164)	(121.3)
CUYJEL	1.890	1.921	1.417	1.499	2.103	123.1
	(1.939)	(1. 942)	(1.428)	(1.466)	(2.134)	(124.3)
KISGID	1.879	1.992	1.387	1.533	2.209	119.3
	(1.901)	(2.024)	(1.397)	(1. 519)	(2.234)	(120.0)

None of the structures show any symmetry as they possess dissimilar WC_α and $C_\alpha C_\beta$ bond distances. It is gratifying that the computed values of the distance particularly the WC_β distance and bond angles (Table 2.7) show good agreement with experimental values. In addition to the σ-type bonding interaction between W and C_α, the π-type interaction between metal d-orbitals and the carbon p-orbital gives substantial double bond character to the WC_α bond. As a result, WC_α bonds show significantly shorter distance than the typical WC_α single bond (2.100 Å). The strongest

evidence that supports the existence of 1,3-MC bond in these complexes is the single bond-like WC_β distance. Both theory and experiment agree that the WC_β distance in the range 2.093 – 2.234 Å is well within the sum of the van der Waals radii of tungsten and carbon (~3.800 Å) and is comparable with the WC_β distance in the 'deprotio' metallacycle CEGGAW (2.050 Å). The good agreement between the gas phase optimized WC_β data, and the corresponding crystal data clearly suggest that the single bond-like WC_β distance cannot be neglected as a consequence of structural restriction imposed in the four-membered ring or due to crystal packing.

2.9.1 QTAIM Analysis

In the QTAIM parlance, affirmation of the bonding interaction between two atoms is verified by locating a (3, -1) bond critical point (BCP)) and the associated bond path (BP) between the interacting atoms. The issue on the use of BP as a universal indicator of bonding is highly debated in the literature and many people have commented that the detection of a BP or BCP is not necessary to verify the bonding interaction between two atoms.[124-131] A BCP or BP is not observed between tungsten and C_β for any of the tungstenacyclobutadienes listed in Figure 2.17. All of them showed a characteristic catastrophe ring critical point (RCP) for the metallacycle. The QTAIM molecular graphs given for the optimized geometries of WEMYUK and CUYJEL in Figure 2.18 along with contours of Laplacian of electron density are useful to understand typical electron density features of the metallacyclobutadiene. Very similar molecular graphs have been obtained for all other systems. In the Chapter 2A it is shown that such a catastrophe nature can be resolved by adjusting the metal-C_β distance to a slightly smaller value than the optimized value as this will lead to the formation of a BCP and the associated BP.[55, 132] Thus the presence of a catastrophe critical point can be considered as the indication of bonding interaction between the metal and C_β. Three eigenvalues associated with the catastrophe RCP are given in Table 2.8. Since the RCP is designated as a (3, +1) critical point, one of the eigenvalues has to be negative and the other two have to be positive. As we can see, one of the positive eigenvalues is very close to zero (eigenvalue 2) which can be considered as an indicator of the catastrophe nature of the RCP. Hence, the system that shows the lowest positive eigenvalue must have the highest

catastrophe character. The smallest positive eigenvalue may become negative with sufficiently strong interaction between W and C_β which will give rise to a (3, -1) BCP critical point.

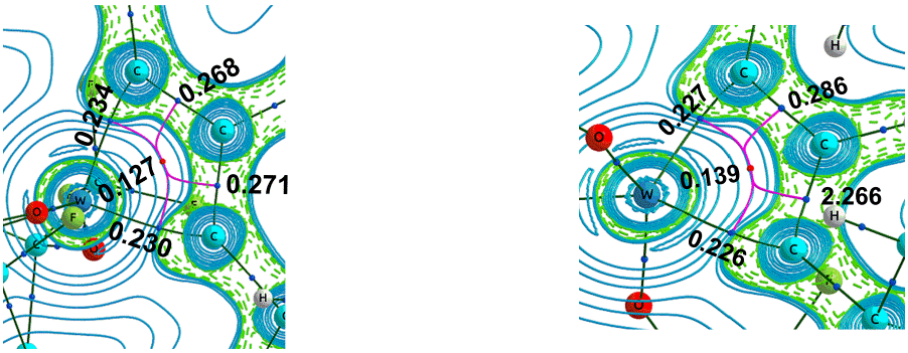

WEMYUK CUYJEL

Figure 2.18 Molecular graphs of WEMYUK and CUYJEL, showing a flat curvature for the meeting point of ring paths along the contours of Laplacian of electron density. Only metallacycle region is shown for clarity and ρ values are in au.

Table 2.8 QTAIM parameters for the WCBD systems and the 'deprotio' metallacycle CEGGAW

WCBD	QTAIM parameters (au)			Eigenvalue at RCP		
	WC_α BCP	$C_\alpha C_\beta$ BCP	WC_β RCP	1	2	3
WEMYIY	0.230	0.271	0.126	-0.108	0.071	0.417
WEMYOE	0.232	0.272	0.129	-0.111	0.070	0.421
WEMYUK	0.232	0.270	0.127	-0.109	0.071	0.416
COMREB	0.226	0.274	0.125	-0.109	0.071	0.406
CONISH	0.232	0.272	0.132	-0.115	0.064	0.428
CUYJEL	0.226	0.276	0.139	-0.125	0.047	0.459
KISGID	0.219	0.274	0.116	-0.099	0.079	0.379
CEGGAW	0.218	0.297	0.176	-0.197	-0.020	0.485

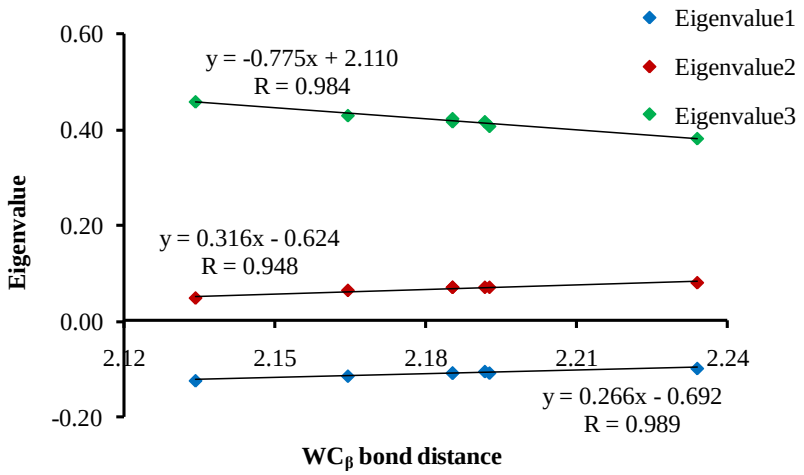

Figure 2.19 Correlation between WC_β bond distances (Å) and eigenvalues at the catastrophe RCP of various WCBD structures.

In Figure 2.19 variation of the eigenvalues with a change in the WC_β distance for various optimized crystal structures is presented. The linear plots given in this figure clearly suggest that with an increase in the WC_β interaction, the most positive eigenvalue (eigenvalue 3) becomes more positive, the least positive eigenvalue (eigenvalue 2) becomes smaller while the magnitude of the negative eigenvalue (eigenvalue 1) remain almost a constant. On the basis of this figure, we can assume that among all the structures, CUYJEL has the highest amount of 1,3-MC bonding character. By extrapolating the eigenvalue plots in Figure 2.19, a value ~1.980 Å for WC_β distance can be suggested at which the system may show a BCP along with a clear BP between W and C_β. To check this, we reduced the WC_β distance of CUYJEL manually and at a distance of 1.990 Å (a saddle point in the potential energy surface) a clear BCP was found along with a BP connecting W and C_β. Thus it is apparent that the absence of a BCP does not indicate the absence of a bonding interaction. Molecular orbital pictures of WEMYUK given in Figure 2.20 prove that the 1,3-MC interaction is mainly arising from significant d_π-p_π interaction between W and C_β.

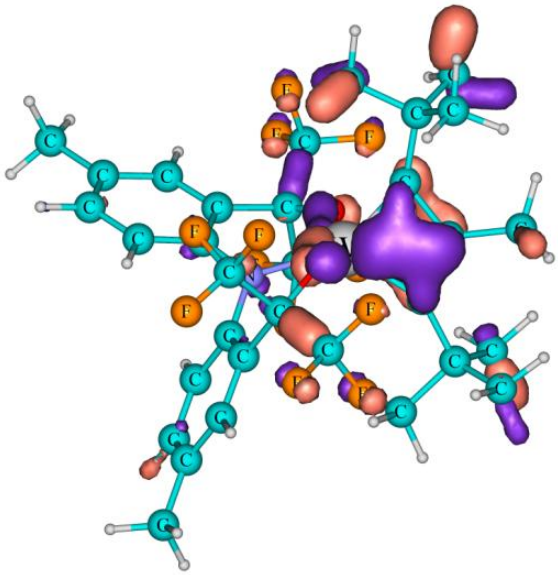

Figure 2.20 Molecular orbital diagram of WEMYUK.

Among the QTAIM parameters given in Table 2.8, the most important in the analysis of 1,3-MC bond are those associated with the catastrophe RCP. The ρ at the RCP is in the range 0.116 - 0.139 au. This indicates a significant build up of electron density between W and C_β. In the case of the 'deprotio' metallacycle CEGGAW, a BCP is observed between W and C_β with ρ value of 0.176 au. This can be considered as a well defined 1,3-MC bond in a metallacycle. Although the C_β of CEGGAW is tri-coordinate, the ρ value of its WC_β bond is useful to compare the strength of the 1,3-MC bond of the WCBD. The WCBD systems are 20 – 34 % smaller than the BCP ρ value of CEGGAW and indicates that the 1,3-MC interaction in the former is proportionally weaker than the latter. In all the metallacycles reported in Table 2, WC_α and $C_\alpha C_\beta$ bonds possess some amount of double bond character, and their BCP ρ values show significantly higher values than a typical WC single bond (0.165 au) and a typical CC single bond (0.240 au).

Among all the WCBD structures given in Figure 2.17, a C_β-H bond is present only in CUYJEL, and this system showed the highest ρ value at the catastrophe RCP. Schrock *et al.* have reported the removal of alcohol from this system, leading to the formation of 'deprotio' metallacycle.[133] The optimised structure of the 'deprotio' metallacycle of

CUYJEL is an energy minimum and in the QTAIM analysis it molecule showed a clear BCP with ρ value 0.175 au for the WC_β bond of length 2.074 Å.

2.9.2 Bond Order Analysis

The bond order parameters depicted in Table 2.9 strongly augment the conclusions drawn from the structural data and QTAIM analysis that tungsten is bonded to C_β for the 1,3-WC bonding. All the WCBD structures show WC_β bond order in the range 0.286 – 0.422 which suggests significant bonding interaction between W and C_β. The CUYJEL system composed of alkoxide ligand has the highest WC_β bond order 0.422. KISGID with imidazolin imidato ligand has the smallest WC_β bond order 0.286 whereas the pincer ligand incorporated structures of Veige *et al.* show WC_β bond order ~0.35.

Table 2.9 Wiberg bond order for the WCBD systems and the 'deprotio' metallacycle CEGGAW

WCBD	Wiberg bond order				
	WC_α	WC_α	$C_\alpha C_\beta$	$C_\alpha C_\beta$	WC_β
WEMYIY	1.385	1.356	1.256	1.175	0.348
WEMYOE	1.386	1.416	1.261	1.181	0.355
WEMYUK	1.419	1.405	1.220	1.222	0.351
COMREB	1.511	1.227	1.358	1.082	0.356
CONISH	1.370	1.450	1.280	1.134	0.395
CUYJEL	1.363	1.430	1.308	1.170	0.422
KISGID	1.119	1.603	1.473	1.035	0.286
CEGGAW	1.314	1.314	1.346	1.347	0.843

2.9.3 ^{13}C NMR Analysis

Schrock *et al.* proposed the use of ^{13}C NMR chemical shift as a measure of WC_β interaction in the case of metallacyclobutane intermediates of alkene metathesis.[4] Similar ^{13}C NMR analysis has been used by Romero and Piers to prove the formation of ruthenacyclobutane intermediate in the Grubbs alkene metathesis mechanism, where

the difference in the chemical shifts observed for the C_α and C_β were very large.[14] In this work, the structure of interest is MCBD. Because of the unusual $_{pt}C$ bonding character of C_β, a large difference in the chemical shift values of C_α (δC_α) and C_β (δC_β) is expected for MCBD. This is indeed true, and in all the cases, the NMR signal of C_β is 52 - 79 ppm smaller than that of C_α (Table 2.10) which is in agreement with the experimental data. We propose that the large difference in the ^{13}C NMR values of C_α and C_β can be considered as a signature of 1,3-MC bonding in the metallacycle.

Table 2.10 Important $C^{13}C$ NMR values calculated in the optimized geometries of MCBD

WCBD	^{13}C NMR			
	δC_α	δC_α	δC_β	δC_α- δC_β
WEMYIY	205.3	218.4	144.8	67.1
WEMYOE	200.4	225.6	152.5	60.5
WEMYUK	207.0	234.7	147.4	73.5
COMREB	204.4	199.3	144.0	57.8
CONISH	199.6	213.6	154.2	52.4
CUYJEL	208.6	222.8	137.0	78.7
KISGID	213.7	214.0	134.4	79.4
CEGGAW	205.2	205.0	191.6	13.5

The elucidation of crystal structures of several MCBD systems of alkyne metathesis clearly suggests that they possess superior stability compared to the 4-membered anti-aromatic cyclobutadiene.[134] It is well known that anti-aromatic to the aromatic transformation of organic moieties can be obtained by the incorporation of a transition metal center *via* chelating effect.[135-136] Aromatic characters of such systems is known as metalloaromaticity.[137] Erdman, and Lawson[138] studied metalloaromaticity in tungstenacyclobutadiene using computational techniques and reported that the nucleus independent chemical shift at the ring center, NICS(0) is -28 ppm for the Schrock's MCBD crystal, BONXOR. The high negative NICS(0) value suggested aromatic stabilization of the MCBD. Apart from NICS(0), NICS at 1 Å above the ring center,

NICS(1) and its zz-tensor component NICS(1)$_{zz}$ have also been used for the study of aromatic nature of a molecule. In Table 2.11, the NICS(0), NICS(1) and NICS(1)$_{zz}$ of all the complexes are reported. NICS(0) in the range -26 to -30 ppm is close to the value reported by Erdman and Lawson for BONXOR and indicate the strong metalloaromatic character of these systems. The high negative values of NICS(1) and NICS(1)$_{zz}$ compared to benzene also indicate the substantial stabilization of the former due to metalloaromaticity.

Table 2.11 NICS indices for optimized geometries of WCBD

WCBD	NICS(0)	NICS(1)	NICS(1)zz
WEMYIY	-25.8	-15.4	-36.8
WEMYOE	-25.8	-15.4	-45.3
WEMYUK	-25.8	-15.1	-34.7
COMREB	-28.9	-17.4	-33.9
CONISH	-28.3	-16.1	-44.7
CUYJEL	-30.1	-17.2	-37.8
KISGID	-26.0	-15.9	-39.4

Recently Herges group developed a methodology to calculate anisotropy of current induced density (ACID) maps and used it to quantify and visualize electron delocalization and aromaticity in molecules.[121-122] The ACID isosurface plot with current density vectors plotted on it gives either diatropic (clockwise) or paratropic (anti-clockwise) circulation of the current density depending on the aromatic or anti-aromatic nature of the molecule. Figure 2.21 depicts such plots to visualize aromatic features for two representative cases, *viz.* WEMYUK and CUYJEL. It is clear from these plots that the MCBD systems possess aromatic delocalization of the π-electrons.

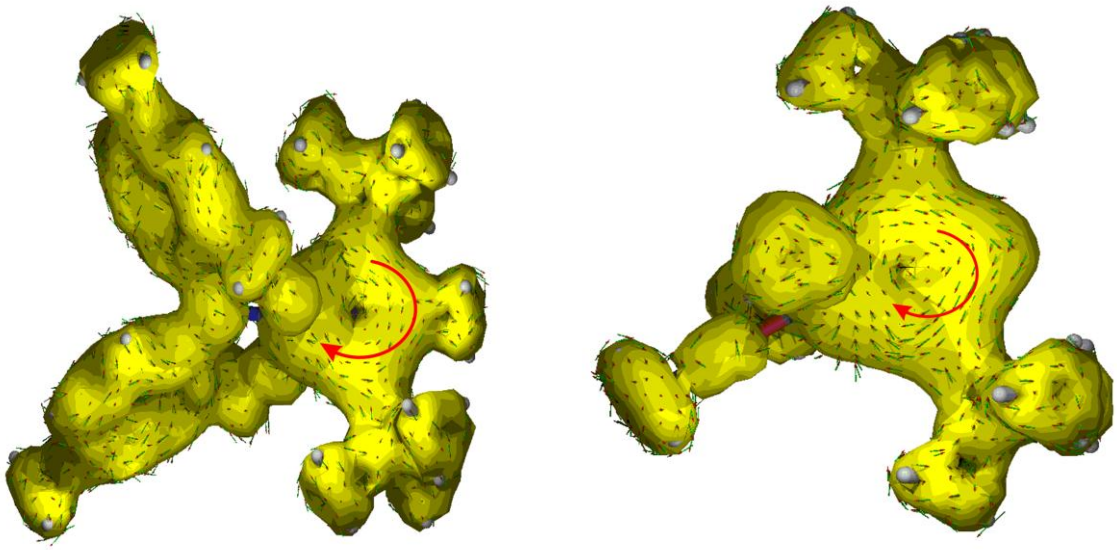

WEMYUK CUYJEL

Figure 2.21 ACID isosurface of WEMYUK and CUYJEL (isosurface value is 0.025 au). The current density vectors plotted on the isosurface shows clockwise circulation (diatropic), indicating the aromatic character of the molecule. A curved red arrow is inscribed in the picture to indicate the direction of the vectors.

2.9.4 Systems with More than One MCBD

Structural, electronic and bonding analyses of the known WCBD structures confirm that the interaction between W and C_β can be considered as a direct bond. This new WC_β bond generally called as 1,3-MC bond defines the planar tetracoordinate state of C_β. Since several WCBD structures exist in stable form, the 1,3-MC bond which contributes to their stability can be utilized to incorporate $_{pt}C$ centers in organometallic complexes. Although the theoretical exploration of $_{pt}C$ chemistry is advanced to some extent, the realistic application of a system containing $_{pt}C$ centers is yet to be achieved. Our results suggest that the consideration of WCBD systems as $_{pt}C$ systems bring in more options to the design of realistic organometallic systems. To explore this revealing thought, we propose the use of tungstenacyclobutadiene as a basic building block to construct complex organometallic structures containing multiple $_{pt}C$ centers. The structural motif given in Figure 2.16b is useful to illustrate the strategies used to develop such expanded

systems in one-, two- and three-dimensions and the proposed models are given in Figure 2.22.

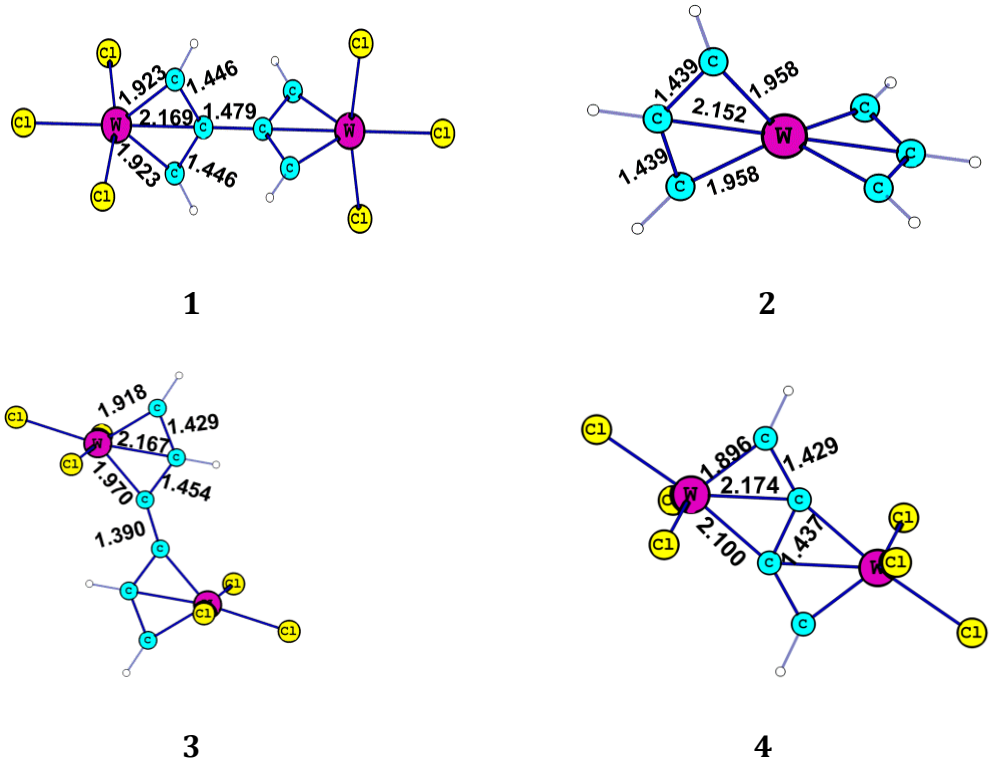

1 **2**

3 **4**

Figure 2.22 Optimized geometries of dimetallacycles containing $_{pt}$C centers.

Assuming the X-direction as the direction of the WC_β bond, an extension of the structure in that direction can be envisaged by connecting two WCBD structures similar to the known chloro-ligated Schrock system BONXOR through the β carbon as shown for model **1.** In **1**, the C_β of the two metallacycles are bonded with a distance of 1.479 Å and the two metallacycles show a symmetric orthogonal arrangement. The WC_β distance 2.169 Å in **1** is similar to any of the 1,3-WC_β bond distance given in Table 2.7. Further, the WC_α bond distance 1.923 Å indicates its double bond character while CC bond distance 1.446 Å indicates significant activation of that bond compared to a typical CC double bond (1.33 Å) or a conjugated aromatic CC bond (1.40 Å). We also consider the formation of two 1,3-WC bonded metallacycles around one tungsten atom. This model **2** is a minimum and both metallacycles in this complex show the characteristic 1,3-WC bond distance of 2.152 Å.

Expansion of the metallacycle in the Y-direction (more towards the direction of C_α) leads to the construction of two types of complexes, *viz.* **3** and **4**. **3** is constructed by connecting C_α of two metallacycles whereas, in **4**, the C_β of one metallacycle serves as the C_α of the other metallacycle meaning that a CC bond is shared by both the metallacycles. Rosenthal *et al.* and many others reported complexes of type **4**.[96, 139-140] Single bond like WC_β distance of 2.167 and 2.174 Å located respectively for **3** and **4** underlines the presence of 1,3-MC interaction in these complexes.

Polymeric 1-dimensional extension of the dimetallacycles **2** - **4** is possible while such an extension of **1** has to be compromised due to chloro ligation. Transition metal acetylide complexes are well discussed in the literature and by using acetylide units to connect metal centers, the linear expansion of **1**-type architecture can also be achieved and the model for such a structure is **5**.[141-143] Model **6** is made by connecting two units of **2** *via* the C_β. The one-dimensional extension of **3** is used to construct **7** while such an extension of **4** would lead to the formation of **8**. All these structures are energy minima, and all of them show single bond-like WC_β distances indicating the presence of 1,3-MC bonding (Figure 2.23). In **7** and **8**, the carbon chain resembles that of a polyene chain suggesting that these systems could be even considered as metal-incorporated polyene. All these extended structures preserve the 1,3-MC bonding features of metallacycles. By combining the expansion patterns shown for the X- and Y-directions, two- dimensional expansions can be created. For instance, **9** is made by connecting **2** with **5**. Similarly, **10** can be made by combining **2** and **6** which can be further extended *via* the α-carbon or β-carbon. All the MCBD units in **9** and **10** possess single bond-like WC_β distances.

Wiberg bond order analysis on the dimetallacycles (Table 2.12) shows strong WC_β interaction in both WCBD region (0.371 – 0.477). Model **4** where one CC bond is shared between the two metallacycle showed the highest WC_β bond order of 0.477. The strongest (1.499) and the weakest WC_α (0.765) bonds are found in **4.** In all the cases, the CC bond order lies between 1.167 and 1.302. QTAIM analysis on these dimetallacycles (Table 2.12) showed a catastrophe ring critical point, where the ring paths meet with a flat curvature. The ρ value at the catastrophe point is nearly 0.133 au, which is close to a typical WC single bond value.

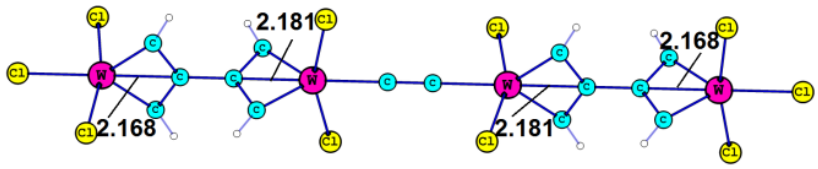

5

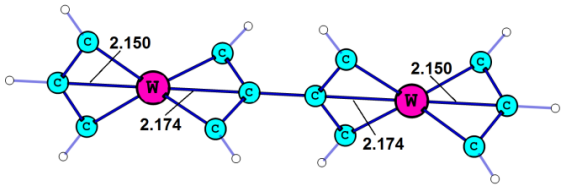

6

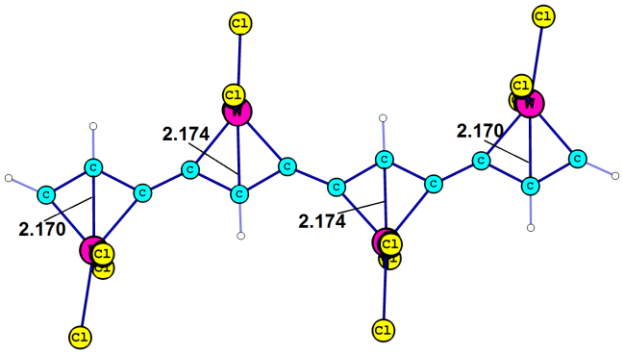

7

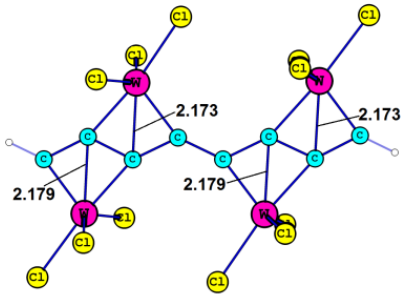

8

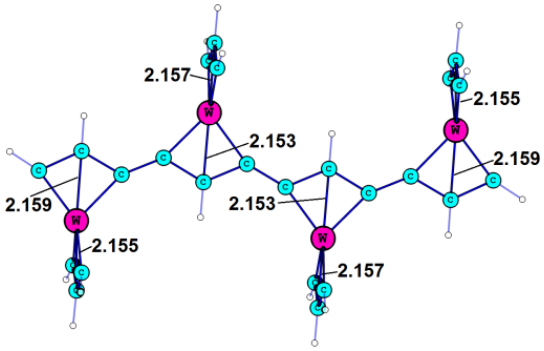

9

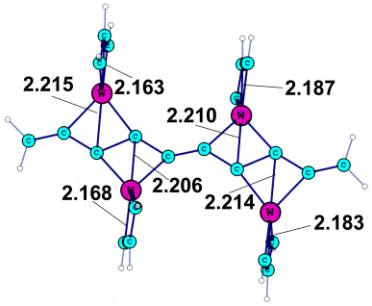

10

Figure 2.23 Models containing more than two metallacycle unit.

Table 2.12 Wiberg bond order, and QTAIM parameters calculated for the dimetallacycle models

MCBD	Wiberg bond order					QTAIM parameters (au)				
	WC_α	WC_α	$C_\alpha C_\beta$	$C_\alpha C_\beta$	WC_β	WC_α BCP	WC_α BCP	CC BCP	CC BCP	WC_β RCP
1	1.466	1.465	1.208	1.209	0.371	0.236	0.236	0.278	0.278	0.131
2	1.274	1.274	1.301	1.302	0.384	0.218	0.218	0.278	0.278	0.135
3	1.452	1.234	1.281	1.167	0.399	0.239	0.215	0.287	0.274	0.132
4	1.499	0.765	1.157	1.192	0.477	0.249	0.165	0.28	0.277	0.135

Negative values for all the three NICS indices (NICS(0), NICS(1) and $NICS(1)_{zz}$) have been observed for the dimetallacycles **1** - **4** (Table 2.13) indicating their metalloaromatic character. ^{13}C NMR analysis of these molecules showed that α and β carbons are markedly different and suggest the presence of 1,3-MC bonding between metal and C_β (Table 2.13). The QTAIM and NMR features of all the 1-dimensional (**5** - **8**) and 2-dimensional (**9** - **10**) extended structures are very similar to the dimetallacycles and suggest that C_β of WCBD region is 1,3-WC bonded and it exists in the planar tetracoordinate state.

Table 2.13 ^{13}C NMR parameters and NICS parameters calculated for the dimetallacycles calculated for the dimetallacycle models

MCBD	^{13}C NMR				NICS(0)	NICS(1)	NICS(1)zz
	δC_α	δC_α	δC_β	δC_β			
1	199.8	199.8	152.2	152.2	-27.7	-16.5	-25.0
2	193.6	193.6	133.9	133.9	-19.2	-7.2	-16.7
3	194.0	197.4	145.2	145.2	-28.9	-17.4	-45.3
4	163.7[a]	163.7[a]	151.8[b]	151.7[b]	-30.8	-17.1	-42.4

[a]terminal carbon, [b]middle carbon

Further extension of 1- and 2-dimensional structures to 3-dimensional networks is possible through proper α- and β- carbon connectivity (Figure 2.24). For example, **11** can be built from two units of **9**. Further, complex **12** can be made by combining two units of **9** along with two units of pyrene. As we can see, these type expansions of the WCBD structures can lead to the formation of metal-organic cavities in the system. In the case of **12**, a well- defined cavity of size (1.06, 0.81, 0.72 nm) in the (X, Y, Z) directions is clearly seen. The 3-dimensional structures **11** and **12** also possess single-bond like WC_β distance (~ 2.2 Å) and all the characteristic QTAIM and NMR features typically seen for a 1,3-WC bonded carbon atom.

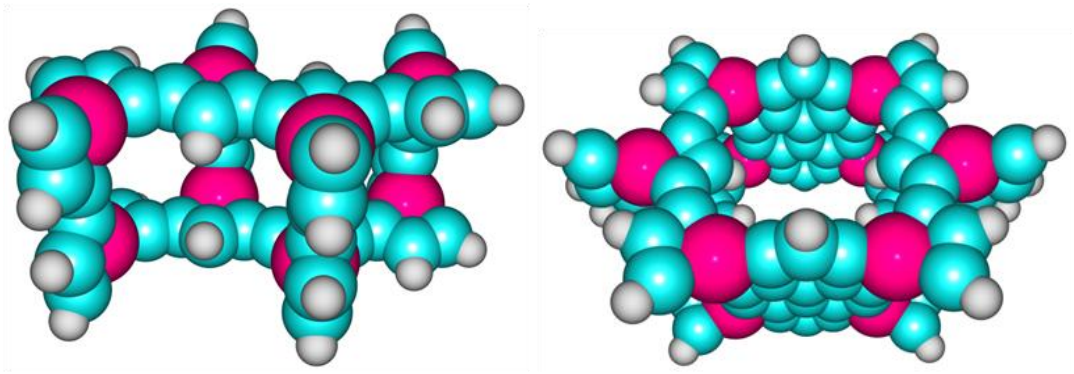

11 **12**

Figure 2.24 3-dimensional WCBD complexes containing multiple $_{pt}C$ centers (color scheme: grey –H, cyan -C, red –W).

2.10 Conclusions

Several tungstenacyclobutadienes available in the CSD have been studied for 1,3-WC bonding interaction. Single bond-like WC_β distance in these complexes is established with a significantly high bond order and appearance of a catastrophe ring critical point in the QTAIM analysis. Large negative NICS(0) values obtained for these molecules point to their metalloaromatic character which is underlined with the diatropic ring current observed in the ACID plot. All these structures showed a large difference in the ^{13}C-NMR signals of C_α and C_β which is considered as a characteristic feature of 1,3-WC bonding. Among the crystal structures, the alkoxide ligated complex CUYJEL reported

by Schrock *et al.* showed the strongest WC_β interaction. In a constrained geometry, this model showed a clear bond critical point between W and C_β. This extra bonding interaction is further confirmed by molecular orbital analysis which clearly showed the d_π-p_π interaction between tungsten and carbon. The 1,3-WC bonding in these metallacycles forces the C_β to exist in a planar tetracoordinate state, $_{pt}C$. Identification of C_β as a $_{pt}C$ center in WCBD pave the way for a new approach to the design of molecules and materials containing multiple $_{pt}C$ centers. Several such molecules have been proposed by extending the WCBD motif in 1-, 2- and 3-dimensions. The presence of 1,3-WC bond as well as metalloaramiticity in all these systems is established on the basis of the characteristic bond order, catastrophe ring critical point in QTAIM, ^{13}C NMR values and various NICS indices. The 3-dimensional structures propose the formation of $_{pt}C$ incorporated metal-organic frameworks.

2.11 References

1. P. Jean-Louis Hérisson and Y. Chauvin, *Die Makromolekulare Chemie*, **1971**, *141*, 161-176.
2. R. H. Grubbs, *Handbook of Olefin Metathesis*, WILEY–VCH Verlag GmbH & Co. KgaA, Weinheim, **2003**.
3. T. M. Trnka and R. H. Grubbs, *Acc. Chem. Res*, **2001**, *34*, 18-29.
4. J. Feldman, W. M. Davis and R. R. Schrock, *Organometallics*, **1989**, *8*, 2266-2268.
5. E. Folga and T. Ziegler, *Organometallics*, **1993**, *12*, 325-337.
6. R. R. Schrock, *Tetrahedron*, **1999**, *55*, 8141-8153.
7. C. Adlhart, C. Hinderling, H. Baumann and P. Chen, *J. Am. Chem. Soc.*, **2000**, *122*, 8204-8214.
8. L. Cavallo, *J. Am. Chem. Soc.*, **2002**, *124*, 8965-8973.
9. S. F. Vyboishchikov, M. Bühl and W. Thiel, *Chem. Eur. J.*, **2002**, *8*, 3962-3975.
10. F. Bernardi, A. Bottoni and G. P. Miscione, *Organometallics*, **2003**, *22*, 940-947.
11. P. Chen, *Angew. Chem. Int. Ed.*, **2003**, *42*, 2832-2847.
12. R. R. Schrock and A. H. Hoveyda, *Angew. Chem. Int. Ed.*, **2003**, *42*, 4592-4633.
13. C. Adlhart and P. Chen, *J. Am. Chem. Soc*, **2004**, *126*, 3496-3510.

14. P. E. Romero and W. E. Piers, *J. Am. Chem. Soc.*, **2005**, *127*, 5032-5033.
15. C. H. Suresh and M.-H. Baik, *Dalton Trans.*, **2005**, 2982-2984.
16. A. Correa and L. Cavallo, *J. Am. Chem. Soc.*, **2006**, *128*, 13352-13353.
17. X. Solans-Monfort, J.-S. Filhol, C. Coperet and O. Eisenstein, *New J. Chem.*, **2006**, *30*, 842-850.
18. M. M. Flook, A. J. Jiang, R. R. Schrock, P. Müller and A. H. Hoveyda, *J. Am. Chem. Soc.*, **2009**, *131*, 7962-7963.
19. A. Poater, F. Ragone, A. Correa, A. Szadkowska, M. Barbasiewicz, K. Grela and L. Cavallo, *Chem. Eur. J.*, **2010**, *16*, 14354-14364.
20. X. Solans-Monfort, R. Pleixats and M. Sodupe, *Chem. Eur. J.*, **2010**, *16*, 7331-7343.
21. D. V. Peryshkov and R. R. Schrock, *Organometallics*, **2012**, *31*, 7278-7286.
22. X. Solans-Monfort, C. Copéret and O. Eisenstein, *Organometallics*, **2012**, *31*, 6812-6822.
23. I. W. Ashworth, I. H. Hillier, D. J. Nelson, J. M. Percy and M. A. Vincent, *ACS Catal.*, **2013**, *3*, 1929-1939.
24. Y. Minenkov, G. Occhipinti and V. R. Jensen, *Organometallics*, **2013**, *32*, 2099-2111.
25. M. R. Reithofer, G. E. Dobereiner, R. R. Schrock and P. Müller, *Organometallics*, **2013**, *32*, 2489-2492.
26. K. Paredes-Gil, X. Solans-Monfort, L. Rodriguez-Santiago, M. Sodupe and P. Jaque, *Organometallics*, **2014**, *33*, 6065-6075.
27. X. Solans-Monfort, C. Copéret and O. Eisenstein, *Organometallics*, **2015**, *34*, 1668-1680.
28. A. Poater, F. Ragone, A. Correa and L. Cavallo, *Dalton Trans.*, **2011**, *40*, 11066-11069.
29. C. A. Urbina-Blanco, A. Poater, T. Lebl, S. Manzini, A. M. Z. Slawin, L. Cavallo and S. P. Nolan, *J. Am. Chem. Soc*, **2013**, *135*, 7073-7079.
30. F. van der EideEdwin and W. E. Piers, *Nat. Chem.*, **2010**, *2*, 571-576.
31. S. Vummaleti, L. Cavallo and A. Poater, *Theor Chem Acc*, **2015**, *134*, 1-6.

32. S. Manzini, C. A. Urbina Blanco, D. J. Nelson, A. Poater, T. Lebl, S. Meiries, A. M. Z. Slawin, L. Falivene, L. Cavallo and S. P. Nolan, *J. Organomet. Chem.*, **2015**, *780*, 43-48.
33. A. Poater, S. V. Chaitanya Vummaleti, E. Pump and L. Cavallo, *Dalton Trans*, **2014**, *43*, 11216-11220.
34. M. R. Churchill, J. W. Ziller, J. H. Freudenberger and R. R. Schrock, *Organometallics*, **1984**, *3*, 1554-1562.
35. J. Feldman, W. M. Davis, J. K. Thomas and R. R. Schrock, *Organometallics*, **1990**, *9*, 2535-2548.
36. M. Yamashita, Y. Yamamoto, K.-y. Akiba, D. Hashizume, F. Iwasaki, N. Takagi and S. Nagase, *J. Am. Chem. Soc.*, **2005**, *127*, 4354-4371.
37. G. Olah, G. S. Prakash, R. Williams and L. Field, Wiley-Interscience, New York, **1987**.
38. H. Kudo, *Nature*, **1992**, *355*, 432-434.
39. E. D. Jemmis, E. G. Jayasree and P. Parameswaran, *Chem. Soc. Rev.*, **2006**, *35*, 157-168.
40. Z.-X. Wang and P. v. R. Schleyer, *Science*, **2001**, *292*, 2465-2469.
41. K. Ito, Z. Chen, C. Corminboeuf, C. S. Wannere, X. H. Zhang, Q. S. Li and P. v. R. Schleyer, *J. Am. Chem. Soc.*, **2007**, *129*, 1510-1511.
42. K.-y. Akiba, M. Yamashita, Y. Yamamoto and S. Nagase, *J. Am. Chem. Soc.*, **1999**, *121*, 10644-10645.
43. J. I. Musher, *Angew. Chem. Int. Ed.*, **1969**, *8*, 54-68.
44. A. E. Reed and P. v. R. Schleyer, *J. Am. Chem. Soc.*, **1990**, *112*, 1434-1445.
45. T. R. Forbus and J. C. Martin, *J. Am. Chem. Soc.*, **1979**, *101*, 5057-5059.
46. T. Yamaguchi, Y. Yamamoto, D. Kinoshita, K.-y. Akiba, Y. Zhang, C. A. Reed, D. Hashizume and F. Iwasaki, *J. Am. Chem. Soc.*, **2008**, *130*, 6894-6895.
47. W. C. McKee, J. Agarwal, H. F. Schaefer and P. v. R. Schleyer, *Angew. Chem. Int. Ed.*, **2014**, *53*, 7875-7878.
48. P. v. R. Schleyer, E. U. Wuerthwein, E. Kaufmann, T. Clark and J. A. Pople, *J. Am. Chem. Soc.*, **1983**, *105*, 5930-5932.

49. F. Scherbaum, A. Grohmann, G. Müller and H. Schmidbaur, *Angew. Chem. Int. Ed.*, **1989**, *28*, 463-465.
50. K. M. Lancaster, M. Roemelt, P. Ettenhuber, Y. Hu, M. W. Ribbe, F. Neese, U. Bergmann and S. DeBeer, *Science*, **2011**, *334*, 974-977.
51. A. D. Becke, *Phys. Rev. A*, **1988**, *38*, 3098-3100.
52. J. P. Perdew, *Phys. Rev. B*, **1986**, *33*, 8822-8824.
53. A. Schäfer, C. Huber and R. Ahlrichs, *J. Chem. Phys.*, **1994**, *100*, 5829-5835.
54. C. H. Suresh and G. Frenking, *Organometallics*, **2010**, *29*, 4766-4769.
55. C. H. Suresh and G. Frenking, *Organometallics*, **2012**, *31*, 7171-7180.
56. C. H. Suresh and G. Frenking, *Organometallics*, **2013**, *32*, 1531-1536.
57. A. Poater, E. Pump, S. V. C. Vummaleti and L. Cavallo, *J Chem Theory Comput.*, **2014**, *10*, 4442-4448.
58. T. A. Keith *AIMAll*, *14.04.17*; TK Gristmill Software, Overland Park KS, USA: **2014**.
59. T. K. Brunck and F. Weinhold, *J. Am. Chem. Soc.*, **1979**, *101*, 1700-1709.
60. F. Weinhold, in *Encyclopedia of Computational Chemistry*, John Wiley & Sons, Ltd, **2002**.
61. T. Helgaker, M. Jaszuński and K. Ruud, *Chem. Rev.*, **1999**, *99*, 293-352.
62. K. Ruud, T. Helgaker, K. L. Bak, P. Jørgensen and H. J. r. A. Jensen, *J. Chem. Phys.*, **1993**, *99*, 3847-3859.
63. T.-L. Choi and R. H. Grubbs, *Angew. Chem. Int. Ed.*, **2003**, *42*, 1743-1746.
64. S. B. Garber, J. S. Kingsbury, B. L. Gray and A. H. Hoveyda, *J. Am. Chem. Soc.*, **2000**, *122*, 8168-8179.
65. P. Gütlich, H. A. Goodwin and D. N. Hendrickson, *Angew. Chem. Int. Ed.*, **1994**, *33*, 425-427.
66. Y. Jean, A. Lledos, J. K. Burdett and R. Hoffmann, *J. Am. Chem. Soc*, **1988**, *110*, 4506-4516.
67. G. Parkin, *Acc. Chem. Res.*, **1992**, *25*, 455-460.
68. R. F. W. Bader, *Atoms in Molecules: A Quantum Theory*, Clarendon Press,Oxford, UK, **1990.**
69. C. H. Suresh and N. Koga, *Organometallics*, **2003**, *23*, 76-80.
70. S. Arndt, R. R. Schrock and P. Müller, *Organometallics*, **2007**, *26*, 1279-1290.

71. L. N. Bochkarev, Y. E. Begantsova, A. L. Bochkarev, N. E. Stolyarova, I. K. Grigorieva, I. P. Malysheva, G. V. Basova, E. O. Platonova, G. K. Fukin, E. V. Baranov, Y. A. Kurskii and G. A. Abakumov, *J. Organomet. Chem.*, **2006**, *691*, 5240-5245.
72. A. J. Jiang, J. H. Simpson, P. Müller and R. R. Schrock, *J. Am. Chem. Soc.*, **2009**, *131*, 7770-7780.
73. S. C. Marinescu, R. R. Schrock, P. Müller, M. K. Takase and A. H. Hoveyda, *Organometallics*, **2011**, *30*, 1780-1782.
74. J. Yuan, R. R. Schrock, P. Müller, J. C. Axtell and G. E. Dobereiner, *Organometallics*, **2012**, *31*, 4650-4653.
75. W. C. P. Tsang, K. C. Hultzsch, J. B. Alexander, P. J. Bonitatebus, R. R. Schrock and A. H. Hoveyda, *J. Am. Chem. Soc*, **2003**, *125*, 6337-6337.
76. C. N. Rowley, E. F. van der Eide, W. E. Piers and T. K. Woo, *Organometallics*, **2008**, *27*, 6043-6045.
77. C. H. Suresh, *J. Organomet. Chem.*, **2006**, *691*, 5366-5374.
78. R. Hoffmann, R. W. Alder and C. F. Wilcox, *J. Am. Chem. Soc.*, **1970**, *92*, 4992-4993.
79. R. Hoffmann, *Pure Appl. Chem.*, **1971**, *28*, 181-194.
80. V. I. Minkin, R. M. Minyaev and R. Hoffmann, *Russ. Chem. Rev.*, **2002**, *71*, 869-892.
81. J. B. Collins, J. D. Dill, E. D. Jemmis, Y. Apeloig, P. v. R. Schleyer, R. Seeger and J. A. Pople, *J. Am. Chem. Soc.*, **1976**, *98*, 5419-5427.
82. P. v. R. Schleyer and A. I. Boldyrev, *J. Chem. Soc., Chem. Commun.*, **1991**, *0*, 1536-1538.
83. Z.-X. Wang and P. v. R. Schleyer, *J. Am. Chem. Soc.*, **2001**, *123*, 994-995.
84. F. A. Cotton and M. Millar, *J. Am. Chem. Soc.*, **1977**, *99*, 7886-7891.
85. R. H. Cayton, S. T. Chacon, M. H. Chisholm, M. J. Hampden-Smith, J. C. Huffman, K. Folting, P. D. Ellis and B. A. Huggins, *Angew. Chem. Int. Ed.*, **1989**, *28*, 1523-1525.
86. F. A. Cotton and E. S. Shamshoum, *J. Am. Chem. Soc.*, **1985**, *107*, 4662-4667.
87. P. Leoni, M. Pasquali, G. Pieri, A. Albinati, P. S. Pregosin and H. Rueegger, *Organometallics*, **1995**, *14*, 3143-3145.
88. W. J. Evans, R. A. Keyer and J. W. Ziller, *Organometallics*, **1993**, *12*, 2618-2633.
89. D. Röttger and G. Erker, *Angew. Chem. Int. Ed.*, **1997**, *36*, 812-827.

90. G. Erker, *Comments Inorg. Chem.*, **1992**, *13*, 111-131.
91. P. Arndt, C. Lefeber, R. Kempe, A. Tillack and U. Rosenthal, *Chemische Berichte*, **1996**, *129*, 1281-1285.
92. G. Erker, W. Fromberg, K. Angermund, R. Schlund and C. Kruger, *J. Chem. Soc., Chem. Commun.*, **1986**, 372-374.
93. R. Gleiter, I. Hyla-Kryspin, S. Niu and G. Erker, *Organometallics*, **1993**, *12*, 3828-3836.
94. J. H. Freudenberger, R. R. Schrock, M. R. Churchill, A. L. Rheingold and J. W. Ziller, *Organometallics*, **1984**, *3*, 1563-1573.
95. M. R. Churchill and J. W. Ziller, *J. Organomet. Chem.*, **1985**, *286*, 27-36.
96. S. Roy, U. Rosenthal and E. D. Jemmis, *Acc. Chem. Res.*, **2014**, *47*, 2917-2930.
97. G. Erker, *Chem.Soc. Rev.*, **1999**, *28*, 307-314.
98. W. Siebert and A. Gunale, *Chem. Soc. Rev.*, **1999**, *28*, 367-371.
99. R. Keese, *Chem. Rev.*, **2006**, *106*, 4787-4808.
100. G. Merino, M. A. Méndez-Rojas, A. Vela and T. Heine, *J. Compu. Chem.*, **2007**, *28*, 362-372.
101. L.-M. Yang, E. Ganz, Z. Chen, Z.-X. Wang and P. v. R. Schleyer, *Angew. Chem. Int. Ed.*, **2015**, *54*, 9468-9501.
102. J. H. Wengrovius, J. Sancho and R. R. Schrock, *J. Am. Chem. Soc.*, **1981**, *103*, 3932-3934.
103. S. F. Pedersen, R. R. Schrock, M. R. Churchill and H. J. Wasserman, *J. Am. Chem. Soc.*, **1982**, *104*, 6808-6809.
104. S. Beer, C. G. Hrib, P. G. Jones, K. Brandhorst, J. Grunenberg and M. Tamm, *Angew. Chem. Int. Ed.*, **2007**, *46*, 8890-8894.
105. J. Zhu, G. Jia and Z. Lin, *Organometallics*, **2006**, *25*, 1812-1819.
106. S. Beer, K. Brandhorst, C. G. Hrib, X. Wu, B. Haberlag, J. Grunenberg, P. G. Jones and M. Tamm, *Organometallics*, **2009**, *28*, 1534-1545.
107. L. G. McCullough, M. L. Listemann, R. R. Schrock, M. R. Churchill and J. W. Ziller, *J. Am. Chem. Soc.*, **1983**, *105*, 6729-6730.
108. L. G. McCullough, R. R. Schrock, J. C. Dewan and J. C. Murdzek, *J. Am. Chem. Soc.*, **1985**, *107*, 5987-5998.

109. S. Roy, E. D. Jemmis, A. Schulz, T. Beweries and U. Rosenthal, *Angew. Chem. Int. Ed.*, **2012**, *51*, 5347-5350.
110. T. Woo, E. Folga and T. Ziegler, *Organometallics*, **1993**, *12*, 1289-1298.
111. Z. Lin and M. B. Hall, *Organometallics*, **1994**, *13*, 2878-2884.
112. G. D. Geske and A. I. Boldyrev, *Inorg. Chem.*, **2002**, *41*, 2795-2798.
113. X. Li, H.-F. Zhang, L.-S. Wang, G. D. Geske and A. I. Boldyrev, *Angew. Chem. Int. Ed.*, **2000**, *39*, 3630-3632.
114. Li-ming Yang , Yi-hong Ding and Chia-chung Sun, *J. Am. Chem. Soc.*, **2007**, *129*, 658-665.
115. P. D. Pancharatna, M. A. Méndez-Rojas, G. Merino, A. Vela and R. Hoffmann, *J. Am. Chem. Soc.*, **2004**, *126*, 15309-15315.
116. G.-L. Chai, C.-S. Lin and W.-D. Cheng, *J. Mater. Chem.*, **2012**, *22*, 11303-11309.
117. M. Wu, Y. Pei and X. C. Zeng, *J. Am. Chem. Soc.*, **2010**, *132*, 5554-5555.
118. D. Andrae, U. Häußermann, M. Dolg, H. Stoll and H. Preuß, *Theoret. Chim. Acta*, **1990**, *77*, 123-141.
119. K. Ruud, T. Helgaker, K. L. Bak, P. Jo/rgensen and H. J. r. A. Jensen, *J. Chem. Phys.*, **1993**, *99*, 3847-3859.
120. P. v. R. Schleyer, C. Maerker, A. Dransfeld, H. Jiao and N. J. R. v. E. Hommes, *J. Am. Chem. Soc.*, **1996**, *118*, 6317-6318.
121. D. Geuenich, K. Hess, F. Köhler and R. Herges, *Chem. Rev.*, **2005**, *105*, 3758-3772.
122. R. Herges and D. Geuenich, *J. Phys. Chem. A*, **2001**, *105*, 3214-3220.
123. M. E. O'Reilly, I. Ghiviriga, K. A. Abboud and A. S. Veige, *Dalton Trans.*, **2013**, *42*, 3326-3336.
124. R. F. W. Bader, *J. Phys. Chem. A*, **1998**, *102*, 7314-7323.
125. E. Cerpa, A. Krapp, A. Vela and G. Merino, *Chem. Eur. J.*, **2008**, *14*, 10232-10234.
126. S. Grimme, C. Muck-Lichtenfeld, G. Erker, G. Kehr, H. D. Wang, H. Beckers and H. Willner, *Angew. Chem. Int. Ed.*, **2009**, *48*, 2592-2595.
127. P. Dem'yanov and P. Polestshuk, *Chem. Eur. J.*, **2012**, *18*, 4982-4993.
128. A. Guevara-Garcia, P. W. Ayers, S. Jenkins, S. R. Kirk, E. Echegaray and A. Toro-Labbe, in *Electronic Effects in Organic Chemistry*, ed. B. Kirchner, **2014**, *vol. 351*,103-124.

129. A. Morgenstern, T. Wilson, J. Miorelli, T. Jones and M. E. Eberhart, *Comput. Theor. Chem.*, **2015**, *1053*, 31-37.
130. J. Overgaard, H. F. Clausen, J. A. Platts and B. B. Iversen, *J. Am. Chem. Soc.*, **2008**, *130*, 3834-3843.
131. L. J. Farrugia, C. Evans, D. Lentz and M. Roemer, *J. Am. Chem. Soc.*, **2009**, *131*, 1251-1268.
132. P. R. Remya and C. H. Suresh, *Dalton Trans.*, **2015**, *44*, 17660-17672.
133. J. H. Freudenberger and R. R. Schrock, *Organometallics*, **1986**, *5*, 1411-1417.
134. A. Lugo, J. Fischer and D. B. Lawson, *J. Mol. Struct.-Theochem*, **2004**, *674*, 139-146.
135. C. Zhu, S. Li, M. Luo, X. Zhou, Y. Niu, M. Lin, J. Zhu, Z. Cao, X. Lu, T. Wen, Z. Xie, P. v. R. Schleyer and H. Xia, *Nat. Chem.*, **2013**, *5*, 698-703.
136. C. Q. Zhu, Y. H. Yang, M. Luo, C. X. Yang, J. J. Wu, L. N. Chen, G. Liu, T. B. Wen, J. Zhu and H. P. Xia, *Angew. Chem. Int. Ed.*, **2015**, *54*, 6181-6185.
137. H. Masui, *Coord. Chem. Rev.*, **2001**, *219–221*, 957-992.
138. F. Erdman and D. B. Lawson, *J.Organomet. Chem.*, **2005**, *690*, 4939-4944.
139. U. Rosenthal, A. Ohff, A. Tillack, W. Baumann and H. Görls, *J.Organomet. Chem.*, **1994**, *468*, C4-C8.
140. P.-M. Pellny, V. V. Burlakov, W. Baumann, A. Spannenberg, R. Kempe and U. Rosenthal, *Organometallics*, **1999**, *18*, 2906-2909.
141. N. J. Long and C. K. Williams, *Angew. Chem. Int. Ed.*, **2003**, *42*, 2586-2617.
142. T. Ren, *Organometallics*, **2005**, *24*, 4854-4870.
143. W.-Y. Wong and C.-L. Ho, *Coord. Chem. Rev.*, **2006**, *250*, 2627-2690.

Chapter 3

Theoretical Evidence for Bond Stretch Isomerism in Grubbs Olefin Metathesis

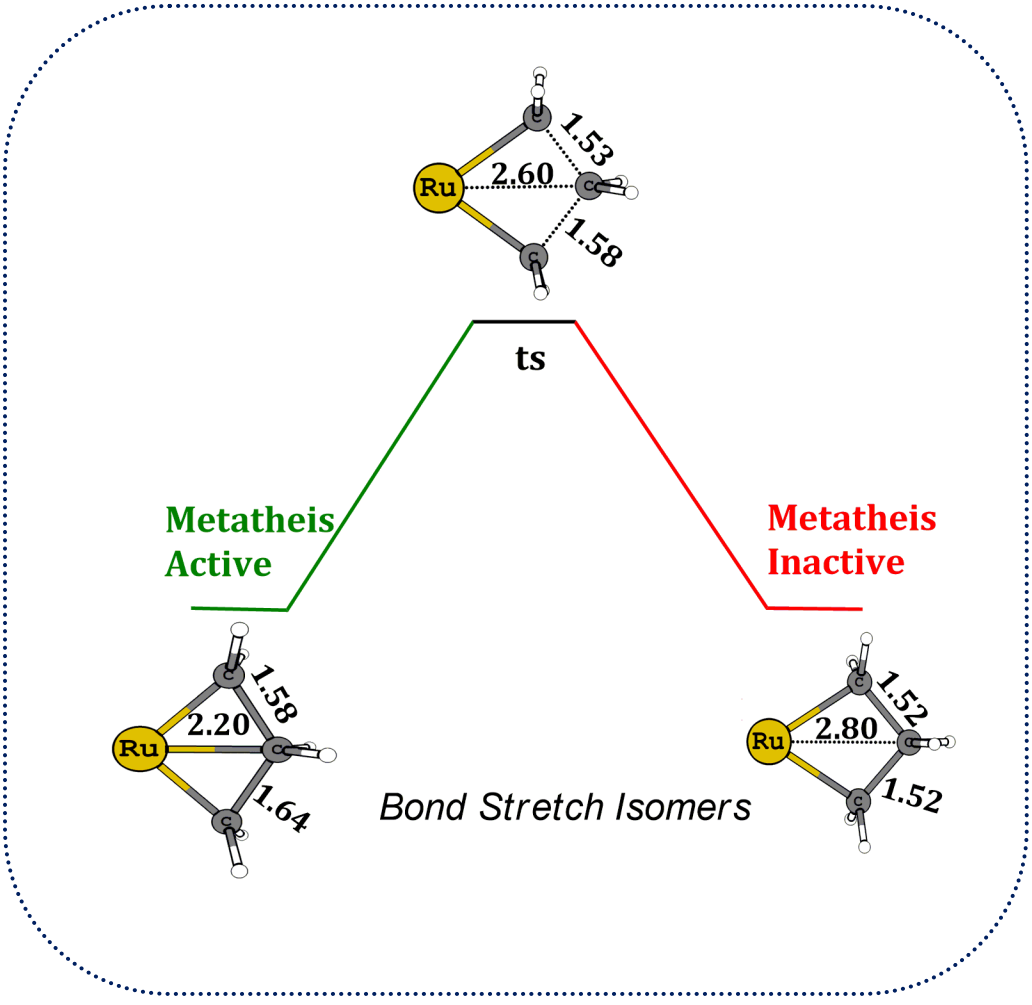

3.1 Abstract

A comprehensive density functional theory study on the dissociative and associative mechanisms of Grubbs first and second generation olefin metathesis catalysis reveals that ruthenacyclobutane intermediate (RuCB) observed in the Chauvin mechanism is not unique as it can change to a non-metathetic ruthenacyclobutane (RuCB′) via the phenomenon of bond stretch isomerism (BSI). RuCB and RuCB′ differ mainly in RuC_α, RuC_β, and $C_\alpha C_\beta$ bond lengths of the metallacycle. RuCB is metathesis active due to the agostic type bonding-assisted simultaneous activation of both $C_\alpha C_\beta$ bonds, whereas an absence of such bonding interactions in RuCB′ leads to typical CC single bond distances and metathesis inactivity. RuCB and RuCB′ are connected by a transition state showing moderate activation barrier. New mechanistic insights invoking BSI explains the non-preference of associative mechanism and the requirement of bulky ligands in the Grubbs catalyst design. The present study lifts the status of BSI from a concept of largely theoretical interest to a phenomenon of intense importance to describe an eminent catalytic reaction.

3.2 Introduction

Bond stretch isomerism (BSI) is the phenomenon of existence of molecules in two isomers differing only in certain bond lengths.[1-2] Hoffmann *et al.* introduced this concept with the help of some hypothetical organic molecules such as $(CH)_5^+$ and $(CH)_4CO$ (Figure 3.1a).[1] For a long time, the blue and green isomers of the inorganic complex *cis-mer*-$MoOCl_2(PMe_2Ph)_3$ reported by Butcher and Chatt[3] was considered as perfect examples of BSI. While the Mo=O bond length was different in blue (1.676 Å) and green (1.803 Å) isomers, rest of the geometric features remains nearly the same. Later many metal oxo complexes, characterized with the help of crystallographic and theoretical techniques were reported to show isomers that differ in the metal-oxygen bond distance (Figure 3.1b).[4-8] Though these observations laid the foundation for BSI, further experimental studies on these complexes proved that the artifact in the crystallographic techniques led to the false identification of two isomers in the crystal

which was also supported by locating only one structure at high level computational studies.[9-12] From a theoretical point of view, one criterion for the existence of BSI is the presence of two minima separated by a significant barrier for interconversion on the potential energy surface. A well known theoretically characterized example of BSI is tetrasilabicyclo[1.1.0]butane system. Schleyer *et al.*[13] showed that this Si_4H_6 molecule exists in two forms which differ in the distance between the bridgehead silicons. Later Boatz and Gordan[14-15] using computational studies at GVB/3-21g* level proposed the existence of bond stretch isomers in tetra-, 1,2,3-tri- and 1,3-disilabicyclo[1.1.0]butane (Figure 3.1c) systems. Experimentally confirmed cases of BSI are rare in the literature. In 2009, Seppelt *et al* [16] showed experimentally and theoretically that hexafluorinated benzene radical cation $C_6F_6^{\cdot+}$ exists in two different isomeric forms such as quinoid (compressed hexagon) and bisallyl (elongated hexagon (Figure 3.1d). Kölle *et al.* reported two isomers of $[(Cp^*RuCl)_2(\mu\text{-}Cl)_2]$ with different Ru–Ru bond distance (2.930 and 3.752 Å), but both differ in the spin states as the shorter is anti-ferromagnetic while longer is ferromagnetic.[17-18] McGrady analyzed $[(Cp^*RuCl)_2(\mu\text{-}Cl)_2]$ using broken symmetry density functional theory and confirmed that the two isomers fulfill all the criteria required for bond stretch isomers as spin crossover in dimetallic complexes involves spin flipping in the metal centers.[19]

It is clear from the above discussion that most of the reported examples of BSI are hypothetical models, and not many examples are known characterized by crystallography techniques.[20-23] Further, there is no report on the observation of BSI in a catalytic reaction which could play a decisive role in the reaction mechanism. A truly organometallic complex showing BSI due to metal-carbon bond length changes is also never reported in the literature. In this context, a recent study from us on Grubbs olefin metathesis takes center stage due to the disclosure that the metallacyclobutane (MCB) intermediate of metathesis may show BSI (Chapter 2A).[24]

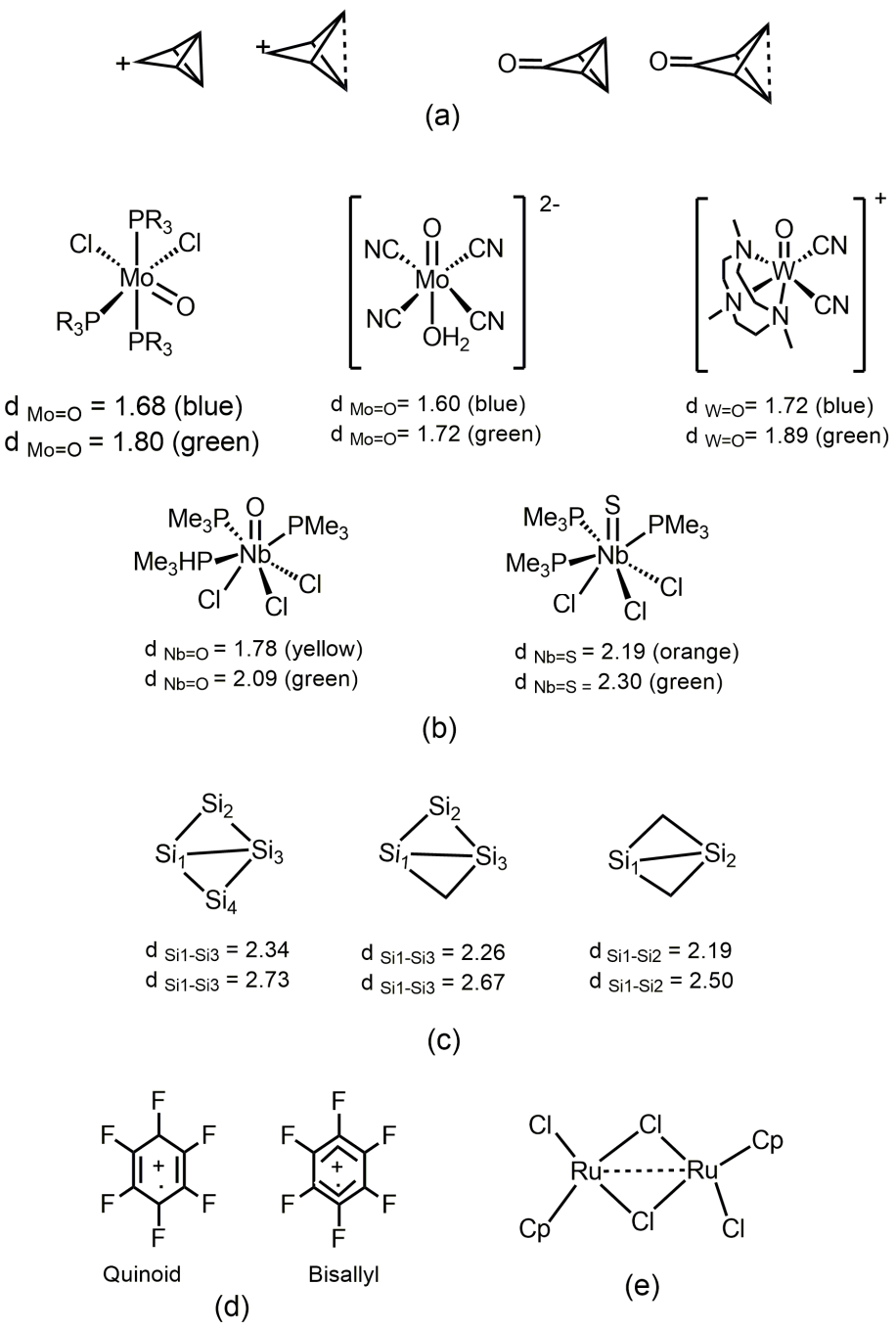

Figure 3.1 Typical cases discussed in the literature for bond stretch isomerism.

Olefin metathesis is a transition metal catalyzed reaction for CC bond formation and is regarded as one of the most elegant methods in organic chemistry.[25-27] Grubbs ruthenium-based complexes and Schrock's tungsten and molybdenum-based complexes are commonly used to catalyze the reaction.[26,27] Olefin metathesis follows a

mechanism called Chauvin mechanism and according to this mechanism the key step of metathesis reaction is the formation of a ruthenacyclobutane (RuCB) intermediate[28] and four possibilities for the RuCB formation are given in Scheme 3.1. The path labeled as 16eD (16-electron Dissociative) is the dissociative pathway where the bulky phosphine ligand dissociates prior to alkene coordination. The metallacycle formed in this case (RuCB1) is a 14-electron complex. The associative *trans* coordination of alkene (with respect to the carbene ligand) is described in the 18eA-D1 (18-electron Associative Dissociative1) path which merges with the 16eD path after the dissociation of the phosphine ligand. The 18eA-D2 (18-electron Associative Dissociative 2) path describes the associative *cis* coordination of alkene followed by dissociation of the phosphine. The 14-electron RuCB2 is the intermediate formed in this path. The 18eA (18-electron Associative) path describes the fully associative mechanism which passes through the 16-electron RuCB3. In every mechanism, the cycloreversion of RuCB intermediate releases the alkene and regenerates the catalyst. The RuCB formation changes the oxidation state of Ru from +2 to +4 meaning that the metal center becomes highly electron deficient. Though 16eD path is the widely accepted mechanism for Grubbs metathesis,[29-38] 18eA path cannot be ruled out for a catalyst designed with sterically less bulky phosphine or small-sized N-heterocyclic carbene ligands.[39]

The RuCB intermediates of olefin metathesis have been characterized with short RuCβ distance (~2.20 Å), long CC bonds (~1.60 Å) and wider CCC angle (~120°) than tetrahedral centers.[24] Herein, we show that the agostic metallacycles RuCB1, RuCB2 and RuCB3 have a tendency to undergo isomerization to non-agostic metallacycles RuCB1′, RuCB2′ and RuCB3′, respectively. In the non-agostic isomers, CC bond attains regular C_{sp3}-C_{sp3} character (~1.52 Å) and Ru-C_{β} distance approaches to ~2.80 Å. We also show that the pairs (RuCB2, RuCB2′) and (RuCB3, RuCB3′) are perfect examples of BSI in organometallics.

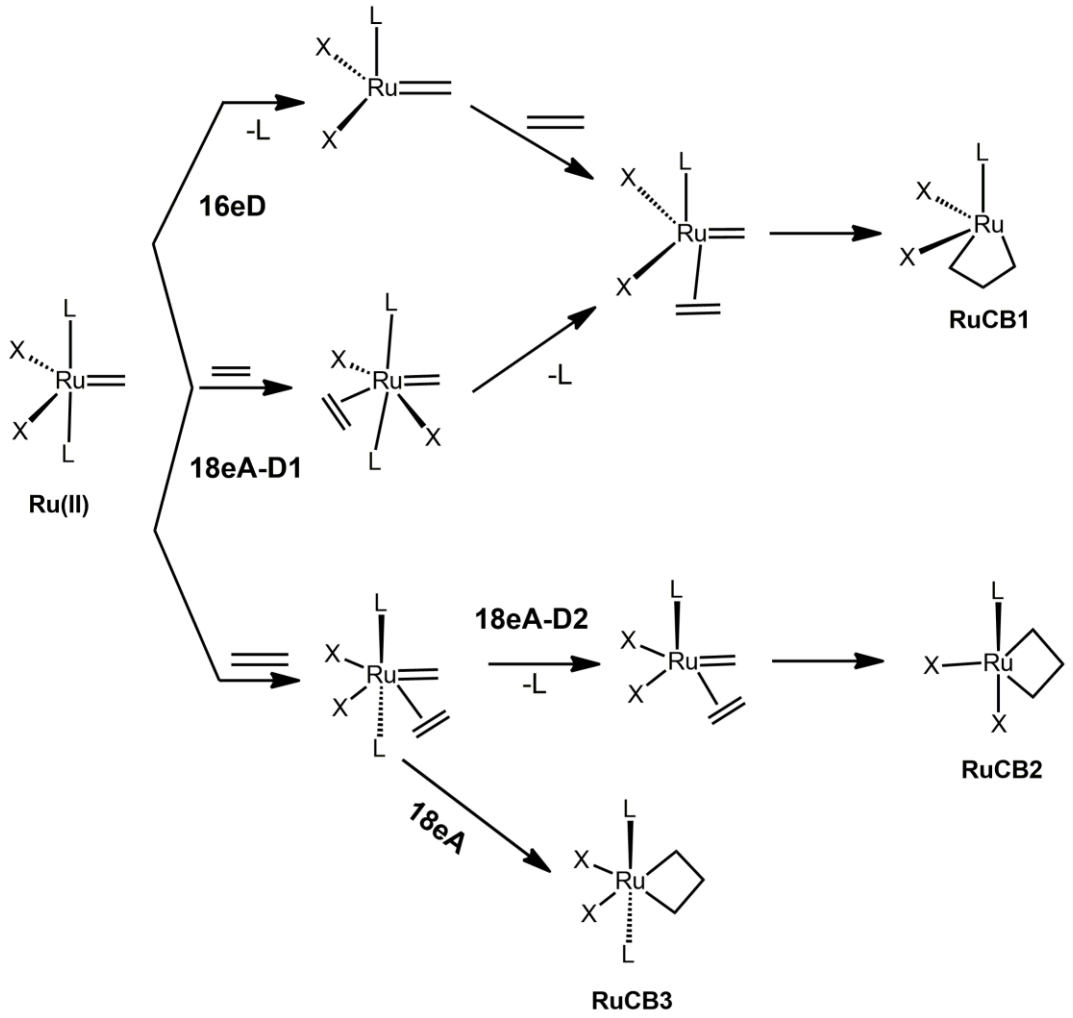

Scheme 3.1 Possible pathways of olefin metathesis by Grubbs catalyst.

3.3 Computational Details

For all molecular systems, the geometry optimization and vibrational frequency calculations have been done with Gaussian 09 program at BP86/Gen1 level of theory.[40-41] In Gen1, 6-31G* basis set[42] is used for lighter atoms and Ru center is described using Stuttgart-Dresden (SDD) effective core potential for the 28 core electrons and the associated double-zeta basis set for the 16 valence electrons.[43] All the transition states have been characterized by one imaginary frequency while all other stationary points showed no imaginary frequencies. Polarizable continuum model (PCM) with dichloromethane as the solvent is used for obtaining the solvation effect incorporated

electronic energy values at BP86/ Gen1 level. The energetic description of the results is based on Gibbs free energy corrected with the solvation effect.[44] Further, many typically used/recommended DFT methods for transition metal complexes, *viz*. along with basis set Gen1 have been used for benchmarking the results on BSI systems. At these DFT levels too, the nature of the stationary points has been verified using analytical vibrational frequency calculations. To check the suitability of the basis set, a diffused triple zeta valence basis set def2-TZVPP is used with the bp86 functional on all atoms.[45]

3.4 Results and Discussion

To demonstrate the role of BSI in olefin metathesis, we examined all four mechanisms described in Scheme 3.1 for two Grubbs first generation catalysts ($(PR_3)_2Cl_2Ru{=}CH_2$ where R = PMe_3 (G1small) or R = PCy_3 (G1big)) and two second generation catalyst ($L'LCl_2Ru{=}CH_2$ where L = H2IMe, L′ = PMe_3 (G2small) or L = H2IMes, L′ = PCy_3 (G2big)). All four catalysts are sketched in Figure 3.2.

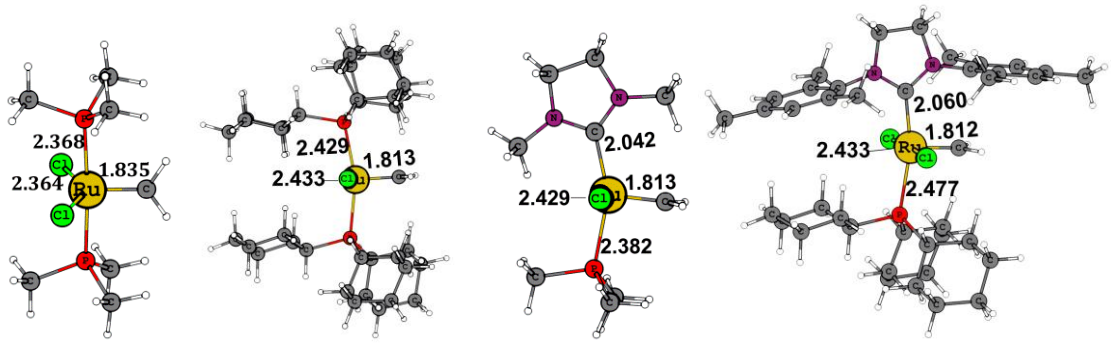

G1small G1 big G2small G2big

Figure 3.2 Structures of various catalyst models studied. All bond distances are given in Å.

3.4.1 16eD Pathway

Figure 3.3 depicts the intermediates and transition state for the 16eD pathway of ethylene metathesis catalyzed by G1small. Other catalyst systems also follow similar pathway and the reaction free energy profile in DCM solvent is described in Figure 3.4. Catalyst initiation occurs by the labile ligand dissociation from the catalyst, which leads

to the strengthening of the RuC, RuP and RuCl bonds in the resulting 14-electron complex **1**.

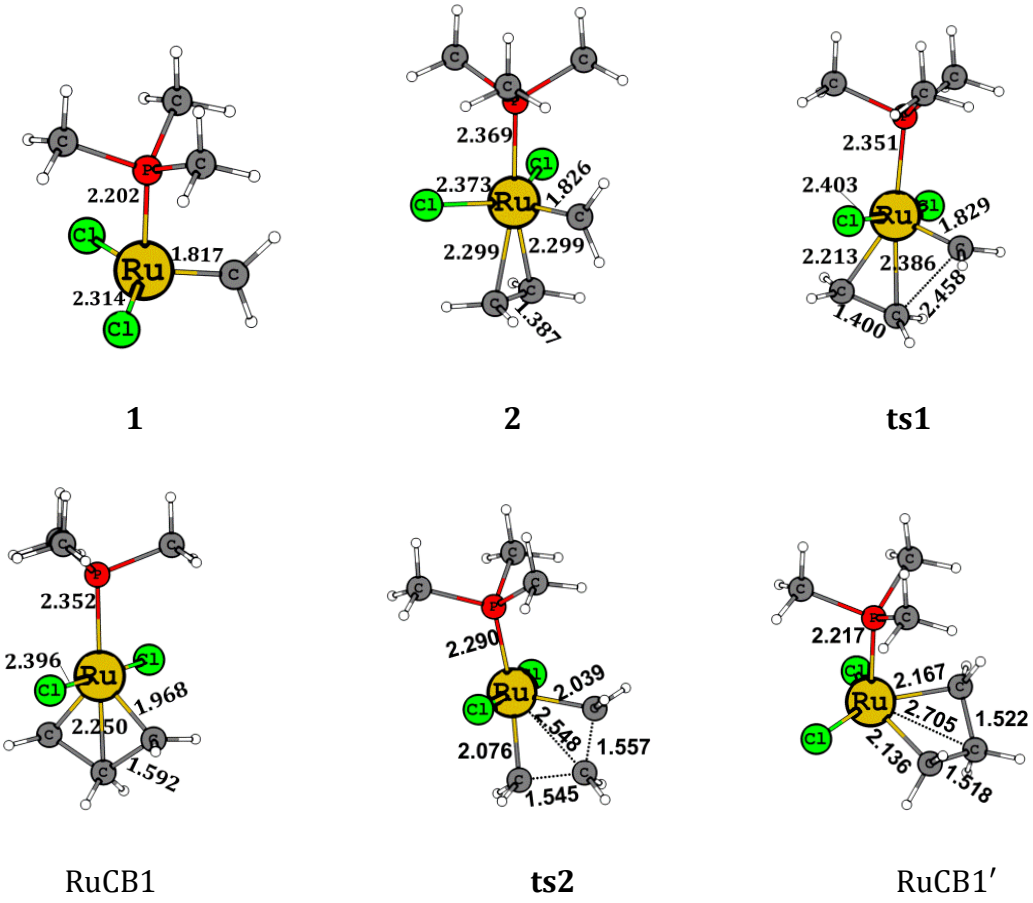

1 **2** **ts1**

RuCB1 **ts2** RuCB1′

Figure 3.3 Intermediates and transition states formed in the 16eD pathway catalyzed G1small.

For the two big systems G1big and G2big, dissociation of PCy3 ligand, results in the stabilization of the system in the solvent. Alkene coordination to **1** leading to **2** increases the entropy of the system. The CC bond formation between an alkene and carbene ligand occurs *via* transition state **ts1**. Figure 3.4 clearly shows that formation of a metallacycle RuCB1 *via* **ts1** is a favoured path as the barrier is very low. For cycloreversion leading to metathesis, RuCB1 has to pass through a transition state exactly similar to **ts1** and the product formed will be the olefin-coordinated complex similar to **2**. In all the cases, cycloreversion is more energy demanding with the

activation free energy ($\Delta G^{\#}$) 6.5, 11.5, 13.2, and 8.9 kcal/mol for G1small, G1big, G2small, and G2big, respectively.

Another possibility is that the metallacycle RuCB1 can transform to another metallacycle RuCB1′ *via* a transition state **ts2**. The dotted lines in Figure 3.4 represent the conversion of agostic RuCB1 to non-agostic RuCB1′ *via* **ts2**, which occurs with $\Delta G^{\#}$ 16.7, 19.8, 24.3 and 30.4 kcal/mol for G1small, G1big, G2small, and G2big, respectively. RuCB1 is significantly more stable than RuCB1′ in all the cases meaning that the metathesis inactive RuCB1′, if formed can be easily converted to metathesis active RuCB1. The 16eD is the most trusted olefin metathesis pathway and the G_{rel} profiles of the realistic catalyst models G1big and G2big completely agree to this.

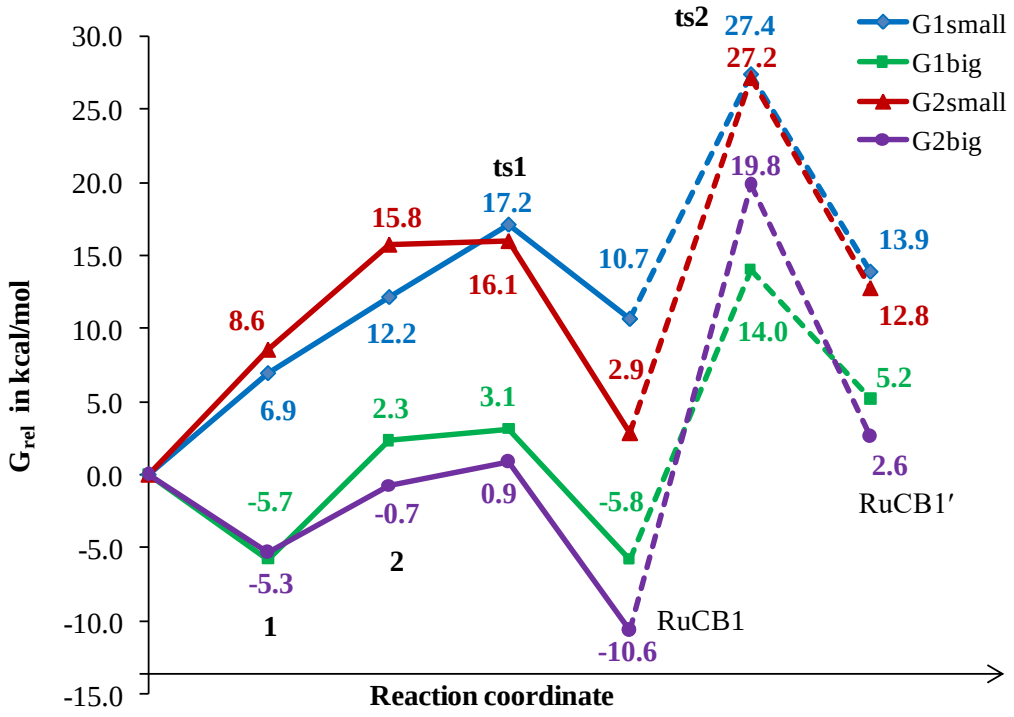

Figure 3.4 Energy profile diagram for the 16eD pathway. Dashed lines represent inter-conversion of RuCB1 to RuCB1′.

3.4.2 18eA-D1 Pathway

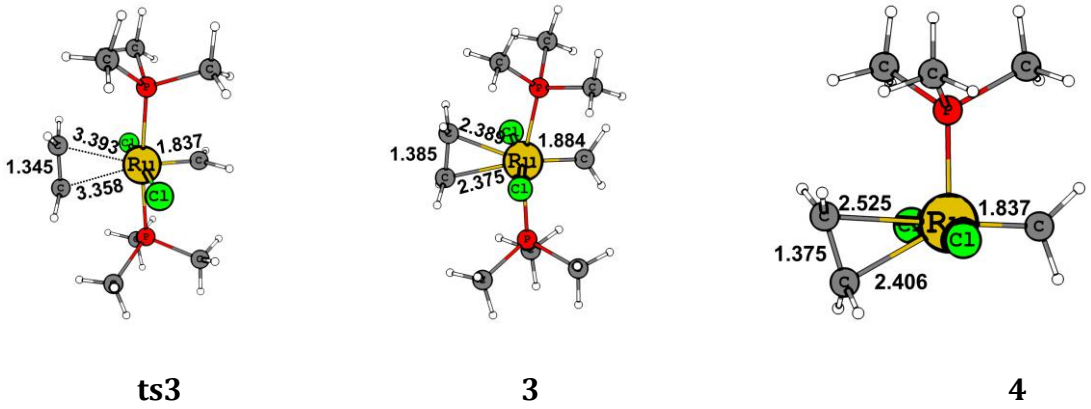

Figure 3.5 Intermediates and transition states formed in the 18eA-D1 pathway catalyzed by G1small.

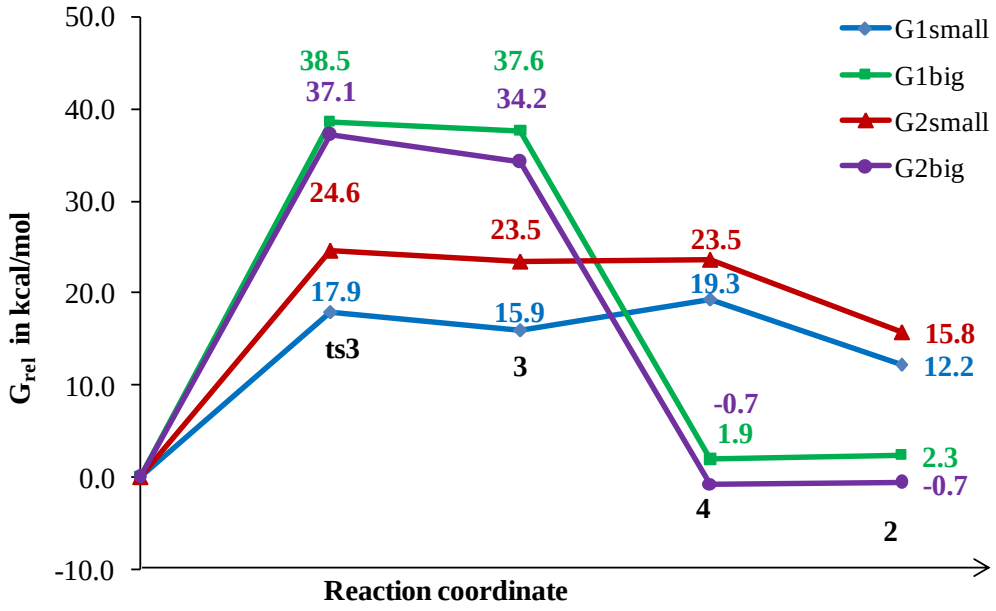

Figure 3.6 Energy profile diagram for the 18eA-D1 mechanism.

In 18eA-D1 path, the crucial step is the coordination of olefin *trans* with respect to the carbene ligand (**3**). The intermediates and transition state of 18eA-D1 path for G1small are given in Figure 3.5 and the reaction free energy profile for all catalyst models are given in Figure 3.6. Although a vacant coordination site on ruthenium center is expected at the *trans* position, the olefin coordination occurs only through the

formation of a high energy transition state (**ts3**) with $\Delta G^{\#}$ 17.9, 38.5, 24.6 and 37.1kcal/mol, respectively for G1small, G1big, G2small and G2big (Figure 3.6). The steric influence of bulky ligands retards the olefin coordination. Further, the *trans* influence of carbene ligand and the π donating character of chloro ligands oppose the olefin coordination. From **3**, a phosphine ligand dissociates to form **4** which subsequently rearranges to **2**. From **2**, the reaction follows the 16eD pathway.

3.4.3 18eA-D2 Pathway

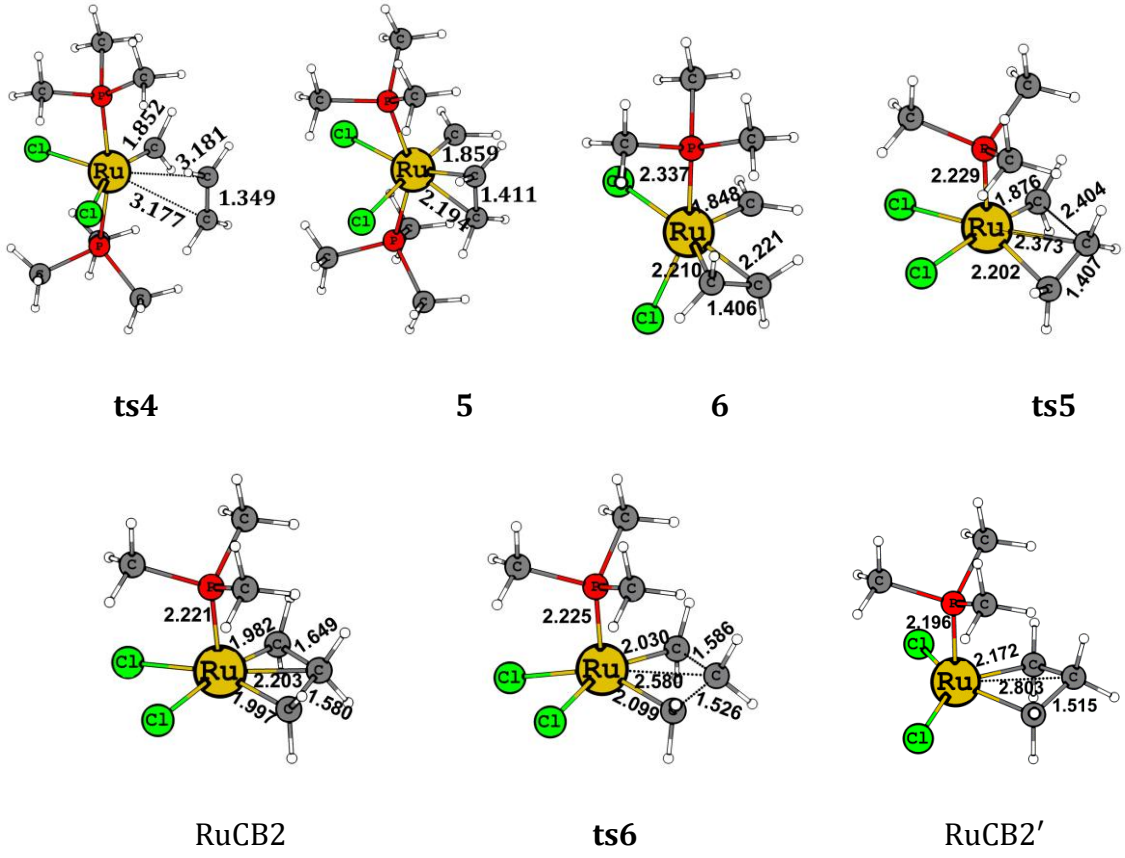

ts4 **5** **6** **ts5**

RuCB2 **ts6** RuCB2′

Figure 3.7 Intermediates and transition states formed in the 18eA-D2 pathway catalyzed by G1small.

In this pathway, *cis* coordination of the alkene with respect to the carbene ligand occurs which requires the formation of a transition state **ts4** (Figure 3.7). The activation barrier for the *cis* coordination is high (Figure 3.8) compared to the *trans* coordination as the steric hindrance is high in the former. The *cis* coordinated 18-electron complex **5**

is relatively stable and ligand dissociation from **5** leads to a more significant drop in G_{rel} except for G1small. The agostic metallacycle RuCB2 is formed from **6** *via* a transition state **ts5**. Further exploration of the mechanism reveals that the RuCB2 undergoes an isomerisation reaction passing through **ts6** to afford a metallacycle RuCB2′ (Figure 3.8). Isomerization of RuCB2 to RuCB2′ *via* **ts6** is more difficult than RuCB2 formation from olefin complex **6** in all except G1small. Further, RuCB2′ of G1small is more stable than RuCB2 while the reverse is true for the others. The G_{rel} profiles clearly suggest that this type of a mechanism can be neglected for all except G1small. Since in smaller systems, metathesis inactive RuCB2′ is more dominating than RuCB2, we may conclude that the use of a sterically less bulky phosphine ligand in catalyst design cannot promote metathesis activity of the catalyst.

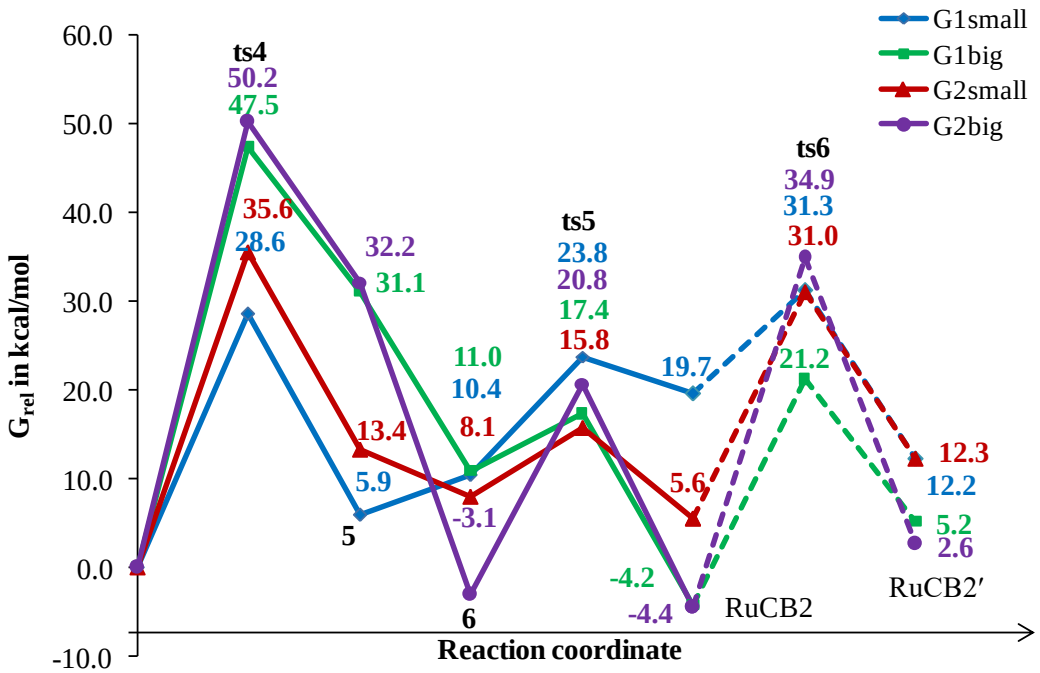

Figure 3.8 Energy profile diagram for the 18eA-D2 mechanism. Dashed lines represent the transformation of RuCB2 to RuCB2′.

3.4.4 18eA Pathway

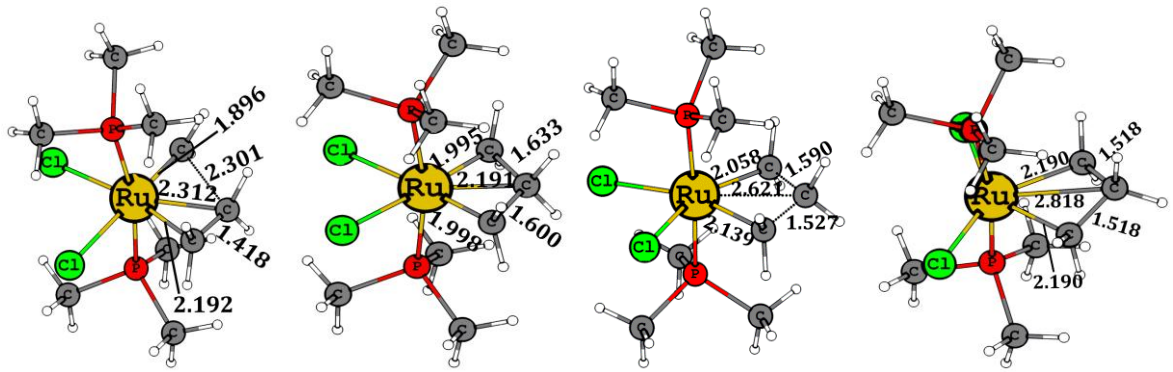

ts7 RuCB3 **ts8** RuCB3′

Figure 3.9 Intermediates and transition states formed in 18eA pathway catalyzed by G1small.

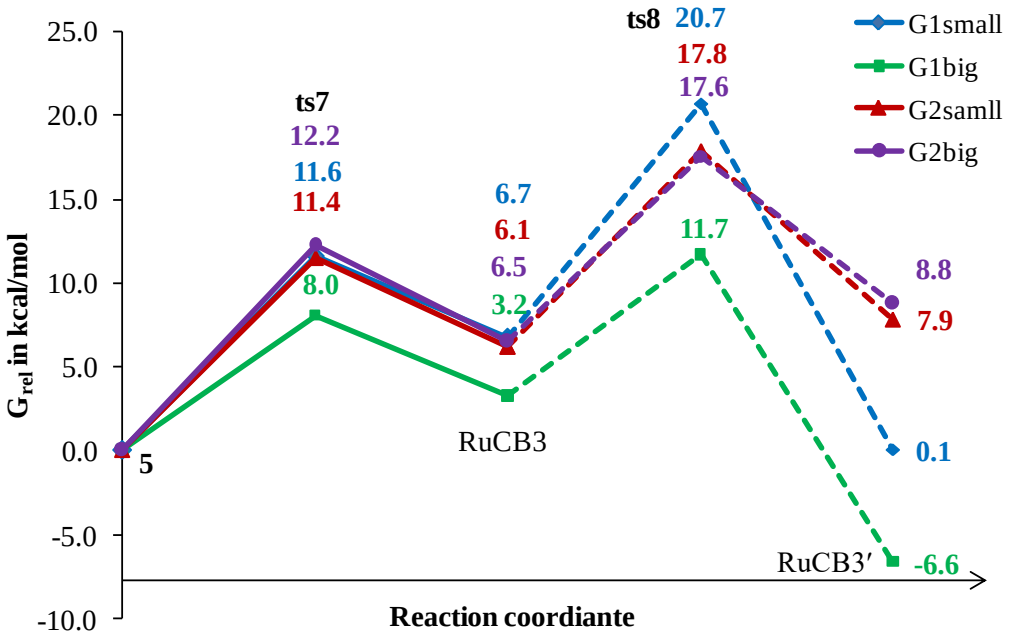

Figure 3.10 Energy profile diagram for 18eA pathway. Dashed lines represent the transformation of RuCB3 to RuCB3′.

The reaction mechanism up to the formation of the olefin complex **5** is common for both 18eA-D2 and 18eA mechanisms. Figure 3.9 depicts the intermediates and transition

states observed for G1small and Figure 3.10 discuss the G_{rel} profile for the remaining part of the mechanism. It is very clear that if the association of olefin and catalyst occurs in a *cis* manner about the carbene ligand, the formation of RuCB3 *via* **ts7** is inevitable as $\Delta G^{\#}$ is 11.6, 8.0, 11.4 and 12.2kcal/mol for G1small, G1big, G2small and G2big, respectively. Further, in this mechanism, RuCB3 has a clear tendency to isomerize to RuCB3′ *via* **ts8** surmounting $\Delta G^{\#}$ 14.0, 8.5, 11.7, and 11.1 kcal/mol for G1small, G1big, G2small and G2big, respectively. G1small and G1big show more stable character for RuCB3′ than RuCB3.

3.4.5 Interpretation of Olefin Metathesis Using BSI

The above-discussed mechanisms apparently bring out the existence of two isomeric metallacycle intermediates in all the possible olefin metathesis pathways. Figure 3.11 gives the structures of these metallacycles observed for 16eD/18eA-D1, 18eA-D2 and 18eA mechanisms for G2big. The significant structural changes noted for agostic to non-agostic transformation are increase in RuC_{α} distance, increase in RuC_{β} distance, decrease in CC distance, decrease in CCC angle (~120^{o} to ~95^{o}), decrease in CRuC angle (~90^{o} to ~62^{o}), and increase in ClRuCl angle (~88^{o} to ~140^{o}). The RuCCC dihedral angle close to zero is observed for all agostic systems, which indicate nearly planar geometry for the metallacycle while a slight puckering at C_{β} is observed for non-agostic complexes. The RuCB1 of 16eD mechanism has trigonal bipyramidal (TBP) configuration while RuCB1′ has square pyramidal (SP) configuration. The change in configuration accounts for distortional isomerism (DI). In fact, BSI can be considered as a subset of DI as both describe distortions of the geometry. The term BSI is applicable to RuCB1 and RuCB1′ if one considers only the structural changes confined to the metallacycle region (Figure 3.11). The RuCB2 of 18eA-D2 mechanism possesses SP geometry for G1small and TBP for others. In the case of G1small, the SP geometry is largely retained when isomerizes to RuCB2′. In other cases, there is a change in geometry from TBP to SP during the isomerization.

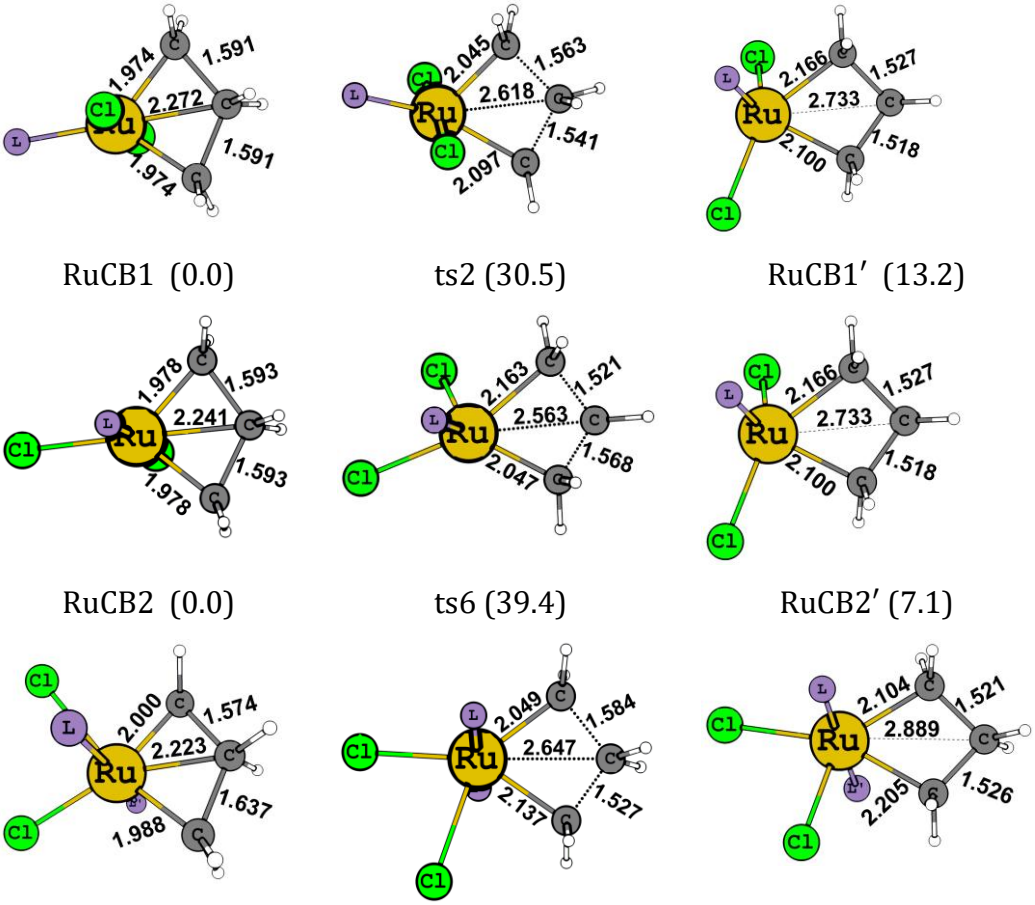

RuCB1 (0.0) ts2 (30.5) RuCB1′ (13.2)

RuCB2 (0.0) ts6 (39.4) RuCB2′ (7.1)

RuCB3 (0.0) ts8 (11.1) RuCB3′ (2.3)

Figure 3.11 Bond stretch isomers and the corresponding transition states located in the 16eD (top row), 18eA-D2 (middle row) and 18eA (bottom row) mechanisms for G2big (G_{rel} in kcal/mol is given in the parenthesis L = H_2IMes and L' = PCy_3).

The structural features strongly indicate that the pairs (RuCB2, RuCB2′) for G1small and (RuB3, RuCB3′) for all are near perfect examples of bond stretch isomers. Other supporting evidence for BSI is the identification of a well-defined transition state for isomerization and the moderate energy barriers for the process.

3.4.6 Study on BSI to Understand the Use of Bulky Ligands in the Catalyst Design

To understand the effect of bulkiness of ligands in the isomerization of agostic to non-agostic complexes, we took phosphine and NHC ligands with varying sizes to design the catalyst and analyzed the transformation RuCB1 to RuCB1′ (16eD path) and RuCB3 to

Table 3.1 Relative free energy for the agostic to non-agostic transition in 16eD and 18eA pathway for different ligands

Ligands	G_{rel} (kcal/mol)					
	16eD pathway			18eA pathway		
	RuCB1	ts	RuCB1'	RuCB3	ts	RuCB3'
PH_3, PH_3	0.0	14.3	1.0	0.0	9.3	-11.2
PH_2Me,PH_2Me	0.0	15.1	1.3	0.0	15.2	-5.5
$PHMe_2$,$PHMe_2$	0.0	16.1	3.6	0.0	14.0	-6.9
PMe_3, PMe_3	0.0	16.7	3.2	0.0	14.0	-6.6
PCy_3, PCy_3	0.0	19.8	11.0	0.0	8.4	-9.9
2I, PMe_3	0.0	20.7	3.9	0.0	13.9	-5.1
2IMe, PMe_3	0.0	24.3	10.0	0.0	11.7	1.7
2IMes, PMe_3	0.0	30.5	13.2	0.0	9.3	-12.3
2IMes, PCy_3	0.0	30.5	13.2	0.0	11.1	2.3

RuCB3′ (18eA path) (Table 3.1). In 16eD mechanism, with an increase in the size of the ligand, a clear increasing trend in the activation energy ($\Delta G^{\#}$) is observed. For catalysts bearing small-sized ligands, relative energy is comparable for RuCB1 and RuCB1′ while a significantly high energy is observed for RuCB1′ in the case of bulky ligands. This suggests that in the first and second generation catalysts, the steric effect of bulky ligands severely hinders the formation of non-agostic isomer RuCB1′ and thus promotes metathesis through RuCB1. In such cases, RuCB1′ appears only as a kinetically driven intermediate, whereas for small-sized ligands, metathesis retarding effect of non-agostic isomer cannot be neglected for the associative mechanism. In 18eA path $\Delta G^{\#}$ for RuCB3 to RuCB3′ transformation is 8.4 to 14.0 kcal/mol, and the non-agostic isomer RuCB3′ is significantly more stable than the agostic one. This observation indicates that associative mechanism must be avoided to improve the metathesis efficiency. In the catalyst design, Grubbs achieved this by incorporating

bulky ligands as such a strategy will prevent the formation of the precursor complex (**5**) needed for RuCB3 formation. Thus the data in Table 3.1 and the reaction profiles (Figure 3.8) establish that the use of bulky ligand is inevitable to improve the efficiency of the ruthenium-based olefin metathesis catalyst. Such a design will promote dissociative mechanism passing almost exclusively through the intermediate RuCB1 by minimizing the formation of the higher energy non-agostic intermediate RuCB1′.

3.4.7 Study on BSI using Different DFT Methods

Table 3.2 Relative energies for the agostic to non-agostic transition in the associative mechanism of $(PMe_3)_2Cl_2Ru(C_3H_6)$ with various DFT methods using Gen1 basis set

Method	G_{rel} (kcal/mol)		
	RuCB3	ts	RuCB3′
BP86	0.0	14.0	-6.6
B3LYP	0.0	9.2	-13.0
B3LYP-D2	0.0	10.9	-10.7
CAM-B3LYP	0.0	11.6	-10.5
B3PW91	0.0	11.2	-11.5
B971	0.0	10.8	-11.5
B97D	0.0	9.8	-11.8
M06	0.0	13.4	-9.7
M06L	0.0	12.9	-9.2
M06-2X	0.0	11.6	-10.0

18eA mechanism involving G1small is studied using a benchmark set of DFT methodologies (Table 3.2). All the methods show two distinct metallacycles, *viz*. the agostic RuCB3 and the non-agostic RuCB3′ on the potential energy surface which are connected by a well-defined four-center transition state with $\Delta G^{\#}$ in the range 9.2 – 14.0

kcal/mol. All the methods consistently show more stable character for RuCB3′ than RuCB3.

3.4 Conclusions

The ruthenacyclobutane (RuCB) is found to be an important intermediate in the Chauvin olefin metathesis mechanism and is characterized by unusual CC-agostic bonding. The present study reveals a new twist to the well established Chauvin mechanism by giving a highly reliable prediction on the formation of yet another ruthenacyclobutane (RuCB'), the metathesis inactive non-agostic system. All possible mechanism of ethylene metathesis analyzed with Grubbs first and second generation catalysts showed the formation of two metallacycles in all the pathways. The metallacycles labelled as RuCB and RuCB′ are found to be isomers differing only in certain bond parameters, especially the RuC_{β} distance. The agostic complex RuCB has shorter RuC_{β} distance and wider CCC bond angle whereas non-agostic complex RuCB′ is characterized with longer RuC_{β} distance. The RuCB1 and RuCB1′ of 16eD pathway, RuCB2 and RuCB2′ of 18eA-D2 pathway, and RuCB3 and RuCB3′ of 18eA pathway fulfil the criteria of bond stretch isomerism at least in the metallacycle region. RuCB3 and RuCB3' are the best examples of BSI as the ligand orientation around the metal center is also conserved in both the isomers.

In summary, this study reveals that the use of bulky ligands in Grubbs catalysts design is inevitable as this strategy minimizes the possibility of the formation of a metathesis inactive metallacycle. In the 18eA mechanism, though RuCB3′ is energetically more stable than RuCB3 in some cases, the use of bulky ligands restricts the coordination of alkene in the first step. However, with smaller ligands, 18eA mechanism is possible and it shows moderate $\Delta G^{\#}$ for RuCB3 to RuCB3′ transformation. More stable character of RuCB3′ than RuCB3 in G1small suggests the isolation of such a compound using a catalyst designed with sterically less bulky ligands. Formation of RuCB3' could also be forced under high pressure by promoting the *cis* coordination of olefin in 18eA mechanism. Yet another point is that a BSI-based interpretation of the

mechanism of a reaction is unknown in chemistry, and rather such a phenomenon is often described as a theoretical concept dealing with conformational and structural changes of certain molecules. Herein, we proved that the BSI-based interpretation is valid for explaining the rational design strategies underlined in the development of Grubbs olefin metathesis catalyst. Hence, the status of BSI is lifted from a concept of largely theoretical interest to a phenomenon of immense importance in catalysis.

3.5 References

1. W. D. Stohrer and R. Hoffmann, *J. Am. Chem. Soc.*, **1972**, *94*, 1661-1668.
2. W. D. Stohrer and R. Hoffmann, *J. Am. Chem. Soc.*, **1972**, *94*, 779-786.
3. A. V. Butcher and J. Chatt, *J. Chem. Soc. A*, **1970**, *0*, 2652-2656.
4. Y. Jean, A. Lledos, J. K. Burdett and R. Hoffmann, *J. Am. Chem. Soc.*, **1988**, *110*, 4506-4516.
5. K. Wieghardt, G. Backes-Dahmann, B. Nuber and J. Weiss, *Angew. Chem. Int. Ed.*, **1985**, *24*, 777-778.
6. F. A. Cotton, M. P. Diebold and W. J. Roth, *Inorg. Chem.*, **1987**, *26*, 2848-2852.
7. M. M. Rohmer and M. Benard, *Chem. Soc. Rev.*, **2001**, *30*, 340-354.
8. Y. Jean, A. Lledos, J. K. Burdett and R. Hoffmann, *J. Chem. Soc., Chem. Commun.*, **1988**, *0*, 140-142.
9. K. Yoon, G. Parkin and A. L. Rheingold, *J. Am. Chem. Soc.*, **1991**, *113*, 1437-1438.
10. K. Yoon, G. Parkin and A. L. Rheingold, *J. Am. Chem. Soc.*, **1992**, *114*, 2210-2218.
11. J. Song and M. B. Hall, *Inorg. Chem.*, **1991**, *30*, 4433-4437.
12. F. P. Di Nicola, M. Lanzi, F. Marchetti, G. Pampaloni and S. Zacchini, *Dalton Trans.*, **2015**, *44*, 12653-12659.
13. P. v. R. Schleyer, A. F. Sax, J. Kalcher and R. Janoschek, *Angew. Chem. Int. Ed.*, **1987**, *26*, 364-366.
14. J. A. Boatz and M. S. Gordon, *J. Phys. Chem.*, **1989**, *93*, 2888-2891.
15. J. A. Boatz and M. S. Gordon, *Organometallics*, **1996**, *15*, 2118-2124.
16. H. Shorafa, D. Mollenhauer, B. Paulus and K. Seppelt, *Angew. Chem. Int. Ed.*, **2009**, *48*, 5845-5847.

17. U. Kölle, J. Kossakowski, N. Klaff, L. Wesemann, U. Englert and G. E. Herberich, *Angew. Chem. Int. Ed.*, **1991**, *30*, 690-691.
18. U. Kölle, H. Lueken, K. Handrick, H. Schilder, J. K. Burdett and S. Balleza, *Inorg. Chem.*, **1995**, *34*, 6273-6278.
19. J. E. McGrady, *Angew. Chem. Int. Ed.*, **2000**, *39*, 3077-3079.
20. P. Comba, A. Hauser, M. Kerscher and H. Pritzkow, *Angew. Chem. Int. Ed.*, **2003**, *42*, 4536-4540.
21. I. Antol, M. Eckert-Maksic, H. Lischka and Z. B. Maksic, *Chem. phys. chem.*, **2004**, *5*, 975-981.
22. K. T. Petrov, B. Pinter and T. Veszpremi, *J. Organomet. Chem.*, **2012**, *706*, 84-88.
23. T. Goswami, S. Paul, S. Mandal, A. Misra, A. Anoop and P. K. Chattaraj, *Int. J. Quantum Chem.*, **2015**, *115*, 426-433.
24. P. R. Remya and C. H. Suresh, *Dalton Trans.*, **2015**, *44*, 17660-17672.
25. R. H. Grubbs, ed., *Handbook of Olefin Metathesis*, WILEY–VCH Verlag GmbH & Co. KgaA, Weinheim, **2003**.
26. T. M. Trnka and R. H. Grubbs, *Acc. Chem. Res*, **2001**, *34*, 18-29.
27. R. H. Grubbs and S. Chang, *Tetrahedron*, **1998**, *54*, 4413-4450.
28. P. Jean-Louis Hérisson and Y. Chauvin, *Die Makromolekulare Chemie*, **1971**, *141*, 161-176.
29. S. F. Vyboishchikov, M. Bühl and W. Thiel, *Chem. Eur. J.*, **2002**, *8*, 3962-3975.
30. C. Adlhart and P. Chen, *J. Am. Chem. Soc.*, **2004**, *126*, 3496-3510.
31. I. W. Ashworth, I. H. Hillier, D. J. Nelson, J. M. Percy and M. A. Vincent, *Chem. Commun.*, **2011**, *47*, 5428-5430.
32. I. W. Ashworth, I. H. Hillier, D. J. Nelson, J. M. Percy and M. A. Vincent, *ACS Catal.*, **2013**, *3*, 1929-1939.
33. C. A. Urbina-Blanco, A. Poater, T. Lebl, S. Manzini, A. M. Z. Slawin, L. Cavallo and S. P. Nolan, *J. Am. Chem. Soc.*, **2013**, *135*, 7073-7079.
34. M. S. Sanford, M. Ulman and R. H. Grubbs, *J. Am. Chem. Soc.*, **2001**, *123*, 749-750.
35. M. S. Sanford, J. A. Love and R. H. Grubbs, *J. Am. Chem. Soc.*, **2001**, *123*, 6543-6554.
36. O. M. Aagaard, R. J. Meier and F. Buda, *J. Am. Chem. Soc.*, **1998**, *120*, 7174-7182.

37. C. Adlhart, C. Hinderling, H. Baumann and P. Chen, *J. Am. Chem. Soc.*, **2000**, *122*, 8204-8214.
38. L. Cavallo, *J. Am. Chem. Soc.*, **2002**, *124*, 8965-8973.
39. E. L. Dias, S. T. Nguyen and R. H. Grubbs, *J. Am. Chem. Soc.*, **1997**, *119*, 3887-3897.
40. A. D. Becke, *Phys. Rev. A*, **1988**, *38*, 3098-3100.
41. J. P. Perdew, *Phys. Rev. B*, **1986**, *33*, 8822-8824.
42. R. Ditchfield, W. J. Hehre and J. A. Pople, *J.Chem. Phys.*, **1971**, *54*, 724-728.
43. K. A. Peterson, D. Figgen, M. Dolg and H. Stoll, *J. Chem. Phys.*, **2007**, *126*, 124101.
44. G. Scalmani and M. J. Frisch, *J. Chem. Phys.*, **2010**, *132*, 114110.
45. A. Schäfer, C. Huber and R. Ahlrichs, *J. Chem. Phys.*, **1994**, *100*, 5829-5835.

Chapter 4

Mechanism of Cyclotrimerization of CC and CN Triple Bonds Using Grubbs Catalysts

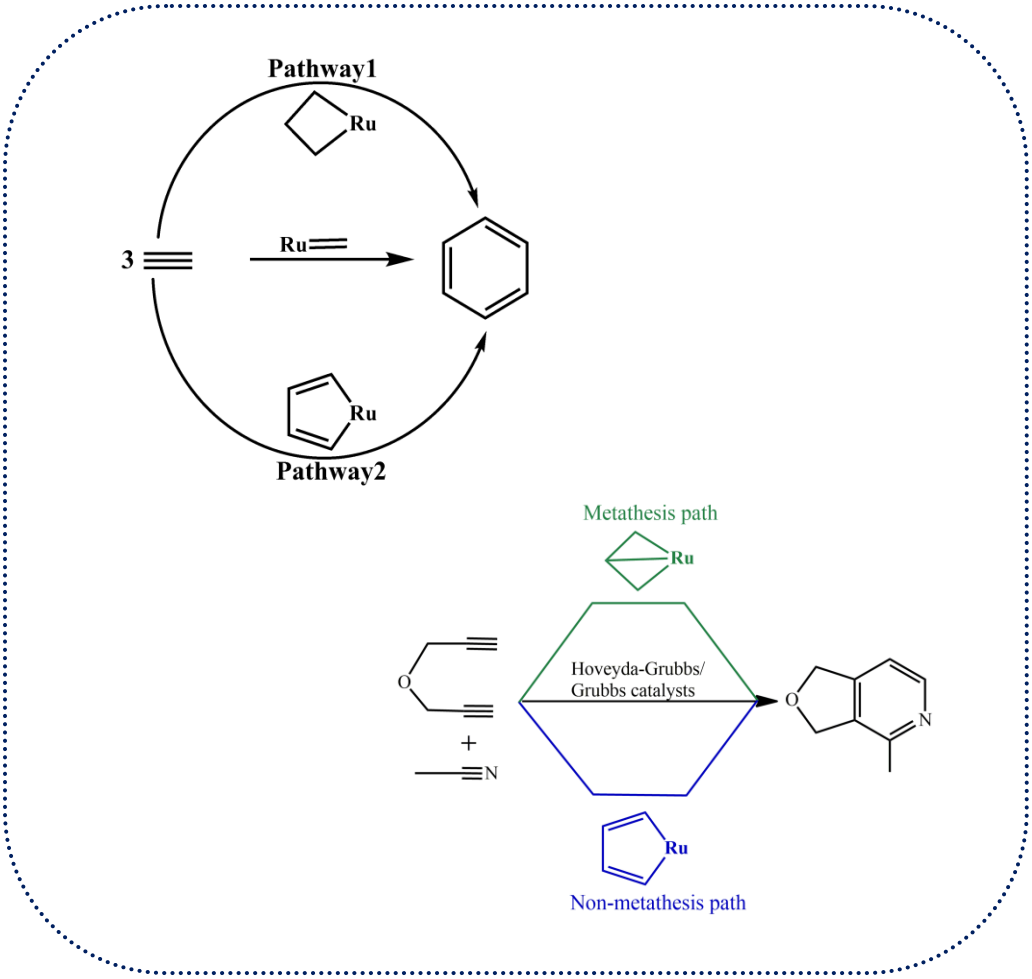

4.1 Abstract

Cyclotrimerization of acetylene by Grubbs first and second generation CC bond metathesis catalysts has been attempted by experimentalists with limited success and lack of reliable information about the mechanism of the reaction hinders further progress in the development of efficient catalysts. Herein, we describe a systematic density functional theory study on the probable mechanisms of this reaction and show that it proceeds either through a fully metathesis pathway (pathway 1) or through an alternate non-metathesis pathway (pathway 2). Pathway 1 consists of four metathesis steps characterized by the formation of metallacyclobutene-like intermediate in each step while pathway 2 passes through a metallacyclopentadiene intermediate. In metathesis pathway, the final ring closing metathesis step for benzene formation competes with another cross metathesis propagation step towards polyene chain expansion. Pathways 1 and 2 show a highly exothermic (~120 kcal/mol) reaction profile due to the tremendous energy gain in converting acetylene triple bonds to aromatic bonds. The reaction is highly influenced by the choice of ligands in the catalyst design, particularly, by reducing the steric influence of ligands, cyclotrimerization of acetylene to benzene appears as a feasible process by Grubbs-type catalysts.

The [2+2+2] cyclotrimerization of diynes and nitrile provides an efficient method for the synthesis of pyridine and its derivatives which can be extended in the total synthesis of natural products. Use of Grubbs type ruthenium catalysts in the cyclotrimerization reaction expands the applicability of Ru(II) catalysts. Two plausible pathways, viz. metathesis and non-metathesis pathways for the cyclotrimerization reaction between a diyne and a nitrile are elucidated with Grubbs second generation and Hoveyda-Grubbs catalysts using DFT techniques. A ruthenacyclobutene like complex is obtained as a stable intermediate in the metathesis pathway while a five membered metallacycle is formed in the non-metathesis pathway. The study reveals the influence of N-substituents on N-heterocyclic ligands (NHC) as well as substituent on carbene ligand in controlling

the energetic of both metathesis and non-metathesis pathways. Incorporating NHC ligand with reduced steric influence in catalyst design is desirable for improving the efficiency of cyclotrimerization reaction of alkynes with nitriles.

4.2 Introduction

Transition metal mediated cyclotrimerization of alkynes and nitriles is a direct and atom economic way for the synthesis of carbocycles and heterocycles.[1-2] This strategy for the synthesis of carbo- and heterocycle derivatives found application in the total synthesis of many natural products and pharmaceutically important molecules.[3-9] Reppe *et al.* were the first to show such a reaction using Ni catalyst.[10] Later many transition metal atoms and complexes have been reported for catalytic activity,[11-20] and among them, cobalt complexes are found to be the most efficient catalysts.[21-25] Yamamoto and co-workers tried ruthenium-based catalysts such as **i**, [CpRuCl(cod)] (Cp = cyclopentadiene, cod = 1,5-cyclooctadiene) in the cyclotrimerization reaction of 1,6-diyne with alkenes, alkynes and nitriles for the synthesis of benzenoid and heterocycle compounds.[26-36] The 'cod' ligand in the catalyst is easily replaceable by the alkynes, and the bulky Cp is used as a control ligand for the chemo and regioselectivity. The intermolecular alkyne cyclotrimerization in an aqueous medium is also recently achieved by Cadierno *et al.* [37] with a Ru(IV) dimer catalyst **ii**, [{Ru(η^3:η^3-$C_{10}H_{16}$)(μ-Cl)Cl}$_2$].

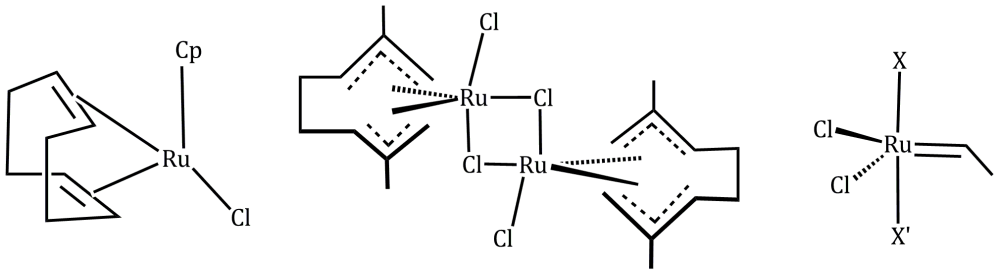

i **ii** **iii**

Figure 4.1 Ruthenium catalysts used in the cyclotrimerization reactions of alkynes (X=PCy_3).

Grubbs ruthenium catalysts, widely used in olefin metathesis reaction,[38-42] have been found to catalyze other non-metathesis reactions such as olefin isomerization.[43-44] Peters and Blechert reported that the Grubbs first generation catalyst **iii**, $[(PCy3)_2Cl_2RuCHPh]$ promotes intra-molecular cyclotrimerization of triynes to benzene derivatives. They proposed a mechanism consisting of four metathesis steps *viz.* three cross metathesis (CM) followed by a ring closing metathesis (RCM) for the reaction (Scheme 4.1).[45] Later Das and Roy used Grubbs first generation catalysts for the intermolecular cyclotrimerization of alkynes for the synthesis of carbohydrate derivatives.[46] Hoven *et al.* used **iii** in the synthesis of amino acid derivatives from appropriately substituted triynes.[47] Witulski *et al.* reported that **iii** could also catalyze the alkyne cyclotrimerization to synthesize indoline derivatives and suggested that the reaction may proceed through a cascade of metathesis steps.[48] Later Grubbs second generation and Hoveyda-Grubbs catalysts also found to be useful in the cyclotrimerization reaction of alkynes with various substrates such as alkynes, nitriles and alkenes.[45-46, 49-50]

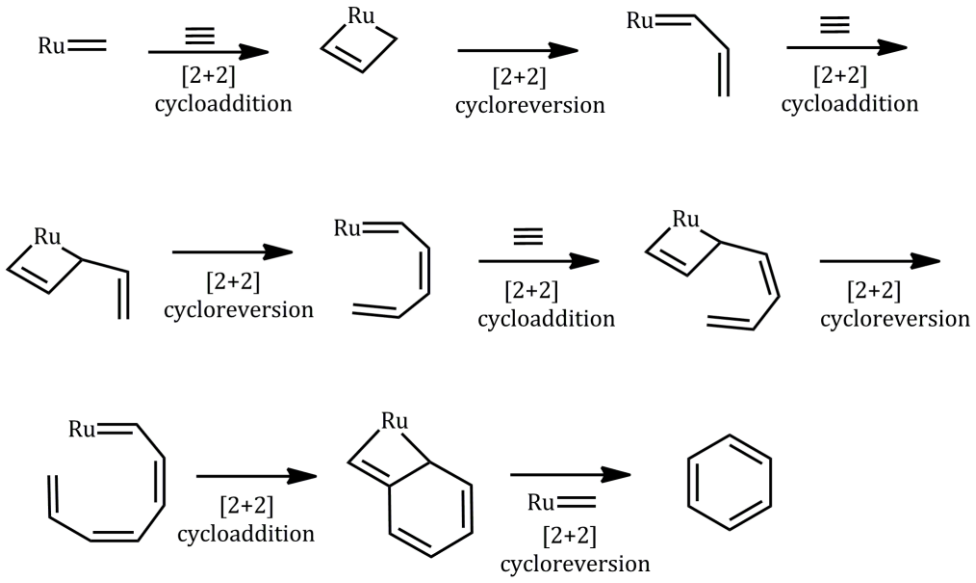

Scheme 4.1 A cascade of metathesis steps suggested for the alkyne cyclotrimerization catalyzed by Grubbs catalysts.

Mechanism described in Scheme 4.1 (first three CM steps) can be compared with that of enyne metathesis which involves the bond reorganization between an alkene and an alkyne, resulting in a conjugated 1,3-diene system.[51-56] Experimental and theoretical studies discussing enyne metathesis mechanism reported a η^3-vinyl carbene complex intermediate in the course of the reaction.[52, 57-58]

The mechanism proposed by Peters and Blechert is fundamentally very different from the typically used and widely accepted trimerization pathway given in Scheme 4.2. Theoretical studies on the mechanism of cyclotrimerization catalyzed by Co, Ru, Ir complexes have shown that a bis-alkyne complex formed in the reaction undergoes CC bond coupling to yield the key metallacyclopentadiene intermediate.[17, 59-63] Coordination of a third alkyne to this intermediate and subsequent CC bond coupling leads to the formation of a bicyclic ring composed of five and four membered rings. The bicyclic system changes to a seven membered metallacycle by the cleavage of the central metal-carbon bond. Further rearrangement involving a CC coupling reaction results in the formation of the benzene complex.

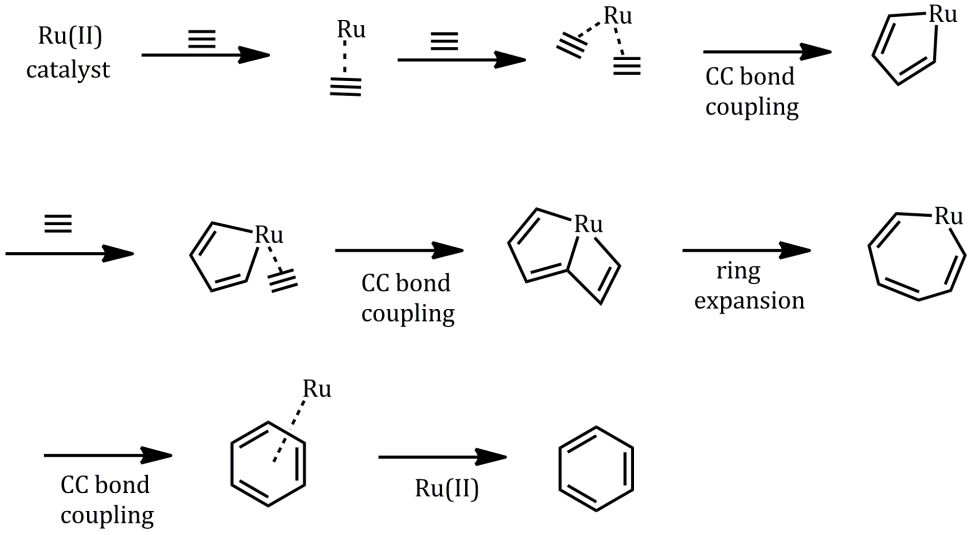

Scheme 4.2 Reaction pathway proposed for the cyclotrimerization of alkynes using Ru(II) catalysts.

It is observed that the Grubbs catalyst undergoes decomposition in strong reaction condition and thus formed modified system can also catalyze non-metathesis

type reactions. Recently Pérez-Castells *et al.* suggested the formation of a non-carbene species from Hoveyda-Grubbs catalyst under strong reaction condition which catalyzes the cyclotrimerization of alkynes and nitriles to pyridine.[64-67] Same group also studied the reaction between a diyne and an alkene leading to cyclohexadiene derivatives in presence of Hoveyda-Grubbs catalyst and proposed that a metathesis pathway similar to Scheme 4.1 can be in competition with a non-metathesis pathway similar to that in Scheme 4.2 and the preference of any of these pathways could depend on the substrates and reaction conditions.[68] in this Chapter, first part discusses the cyclotrimerization of acetylene to benzene and Part B describes the incorporation of a nitrile group in the cyclotrimerization leading to a heterocycle.

4.3 Computational Details

Optimization of the geometries and frequency calculations are done at BP86/Gen1 level of theory.[69-70] Further single point calculations in solvent (dichloromethane) is done at the BP86-D2/Gen2 level of theory[71] using the SMD solvation model[72] implemented in Gaussian 09. In Gen 1, ruthenium center is defined with LANL2DZ basis set and effective core potential while 6-31G* basis set is used to define other atoms. In Gen2, ruthenium center is described with LANL2DZ basis set augmented with f polarization function and effective core potential while lighter elements are described using 6-31+G** basis set. We did gas phase optimization followed by solvent single point calculation to calculate free energy as it gives energetics very similar to a full optimization procedure in solvent phase. The Gibbs free energy of every system is estimated by adding the thermal correction to Gibbs free energy calculated at BP86/Gen1 level and the total energy obtained at BP86-D2/Gen2 level. The Gibbs free energies are calculated at the standard reaction conditions, *viz*. temperature 298.15 K and pressure 1 atm. All transition states are characterized by a single imaginary frequency along the reaction coordinate whereas all intermediates are confirmed to be a minimum by locating zero imaginary frequency in the vibrational analysis. Further Intrinsic reaction coordinate (IRC) technique is used to confirm the reactant to product connectivity of some important transition states.[73]

Part A: Mechanistic Studies on Acetylene Cyclotrimerization Catalyzed by Grubbs First and Second Generation Catalysts

4.4 Results and Discussion

Cyclotrimerization of acetylene to benzene is an attractive reaction path for the synthesis of benzene and its derivatives. In the present study, we investigate the possibility of acetylene cyclotrimerization using Grubbs first and second generation catalysts (Figure 4.2). The reaction may follow a fully metathesis pathway as shown in Scheme 4.1 by the carbene catalyst or it may proceed through a non-metathesis pathway as shown in Scheme 4.2 with the intervention of a non-carbene species generated by the decomposition of the catalyst. This study reveals intriguing aspects of the mechanism and suggests decisive modification on the catalyst for the viable cyclo trimerization of acetylene. Mechanistic studies on the metathesis (pathway 1) and non-metathesis (pathway 2) pathways of acetylene cyclotrimerization are examined using Grubbs first generation catalysts **1** and **1′**. Catalyst **1** is a real catalyst model of formula $(PCy_3)_2Cl_2RuCHMe$ while **1′** is a smaller version of **1** ($(PMe_3)_2Cl_2RuCHMe$). Further Grubbs second generation catalysts **2** and **2′** are tested to understand how ligand environment is affecting the reaction path.

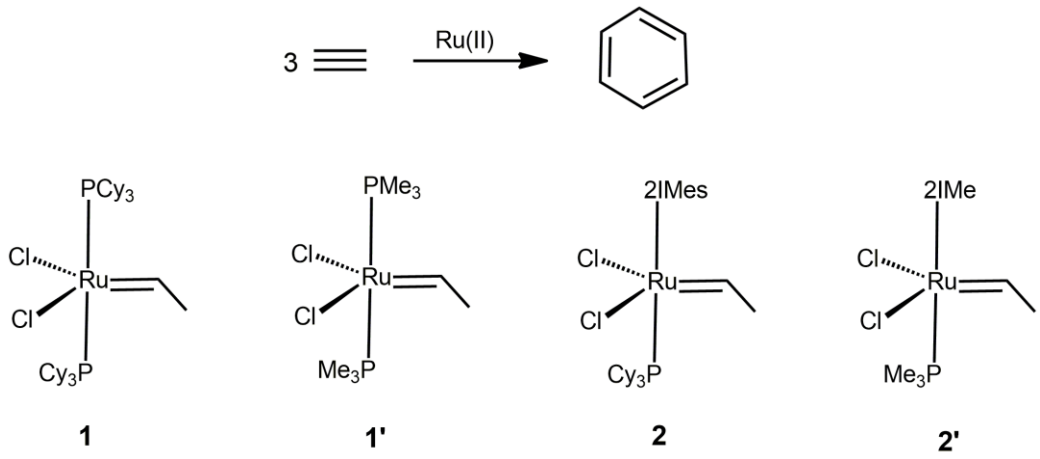

Figure 4.2 Representation of the reaction and catalysts used in the study.

4.4.1 Pathway 1: Metathesis Pathway

Figure 4.3 describes the intermediates and transition states located in the metathesis pathway for the reaction of three units of acetylene to yield benzene catalyzed by **1**. Metathesis reaction pathway begins with the dissociation of the labile ligand from **1** to generate the catalytically active carbene complex **1a:** (':' indicates the carbene character). One of the acetylenes coordinates to the metal center in **1a:** to yield **1a:C_2H_2**. The C-C bond coupling (2+2 cycloaddition) in **1a:C_2H_2** *via* the transition state **1ts1** gives the ruthenacyclobutene-like complex **1a$_{4cyc}$** and is confirmed by doing IRC. The metallacycle **1a$_{4cyc}$** opens up with almost no barrier to cross and generates the second ruthenium carbene complex **1b:** which becomes the active complex in the next metathesis step.[74] Subsequent addition of alkyne to the metal center in **1b:** proceeds through transformations similar to that in the first metathesis step. For instance, **1b:C_2H_2** passes through **1ts2** to yield **1b$_{4cyc}$** and the subsequent ring opening gives the third carbene complex **1c:**. Similarly further propagation in the reaction can be described from **1c:** by **1c:C_2H_2**, **1ts3**, **1c$_{4cyc}$** and **1d:**. Since in **1d:**, the carbene carbon is conjugated with a chain of six unsaturated carbon centers, a six-membered ring closing metathesis (RCM) process could be envisaged. Formation of **1e** from **1d:** is considered by allowing the terminal double bond of the carbon chain to coordinate with the metal center. The **1ts4** describes the C-C bond coupling in **1e** and the resulting system is the benzene complex **1a:C_6H_6**. Dissociation of benzene from this complex regenerates **1a:**. Considering the structural features, a shortening in the RuP (~2.25 Å) and RuCl (~2.36 Å) bonds are observed in the monophosphine carbene complexes **1a:**, **1b:**, **1c:** and **1d:** compared to the catalyst **1**. A gradual, but minor lengthening of the RuC: bond with increase in the alkene chain length is also observed, as the RuC: distances are 1.83, 1.85, 1.86 and 1.87 Å respectively for **1a:**, **1b:**, **1c:** and **1d:**. In the transition state corresponding to the CC bond coupling steps, the CC interaction distance is found to be in the range 2.12 to 2.28 Å.

The metathesis reaction pathway using the smaller catalyst **1′** is very similar to that of **1**. The intermediates and transition states formed in the course of the reaction are very similar to that given in Figure 4.3. The free energy reaction profile of **1′** is

compared with that of **1** in Figure 4.4. Both **1** and **1′** show a highly exergonic reaction profile as the triple bonds are converted to aromatic CC bonds. Dissociation of PR_3 ligand is essential for the reaction to get initiated and the free energy change is highly in favor for this process for **1** and **1′**. The activation barrier ($\Delta G^{\#}$) located for the first, second and third metathesis steps are 9.5, 3.9, and 13.2, kcal/mol, respectively for catalyst **1**. With the small catalyst **1′** though the reaction energy profile shows a more exothermic character, $\Delta G^{\#}$ for each metathesis step is comparatively high *viz.* 12.6 kcal/mol for first, 18.9 kcal/mol for second and 18.6 kcal/mol for third metathesis step. The last RCM step for **1** passing through **1e** and **1ts4** has $\Delta G^{\#}$ of 16.6 kcal/mol (Figure 4.4b) while **1′** passing through **1′e** and **1′ts4** shows a small value 10.7 kcal/mol (Figure 4.4c). The high activation barrier for final RCM for **1** may be attributed to the energy required for folding up of the long alkyl chain and to the steric hindrance by bulky ligands. On the basis of energetics of the final RCM step, smaller catalyst **1′** can be considered as catalytically more active than the bulky catalyst **1** for acetylene trimerization reaction *via* metathesis pathway.

Highly exothermic nature of the reaction and the moderate reaction barriers depicted in Figure 4.4 propose a theoretical suggestion that Grubbs olefin metathesis catalysts has the ability to perform as an efficient trimerization catalysts for acetylenes. However, a remarkable catalytic activity of Grubbs catalysts with bulky ligands for trimerization reactions is never reported. From the reaction profile, it is clear that the efficiency of the RCM step (**1d:** to **1e** or **1′d:** to **1′e**) determines the success of such a reaction. But it is very likely that the fourth carbene intermediate **1d:** or **1′d:** may undergo yet another cross metathesis step and subsequent propagation of similar reaction may lead to the expansion of the alkylidene chain in presence of excess acetylene.[75-76] In Figure 4.4b, the reaction profile for the cross metathesis step of **1d:** and in Figure 4.4c the same for **1′d:** is represented using dotted line. Also Figure 4.5 gives the reaction intermediates and transition states for **1d:** to **1f:** conversion. The formation of the metallacycle intermediate $\mathbf{1d_{4cyc}}$ or $\mathbf{1'd_{4cyc}}$ is more facile than RCM and leads to a more exothermic product than the benzene complex in the case of bulky catalyst **1**. The reaction may continue with more metathesis steps leading to further

propagation of the alkene chain especially with acetylenes. In the case of **1′** the activation barrier reported for RCM (10.7 kcal/mol) is lesser than that required for the propagation step (17.3 kcal/mol). Thus in the case of **1** it is clear that benzene formation can occur only as a minor pathway through a RCM step and most likely, the reaction is highly biased towards the open chain metathesis transformation. But for **1′**, the smaller catalyst system, the cyclotrimerization reaction can lead to the benzene formation.

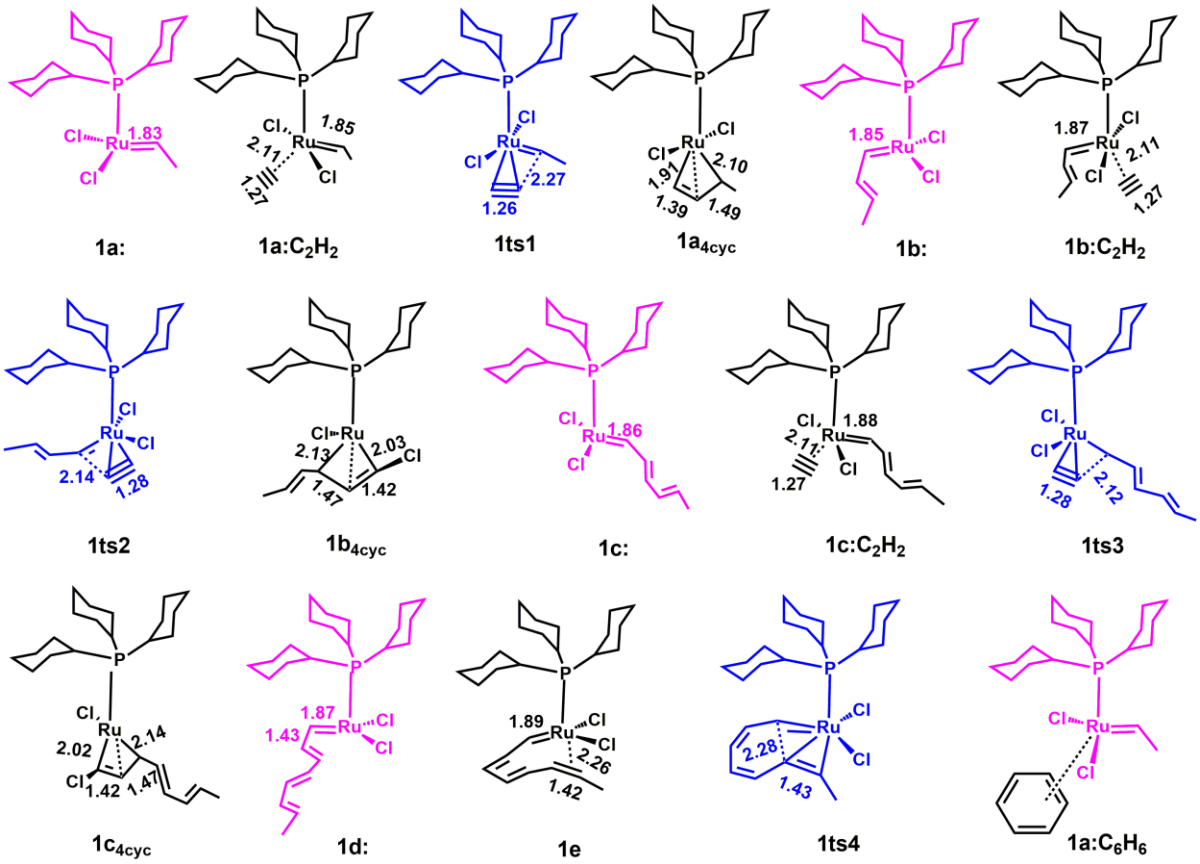

Figure 4.3 Acetylene cyclotrimerization *via* metathesis route for the Grubbs first generation catalyst **1**. The active form of the catalyst at various stages (**1a:**, **1b:**, **1c:**, **1d:**) are shown in red color, and the transition states are shown in blue color. All bond lengths are in Å

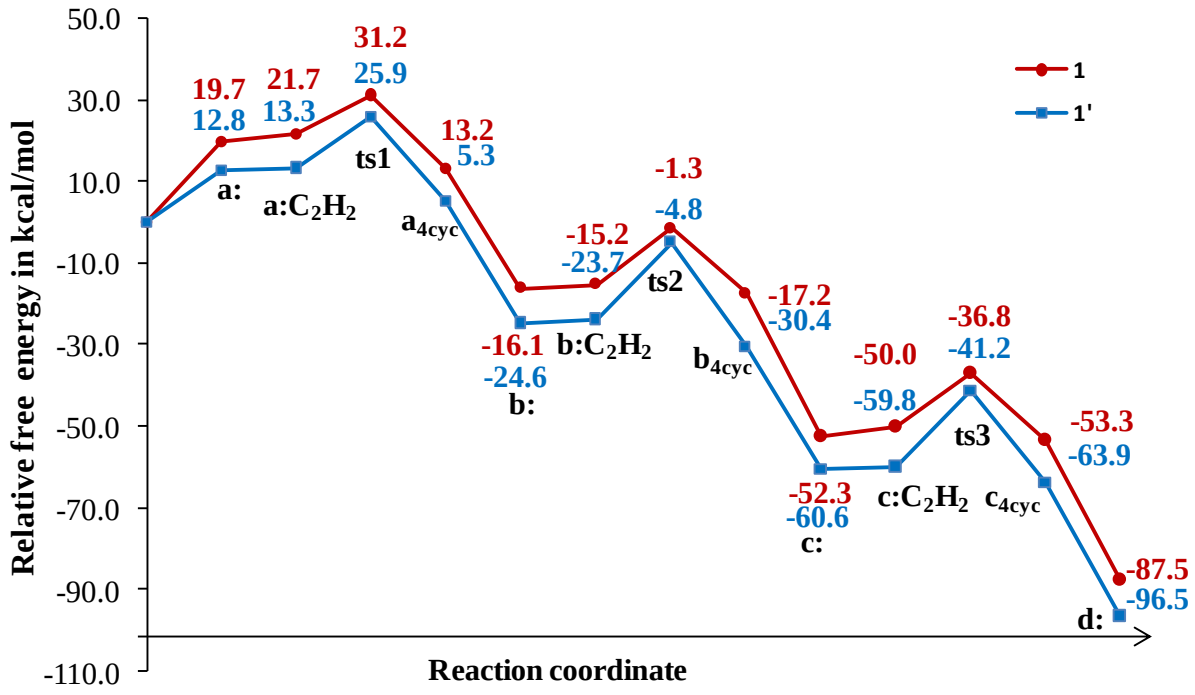

(a)

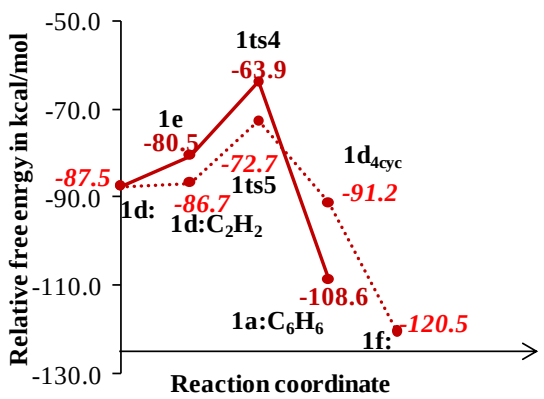

(b)

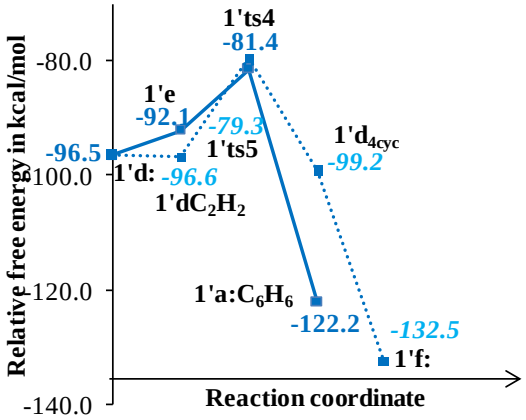

(c)

Figure 4.4 Gibbs free energy profile for the metathesis pathway of cyclotrimerization of acetylenes catalyzed by catalyst **1** and **1′.** (a) reaction profile up to the formation of **1d:** and **1′d:**. Competition between the RCM (solid line) and propagation step (dotted line) depicted for (b) catalyst **1** and (c) catalyst **1′**

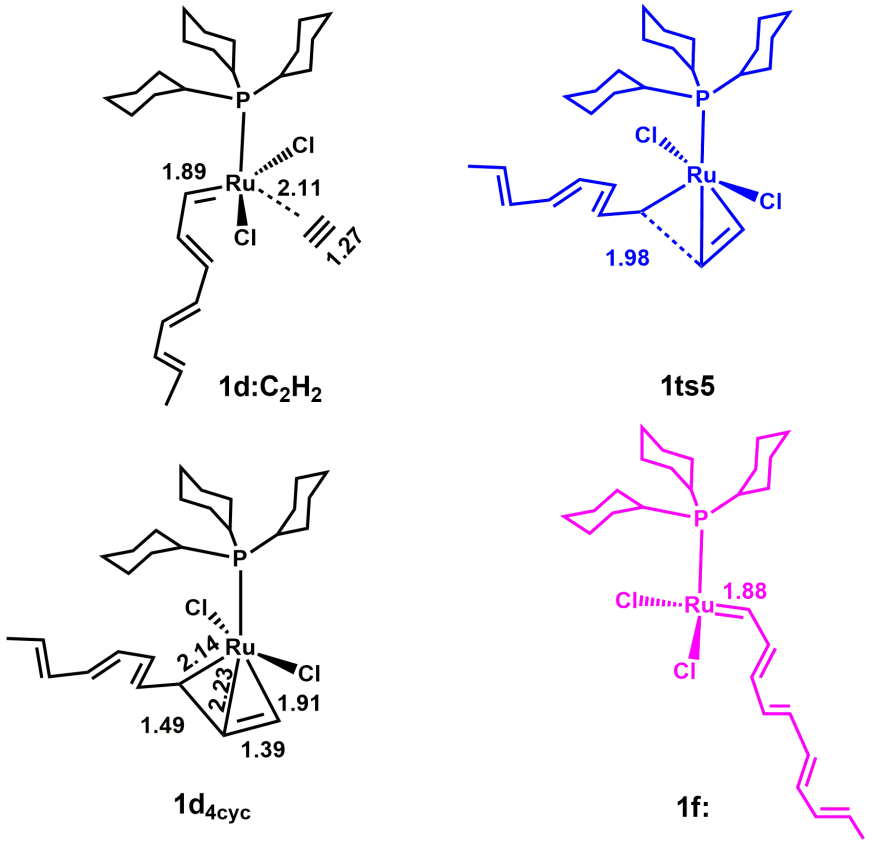

Figure 4.5 Reaction intermediate and transition state involved in the propagation step using catalyst **1**.

So far most of the trimerization reaction of alkynes *via* a cascade of metathesis step is reported only for first generation catalysts.[45-47] To understand how N-heterocyclic carbene (NHC) of Grubbs second generation catalysts affect the reaction pathway we took two catalysts **2** and **2′**. **2** is a realistic model of Grubbs second generation catalyst with bulky mesityl group in the nitrogen of NHC and PCy_3 ligand as the labile ligand. **2′** is the smaller version of **2** with methyl group on NHC and PMe_3 group as labile ligand. The reaction *via* metathesis pathway using **2** and **2′** are similar to that of first generation catalysts given in Figure 4.3 and 4.4. The key to trimerization reaction is the formation of the intermediate **e** wherein the terminal double bond of the alkene chain coordinates to the metal center. Reaction energy profile for this crucial step using **2** and **2′** are given in Figure 4.6. It is clear from Figure 4.6 that the probability

for a ring closing metathesis is less, and a cross metathesis leading to the polyene chain is favored for both **2** and **2′.**

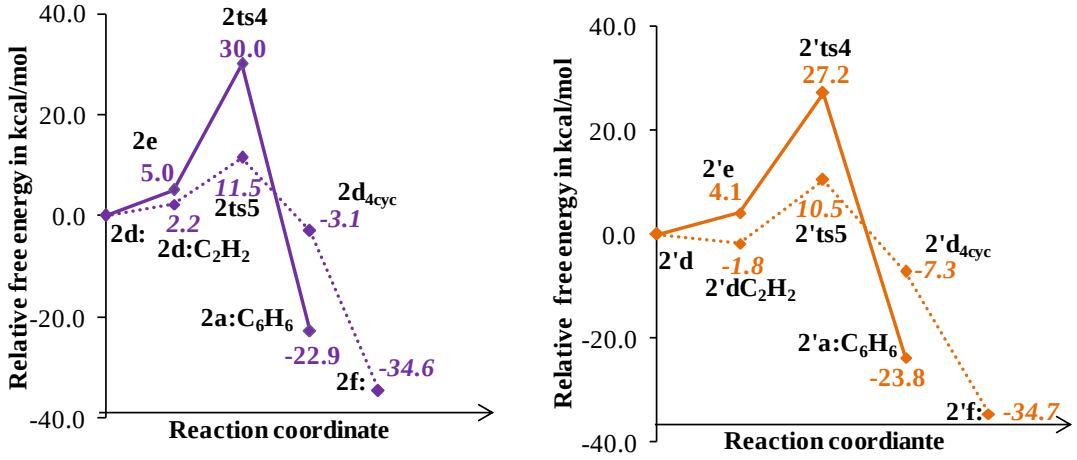

Figure 4.6 Reaction free energy profile for the metathesis pathway catalyzed by **2** and **2′**. The solid line represents the RCM and dotted line represents the propagation step.

The metallacycle intermediates located in metathesis pathway of trimerization reaction *viz.* **1a**$_{4cyc}$, **1b**$_{4cyc}$, **1c**$_{4cyc}$ are different from the normal metallacyclobutanes of alkene metathesis or metallacyclobutadienes of alkyne metathesis. The metallacycle intermediates of alkene and alkyne metathesis are characterized by short RuC_{β} distance and long CC bonds. But metallacycles observed herein do not possess any such characteristic bonding features. Instead the metal center has an η^3 type interaction with the carbon fragment. Such η^3 vinyl carbene complexes are reported by Grubbs *et al.*[77] and is further confirmed by mechanistic studies on the enyne metathesis.[75, 78] Recently Solans-Monfort reported molybdacylobutene as a short lived intermediate in the ring closing enyne metathesis catalyzed by molybdenum alkylidene complexes.[79] Here also the ruthenacyclobutene-like ring structures observed in the metathesis reaction pathway immediately opens up to a carbene structure. We are able to locate a transition state to define the ring opening of **a**$_{4cyc}$ (Figure 4.7). The activation barrier recorded for the **a**$_{4cyc}$ cleavage for **1** is 2.7 kcal/mol while the barrier for **1′** is 1.3 kcal/mol**.** Though these transition states are almost barrier-less, their identification confirms the presence of ruthenacyclobutene-like structures in the metathesis pathway. Also the metal chlorine distance increases gradually along the series **1a**$_{4cyc}$, **1b**$_{4cyc}$ and **1c**$_{4cyc}$

while a C_α-Cl distance decreases. In fact, in **1b$_{4cyc}$** and **1c$_{4cyc}$** the C_α-Cl distance is 1.87 Å and it suggests a bond between the two. This again confirms that the metallacycle is not the regular metallacycles observed in the course of the metathesis and can be treated as η^3 vinyl complexes. On ring opening, the chlorine atom bonded to C_α in **1b$_{4cyc}$** and **1c$_{4cyc}$** migrates back to the metal center to form the new carbene complex (Figure 4.3).

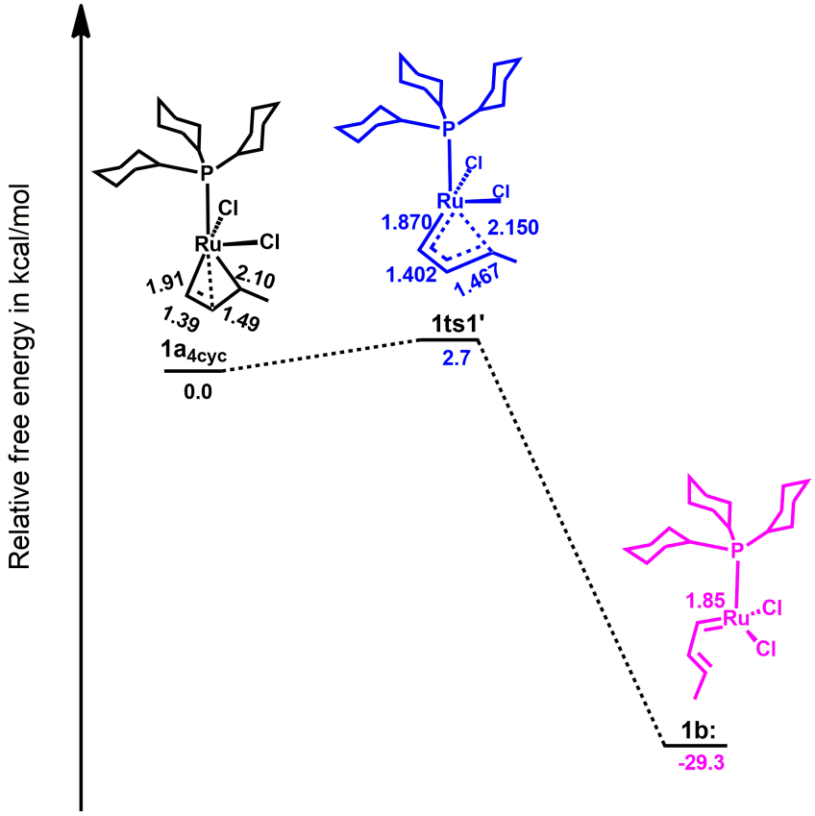

Figure 4.7 Reaction free energy profile for the ring opening of the **1a$_{4cyc}$** structure.

4.4.2 Pathway 2: Non-metathesis Pathway

The non-metathesis reactions exhibited by ruthenium carbene complexes broaden the applicability of the catalyst. Though the mechanism through which such reactions proceed is not known, the non-metathesis active species are reported as decomposition products of the catalysts generated under strong reaction conditions. The modified catalyst in the decomposition pathway is found to be devoid of carbene center. Recently Cavallo and co-workers reported Ru-halide bond energies in the range 25 – 43 kcal/mol for several ruthenium olefin metathesis catalysts and proposed that such bond breaking

event is possible for them.[80-81] Here, the Ru-chloro bond migration is considered as a plausible decomposition pathway for the catalyst to generate a metathesis inactive species. The chloro ligand could migrate to the carbene carbon (defined by a transition state **ts6**) to get the catalytically active species **g** where Ru is in +2 oxidation state. This species with a 14e configuration resembles that of CpRuCl complex, well known for [2 + 2 + 2] type cycloadditions with diynes and nitriles.[82] The chloro ligand migration to carbene center leads to the formation of complex **g** (Figure 4.8), a possible catalyst for cyclotrimerization of acetylene *via* a non-metathesis pathway. This complex has the potential to undergo further reaction as a vacant space is created on the metal center for the acetylene coordination.

In the case of **1**, acetylene coordinates to the metal center in the space generated by the chloro migration (**1g-C_2H_2**). The process is energy demanding as the coordination increases the steric crowding around the metal center. Phosphine dissociation from the sterically crowded system **1g-C_2H_2** is quite easy and one of the RuP bonds cleaves spontaneously to give **1h**. Next step is the formation of the bis-alkyne complex **1h-C_2H_2**. Subsequent steps of the reaction are very similar to the pathway shown in Scheme 4.2, *viz*. CC bond coupling between the coordinated alkynes *via* **1ts7**, formation of ruthenacyclopentadiene (**1i$_{5cyc}$**), coordination of the third alkyne to ruthenium (**1i$_{5cyc}$-C_2H_2**), CC bond coupling between alkyne and the metallacycle (**1ts8**), formation of a bicyclic intermediate complex (**1j**), formation of ruthenacycloheptatriene (**1k$_{7cyc}$**) *via* transition state **1ts9** and CC bond coupling within the metallacycle *via* **1ts10** to form the benzene complex **1a:C_6H_6**. Activation barrier for the transition states **1ts7**, **1ts8**, and **1ts9** are small, *viz*. 8.9, 16.9, and 12.2 kcal/mol, respectively while the activation barrier for **1ts10** is significantly high (28.3 kcal/mol). Acetylene trimerization *via* non-metathesis pathway catalyzed by smaller catalyst **1′** shows intermediates and transition states similar to that discussed for **1**. The reaction free energy profile for **1′** is compared with that of **1** in Figure 4.9. The smaller catalyst **1′** shows a more exothermic profile and the activation barrier for **ts7**, **ts8**, **ts9**, and **ts10** are 8.5, 9.3, 9.6 and 16.7 kcal/mol respectively. Catalytic transformation involving chloro migration is the rate determining step of the reaction. The activation barrier

required for this transformation in **1** (36.6 kcal/mol) is higher than that located for **1′** (23.3 kcal/mol). The remaining portions of the reaction profile of **1** and **1′** are very similar.

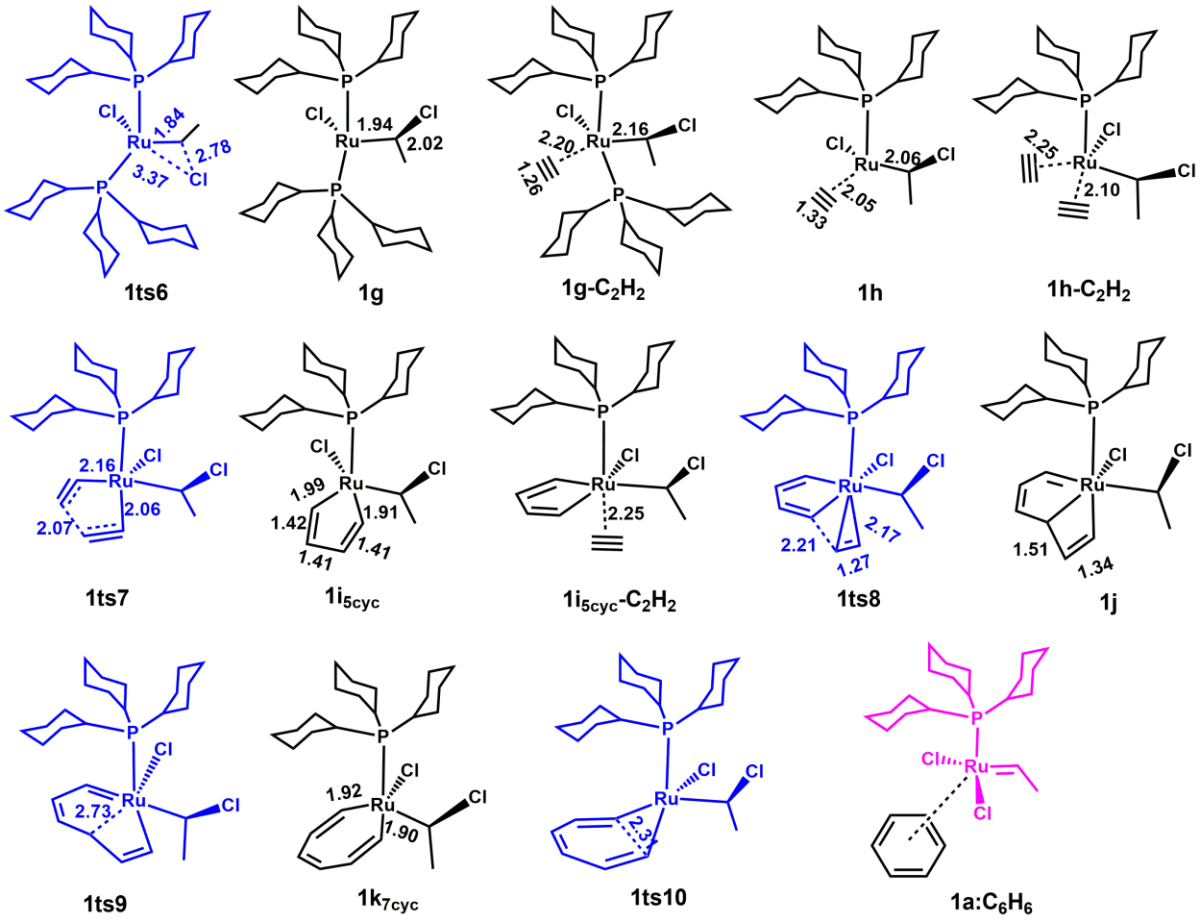

Figure 4.8 Acetylene cyclotrimerization *via* non-metathesis route for Grubbs first generation catalyst **1**. Transition states are shown in blue colour. All bond lengths in Å.

The rate determining step of the non-metathesis step (chloro ligand migration) is attempted with second generation catalysts **2** and **2′**. The activation barrier for the chloro migration in **2** and **2′** is 40.2 and 24.1 kcal/mol, respectively. These results indicate that with smaller ligands the catalyst transformation will be easier. Also the coordination of acetylene slightly stabilizes the system as the steric crowding is less around the metal center. In contrary to the big catalyst systems, dissociation of the labile ligand requires ~30 kcal/mol of energy for smaller version. Therefore, chloro

migration appears feasible than phosphine dissociation. Once the phosphine ligand dissociates, the second acetylene coordination and CC bond coupling occur easily to form a stable ruthenacyclopentadiene. The remaining rearrangements are very similar to that shown for first generation catalyst.

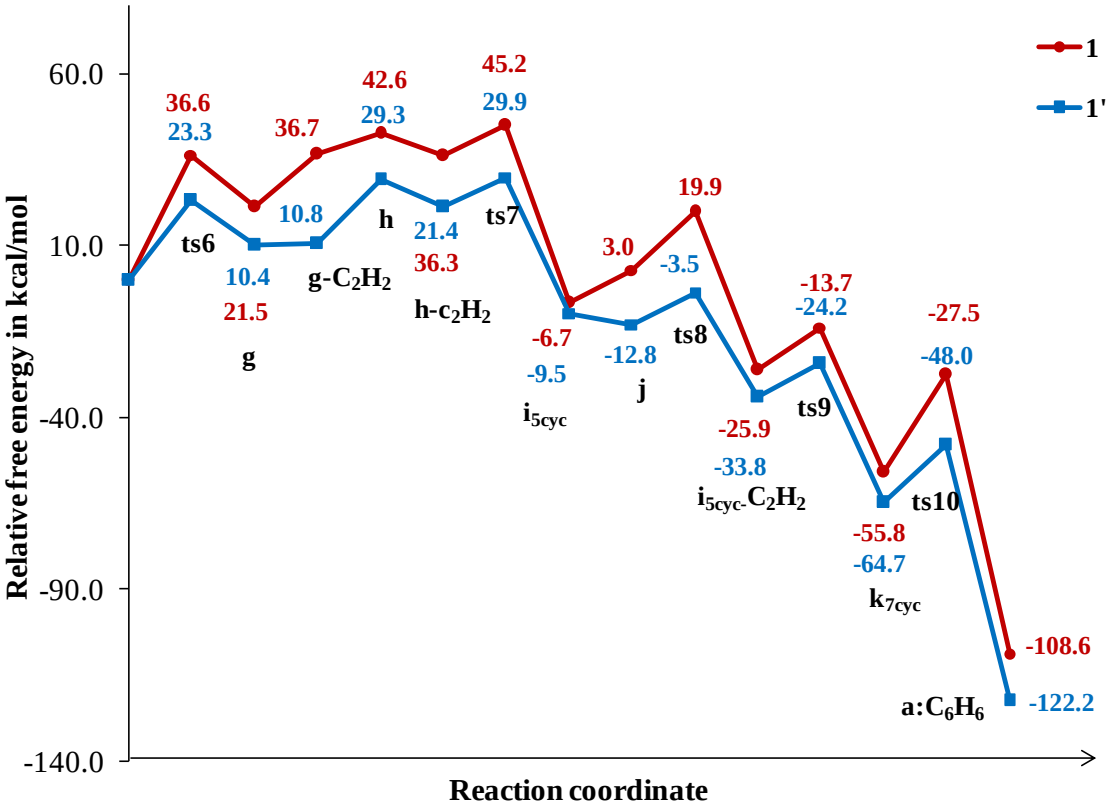

Figure 4.9 Relative Gibbs free energy profile for the non-metathesis pathway of acetylene trimerization catalyzed by **1** and **1′**.

4.5 Conclusions

Mechanistic study on the cyclotrimerization of acetylene using Grubbs first and second generation catalysts shows two probable pathways. Both pathways are highly exergonic, and the final product is stabilized by ~120 kcal/mol. Metathesis pathway is defined by three successive cross metathesis (CM) followed by a ring closing metathesis (RCM). The metathesis reaction pathway is found to be a feasible path for cyclotrimerization as the activation barrier for the reaction is moderate in all the steps.

Chance of acetylene coordination to complex **d:**, leading to a fourth CM instead of the RCM is high with all the catalysts except **1'**. This suggests that the Grubbs first generation catalyst could be modified by reducing the steric influence to prefer the RCM over CM to get a new efficient reaction for benzene synthesis. Catalytic transformation of Grubbs catalyst is also explored in the non-metathesis pathway. Though, the chloro ligand migration from the metal center to the carbene is an energy demanding process, it may compete with phosphine dissociation step in the case of catalysts made with less bulky and strongly coordinating phosphine ligands. The smaller version of the first generation catalyst **1'** show significant reduction in the activation barrier for the chlorine migration compared to their original catalysts. Again a proper tuning of the steric influence of the coordinating ligands is evident in the non-metathesis reaction profile of **1'** to achieve cyclotrimerization *via* non metathesis pathway. In summary, by reducing the steric influence and improving the coordination strength of phosphine ligands in Grubbs catalysts, efficient catalysts could be developed for cyclotrimerization of acetylene.

Part B: Grubbs and Hoveyda-Grubbs Catalysts for Pyridine Derivative Synthesis: Probing the Mechanistic Pathways Using DFT

4.6 Results and Discussions

Pérez-Castells group used Grubbs second generation catalyst in the cyclotrimerization of diynes with alkynes, where they reported a modification of Grubbs system for the formation of a catalytically active non-carbenic species.[66-68] They developed a new strategy for the pyridine derivative synthesis by the cyclotrimerization of a diyne with nitriles (Scheme 4.3) using Hoveyda-Grubbs catalyst.[83] Their reaction typically happened at high temperature (90^{o} C) and in presence of excess amount of activated nitrile (5 equivalent with respect to diyne). This reaction is important since it can be used in the total synthesis of natural products with nitrogen containing heterocycles. Though pyridine derivative synthesis using transition metal complexes is already

known,[84-87] use of Grubbs catalyst system in the cyclotrimerization is significant as the catalyst is well-known for its stability and functional group tolerance.[39] In this study, the reaction between a dipropargyl ether and acetonitrile leading to the formation of a heterocyclic molecule using Hoveyda-Grubbs catalysts and Grubbs second generation catalyst are considered for a detailed study on the mechanistic aspects covering both metathesis and non-metathesis pathways. Here, we are extending the scope of the cyclotrimerization reaction to an experimentally reported reaction of a pyridine heterocycle formation using the Hoveyda-Grubbs and Grubbs second generation catalysts (Scheme 4.3).

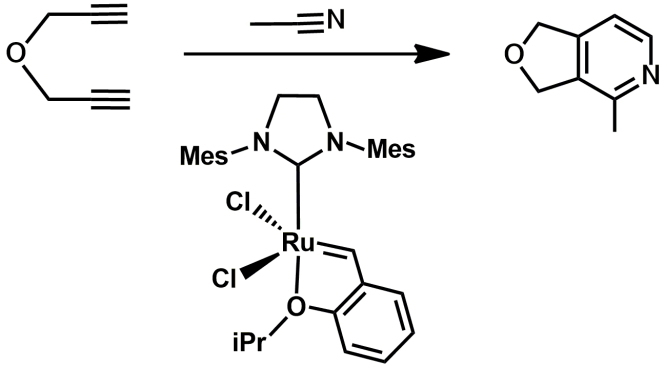

Scheme 4.3 Reaction between a diyne and nitrile catalyzed by Hoveyda-Grubbs catalyst leading to the formation of a pyridine derivative.

Four catalyst models, **2**, **2′**, **3**, **3′** (Figure 4.10) are selected for this study. **2** is Grubbs second generation catalyst[42] with the typical PCy_3 as the labile ligand. **3** is the Hoveyda-Grubbs catalyst[88-89] characterized by the isopropoxy unit and the bulky N-heterocyclic ligand in the coordination environment of Ru. Catalyst models **2′** and **3′** are the smaller versions of **2** and **3** respectively with a methyl group on the NHC nitrogen. In **2′**, the labile ligand is PMe_3. Reducing the ligand bulk has only a minor influence on the geometrical parameters of the catalysts (Figure 4.10). The steric interaction between the bulky mesityl groups and chloro ligands keeps the NHC ring coplanar with the ruthenium carbene bond in **3** and **2** while in the case of **3′** and **2′**, the reduced steric influence promotes orientation of NHC ring towards the direction of chloro ligands.

Both metathesis (Scheme 4.1) and non-metathesis (Scheme 4.2) pathways are modeled using all the four catalyst models discussed in (Figure 4.10).

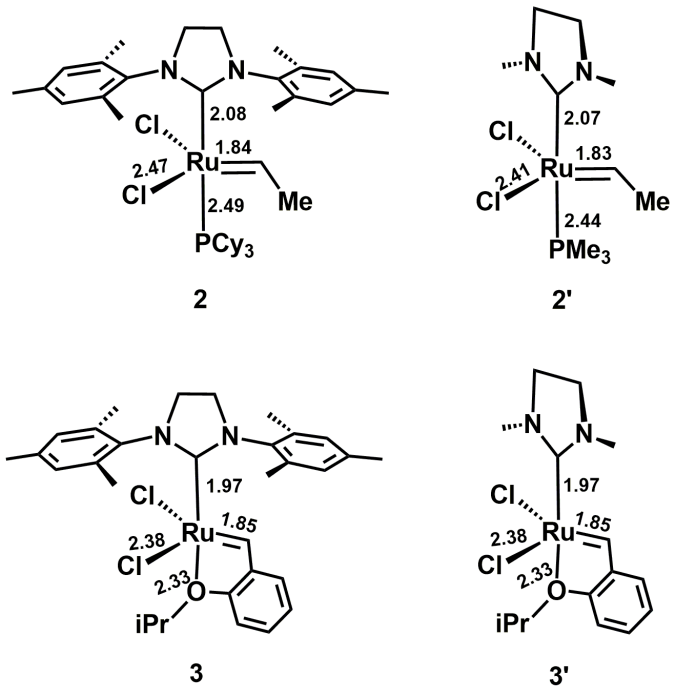

Figure 4.10 Hoveyda and Grubbs catalyst models used in the study.

4.6.1 Pathway 1: Metathesis Pathway

Figure 4.11 shows various intermediates and transition states formed in the metathesis pathway using Hoveyda-Grubbs catalyst **3**. For all the catalysts, a dissociative mechanism is considered for the metathesis.[90-91] In the case of **3**, the ruthenium oxygen bond cleave to get an active form of the catalyst **3a**. To **3a**, one of the CC triple bonds from the diyne coordinates by a bottom bound attack to form **3b**. CC bond coupling between CC triple bond and ruthenium carbene bond occurs in the next step *via* **3ts1** which yields the ruthenacyclobutene like intermediate **3c**. Here the triple bond coordination and CC coupling resemble the mechanism of enyne metathesis, a reaction that describes the formation of a 1,3-diene due to the coupling of an alkene and an alkyne in presence of a catalyst.[51, 78] Though ruthenacyclobutene is not reported as intermediate in enyne metathesis, η^3 vinyl carbene ruthenium complexes are identified in the mechanism.[57, 77, 79] Here **3c** possesses a non planar structure while the

metallacycles reported for olefin and alkyne metathesis exhibit planar structure due to 1,3-metal-carbon bonding interactions.[72]

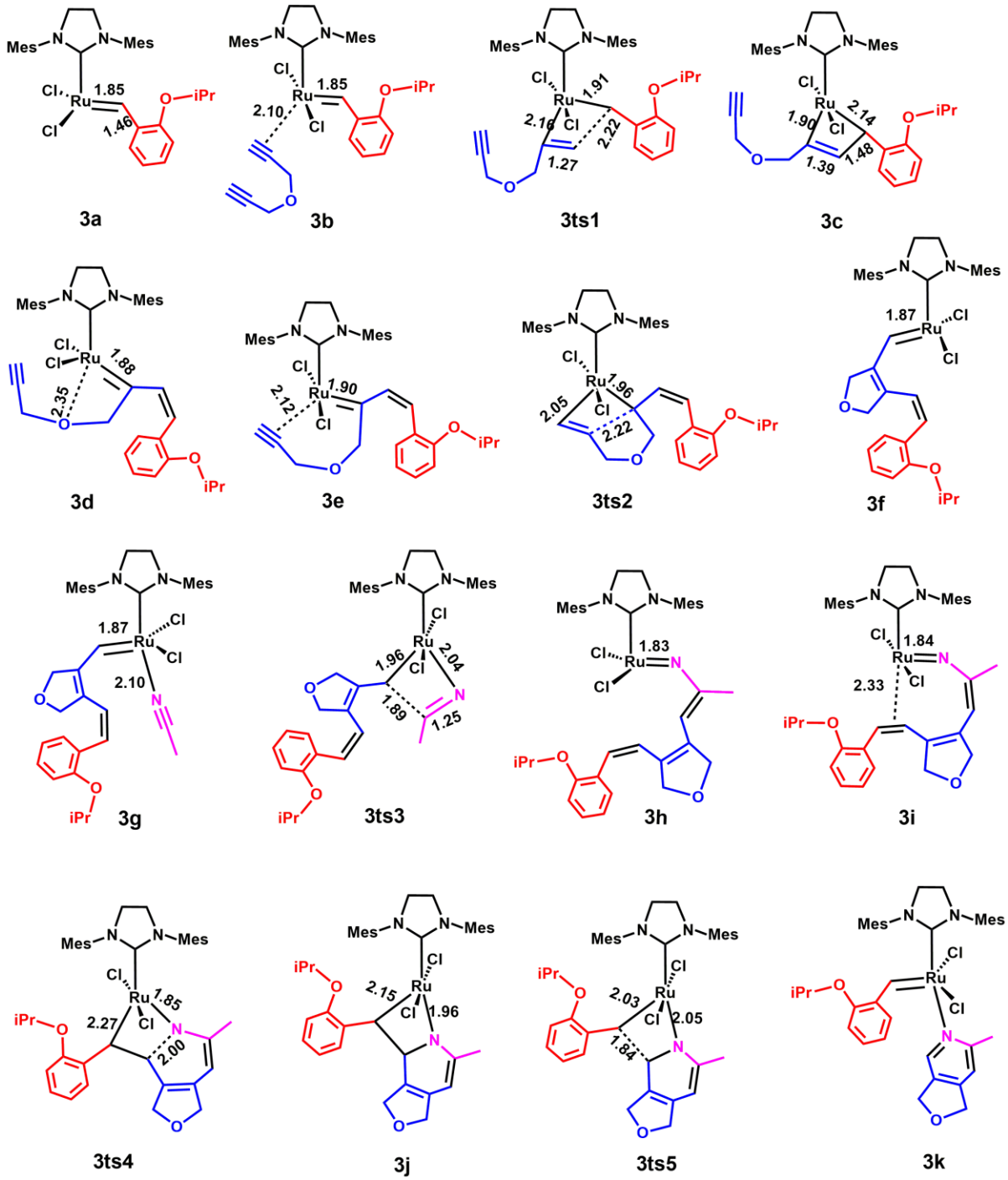

Figure 4.11 Intermediates and transition states formed in metathesis pathway of catalyst model **3** (distances in Å) (Colour code: portions from diyne, benzyl and acetonitrile units).

In **3c**, RuC_α bond distance for the saturated C_α is 2.14 Å and for the other C_α is 1.90 Å suggesting that the former could undergo RuC bond rupture to yield the intermediate **3d**. The ether oxygen functionality of **3d** shows coordination to the metal center (RuO distance 2.35 Å) and suggests that **3d** largely retains the structural and electronic properties of the Hoveyda-Grubbs catalyst. **3d** has a four-membered oxygen incorporated metallacycle while that in the original catalyst is five-membered. In the next metathesis step, the second alkyne bond of diyne coordinates to the metal by replacing the RuO interaction (**3e**). **3e** has a distrorted triogaonal bipyramidal configuration with chloro ligands at the apical position and the ClRuCl bond angle changes from 160^o in **3d** to 169^o in **3e**. The second CC bond coupling occurs *via* **3ts2**. The product of this reaction **3f** resembles that of the active form of a typical Grubbs second generation catalyst. Here a metallacycle formation is not observed which may be attributed to the ring strain effect. In the next step, acetonitrile coordinates to **3f** through its nitrogen (**3g)** and subsequently undergoes insertion into the ruthenium carbene bond *via* the transition state **3ts3**. The product of this step **3h** shows a short RuN bond of distance 1.83 Å. This indicates double bond character to RuN bond and the formation of a ruthenium nitrene complex. Fourth metathesis step is a ring closing step, where the alkene functionality adjacent to the phenyl ring (formed in the first metathesis step) coordinates to the metal (**3i)** and couples with RuN bond to give the transition state **3ts4**. **3ts4** yileds a heterometallacycle **3k** which subsequently undergoes a C-C bond rupture *via* **3ts5** to produce the pyridine derivative **3k** which is coordinated to the ruthenium center.

Grubbs second generation catalyst **2** follows the reaction in a way similar to that given in Figure 4.11. The labile phosphine ligand dissociates from the catalyst to get an active form of the catalyst **2'**. Also, smaller versions of **2** and **3**, *viz.* **2′** and **3′** follow the metathesis reaction pathway in the same way as shown in Figure 4.11. Irrespective of the ligands, the intermediates and transition states located in the reaction pathways are very similar.

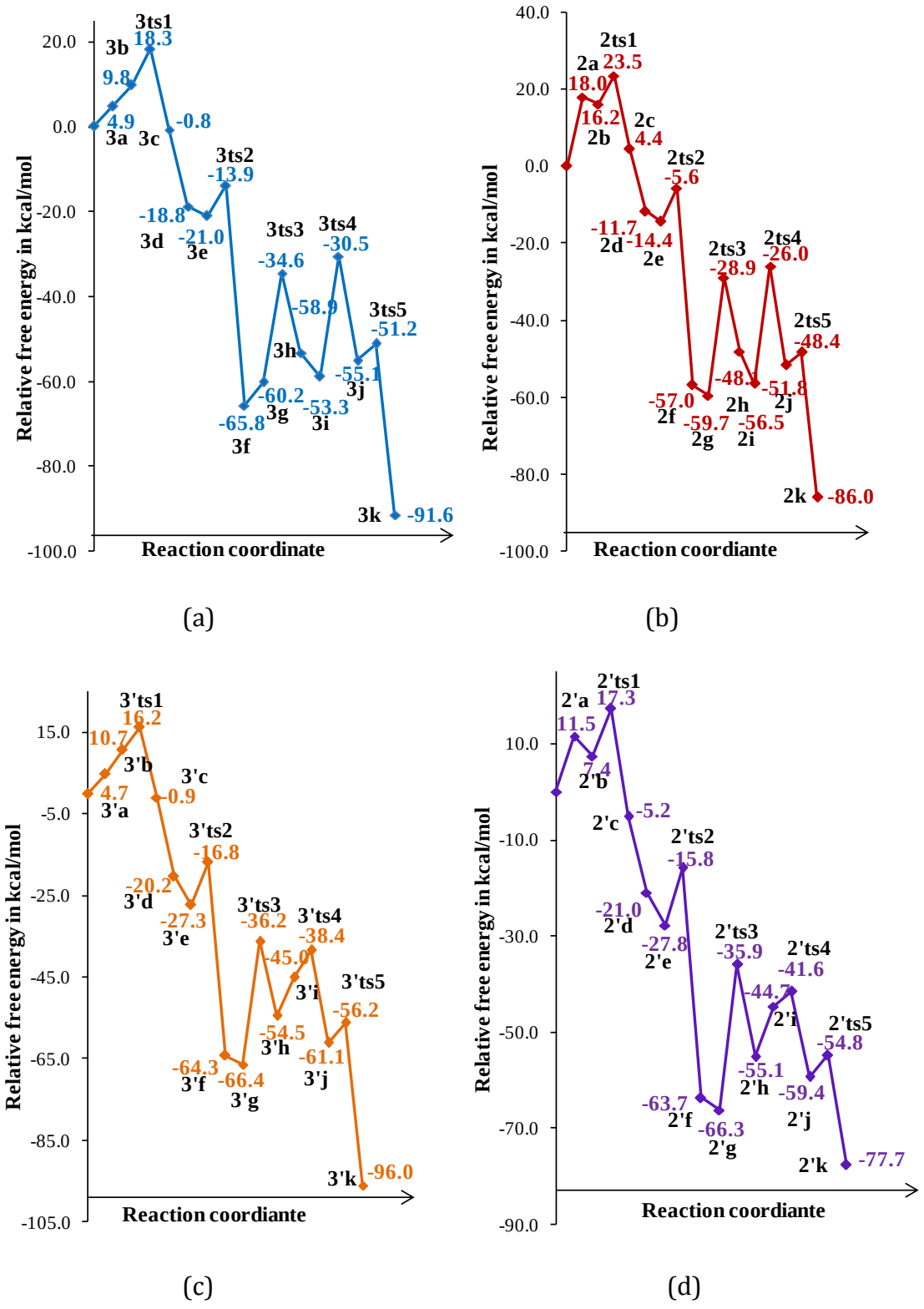

Figure 4.12 Reaction profile for the metathesis pathway of (a) catalyst **3** (b) catalyst **2** (c) catalyst **3'** and (d) catalyst **2'**.

Reaction energy profiles for the trimerization reaction *via* metathesis pathway using all the four catalysts are given in Figure 4.12. These profiles show highly exothermic character of the reaction as the triple bonds are converted to aromatic bonds. The RuO bond dissociation requires 4.9 and 4.7 kcal/mol in **3** and **3′**. The phosphine ligand dissociation from **2** and **2′** requires 16.2 and 11.5 kcal/mol respectively. Once the active form of the catalyst is formed, alkyne coordinates in the vacant space. Metathesis reaction pathway of the Hoveyda-Grubbs-type catalyst models shows a slight difference in the energy profile compared to that of Grubbs second generation catalysts. Since **3** and **3′** has bulky group attached to the carbene carbon, the alkyne coordination experiences a steric hindrance, and thus a high energy is noted in the reaction profile for the alkyne coordination. The reaction profiles in Figure 4.12 clearly indicate that the ligand bulk on the carbene carbon has significant influence on the first two cross metathesis steps. Nitrile coordination and further coupling reactions are influenced by the ligand bulk on the NHC. Activation barrier for the first cross metathesis (**ts1**) is in the range 5.5 to 9.9 kcal/mol while the second cross metathesis (**ts2**) barrier is in the range 7.1 to 12.0 kcal/mol. The bulky catalysts **3** and **2** show smaller activation barrier in both first and second metathesis steps compared to their smaller analogue. The third metathesis (**ts3**) involving the CN bond coupling is a high energy demanding process (~30.0 kcal/mol) for all catalysts. The final ring closing metathesis step (**ts4**) has an activation barrier of 28.4, 30.5, 6.6, and 4.6 respectively for **3**, **2**, **3′** and **2′**. The CC coupling defined by **ts4** leads to a metallacycle structure **j** for all. The metallacycle **j**, opens up immediately to form the final product **k** and the activation barrier required for the ring opening is in the range 3.3 to 4.9 kcal/mol.

Though the synthesis of pyridine and pyridone type molecules *via* metathesis based approach is already reported,[49, 92-93] the present study is the first one on mechanistic aspects that unravels a cascade of metatheses for pyridine synthesis. In the mechanism, the metallacyclobutene structure **c** is clearly seen as an intermediate in all the catalyst models which opens up to an active catalyst **d** in a barrier less process. The minimum energy state of **3c** is also validated by locating its structure using different DFT methods. The rate limiting step of the reaction is the CC bond coupling between

carbon of acetonitrile and C_α of the catalyst (*via* **ts3**) for the smaller catalysts models (~30.0 kcal/mol). For the bulky catalysts models **2** and **3** the final RCM is a high energy process (~30.0 kcal/mol). In all the **g** intermediates, end-on coordination of acetonitrile yields the most stable complex which promotes the CC bond coupling.

4.6.2 Pathway 2: Non-metathesis Pathway

We invoke the chloro ligand migration in describing the non-metathesis pathway. Ru-chloro bond cleavage creates a vacant site for the alkyne to coordinate with Ru in a distorted trigonal pyramidal configuration. The chloro ligand migration to carbene carbon elongates the RuC_α bond by ~0.13 Å indicating single bond character of the bond and loss of metathesis activity of the complex. For all the catalyst models, the transformed '**l**' type species are used for exploring the cyclotrimerization pathway given in Scheme 4.2. Such a pathway is well known in the case of CpRuCl, reported by Yamamoto *et al.*[82]

In the non-metathesis pathway for **3** (Figure 4.13), coordination of the first alkyne unit occurs on **3l** to yield **3m**. In the next step, RuO bond cleavage (**3n)** promotes the coordination of the second alkyne unit to Ru (**3o**). The next stage of the reaction describes an intramolecular [2+2] cycloaddition between the coordinated alkyne units in **3o** *via* **3ts7** leading to the formation of a stable ruthenacyclopentadiene intermediate **3p**. At this stage, coordination of acetonitrile to Ru is invoked (**3q)**. Subsequently, CC bond coupling occurs between acetonitrile and C_α of metallacyclopentadiene through the transition state **3ts8** which give rise to the formation of a [3.2.0] bicyclic ring **3r**. This intermediate opens up at the central RuC bond through **3ts9** to a seven-memberd metallacycle **3s**. **3s** undergoes ring contraction reaction by promoting N-C bond formation *via* **3ts10**. The desired heterocyclic product is formed from this transition state which shows coordination of the pyridine nitrogen to ruthenium. During this process, the chloro ligand migrates back to ruthenium to regenerate the catalytically active species.

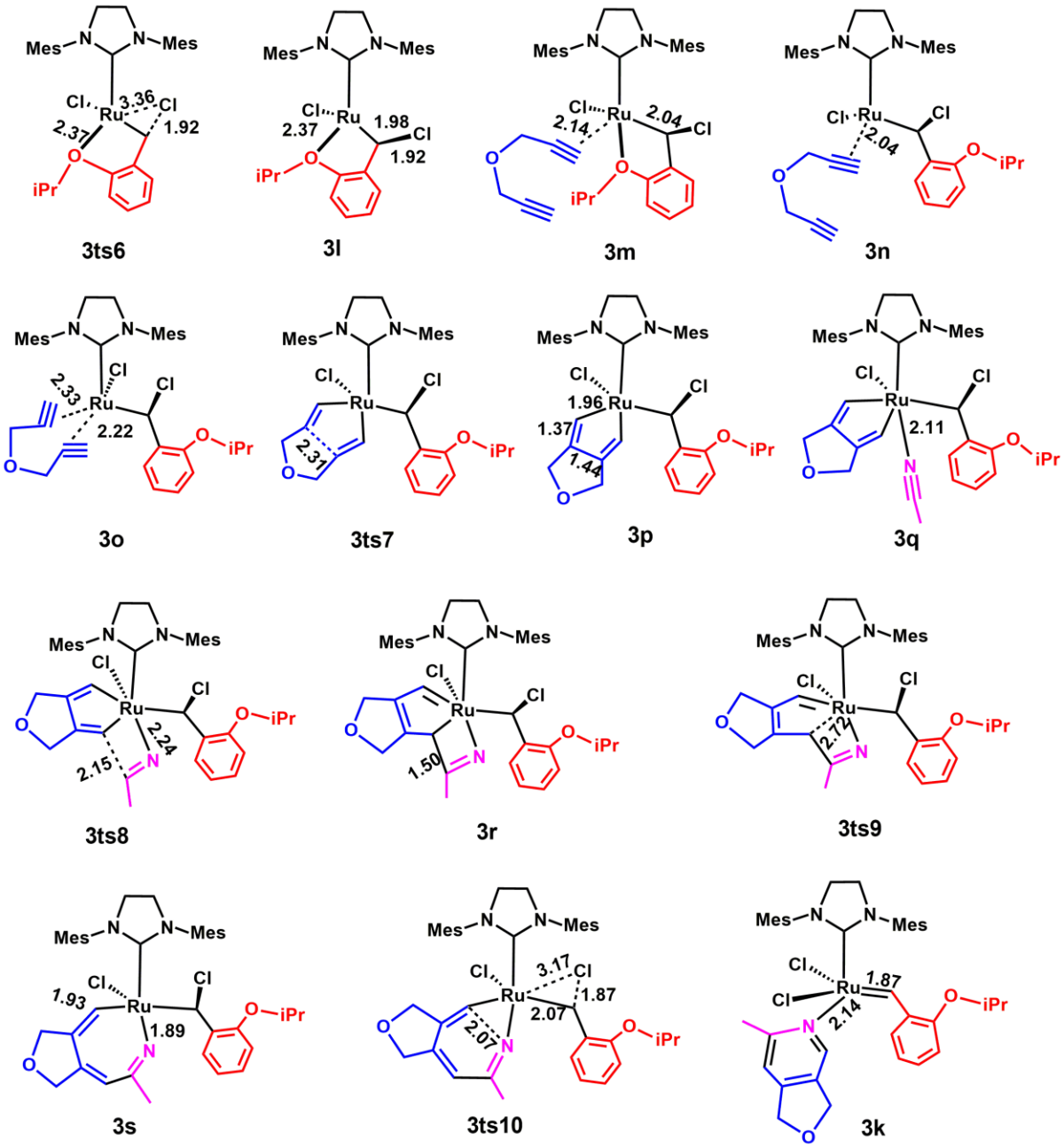

Figure 4.13 Intermediates and transition states formed in non-metathesis pathway of **3** (distances are given in Å) (Colour code: portions from diyne, benzyl and acetonitrile units).

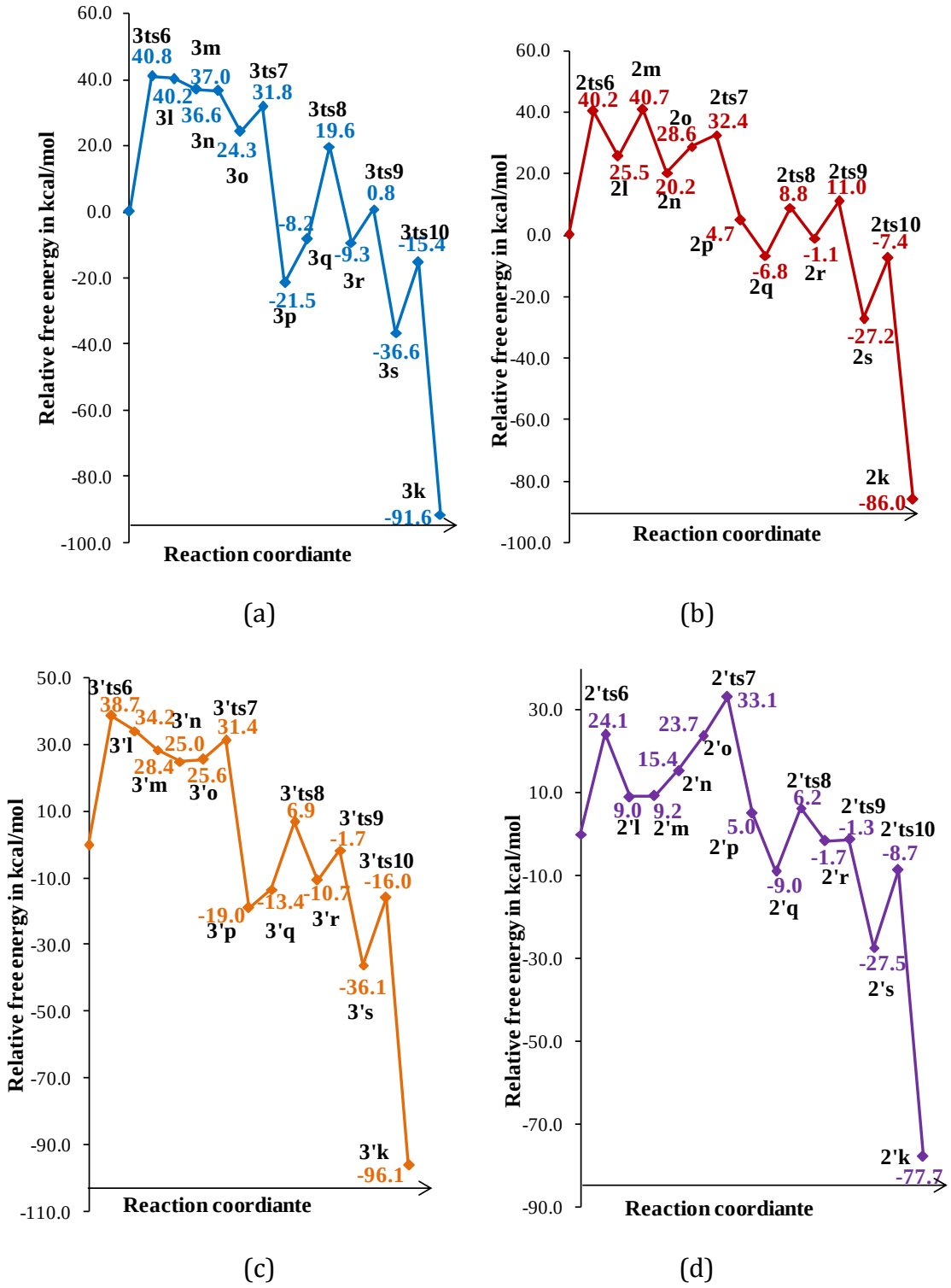

Figure 4.14 Reaction profile for the non-metathesis pathway of (a) catalyst **3** (b) catalyst **2** (c) catalyst **3'** and (d) catalyst **2'**.

Reaction pathway similar to **3** is observed for the cyclotrimerization reaction catalyzed by Grubbs second generation catalyst **2** and smaller catalyst models **2'**and **3'**. The relative free energy profiles for the non-metathesis pathway catalyzed by all four catalysts are given in Figure 4.14. Chloro migration from the metal center to the carbene carbon requires 40.8 and 40.2 kcal/mol respectively for **3** and **2**. The smaller Hoveyda-Grubbs-type catalyst **3'** requires 38.7 kcal/mol for the chloro migration, while an activation barrier of 24.1 kcal/mol observed for catalyst transformation in **2'**. These barrier heights indicate that the non-metathesis pathway needs severe reaction conditions except for **2'**. Also, the modified catalyst **l** for Grubbs second generation catalyst **2** and **2'** appears more stable than that obtained for **3** and **3'**. Alkyne coordination to the metal center slightly stabilizes the catalyst systems in the case of **3** and **3'** while slight destabilization is observed for **2** and **2'** due to steric influence from phosphine ligand. Further, dissociation of the labile ligand from complex **m** (Ru-O bond cleavage for **3** and **3'** and phosphine ligand dissociation for **2** and **2'**) occurs spontaneously with lowering of free energy for all the catalysts except **2'** that reduces the steric crowding around the metal. In **2'm**, ligand dissociation is energy demanding by 6.2 kcal/mol while the sterically the most crowded **2m** shows a large drop in free energy. Activation barrier for the CC bond coupling (**ts7**) is in the range of 3.8 to 9.4 kcal/mol for all the catalyst models. The CC coupling *via* **ts7** results in a stable ruthenacyclopentadiene intermediate (**p**). Coordination of nitrile to **p** causes a slight increase in free energy for **3** and **3'**. Activation barrier for the coupling between RuC and CN bond (**ts8**) requires 27.8 and 20.3 kcal/mol for Hoveyda-Grubbs-type catalysts **3** and **3'** while the value is 15.6 and 15.2 kcal/mol respectively for **2** and **2'**. The activation barrier for the final CN coupling in **s** is 21.2, 19.8, 20.1, 18.8 kcal/mol respectively for **3**, **2**, **3'** and **2'**.

Both metathesis and non-metathesis pathway suggest that smaller versions of the catalysts are good choice for the cyclotrimerization reaction. Both **3'** and **2'**, the smaller versions of the Hoveyda-Grubbs and Grubbs second generation catalysts respectively showed relatively lower activation free energy values in both metathesis and non-metathesis pathways. Comparison of reaction profiles in Figure 4.12

(metathesis) and Figure 4.14 (non-metathesis) may suggest that metathesis is the obvious choice for describing the pyridine ring formation. However, by invoking the possibility that the catalyst undergoes decomposition at the condition used for the reaction, *viz*. 90° C by Pérez-Castells *et al*., the metathesis pathway may be ruled out. Otherwise, the chance for benzene ring formation is higher than the pyridine ring formation. We looked at this alternate possibility by proposing the coordination of a second diyne with metal center in **3g** instead of the coordination of acetonitrile (Figure 4.16). Such a pathway showed the facile formation of the CC bond with activation free energy 11.0 kcal/mol (Figure 4.15) which is 21.0 kcal/mol lower than the CC bond formation *via* the coordination of acetonitrile (**3ts4**). In fact, this pathway explains the formation of the carbocycle (a benzene derivative) byproduct reported by Pérez-Castells *et al*. It may be noted that the alternate pathway suggests the use of excess diyne while the actual reaction conditions used excess amount of activated nitrile (5 equivalents with respect to diyne concentration) which is favorable for the non-metathesis pathway at 90° C. An alternate non-metathesis pathway for the byproduct formation is not observed.

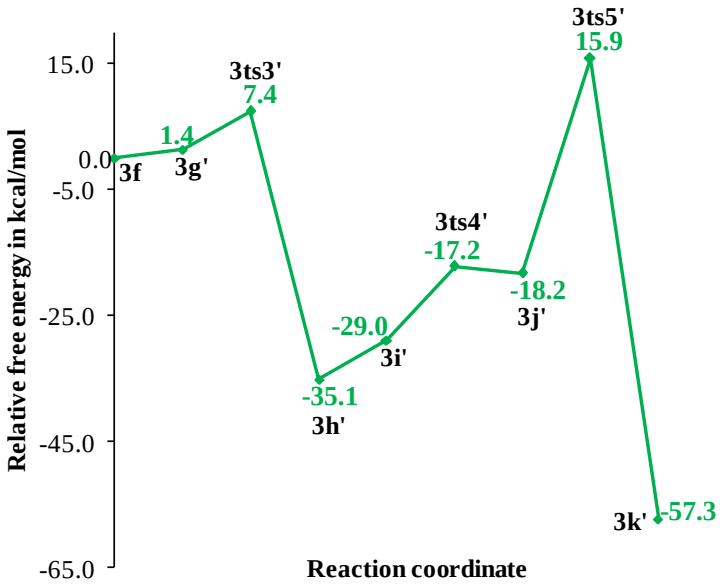

Figure 4.15 Reaction free energy profile for the second diyne coordination resulting in **3k'**.

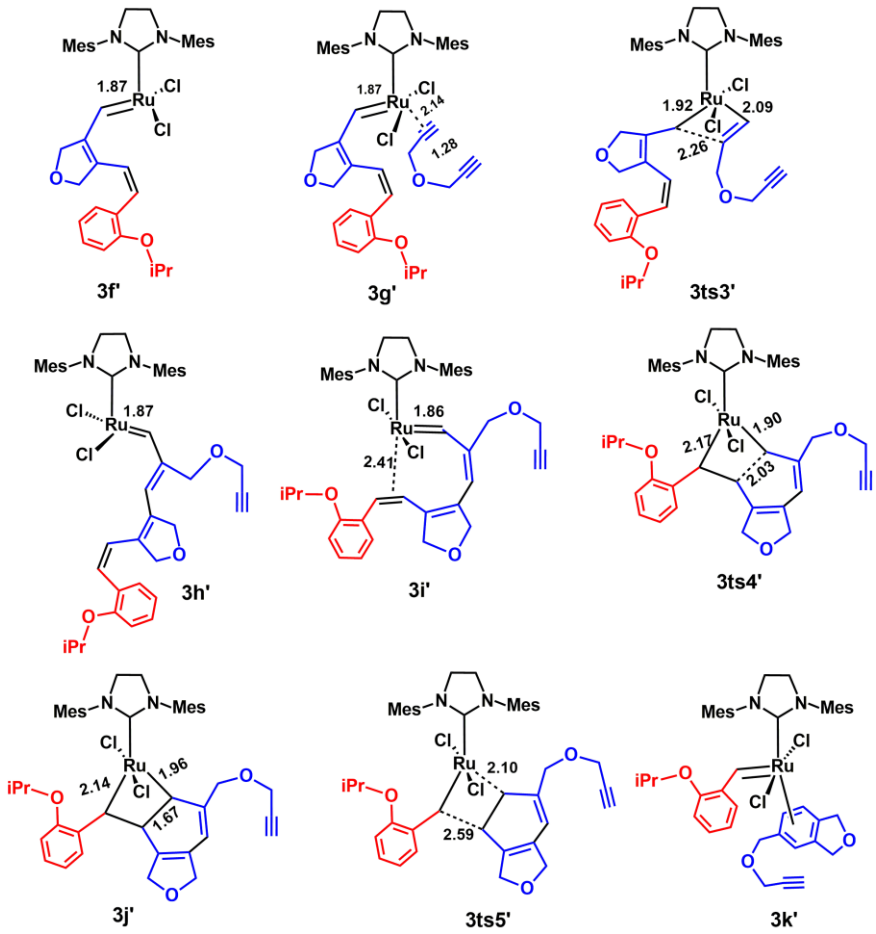

Figure 4.16 Intermediates and transition states formed in the metathesis pathway *via* second diyne coordination for **3**(distances are given in Å). (Colour code: portions from diyne, and benzyl units).

4.7 Conclusions

The cyclotrimerization between diyne and acetonitrile is a highly exothermic reaction which involves the conversion of triple bonds to aromatic bonds. Both Hoveyda-Grubbs and Grubbs second generation catalysts and their simpler versions show metathesis and non-metathesis pathways for the cyclotrimerization. The bulky mesityl group as well as the isopropoxy group influence the stability of the intermediates and thus play a vital role in the mechanism. In metathesis pathway of **2** and **3**, the second step yields a Hoveyda-type catalyst and subsequently the second alkyne unit coordinates to the metal by the loss of Ru-O bond. When the mesityl group in **2** and **3** is replaced by

methyl groups (**2**' and **3**'), second alkyne coordination occurs without the intervention of the oxygen coordinated species. In general, metathesis pathway follows Scheme 4.1, where the rate determining step is the CC bond formation between the coordinated acetonitrile and the carbene center of the catalytically active species. For non-metathesis pathway, the catalytically active species is generated by migrating the chloro ligand to the carbene center. The resulting species is metathesis inactive while the creation of a vacant coordination on Ru promotes the coordination of the first alkyne unit and subsequent reactions thereafter as per Scheme 4.2. Here the proposed ruthenium carbon bond deactivation for non-metathesis requires higher energy for catalysts **2** and **3** with bulky mesityl group on the NHC than their smaller versions. In all cases, the first step leading to catalyst transformation emerges as the most crucial for non-metathesis activity. Decreasing the bulkiness of the NHC ligand enhances non-metathesis pathway of cyclotrimerization. Typically pyridine ring formation reactions are done at high temperature with excess amount of activated nitriles. If the catalyst is not decomposed under such circumstances, only a metathesis pathway can be invoked for the formation of the heterocycle because the more facile route to benzene ring formation may be suppressed by the excess amount of nitrile present in the reaction. If the catalyst undergoes decomposition, the non-metathesis pathway has to be invoked to describe the outcome of the reaction. Hence we feel that it is very important to find out experimentally the nature of the active catalytic species in the reaction to make further progress in the design of efficient catalysts for pyridine synthesis.

4.8 References

1. S. Saito and Y. Yamamoto, *Chem. Rev.*, **2000**, *100*, 2901-2916.
2. J. A. Varela and C. Saá, *Chem. Rev.*, **2003**, *103*, 3787-3802.
3. D. O'Hagan, *Nat. Prod. Rep.*, **1997**, *14*, 637-651.
4. L. Jayasinghe, C. P. Jayasooriya, N. Hara and Y. Fujimoto, *Tetrahedron Lett.*, **2003**, *44*, 8769-8771.
5. Y.-W. Kim, J. C. Hackett and R. W. Brueggemeier, *J. Med. Chem.* , **2004**, *47*, 4032-4040.

6. S.-J. Su, H. Sasabe, T. Takeda and J. Kido, *Chem. Mater.*, **2008**, *20*, 1691-1693.
7. W. Aida, T. Ohtsuki, X. Li and M. Ishibashi, *Tetrahedron*, **2009**, *65*, 369-373.
8. K. M. John A. Joule, ed., *Heterocyclic Chemistry, 5th Edition*, Wiley-Blackwell, **2010**.
9. C. W. Lee and J. Y. Lee, *Adv. Mater.*, **2013**, *25*, 596-600.
10. W. Reppe and W. J. Schweckendiek, *Justus Liebigs Annalen der Chemie*, **1948**, *560*, 104-116.
11. C. Bianchini, K. G. Caulton, T. J. Johnson, A. Meli, M. Peruzzini and F. Vizza, *Organometallics*, **1995**, *14*, 933-943.
12. C. Breschi, L. Piparo, P. Pertici, A. M. Caporusso and G. Vitulli, *J. Organomet. Chem.*, **2000**, *607*, 57-63.
13. D. Suzuki, H. Urabe and F. Sato, *J. Am. Chem. Soc.*, **2001**, *123*, 7925-7926.
14. P. I. Dosa, G. D. Whitener, K. P. C. Vollhardt, A. D. Bond and S. J. Teat, *Org. Lett.*, **2002**, *4*, 2075-2078.
15. M. Shanmugasundaram, M. S. Wu, M. Jeganmohan, C. W. Huang and C. H. Cheng, *J. Org. Chem.*, **2002**, *67*, 7724-7729.
16. T. Takahashi, Y. Z. Li, P. Stepnicka, M. Kitamura, Y. J. Liu, K. Nakajima and M. Kotora, *J. Am. Chem. Soc.*, **2002**, *124*, 576-582.
17. Y. Yamamoto, A. Nagata, H. Nagata, Y. Ando, Y. Arikawa, K. Tatsumi and K. Itoh, *Chem. Eur. J.*, **2003**, *9*, 2469-2483.
18. T. Oshiki, H. Nomoto, K. Tanaka and K. Takai, *Bull. Chem. Soc. Jpn.*, **2004**, *77*, 1009-1011.
19. S. Kotha, E. Brahmachary and K. Lahiri, *Eur. J. Org. Chem.*, **2005**, *2005*, 4741-4767.
20. P. R. Chopade and J. Louie, *Adv. Synth. Catal.*, **2006**, *348*, 2307-2327.
21. A. F. Moretto, H.-C. Zhang and B. E. Maryanoff, *J. Am. Chem. Soc.*, **2001**, *123*, 3157-3158.
22. B.-H. Xu, D.-H. Wu, Y.-Z. Li and H. Yan, *Organometallics*, **2007**, *26*, 4344-4349.
23. G. Hilt, C. Hengst and W. Hess, *Eur. J. Org. Chem.*, **2008**, *2008*, 2293-2297.
24. A. H. M. Elwahy and K. Hafner, *Eur. J. Org. Chem.*, **2010**, *2010*, 265-274.
25. C. C. Eichman, J. P. Bragdon and J. P. Stambuli, *Synlett*, **2011**, *2011*, 1109-1112.

26. Y. Yamamoto, H. Kitahara, R. Ogawa, H. Kawaguchi, K. Tatsumi and K. Itoh, *J. Am. Chem. Soc.*, **2000**, *122*, 4310-4319.
27. Y. Yamamoto, R. Ogawa and K. Itoh, *Chem. Commun.*, **2000**, 549-550.
28. Y. Yamamoto, S. Okuda and K. Itoh, *Chem. Commun.*, **2001**, 1102-1103.
29. Y. Yamamoto, H. Takagishi and K. Itoh, *Org. Lett.*, **2001**, *3*, 2117-2119.
30. Y. Yamamoto, K. Kinpara, T. Saigoku, H. Takagishi, S. Okuda, H. Nishiyama and K. Itoh, *J. Am. Chem. Soc.*, **2004**, *127*, 605-613.
31. D. D. Young, R. S. Senaiar and A. Deiters, *Chem. Eur. J.*, **2006**, *12*, 5563-5568.
32. A. Dachs, S. Osuna, A. Roglans and M. Solà, *Organometallics*, **2010**, *29*, 562-569.
33. Z. Liu, R. Cheng, X. He, X. Wu and B. Liu, *J. Phys. Chem. A*, **2012**, *116*, 7538-7549.
34. S. Y. Yun, K.-P. Wang, M. Kim and D. Lee, *J. Am. Chem. Soc.*, **2012**, *134*, 10783-10786.
35. C.-H. Guo, H.-S. Wu, M. Hapke and H. Jiao, *J. Organomet. Chem.*, **2013**, *748*, 29-35.
36. Y. Yamamoto, in *Transition-Metal-Mediated Aromatic Ring Construction*, John Wiley & Sons, Inc., **2013**, pp. 71-125.
37. A. Sorkau, K. Schwarzer, C. Wagner, E. Poetsch and D. Steinborn, *J. Mol. Catal. A: Chem.*, **2004**, *224*, 105-109.
38. R. H. Grubbs, ed., *Handbook of Olefin Metathesis*, Wiley-VCH: Weinheim, Germany.
39. T. M. Trnka and R. H. Grubbs, *Acc. Chem. Res*, **2001**, *34*, 18-29.
40. R. H. Grubbs and S. Chang, *Tetrahedron*, **1998**, *54*, 4413-4450.
41. R. H. Grubbs, *Angew. Chem. Int. Ed.*, **2006**, *45*, 3760-3765.
42. G. C. Vougioukalakis and R. H. Grubbs, *Chem. Rev.*, **2010**, *110*, 1746-1787.
43. A. Mukherjee, *Synlett*, **2006**, 1128-1129.
44. B. Alcaide, P. Almendros and A. Luna, *Chem. Rev.*, **2009**, *109*, 3817-3858.
45. J. U. Peters and S. Blechert, *Chem. Commun.*, **1997**, 1983-1984.
46. S. K. Das and R. Roy, *Tetrahedron Lett.*, **1999**, *40*, 4015-4018.
47. G. B. Hoven, J. Efskind, C. Rømming and K. Undheim, *J. Org. Chem.*, **2002**, *67*, 2459-2463.
48. B. Witulski, T. Stengel and J. M. Fernandez-Hernandez, *Chem. Commun.*, **2000**, 1965-1966.

49. W. A. L. van Otterlo and C. B. de Koning, *Chem. Rev.*, **2009**, *109*, 3743-3782.
50. C. Kang, E.-H. Kang and T.-L. Choi, *Macromolecules*, **2017**, *50*, 3153-3163.
51. C. S. Poulsen and R. Madsen, *Synthesis-Stuttgart*, **2003**, 1-18.
52. H. Clavier, A. Correa, E. C. Escudero-Adán, J. Benet-Buchholz, L. Cavallo and S. P. Nolan, *Chem. Eur. J.*, **2009**, *15*, 10244-10254.
53. G. C. Lloyd-Jones, A. J. Robinson, L. Lefort and J. G. de Vries, *Chem. Eur. J.*, **2010**, *16*, 9449-9452.
54. A. G. D. Grotevendt, J. A. M. Lummiss, M. L. Mastronardi and D. E. Fogg, *J. Am. Chem. Soc.*, **2011**, *133*, 15918-15921.
55. F. Nunez-Zarur, X. Solans-Monfort, L. Rodriguez-Santiago and M. Sodupe, *ACS Catal.*, **2013**, *3*, 206-218.
56. J. R. Griffiths, J. B. Keister and S. T. Diver, *J. Am. Chem. Soc.*, **2016**, *138*, 5380-5391.
57. J. J. Lippstreu and B. F. Straub, *J. Am. Chem. Soc.*, **2005**, *127*, 7444-7457.
58. F. Nuñez-Zarur, X. Solans-Monfort, L. Rodríguez-Santiago, R. Pleixats and M. Sodupe, *Chem. Eur. J.*, **2011**, *17*, 7506-7520.
59. K. Kirchner, M. J. Calhorda, R. Schmid and L. F. Veiros, *J. Am. Chem. Soc.*, **2003**, *125*, 11721-11729.
60. R. Schmid and K. Kirchner, *J. Org. Chem.*, **2003**, *68*, 8339-8344.
61. Y. Yamamoto, T. Arakawa, R. Ogawa and K. Itoh, *J. Am. Chem. Soc.*, **2003**, *125*, 12143-12160.
62. A. A. Dahy, C. H. Suresh and N. Koga, *Bull. Chem. Soc. Jpn.*, **2005**, *78*, 792-803.
63. A. A. Dahy and N. Koga, *Organometallics*, **2015**, *34*, 4965-4974.
64. S. Hanessian, S. Giroux and A. Larsson, *Org. Lett.*, **2006**, *8*, 5481-5484.
65. Á. Mallagaray, S. Medina, G. Domínguez and J. Pérez-Castells, *Synlett*, **2010**, *2010*, 2114-2118.
66. G. Dominguez and J. Perez-Castells, *Chem. Soc. Rev.*, **2011**, *40*, 3430-3444.
67. A. Mallagaray, K. Mohammadiannejad-Abbasabadi, S. Medina, G. Dominguez and J. Perez-Castells, *J. Org. Biomol. Chem.*, **2012**, *10*, 6665-6672.
68. S. Alvarez, S. Medina, G. Dominguez and J. Perez-Castells, *J. Org. Chem.*, **2015**, *80*, 2436-2442.
69. A. D. Becke, *Phys. Rev. A*, **1988**, *38*, 3098-3100.

70. J. P. Perdew, *Phys. Rev. B*, **1986**, *33*, 8822-8824.
71. S. Grimme, J. Antony, S. Ehrlich and H. Krieg, *J. Chem. Phys.*, **2010**, *132*.
72. A. V. Marenich, C. J. Cramer and D. G. Truhlar, *J. Phys. Chem. B*, **2009**, *113*, 6378-6396.
73. S. Maeda, Y. Harabuchi, Y. Ono, T. Taketsugu and K. Morokuma, *Int. J. Quantum Chem.*, **2015**, *115*, 258-269.
74. A. J. Jiang, J. H. Simpson, P. Müller and R. R. Schrock, *J. Am. Chem. Soc*, **2009**, *131*, 7770-7780.
75. S. T. Diver, *Coord. Chem. Rev.*, **2007**, *251*, 671-701.
76. B. O. Ozturk, B. Sariaslan and S. K. Sehitoglu, *J. Organomet. Chem.*, **2016**, *822*, 13-19.
77. T. M. Trnka, M. W. Day and R. H. Grubbs, *Organometallics*, **2001**, *20*, 3845-3847.
78. S. T. Diver and A. J. Giessert, *Chem. Rev.*, **2004**, *104*, 1317-1382.
79. X. Solans-Monfort, *Dalton Trans.*, **2014**, *43*, 4573-4586.
80. H.-Y. Wang, W.-L. Yim, Y.-L. Guo and J. O. Metzger, *Organometallics*, **2012**, *31*, 1627-1634.
81. L. Falivene, A. Poater, C. S. J. Cazin, C. Slugovc and L. Cavallo, *Dalton Trans.*, **2013**, *42*, 7312-7317.
82. Y. Yamamoto, K. Kinpara, T. Saigoku, H. Takagishi, S. Okuda, H. Nishiyama and K. Itoh, *J. Am. Chem. Soc.*, **2004**, *127*, 605-613.
83. S. Alvarez, S. Medina, G. Domínguez and J. Pérez-Castells, *J. Org. Chem.*, **2013**, *78*, 9995-10001.
84. G. Dazinger, M. Torres-Rodrigues, K. Kirchner, M. J. Calhorda and P. J. Costa, *J. Organomet. Chem.*, **2006**, *691*, 4434-4445.
85. A. A. Dahy, K. Yamada and N. Koga, *Organometallics*, **2009**, *28*, 3636-3649.
86. T. Hashimoto, K. Kato, R. Yano, T. Natori, H. Miura and R. Takeuchi, *J. Org. Chem.*, **2016**, *81*, 5393-5400.
87. F. Ye, M. Haddad, V. Michelet and V. Ratovelomanana-Vidal, *Org. Chem. Front.*, **2017**, *4*, 1063-1068.
88. J. S. Kingsbury, J. P. A. Harrity, P. J. Bonitatebus and A. H. Hoveyda, *J. Am. Chem. Soc.*, **1999**, *121*, 791-799.

89. S. B. Garber, J. S. Kingsbury, B. L. Gray and A. H. Hoveyda, *J. Am. Chem. Soc.*, **2000**, *122*, 8168-8179.
90. J. B. Collins, J. D. Dill, E. D. Jemmis, Y. Apeloig, P. v. R. Schleyer, R. Seeger and J. A. Pople, *J. Am. Chem. Soc.*, **1976**, *98*, 5419-5427.
91. I. W. Ashworth, I. H. Hillier, D. J. Nelson, J. M. Percy and M. A. Vincent, *Chem.Commun.*, **2011**, *47*, 5428-5430.
92. T. J. Donohoe, L. P. Fishlock and P. A. Procopiou, *Synthesis*, **2008**, *2008*, 2665-2667.
93. T. J. Donohoe, L. P. Fishlock and P. A. Procopiou, *Org. Let.*, **2008**, *10*, 285-288.

List of Publications

(i) Articles in journals

1. Hypercoordinate β-carbon in Grubbs and Schrock olefin metathesis metallacycles. **P. R. Remya**, and C.H. Suresh, *Dalton Trans.*, **2015**, *44*, 17660-17672.

2. Planar tetracoordinate carbon in tungstenacyclobutadiene of alkyne metathesis and expanded structures. **P. R. Remya**, and C.H. Suresh, *Dalton Trans.*, **2016**, *45*, 1769-1778.

3. Theoretical evidence for bond stretch isomerism in Grubbs olefin metathesis. **P. R. Remya**, and C.H. Suresh, *J. Comput. Chem*., **2017**, *38*, 1704-1711.

4. Mechanistic studies on acetylene cyclotrimerization catalyzed by Grubbs first and second generation catalysts. **P. R. Remya**, and C.H. Suresh, *Molecular Catal.,* **2017**, *441*, 63-71.

5. Grubbs and Hoveyda-Grubbs catalysts for pyridine derivative synthesis: probing the mechanistic pathways using DFT. **P. R. Remya**, and C.H. Suresh, *Molecular Catal.* **2018**, *450*, 29-38.

(ii) Published contributions to academic conferences

1. Presented a poster entitled "Grubbs and Hoveyada catalyst for pyridine derivative synthesis: Probing the metathetic and non-metathetic pathways using DFT" in the Transcending Frontiers in Organic Chemistry (TFOC), held at CSIR-NIIST, during October 09 - 11, 2014

2. Presented a poster entitled "Planar Tetracoordinate (C_{pt}) and Hypervalent Carbon (C_{hyper}) in Metathesis Reaction- a DFT study " in the Theoretical Chemistry Symposium (TCS), held at CSIR-NCL, Pune, during December 18 - 21, 2014

3. Presented a poster entitled "Bond Stretch Isomerism in Olefin Metathesis" in the Theoretical Chemistry Symposium (TCS), held at University of Hyderabad, Hyderabad, during December 14 - 17, 2016